Investigation towards applicability of polybenzimidazole (PBI) based polymeric ionic liquids (PILs) for gas permeation and fuel cells

Thesis Submitted to AcSIR

For the Award of the Degree of

DOCTOR OF PHILOSOPHY

In

CHEMICAL SCIENCES

AcSIR

By

Anita Kumari Rewar
(Registration Number: 10CC11J26069)

Under the guidance of
Dr. Ulhas K. Kharul

Polymer Science and Engineering Division
CSIR-National Chemical Laboratory
Pune - 411008, India.

December 2015

Certificate

This is to certify that the work reported in this Ph.D. thesis entitled **"Investigation towards applicability of polybenzimidazole (PBI) based polymeric ionic liquids (PILs) for gas permeation and fuel cells"** submitted by **Ms. Anita Rewar** to Academy of Scientific and Innovative Research (AcSIR) in the fulfillment of the requirements for the award of the Degree of **Doctor of Philosophy in Chemical Sciences**, embodies original research work under my supervision. I further certify that this work has not been submitted to any other University or Institution in part or full for the award of any degree or diploma. Research material obtained from other sources has been duly acknowledged in the thesis. Any text, illustration, table etc., used in the thesis from other sources, have been duly cited and acknowledged.

Research Guide

Dr. Ulhas Kharul

Research Co-guide

Dr. K. Sreekumar

Declaration by the Candidate

I declare that the thesis entitled "**Investigation towards applicability of polybenzimidazole (PBI) based polymeric ionic liquids (PILs) for gas permeation and fuel cells**" is my own work conducted under the supervision of **Dr. U. K. Kharul** at Polymer Science and Engineering Division and **Dr. K. Sreekumar** at Physical & Materials Chemistry Division, **CSIR-National Chemical Laboratory**, Pune, India. I further declare that to the best of my knowledge, this thesis does not contain any part of work, which has been submitted for the award of any degree either of this University or any other University without proper citation.

Anita Kumari Rewar

Research Student

Dedicated to my Parents

Acknowledgements

thanks my nephew Aryan and niece Pranjal whose presence in my life is always refreshing, making me feel relax and comfortable.

Finally, I am grateful to the God for my continuous source of inspiration and giving me a beautiful and healthy life.

Anita Rewar

Contents

Chapter 3.   Polymeric ionic liquids (PILs) possessing partial ionic liquid character: Gas permeation studies

Chapter 4. PILs possessing partial ionic liquid character: Effects of anion exchange on their physical and gas permeation properties

Chapter 5. Effect of amino acid as an anion on physical and gas sorption properties of PBI based Polymeric ionic liquids

Chapter 6. PIL–PBI blend membranes: Physical and electro-chemical evaluations towards their applicability as membranes for PEMFC and AEMFC

Chapter 7. New polymeric ionic liquids (PILs) as membrane materials for fuel cell (PEMFC and AEMF)

List of Schemes

List of Figures

List of Tables

Chapter 1

Introduction and Literature survey

This chapter describes the background and motivation of the present thesis, the context and the progressive development of the state of the art of polymeric ionic liquids (PILs) as new alternatives for CO_2 separation. A brief review of current green energy scenario (especially fuel cell) and use of PILs as proton and anion transport membranes for alternate energy production in fuel cell is presented.

1.1 The context

Change in climate and necessity to use renewable energy sources are two of the most critical challenges for the society [Jacobson (2009)]. The key problem associated with these is to control the CO_2 emission resulting due to burning of fossil fuels [Li (2012)]. Over the fifty years, CO_2 concentration in the atmosphere has increased from about 310 ppm in 1960 to over 390 ppm in 2010 [Liu (2012)]. The world population expected to increase to about 9.2 billion in 2050, which was 6.8 billion in 2010. Rationally, this expansion is projected to be accompanied by equivalent increase in energy consumption (from 15 TW to more than 40 TW) [Adewole (2013)]. Global temperatures are anticipated to rise between 1.4 and 5.8 °C by 2100 in the absence of climate change policies [Powell (2006)]. As a result, it is expected that the world will face more challenges of climate change associated problems, than it is facing presently. To address these issues, there can be two possible solutions; (i) development of methods which would effectively reduce CO_2 concentration in the atmosphere and (ii) development of new renewable energy sources that can minimize and then ultimately replace use of fossil fuel. Consequently, these are the central aspirations, which led to investigations of new membrane material design, synthesis and evaluations as given in this thesis. Polymeric ionic liquid (PIL) membranes were investigated with two applications in mind, viz., CO_2 separation and fuel cell [proton exchange membrane fuel cell (PEMFC) and anion exchange membrane fuel cell (AEMFC)]. Since ionic liquids (ILs) are prior art in these areas, a brief survey on them in included in the beginning of this chapter.

1.2 Ionic Liquids (ILs)

The first IL was discovered by Paul Walden in 1914. He had observed the special physical properties of ethylammonium nitrate [Walden (1914)], such as it is an odorless and colorless to slightly yellowish liquid with a melting point of 12 °C. Although, at that time ILs could not attract attention, they have acquired a substantial growth and interest over the last 20-25 years, as they have some specific properties. ILs have lower melting temperature because of the low intermolecular interactions, poor packing efficiency of their asymmetric ions and delocalization of their charges. Despite their broad definition as compounds, ILs consist of exceptional combination of some intrinsic properties such as negligible volatility [Earle (2000)], low flammability (with some rare exceptions) [Smiglak (2006)], thermal stability [Anderson (2007)], and high ion conductivity [Ohno (2004)]. However, most attractive feature is their tunability in anion and cation [Kohno (2012)]. According to the commonly accepted definition, an ionic liquid is a salt, in which, ions (organic cations and either organic or inorganic anions) are poorly coordinated, which results in their low melting point, usually, below 100 °C (or even at room temperature) and solvent like nature. They are thus termed as room temperature ionic liquids, RTILs [Plechkova (2008)]. This general definition has been used to differentiate ILs from traditional salts, which melt at very high temperatures (*e.g.* sodium chloride melts at 801 °C) [Tome (2014a)]; and from usual liquids that are non-ionic. Nowadays, there is considerable interest in the synthesis of ILs which incorporates functional groups introduced in either the cation or anion and their synthesis is targeted by a particular application. These types of ILs are called as "task-specific" ILs [Lee (2006), Green (2009)]. Some examples of specific application include metal ion extractants [Domanska (2009), Green (2009)], electroactivity [Buzzeo (2004), Green (2009)], use as catalytic materials [Mehnert (2005), Green (2009)] and CO_2 separation [Yang (2011)].

The most commonly found cations and anions for ILs are presented in Figure 1.1. It is possible to achieve specific properties in ILs by choosing the proper combination of a cation and an anion [Green (2009)]. These characters make them extremely unique and incomparable to other organic solvents. Most of the academic and industrial research activities related to ILs were associated with their applications in green chemistry [Mecerreyes (2011)]. ILs are attracting more interests towards CO_2 separation due to their high CO_2 sorption capacity [Xiong (2012), Zhijun (2012), Privalova (2012), Carlisle (2013a), Calleja (2013)].
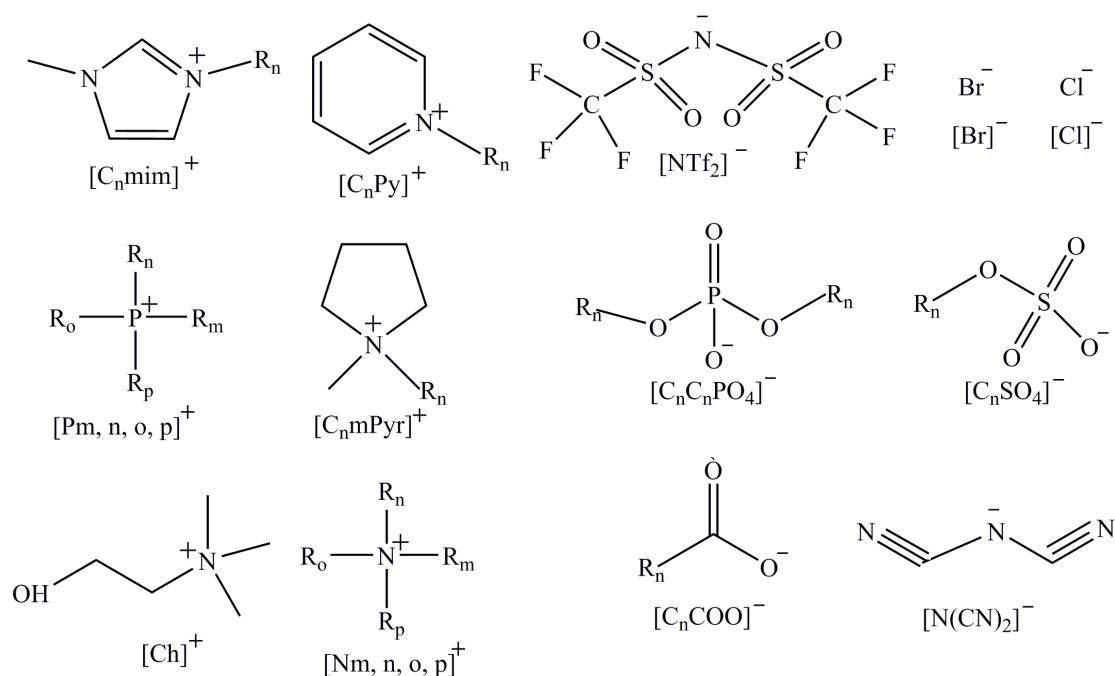
Figure 1.1 Cations and anions commonly used in ionic liquids.

ILs are widely investigated as membranes for CO_2 separation by making supported ionic liquid membrane (SILM) [Fernandez (2007), Neves (2010), Miquel (2011), Tome (2013a)]. A requirement of high membrane thickness ~150 μm for making SILMs [Bara (2009a)], their practical applicability possible only up to few atmospheres of differential pressure [Neves (2010), Cserjesi (2010), Albo (2012)] and issues with their long term stability [Bara (2009a)] are major hurdles towards their successful utilization. To conquer above issues, polymeric ionic liquids (PILs) are being explored as promising alternatives [Yuan (2013)]. PILs possess characteristics of ionic liquids and macromolecular architecture combined together; leads to a unique combination of properties such as high CO_2 sorption, faster CO_2 adsorption/desorption rates, good thermal stability and anticipated flexibility due to their polymeric nature [Mecerreyes (2011), Yuan (2013)]. A brief literature survey on PILs is given below.

1.3 Polymeric ionic liquids (PILs)

1.3.1 Basic introduction of PILs

Polymeric ionic liquids or poly(ionic liquid)s or polymerized ionic liquids (PILs), as referred in the literature, are polymeric in nature and represents a specific class of

polyelectrolytes, which has an IL species in its repeating units [Green (2009), Mecerreyes (2011), Yuan (2013), Mecerreyes (2015a), Mecerreyes (2015b)]. Basically, PIL's concept was proposed in the 1990s in pursuit of solid electrolytes that could potentially substitute ILs in electrochemical devices [Tominaga (1998), Hirao (2000), Ohno (2004)]. In PIL structure, individual IL species are covalently connected through a polymeric backbone to present a macromolecular architecture [Mecerreyes (2015a)], as presented in Figure 1.2. This structural configuration of PILs possesses characteristics of ionic liquids and macromolecular architecture combined together. This creates new properties that are not usually found in ILs. The physical properties of PILs and ILs are often close but not necessarily related to each other. PILs possess enhanced mechanical stability, dynamic chains, durability, improved process-ability and spatial controllability than that of the IL moieties. In the bulk state, ILs turn liquid below 100 °C or even at room temperature, while, except some PILs, most of them are solids, however, with a relatively lower glass transition temperature [Mecerreyes (2015a)]. PILs have been widely studied in last five years. The rapid progress in PIL chemistry has delivered many novel and versatile polyelectrolytes that are useful for fundamental research and also provide qualified materials to solve problems in many devices and systems [Mecerreyes (2015a)].
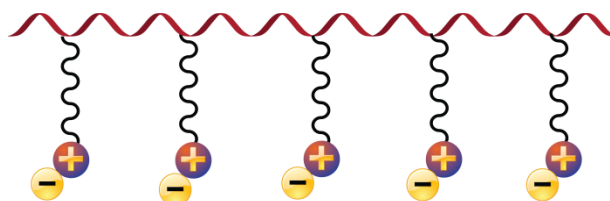
Figure 1.2 Basic structure of polymeric ionic liquid.

1.3.2   Structure and synthesis of PILs

PILs are a category of unique type of polyelectrolytes. The backbone of a PIL can be cationic or anionic. These cationic or anionic repeating units construct the polymer chain. There are two basic strategies for the synthesis of PIL [Yuan (2011), Mecerreyes (2015a)]:

(A) Direct polymerization of IL monomers,

(B) Chemical modification of existing polymers.

In each pathway, various polymerization techniques are involved, such as conventional and controlled free radical polymerization, step-growth polymerization, ring opening metathesis polymerization, *N*-quaternization and many more. From a synthetic perspective, each of these

strategies directs different structural parameters of PILs and exhibits their own distinct advantages as well as limits with respect to the PIL properties and molecular design [Ohno (2004), Ogihara (2006), Tang (2007), Tang (2009), Yuan (2011)]. These methods are briefly described below.

(A)   Direct polymerization of IL monomer

An IL monomer possesses the polymerizable functionality in its chemical structure. It provides the path to polymerize them into the PIL form. The common IL structures are illustrated in Figure 1.3. The classification is based on the relative position of the polymerizable unit in the IL monomer. The polymerizable functionality can be attached to the cation or anion, depending upon the desired polymer structure [Yuan (2011), Mecerreyes (2015a)]. Moreover, an IL monomer may copolymerize with other monomers to adjust the charge distribution pattern in the polymer chain and subsequently modify the physical and chemical properties of formed PILs. The property variations include solubility and aggregation behaviour in different solvents as well as, chemical, thermal and conductive properties.
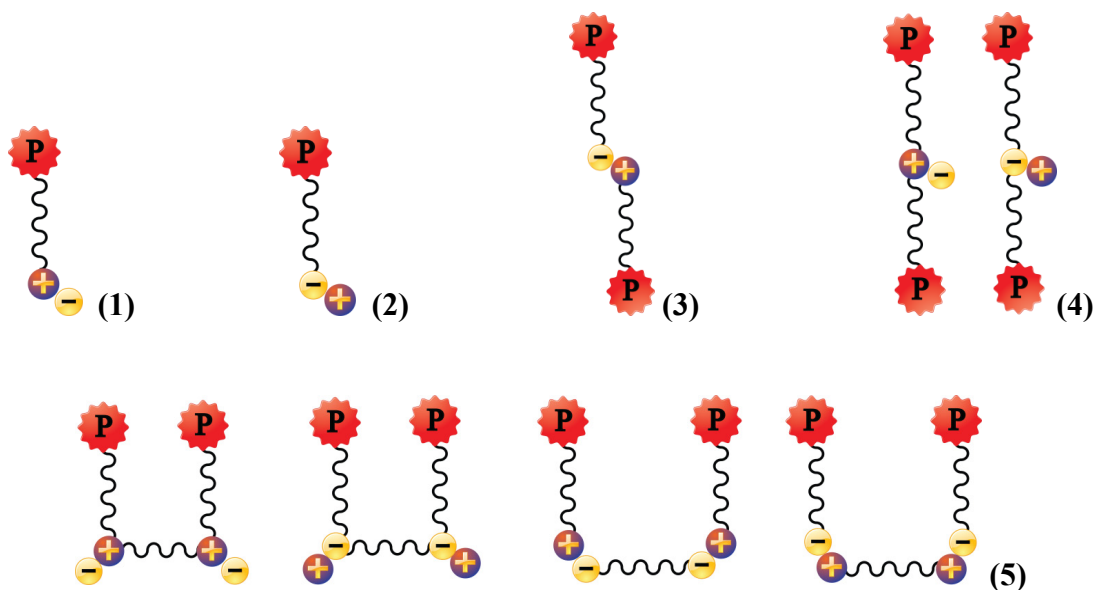
Figure 1.3 Basic structures of IL monomer, where "p" is a polymerizable unit.

Direct polymerization of ionic liquids monomer is grouped based on their polymerization process and monomer used, such as (a) Free radical polymerization, (b) Controlled/living radical polymerization, (c) Condensation polymerization, etc.

(B)   Chemical modification of existing polymers

 (i)   *N*-quaternization of polymers

PILs can also be synthesized by the *N*-quternization of previously synthesized polymers (e.g. polybenzimidazoles, polyimides etc.) [Kumbharkar (2014), Bhavsar (2014a), Bhavsar (2014b), Bhavsar (2014c), Shaplov (2015)]. These types of PILs have cation inside the backbone and are mechanically more stable and also have film forming ability, such as polybenzimidazole based PILs are stable even upto 20 atm.

(ii)   Anion exchange of previously synthesized PILs

PILs having organic or inorganic non-halide anions (BF_4^-, PF_6^-, $CF_3SO_3^-$, $(CF_3SO_2)_2N^-$, $(CF_3CF_2SO_2)_2N^-$, ClO_4^-) can be prepared by an anion exchange reaction with pre-synthesized PILs containing halide as anions [Marcilla (2004), Green (2009), Mecerreyes (2011), Yaun (2011), Bhavsar (2012), Yuan (2013)]. It has been well reported that the solubility characteristics of the PILs can be tuned by anion exchange of halide containing PILs by other anions [Mecerreyes (2015a)]. The various physical and chemical properties change with the anion of the PILs such as morphology, thermal properties, electrochemical properties, hydrophobic-hydrophilic characteristics, gas separation performances, etc., [Green (2009), Mecerreyes (2011), Yaun (2011, 2013)].

1.3.3   Physico-chemical properties of polymeric ionic liquids

1.3.3.1 Solution properties

The solution property of the PILs is one of the important properties in which the counter anion has very strong influence. For example, poly(1-vinyl-3-ethylimidazolium) having bromide anion is soluble in water as a conventional polyelectrolyte. When the bromide anion was exchanged with tetrafluroborate or hexafluraphosphate, the PILs become insoluble in water, but they develop solublity in methanol and polar solvents such as acetone, dimethylsulfoxide and dimethyl formamide. Similar behaviour has been observed with PILs having imidazolium, alkylammonium, pyridinium or guanidinium cationic backbones [Ito (2000), Marcilla (2004), Mecerreyes (2011)]. This conveys that influence of the anion is more in determining the solubility of PILs than that of the cation. Behaviour of PILs in the solution was expected to be similar as that of polyelectrolyte [Mecerreyes (2011)]. Due to repulsive electrostatic interaction

among ionic groups, the conventional polyelectrolyte shows unique viscoelastic behaviour in aqueous solution. Polyelectrolytes have remarkably different rheological properties than that of neutral polymers. The chains of polyelectrolytes are nearly rod-like and are located far apart from each other due to repulsive interactions. The polymer chains expand with the decrease in polymer concentration, known as the "polyelectrolyte effect" [Mecerreyes (2011)]. In the presence of salts or external electrolyte, the polyelectrolyte behaves like non-ionic polymer and there may not be chain expansion in the solution. PILs are also show the polyelectrolyte behaviour in polar organic solvents such as dimethylformamide or acetonitrile [Mecerreyes (2011)].

1.3.3.2 Solid state properties

In most of the cases, PILs are non-crystalline amorphous materials. This may be due to the mobile nature of the counter-anion, which makes crystallization processes difficult. As compared to polyelectrolytes, PILs are less hygroscopic and less fragile. This may be due to the important feature that the glass transition temperature (T_g) of PILs not only depends on the chemical composition of the polyelectrolyte backbone, but also on the type of the counter-anion [Vygodskii (2006), Hunley (2010), Mecerreyes (2011)]. It is important to know that some of the PILs present mesophase due to their self assembling behaviour [Mecerreyes (2011)]. One of the important applications of PILs is as ion conducting solid polymer electrolytes. Recently, Shaplov et al., have studied the factors affecting ionic conductivity of PILs [Shaplov (2010)]. The conductivity of PILs depends on the chemical nature of polymer backbone, nature of counter-ion, T_g, mesophase morphology, temperature and pressure. Although, there are several other external factors such as impurities, presence of water in the polymer, external humidity, measurement techniques and type of electrolytes, affecting the conductivity.

1.3.4   Applications of polymeric ionic liquids

The PILs have been used in a variety of applications such as new generation polyelectrolyte materials in energy devices (PEMFC, lithium ion batteries, dye sensitized solar cells, supercapacitors, field effect transistors, light-emitting electrochemical cells), biosensors, anion sensitive materials, electromagnetically active polymers, nanocomposites and many other applications are emerging [Green (2009), Mecerreyes (2011), Yaun (2011, 2013)]. PILs as CO_2 separation membrane materials also look promising due to their high CO_2 sorption, high

absorption-desorption rates and appreciable thermal stability [Green (2009), Mecerreyes (2011), Yaun (2011, 2013)]. The application of PILs in CO_2 separation and fuel cell (PEMC and AEMFC) is briefly described in following sections.

1.4 CO_2 separation

The climate change due to global warming and renewable energy source are two of the most important challenges for the world [Jacobson (2009), Mecerreceys (2015a), Mecerreceys (2015b)]. Continuous rising earth's temperature due to increasing emission of green house gases such as carbon dioxide (CO_2), nitrous oxide (NO), water vapour (H_2O), methane (CH_4) is of key concern. Among all the culprit gases, CO_2 has a major role. Consequently, it is very important to mitigate anthropogenic CO_2 emissions, which release from the burning of fossil fuels (a primary source of energy for the world). To mitigate this issue (reduction of the CO_2) there are numerous ways, such as replacing current fossil fuel-based energy by more environment friendly sources (renewable energy), higher efficiency processes for energy production and carbon capture and storage (CCS) [Tome (2014a)]. In this context, CCS is a strategy that provides a short-term solution to lesser climate change until renewable energy technologies become mature [Anderson (2004)].

Although there could be many technological solutions for CCS process [Handford (2014)], existing methods for CO_2 separation are highly energy intensive [Haszeldine (2009)] and new, cost-effective technologies need to be developed. Design of materials with the capability to effectively separate CO_2 from other sources is most significant, as the material cost and regeneration are the vital contributors in the total cost of the system [Kenarsari (2013)].

1.4.1 CO_2 separation technologies

Recently, numerous challenges are being faced in order to achieve improved processes and materials. However, improving the CO_2 separation efficiency of a material has huge potential for lowering the cost of CO_2 capture in near-term and represents one of the prime challenges [Alessandro (2010)]. There are three major CO_2 capture processes as shown in Figure 1.4. The CO_2 separation is required in numerous applications such as from the natural gas production, flue gas, water gas shift reaction, enhanced oil recovery and landfill gas upgradation,

etc. In each application, mixture of different gases is found, separation of which imposes distinct requirements and have their own limitations.
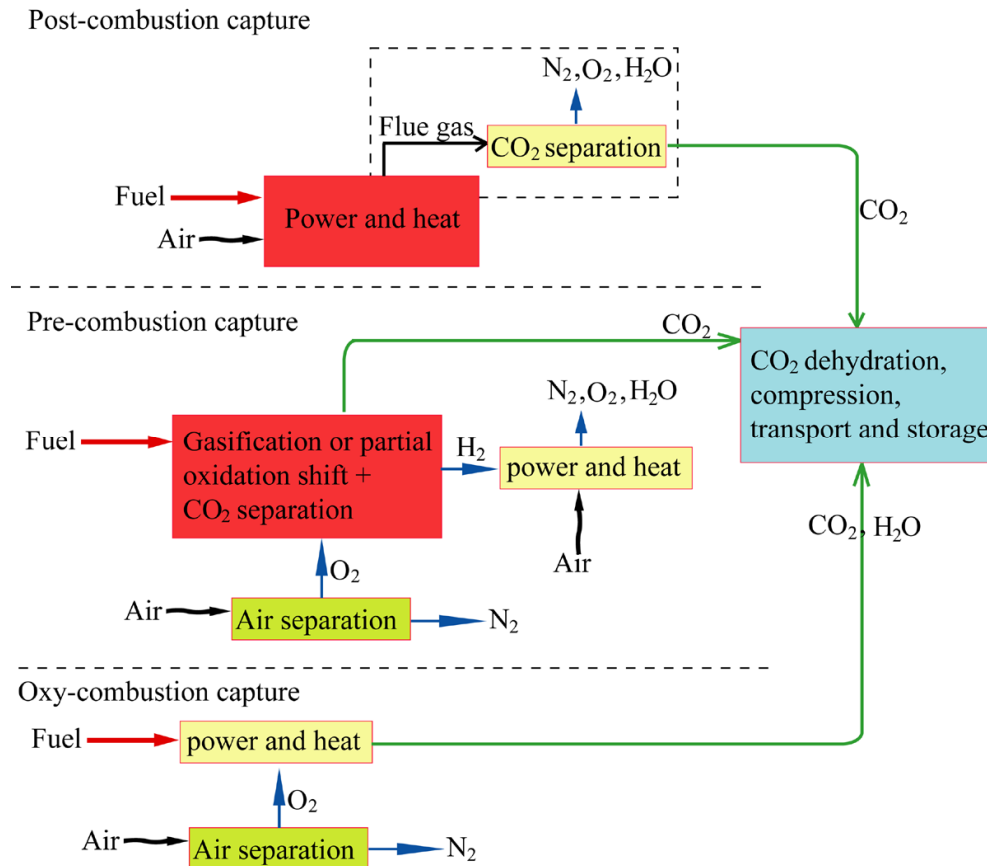
Figure 1.4 Schematic of post, pre and oxy combustion.

1.4.1.1 Absorption

The absorption process is of mainly two types, *viz.*, chemical and physical absorption. The operation of physical absorption is based on Henry's Law. CO_2 is absorbed under a low temperature and high pressure and desorbed at reduced pressure and increased temperature. This technology has been widely applied to many industrial processes including synthesis gas, nature gas and hydrogen production with high CO_2 contents [Olajire (2010), Yu (2012)]. Currently, the amine based sorption system is the most utilized technology for the CO_2 capture in industrial streams [Li (2012)]. When an amine is reacted with CO_2, it forms carbamic acid [Sanders (2013)], which is quite unstable and would decompose to the original amine and CO_2 at temperatures around >100 °C [Sanders (2013)]. Thus, amine can be regenerated, wherein CO_2 is

collected at higher temperatures. For chemical absorption, other inorganic solvents such as aqueous sodium and potassium carbonate and aqueous ammonia solutions have also been used [Alessandro (2010)]. For this process, although monoethanolamine is one of the favorite amines, other amines such as diethanolamine, methyl diethanolamine and triethanolamine have also been utilized [Sanders (2013)]. However, inspite of their high CO_2 solubility, amines are highly corrosive in nature and they have low thermal stability. This, reduce their reusability and make desorption process difficult on larger scale. These drawbacks along with high heat of dissolution with CO_2 make the amine scrubbing process highly energy intensive [Wang (2011, 2012), Sistla (2012)].

1.4.1.2 Adsorption

Adsorption can be of two types, *viz.*, physisorption (Van der Waals) and chemisorption (covalent bonding) [Alessandro (2010)]. Many materials have the ability to selectively adsorb CO_2 into small holes, pores and their external surfaces under specific pressure and temperature conditions [Aaron (2005)]. The two important methods for adsorption are pressure swing adsorption (PSA) and temperature swing adsorption (TSA). In both the cases, adsorption rate depends on partial pressures of CO_2, temperature, surface forces, available surface area of the sorbent and its pore size [Aaron (2005)]. Probable mechanisms of adsorptive separation includes: (i) the molecular sieving effect, which is based upon size/shape exclusion of certain components of a gas mixture, (ii) the thermodynamic equilibrium due to preferential adsorbate-surface or adsorbate packing interactions and (iii) the kinetic effect due to differences in the diffusion rates of different components of a gas mixture [Alessandro (2010)]. There are two major drawbacks that make adsorption unfavourable as an individual process. The system cannot easily handle large concentrations of CO_2 (usually between 0.04 % and 1.5 %), while most power plants have much higher concentrations of CO_2 in flue gases (~ 15 %). Secondly, available sorbents are not selective enough for the CO_2 separation from flue gases [Aaron (2005),].

1.4.1.3 Cryogenic distillation

This separation process is based on the difference in boiling point of gases in various gaseous mixtures. Cryogenic separation is used commercially for the CO_2 separation when high

CO_2 concentrations are typically more than 50% [Mondal (2012)]. The triple point and critical temperature of CO_2 is -56.8 and 31.6 °C, respectively. CO_2 can be liquefied by cooling and compression between these temperatures [Plasynski (2000), Bhavsar (2014c)]. The high energy consumption and cost is the major disadvantage of cryogenic method. Since the concentration of CO_2 in flue gas is around 15%, to compress the rest 85% gases, considerable amount of energy is required. Thus, the major drawback of cryogenic separation is that the technique is highly energy demanding for regeneration and can considerably decrease the overall power plant efficiency [Mondal (2012)]. Moreover, tendency for blockage of process equipment is quite high [Shimekit (2012)].

1.4.1.4 Membrane based separation

A membrane is a selective barrier that allows passage of certain constituents and retains other [Mulder (1996)]. Membrane technology exhibit several advantages over the above mention technologies for separation process. These include simplicity of installation and operation, smaller footprint and flexibility of operation due to compactness of modules, no extra agents are required (e.g. amines in absorption process). Continuous mode of operation is possible with complete or partial recycles of retentates/permeates. A possibility of incorporation with other separation process to achieve improved economy is possible in a hybrid process. It is possible to "tailor" the membranes material/process to achieve specific separation task [Sridhar (2015), Li (2005)]. As membrane process is a physical separation (no requirement of any chemical and solvent), they are environment friendly.

Membrane material can be metallic, polymeric or inorganic in nature. In most of the commercial applications, polymeric membranes are used. Although, there are number of advantages by using membranes for separation process and various polymeric materials have been investigated for commercial gas separation application, there is a need to develop new membrane materials in order to achieve high separation performance. This is especially required to address drawbacks such as temperature withstands ability of polymeric membranes and mitigate plasticization (that reduces selectivity). The major class of polymers which are employed for commercial gas separation membranes are cellulose acetate, poly(dimethylsiloxane), polyimides, polycarbonates, polysulfone and poly(phenylene oxide) [Bernardo (2009)]. A tradeoff can be found in the permeability-selectivity relationship, wherein

the membrane material which is more permeable is usually less selective and vice-versa [Aaron (2005), Bernardo (2009), Salleh (2011), Tome (2013)]. It is also known that polymeric materials are not suitable to use at harsh environmental conditions, e.g., those prone to corrosion and high temperatures [Salleh (2011)]. Plasticization of membrane material by CO_2, partial pressure and temperature is also known [Kapantaidakis (2003)]. This phenomenon adversely affects the gas separation [Bernardo (2013)]. Therefore, long term performance and stability of the membranes at high pressure and temperature are essential to maintain the robustness of the polymeric membrane based systems [Shao (2009)]. For achieving these, an understanding towards basic aspects of gas permeation in polymeric membranes is necessary.

1.4.2   Gas separation membranes: Theoretical considerations

Gas-transport mechanisms in polymeric membrane are generally Knudsen diffusion, molecular sieving and solution-diffusion [Koros (1993), Mulder (1996), Koros (2000), George (2001), Shao (2009)], as given schematically in Figure 1.5.
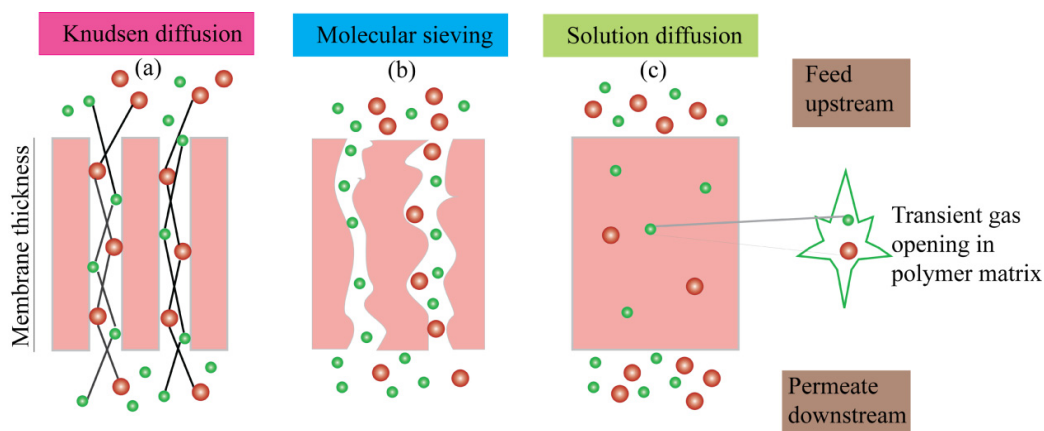
Figure 1.5 Mechanism of gas transport through the membrane, a) Knudson diffusion, b) molecular sieving and c) solution diffusion [Koros (1993)].

These transport mechanisms can be applicable based on the properties of gases and polymeric membrane material [Shao (2009)]. In porous membranes, the mechanism of gas separation is primarily governed by Knudsen diffusion and molecular sieving. In Knudson diffusion, flow is inversely proportional to the square root of the molecular mass of diffusing species [George (2001)]. This mechanism is applicable in mesoporous and macroporous membranes [Javaid (2005)]. According to molecular sieving mechanism, the diffusion rate is

higher for smaller gas molecule than that of larger gas molecule [Shao (2009)]. Nevertheless, the molecular-sieving mechanism may not be useful for the separation of similar-size penetrants (e.g. O_2 and N_2).

The solution-diffusion mechanism is largely applicable for gas transport through dense polymeric membranes [Shao (2009)]. According to this mechanism, solution equilibrium is supposed to be establishing between the upstream gas and the gas dissolved in the polymeric membrane. Subsequently, diffusion of the penetrant gas molecules in the polymeric membrane matrix [Stern (1994)] takes place. This mechanism mainly occurs in three steps:

(i) Sorption of the gas molecules (penetrants) at the upstream side of the membrane,

(ii) Activated diffusion of the penetrants gas molecules across the membrane matrix and

(iii) Desorption of the penetrants molecules at the downstream surface of the membrane [Shao (2009)].

The diffusion of gas molecules through the polymeric membrane could be expressed by Fick's first law [George (2001), Javaid (2005)], as explained below.

$$J = -D\left(\frac{dC}{dx}\right) \tag{1.1}$$

where, J is the flux of the gas through the polymeric membrane, D is the diffusion coefficient, and dC/dx is the concentration gradient of the penetrant gas across the membrane. At steady state, the flux is a constant. If D is assumed to be constant, Eq. (1.1) can be integrated as

$$J = D\left(\frac{C_0 - C_1}{l}\right) \tag{1.2}$$

where C_0 and C_1 are the concentration of the gas on the upstream and downstream sides, respectively, and *l* is the membrane thickness. At low pressures, Henry's law is expressed in the concentration of the gas in the membrane as,

$$C = S.p \tag{1.3}$$

where, S is the Henry's solubility constant and p is the gas pressure. By substituting Eq. (1.3) into Eq. (1.2) we get:

$$J = D.S \frac{(p_0 - p_1)}{l} = P \frac{(p_0 - p_1)}{l} \tag{1.4}$$

where, P is permeability of the gas and according to Eq. (1.4), it can be defined as:

$$P = D \cdot S \tag{1.5}$$

In the real systems, both the solubility coefficient (S) and the diffusion coefficient (D) can be the function of concentration. In gas separation with polymeric membranes, selectivity is defined as the ratio of the individual gas permeabilities. Based on single gas permeability of species "A" and "B", an ideal selectivity can be written as,

$$\alpha(A/B) = \frac{P_A}{P_B} = \frac{D_A . S_A}{D_B . S_B} \tag{1.6}$$

The selectivity is thus a function of differences in both, the diffusivity and solubility coefficients of the two gases [Javaid (2005)].

1.4.3   Membrane materials for gas separation

The membrane materials for gas separation have been selected based on their physical and chemical properties, as these membrane materials should be designed in an advanced way to separate specific gaseous mixture. Furthermore, these robust (i. e., stable) materials are required to be applied in the gas separation processes. As an overall perspective, gas separation properties of a polymeric membrane depend upon the material properties (permeability, separation factors), membrane structure and thickness, the membrane configuration (i. e., flat sheet membrane, hollow fiber) and the module design [Bernardo (2009)].

The inorganic and polymeric membranes can be designed to attain solubility based gas separations. These both type of materials having their own advantages and disadvantages. Present research focuses on design of the membrane that offers high flux with high selectivity [Javaid (2005)]. The aim of developing the carbon-based molecular sieves and inorganic membranes (e. g., silica, zeolites, etc) are mainly because they can withstand high temperature as well as chemicals. However, these materials have disadvantages such as high cost, brittleness, modest reproducibility, low membrane area to module volume ratio, low permeability with the membranes that has high selectivity (e. g., metal oxides at temperatures below 400 °C) and difficult sealing at high temperatures [Bernardo (2009)]. Polymeric membranes are attracting great interest in the area of gas separation [Javaid (2005)]. Polymers are available in a wide

range, which can be used for a particular application. The flux performance increases with decreasing thickness of the membranes. Therefore, they are cast on the support to form integrally skinned top layer. Phase separation process is used for achieving the integrally skinned membranes. The polymer which provides the combination of high permeability and selectivity are most desirable.

Polymeric membranes used for gas separation are divided into two types, glassy and rubbery in nature. Glassy membranes are commonly operated below their glass transition temperatures and are rigid (glass like) in nature. While, rubbery polymeric membranes are used above their glass transition temperatures and are flexible, soft in nature. In general, rubbery polymers are more permeable but less selective; while glassy polymers are less permeable but have high selectivity. Glassy polymers encompass more shares in the industrial separations because of their high selectivity and good mechanical properties [Shekhawat (2006)].

1.4.3.1 Gas transport in rubbery polymers

The segmental mobility of the rubbery polymers is the most important property; consequently, molecules can diffuse easily [George (2001)]. At low gas pressures, sorption in rubbery polymer is linear with the pressure axis, which can be described by Henry's law [Barbari (1994)], as given below;

$$C = k_D \cdot P \qquad (1.7)$$

where, C is the concentration of gas in the polymer, k_D is a Henry's law constant and P is the gas pressure. The units normally used for C and P in the literature are $cm^3(STP)/cm^3$ of the polymer and atm, respectively. In the presence of highly active gases and vapors, the deviation from the Henry's law is observed in rubbery polymers. The k_D (Henry's law constant) can be related to the Lennard-Jone's force constant, which determines the value of condensation of the gas [Michaels (1961)]. As an alternative, boiling point or critical point can also be used as a correlating parameter. Diffusion coefficient for gas in rubbery polymer may be described by eq. given below [Barrer (1939), Stern (1980)],

$$D = D_0 . \exp(-E/RT) \qquad (1.8)$$

D_0 is the pre-exponential factors, E is activation energy, R is gas constant and T is temperature. The activation energy (E) is an energy that must be concentrated in the polymer adjacent to diffusing molecule, on order to open a passage of enough free volume to allow the penetrant to

execute a diffusional jump. The concept of "free-volume" or "empty" volume used to describe the transport of gases and liquids in polymers is well reviewed [Shao (2009)].

1.4.3.2 Gas transport in glassy polymers

The restricted chain mobility is the characteristic of glassy polymers [George (2001)]. Therefore, the mechanism of gaseous diffusion in glassy polymer is more complex as compared to rubbery polymers. The structure of glassy polymeric membranes is composed of two components: matrix phase and microvoids (called as frozen free volume or free volume holes), which is distributed in the matrix phase. In glassy polymer, transport properties, viz., sorption (S), diffusion (D) and permeability coefficient (P) of gases are described by solution-diffusion mechanism. Different type and levels of interactions between the penetrant and membrane affect the gas transport [Tsujita (2003)]. A number of models have been proposed to explain the transport mechanism in glassy polymer and the parameters D, S and P [Stern (1994)]. The most precise and widely used model to explain the gas sorption in glassy polymers at low to moderate pressure is the 'dual mode sorption model' [Barbari (1994)]. According to this model, there are two distinct populations of penetrant molecules to stay within the glassy polymers. The one, in which, penetrant molecules are sorbed by normal dissolution mechanism (dissolved or Henry's law population) and another, in which penetrant molecules exists in pre-existing gaps that are frozen into the glassy polymer (the hole or Langmuir population) [Barbari (1994)]. This is shown in Figure 1.6 [Tsujita (2003)].
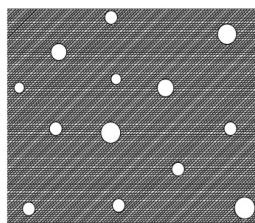
Figure 1.6 Schematic representation of polymeric glassy state depicting the matrix and the microvoids [Tsujita (2003)].

In the polymer matrix, equilibrium exists between penetrant molecules in Henry and Langmuir sites. The dual-mode sorption is normally described by the sum of two contributions as follows (Figure 1.7) [Tsujita (2003)]:
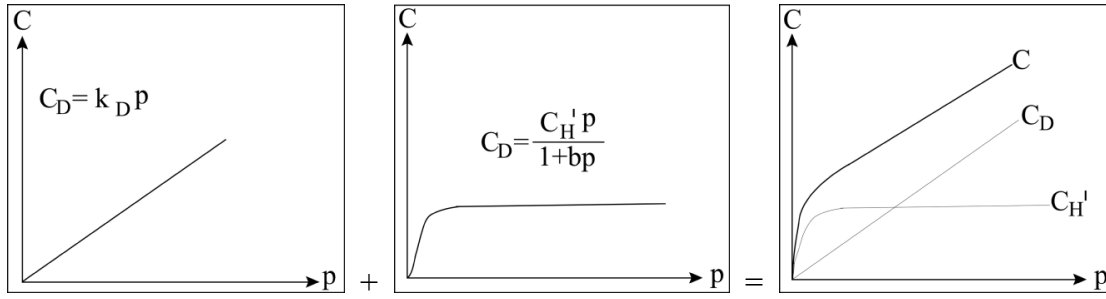
Figure 1.7 Schematic representation of dual-mode sorption, Henry sorption and Langmuir sorption [Tsujita (2003)].

$$C = C_D + C_H = k_D.P \frac{C'_H.b.p}{(1 + b.p)} \tag{1.9}$$

where, C is the total sorption amount in glassy polymeric membrane, C_D is Henry mode sorption, C_H is Langmuir sorption amount, p is applied gas pressure, k_D is Henry's solubility coefficient, C'_H is Langmuir saturation constant and b is Langmuir affinity constant.

The dual-mode sorption equation (1.9) gives a linear relationship with pressure in the high pressure region [Tsujita (2003)]. The linear slope communicates to the Henry's solubility coefficient in the high pressure region while, the intercept of the extrapolated line to the C axis is the Langmuir saturation constant (Figure 1.7). The dual mode sorption parameters k_D, C'_H, and b can be obtain by curve fitting using a nonlinear least squares method by using gas sorption isotherm observed experimentally. The C'_H is correlated to the unrelaxed volume (eq. 1.9), which quantitatively provides the value of the deviation from equilibrium in the glassy state, i.e. the difference between the specific volume of glassy state and liquid states ($V_g - V_l$).

$$C'_H = \left(\frac{V_g - V_l}{V_g} \right) \frac{22400}{V_p} \tag{1.10}$$

where, V_p is the molar volume of sorbant gas estimated from the sorption isotherm. If the sorbed gas is polar in nature and condensable, the gas sorption may exhibit an anomalous isotherm. For example, some glassy polymers are plasticized to rubbery state by CO_2 in their matrix owing to their interactions [Wang (1996)]. Therefore, a linear relationship in the high pressure range does not arise over a wide pressure range, due to the effects of plasticization at high pressure by sorbent gas.

Most frequently used glassy polymeric membranes for gas separation are cellulose acetate (CA), polysulfone (PSF), polyimide (PI), while; polydimethylsiloxane (PDMS) is the commonly used rubbery polymers for vapor separation. These polymers exhibit their own advantages and disadvantages. For CO_2 separation in particular, these include low selectivity, plasticization and inability to withstand high temperatures of flue gas. Consequently, the current goal of the research in this area is to develop new membrane materials with high CO_2 sorption capacity, which ultimately would lead to high selectivity over the other gases. This would eventually improve the gas separation performance and reduce the cost of overall process.

1.4.4 ILs for CO_2 separation

Recently, ionic liquids (ILs) as the new class of materials are proposed, since they have remarkably high CO_2 solubility as well as CO_2 based selectivity over the other gases. One can tune their physical and chemical properties by using CO_2 specific cations and anions or by adding functional groups. Large efforts have been put on the theoretical understanding and experimental determination of gas solubility in ILs [Hu (2011), Shannon (2012), Sistla (201]. It has been proved that the anion of ILs has more effect on CO_2 solubility than that of cation [Cadena (2004), Anthony (2005), Anderson (2007), Muldon (2007)]. The effect on CO_2 sorption by different functional groups such as alkyl, hydroxyl, ether, amine, fluorine and nitrile has also been investigated [Bates (2002), Camper (2006), Carlisle (2008), Smith (2008), Almantariotis (2010)]. A huge amount of literature on ILs for CO_2 separation has been reported. A range of functional group have been employed in ILs which is specifically designed for CO_2 separation such as acetate [Gurau (2011), Wang (2012), Wu (2012)] amino acids [Goodrich (2010, 2011)], imidazole and pyrrolide [Wang (2010)].

Utilization of ILs in membrane configuration by making supported ionic liquid membranes (SILMs) is widely attempted [Fernandez (2007), Neves (2010), Miquel (2011), Tome (2013)]. A variety of ILs have been studied to develop SILMs for CO_2 separation [Scovazzo (2004), Baltus (2005), Morgan (2005), Cserjesi (2009), Neves (2009), Scovazzo (2009), Zhao (2010), Neves (2010), Jindaratsamee (2012)]. It is noteworthy that some of the SILMs have good CO_2 separation performance with permeability/selectivity that is close to "Robeson upper bound" [Robeson (2008)], an empirical representation of permeation properties. Although, SILMs have good separation performance, they require high membrane thickness of ~

150 mm for effective making SILMs [Bara (2009)]. Their practical applicability is possible only up to few atmospheres of differential pressure [Neves (2010), Cserjesi (2010), Albo (2012)] and issues with their long term stability [Bara (2009)] are major hurdles towards successful utilization of SILMs. To conquer such issues, PILs are being explored as promising alternatives [Yuan (2013)].

1.4.5 PILs for CO_2 separation

PILs possess characteristics of ionic liquids and macromolecular architecture combined together; leading to a unique combination of properties such as high CO_2 sorption, faster CO_2 adsorption/desorption rates, good thermal stability and anticipated flexibility due to their polymeric nature [Mecerreeyes (2011), Yuan (2013)]. A range of PILs have been studied to investigate CO_2 sorption [Tang (2005a), Tang (2005b), Tang (2005c), Tang (2009), Xiong (2012), Bhavsar (2012), Wilke (2012), Fang (2013), Bhavsar (2014c), Shaligram (2015)]. The first PIL was reported in 2005 by Radosz et. al., which was based on imidazolium cation and tetrafluoroborate (BF_4) and hexafluorophosphate (PF_6) as anions. They showed higher CO_2 absorption capacity and faster absorption/desorption rates than that of corresponding ILs [Tang (2005a), Tang (2005b)]. It was reported that ammonium based PILs have more CO_2 sorption capacity than that of imidazoilum based PILs [Tang (2005c)]. Later on, effects of anions on governing the CO_2 sorption properties were reported by various groups [Bhavsar (2012), Miquel (2013)]. PILs are recognized as the potential materials for CO_2 separation, especially with CO_2/CH_4 and CO_2/N_2 gas pairs [Camper (2006), Bara (2007), Bara (2008a), Bara (2008b)]. Although PILs make stable film, their key problem is considerable decline in permeability and diffusivity with time [Mecerreyes (2015)] and more significantly, inability to form a stable film [Tang (2005a), Hu (2006)]. To conquer these, different strategies have been employed to design robust PIL-based membrane, which would exhibit good CO_2 separation performance, in particular natural gas purification (CO_2/CH_4) and flue gas separation (CO_2/N_2). Four different membrane arrangements proposed are described below [Mecerreyes (2015)].

(i) Pure PIL membranes exhibiting different functional groups into their polycation,

(ii) Synthesis of copolymers of PIL to control chain packing and segmental motion for increasing the mechanical stability and gas permeability of the membranes,

(iii) Blending of PILs with free ILs to form homogeneous composite membranes and

(iv) Preparation of mixed matrix membranes by the incorporation of zeolites into PILs.

1.4.5.1 Neat PIL membranes

Camper et al. [2006] have proposed PILs as the gas separation membrane materials for the first time [Camper (2006)]. Authors studied the immobilized IL membranes for gas permeation study and postulated that membrane preparation by the polymerization of these IL monomers would be promising for CO_2 separations. Then the first pure or neat PIL membrane for CO_2 separation was prepared by Bara et al. [Bara (2007)]. They studied the effect of chemical structure and alkyl substituent chain length of PILs on gas permeability. They found that the polymer backbone had a little effect on the gas permeation properties of the membranes, while both the permeability and the CO_2 permselectivity of all gases were largely dependent of the alkyl chain length attached to the imidazolium polycation [Bara (2007)]. In order to improve the CO_2 permeation of PIL membranes, Nobel et al., have synthesized functionalized imidazolium-based PILs containing polar groups, namely, oligo(ethylene glycol) and alkylterminated nitrile [Bara (2008c)]. The introduction of pendant nitrile groups decreased the permeability of CO_2, while the PILs combining oligo(ethylene glycol) units had the CO_2 permeability similar to their alkyl analogues [Bara (2008c)]. These PILs have not increased the permeability of CO_2 but the permselectivity (CO_2/N_2 and CO_2/CH_4) was improved significantly. By the incorporation of multifunctional styrene IL monomers, cross-linked PIL membranes with different spacer groups were also synthesized [Bara (2008c)]. Although these cross-linked PIL membranes had almost similar permeselectivity to previous ones for CO_2/N_2 and CO_2/CH_4, CO_2 permeability was decreased. Therefore this approach seems to be less successful. Polystyrene and polyacrylate backbone-based PILs and several other PILs with functionalized imidazolium cations bound to a polyethylene backbone have also been evaluated [Carlisle (2013)]. These results demonstrated that the difference of CO_2 permeability in different PILs is because of diffusivity [Carlisle (2013)]. PIL with disiloxane-functionalized vinylimidazolium cation showed high CO_2 permeability (130 Barrer), although it was less selective ($CO_2/N_2 = 14$, $CO_2/CH_4 = 8.7$) [Carlisle (2013)]. On the other hand, PILs containing fluoroalkyl substituents contributed only to a little increase in the CO_2/CH_4 permselectivity, without changing the CO_2 permeability. Li et al. [2012] have synthesized three PILs with alkyl-functionalized vinylimidazolium-based using dicyanamide (DCA) as counter-anion. They found the same results as Bara et. al., have observed

previously for styrene and acrylate backbone based PILs. It was reported that with increasing the chain length from ethyl to hexyl, CO_2 permeability increased but the CO_2/N_2 permselectivity of the membranes was reduced [Li (2012)]. Noble and group have also developed PILs in which cationic part is situated in the main chain backbone [Carlisle (2010)]. Recently, Tome et al. [2013] have proposed the pyrrolidinium cation and the Tf_2N anion containing PILs for CO_2 separation [Tome (2013)]. It was observed that the permeability and permselectivity of these type of membranes was in the same order as found with imidazolium based PILs with Tf_2N containing anion.

1.4.5.2 PIL copolymer membranes

PIL copolymers are attracting great interest [Mecerreyes (2011), Yuan (2013)]. The synthesis of copolymer is one of the important pathways to prepare CO_2 specific PILs [Hu (2006), Li (2010), Chi (2013), Kammakakam (2013), Nguyen (2013)]. The first PIL copolymers were evaluated for CO_2 separation by Radosz and cowerkers [Hu (2006)]. The main objective was to prepare less brittle PIL membranes by the grafting of poly(ethylene glycol) PEG onto glassy ammonium-based PILs [Hu (2006)]. The formed copolymer membranes were found to be mechanically and chemical stable, with the CO_2 permeability of 40 Barrer and CO_2/N_2 permselectivity of 70 [Hu (2006)]. Recently, Li and Coleman have synthesized random block copolyimides having diamino functional IL monomeric units and the formed membranes were freestanding. In these copolyimides, the incorporated IL monomeric units reduced the gas permeability (solubility as well as diffusivity) with the small increase in CO_2/CH_4 selectivity as compared to that of pure block copolyimide [Li (2010)]. Furthermore, Chi et al. have synthesized graft copolymers based on poly(vinyl chloride) (PVC) main backbone and imidazolium based PIL as a side chain via atom transfer radical polymerization [Chi (2013)]. The resulting membranes showed increased CO_2 permeability with a small decrease in CO_2/N_2 permselectivity. Noble's group has synthesized a series of new type of phase-separated block copolymers by combining an imidazolium-based PIL and an alkyl non-ionic polymer [Nguyen (2013)]. In order to increase the flexibility in the polymer chain and to increase their permeability and selectivity, Tome and group explored use of PILs with mixtures of counteranions [Tome (2013)]. They have synthesized a new PIL copolymer family having pyrrolidinium cation unit with different counter anion mixture by the quantitative anion

exchange method. Pyrrolidinium random copymer and [C4pyr][Nf$_2$T] composite membranes have been prepared as neat copolymer membranes, which were brittle in nature. Good combination of CO$_2$ permeability and selectivity was observed. The chain interaction and packing in polymer depended on the structure of counter-anion [Tome (2013)]. This study has demonstrated that the gas permeation of pyrrolidium based PILs can be increased by the changing counter-anion mixture in the polymer matrix.

1.4.5.3 PIL-IL composite membranes

The main reason of decreasing the gas transport through PIL membranes as compared to SILMs is due to decrease in permeability through the solid polymer matrix. By making PIL-IL blends, it was expected to have high CO$_2$ permeable membranes, while simultaneously maintaining their mechanical stability and permeation characteristics. ILs in PILs are different than that of plasticizers in conventional polymers, not only because of their negligible volatility but also they have the ability to strongly interact with the charged backbone of the PIL through electrostatic interactions. Bara et al. [2008d] prepared stable PIL-IL composite membranes via polymerization of an IL monomer in the presence of a non-polymerizable IL (also called "free IL"). By incorporation of this free IL in the PIL, the CO$_2$ permeability of resulting composite membrane is increased by 4 times with the slight reduction in permselectivity (CO$_2$/N$_2$ and CO$_2$/CH$_4$) than that of neat PIL membrane. In second strategy, Bara and group had tried the composite membranes with the different anion of the free IL. They blended PIL and 20 wt% of imidazolium based free IL, possessing four different anions. The PIL-IL membrane containing 20 wt% of free [C$_2$mim][Nf$_2$T] exhibited CO$_2$ permeability of 60 Barrer; while membranes with IL possessing other anions possessed CO$_2$ permeability of 41 to 43 Barrer. This could be because of the larger molar volume of IL with Nf$_2$T anion, which allowed the faster gas diffusion in the resulting composite membrane [Bara (2008a)]. Imidazolium-based ILs functionalized with alkyl, fluoroalkyl, ether, nitrile, and siloxane groups were incorporated into PIL [Bara (2009b)]. It was observed that all PIL-IL composites have almost similar CO$_2$ permeability and permselectivity over N$_2$ and CH$_4$. Tome and group studied the gas separation behavior of the whole material range from neat PIL to pure IL, encompassing the PIL-IL composites [Tome (2013)]. For this study, they have chosen P[DADMA][Nf$_2$T] with different amounts of free [C$_4$pyr][Nf$_2$T] (0, 20, 40, 60, 80, and 100 wt%). They found increased permeability and

diffusivity of CO_2, N_2, and CH_4 as compared to neat P[DADMA][Nf_2T]. Enhancement of polymer chain mobility and consequently a lower resistance to gas diffusion created by the free ion pairs was said to be the reason for this. They found that CO_2/N_2 is a more favorable separation than that of CO_2/CH_4. To prepare the PIL-IL composite membranes, Carlisle et al. [2012] have prepared a series of membranes by photopolymerization of oligo(ethylene glycol)-functionalized cross-linking and non-cross-linking vinylimidazolium IL monomers in the presence of free IL, viz., [C_2mim][Nf_2T]. They have investigated the effect of the cross-linker content as well as the free IL loading on the CO_2 separation performance. An increase in CO_2 permeability was observed at the three concentrations (45, 65, 75 wt%) of IL loading, while the CO_2/N_2 and CO_2/CH_4 permselectivity was almost similar with increasing IL loading in composite membranes [Carlisle (2012)]. They concluded that the gas diffusivity through the membranes can be increased by decreasing the cross-linker concentration [Carlisle (2012)]. These PIL-IL composite studies showed that via the addition of IL in the PIL, CO_2 permeability of PIL based membranes can be increased with little sacrifice in permselectivity [Mecerreyes (2015)]. It was also observed that properties of free IL also affect the CO_2 separation performance of the resulting composite membranes. Accordingly, both, the choice of free IL and PIL are crucial to improve the performance of the resulting blend membranes.

1.4.5.4 PIL-IL-Zeolite mixed matrix membranes

A new class of membrane materials containing organic and inorganic component together is called as mixed matrix membranes (MMMs). MMMs have been identified as a potential solution to come over the trade-off issues in polymeric membranes [Nobel (2011)]. MMMs are fabrication of an inorganic solid (dispersed phase) into a continuous polymer matrix. Theoretically, these composite membranes can present ease in processing polymeric material with enhanced CO_2 permeability offering high separation performance [Dong (2013)]. Recently, MMMs comprising PIL, IL and free inorganic partials are reported to improve CO_2 separation performance [Hudiono (2010, 2011), Hao (2013)]. The first PIL-IL containing MMMs membranes was prepared by Hudiono et al in 2010, by using zeolite SAPO-34 as inorganic filler [Hudiono (2010)]. This study proved that IL component in MMMs is enhancing the CO_2 permeability. It also improved the adhesion at the interface of PIL and zeolite [Hudiono (2010)]. The MMM membranes were able to increase the CO_2 permeability as well as permselectivity

than that of neat PIL membrane, but the performance was still below the Robson upper limit [Hudiono (2010)]. The same group has studied the MMMs by varying the free IL and SAPO-34 in the membranes and found that the gas separation performance can be tuned by varying the loading of zeolite and free IL [Hudiono (2011)]. Hao et al. [2013], have prepared MMMs of PIL-IL-ZIF-8 and found that with increasing amount of ZIF-8 in presence of free IL, gas permeation increased and gas selectivities decreased slightly [Hao (2013)].

Although, significant research has been attempted for a complete understanding of the relationship between molecular compositions, macromolecular structure and gas permeation properties, the challenges regarding PIL-membrane permeability and stability at elevated pressure and temperature remain unresolved.

1.5 Fuel cell

In recent days, world's energy consumption is dependant mainly on the combustion of fossil fuels and this has adverse futuristic impact on world's economics and ecology. Consequently, electrochemical energy is under serious consideration as an alternative power source. These electrochemical systems include batteries, electrochemical capacitors (ECs) and fuel cells [Winter (2004)]. These three systems have different energy storage and conversion mechanism, but still have some common features. They consist of two electrodes in contact with an electrolyte [Winter (2004)]. A fuel cell is an electrochemical "device" that continuously converts chemical energy into electric energy (and some heat) for as long as fuel and oxidant are supplied [Hoogers (2003)].

1.5.1 General design and features

This chemical reaction takes place at electrodes, anode and cathode. Every fuel cell has an electrolyte which transfers ion from anode to cathode or vice-versa. When hydrogen is used as fuel, it generates energy, heat and water. Thus, it is a so-called, *zero emission engine* [Hoogers (2003)]. Fuel cell operates by simple combustion reaction as given below.

$$2H_2 + O_2 \longleftrightarrow H_2O \tag{1.11}$$

Fuel cells have similarity with batteries, as they have similar electrochemical procedure for the power generation. Unlike batteries, fuel cell does not need to recharge, it operates quietly, efficiently and continuously.

Fuel cells have ability to get commercialized as they can fulfil the global power needs. They have high efficiency without environmental loss. There are various advantages and challenges of using fuel cell such as; fuel cells have the potential for a high operating efficiency, pollution free technique, various ways to supply fuel (different type of fuel), low maintenance (as there are no moving parts) and they produce regular energy as long as fuel is provided. Some of the limitations of fuel cells include high cost, expensive fuel reformation technology gradual decrease in performance, catalyst degradation and electrolyte poisoning.

1.5.2   Main applications

The fuel cell was used for the first time in Gemini and Apollo programs for electricity and drinking water generation [Hoogers (2003)]. Now a days, extensive research has been going on to improve the fuel cell efficiency and application. Fuel cells are used mainly projected to be used for three applications, transportation, portable and stationary applications.

1.5.3   Types of fuel cell

Fuel cells are classified based on the kind of electrolyte they employ. This classification also define the electro-chemical reaction that occurs in the cell, the type of catalyst, operational temperature, type of fuel which they use other associated factors. There are five major types of fuel cells that have been demonstrated, as shown in following Table 1.1. Each one has its own advantages, disadvantages and potential applications [Ramani (2006)].

Table 1.1 Classification of fuel cells.

Fuel cell type	Electrolyte used	Operating temperature (°C)	Electrode reaction
Polymer electrolyte	Polymer membrane	60-140	Anode: $H_2 = 2H^+ + 2e^-$ Cathode: $1/2\ O_2 + 2H^+ + 2e^- = H_2O$
Direct methanol	Polymer membrane	30-80	Anode: $CH_3OH + H_2O = CO_2 + 6H^+ + 6e^-$ Cathode: $3/2\ O_2 + 6H^+ + 6e^- = 3H_2O$
Alkaline	Potassium hydroxide	150-200	Anode: $H_2 + 2OH^- = H_2O + 2e^-$ Cathode: $1/2\ O_2 + H_2O + 2e^- = 2OH^-$
Phosphoric acid	Phosphoric acid	180-200	Anode: $H_2 = 2H^+ + 2e^-$ Cathode: $1/2\ O_2 + 2H^+ + 2e^- = H_2O$
Molten carbonate	Lithium/potassium carbonate	650	Anode: $H_2 + CO_3^{2-} = H_2O + CO_2 + 2e^-$ Cathode: $1/2\ O_2 + 2H^+ + 2e^- = H_2O$
Solid oxide	Yittria stablized zirconia	1000	Anode: $H_2 + O^{2-} = H_2O + 2e^-$ Cathode: $1/2\ O_2 + 2e^- = O^{2-}$

1.5.4   Proton exchange membrane fuel cell (PEMFC)

PEMFC is made up of one anode (the electrode where hydrogen oxidizes), one cathode (the electrode where oxygen reduces) and a solid proton conducting polymeric membrane, normally known as 'polymer electrolyte membrane' or 'proton exchange membrane' which acts as a solid electrolyte. It is the heart of fuel cell that acts as a proton conductor, barrier to prevent the fuel cross over and a mechanical separator between anode and cathode. The membrane is sandwiched between two electrodes (consisting of catalyst layers, containing platinum deposited on carbon), is typically of ~ 50 µm thick. The formed sandwich is called as membrane electrode assembly (MEA).

1.5.4.1 Working principle of fuel cell

Hydrogen is oxidized on the anode and oxygen is reduced on the cathode. Protons are transported from the anode to the cathode through the electrolyte membrane and electrons are carried to the cathode over the external circuit and generate electricity. On the cathode side, hydrogen ions meet with the oxygen and electrons to form water and heat (Figure 1.8). Typically the fuel cell working potential ranges from 0.6-0.8 V, and produce the current density (current per active area) of 0.2-1 A/cm^2.
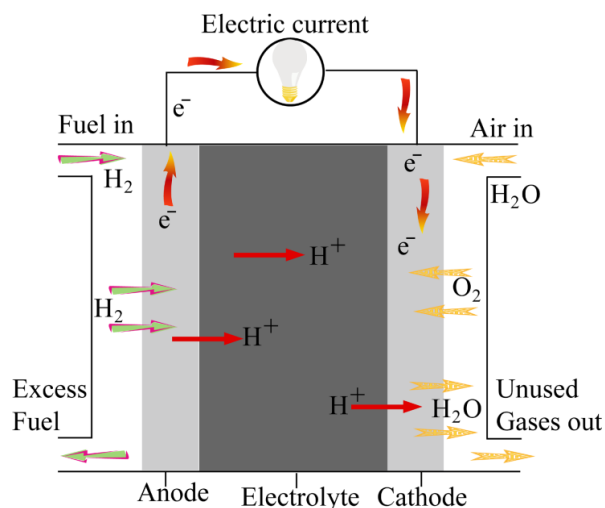
Figure 1.8 Schematic and key feature of proton exchange membrane fuel cell.

During the conversion of chemical energy of into electrical energy, heat and water are also produced in the catalyst layers that have a thickness of ~ 5-30 µm. Reactions taking place in fuel cell are:

Anode: H_2 (g) $\longrightarrow$ $2H^+$ (aq) + $2e^-$ (1.12)

Cathode: $1/2$ O_2 (g) + $2H^+$ (aq) + $2e^-$ $\longrightarrow$ H_2O (1.13)

Overall: H_2 (g) + $1/2$ O_2 (g) $\longrightarrow$ H_2O + electrical energy + waste heat (1.14)
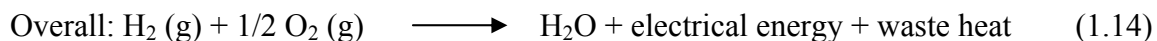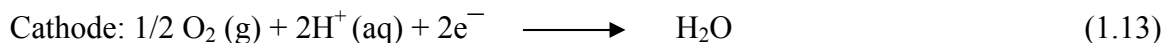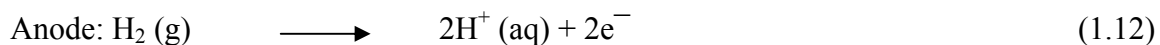
Various reactants are transported by the diffusion and convection to the catalyzed electrode surface, where electrochemical reactions take place.

In most of the applications, many cells are connected in series to make a fuel cell stack. These repeating cells are separated by flow field plates. Typically, a PEM fuel cell stack is constructed of bipolar plates, membrane electrode assemblies (MEA) and end plates. The bipolar plates are made up of graphite or metal and they serve to distribute gases through the flow channel as well as transfer electrons to the load. The flow channels pass reactants to enter into the MEA. The MEA has a thickness of around 500-600 μm and consist of five layers: the proton exchange membrane, the anode as well as cathode catalyst layers and the anode as well as cathode gas diffusion layers. The main functions of different components are given in Table 1.2 and the schematic of fuel cell is given in Figure 1.9.
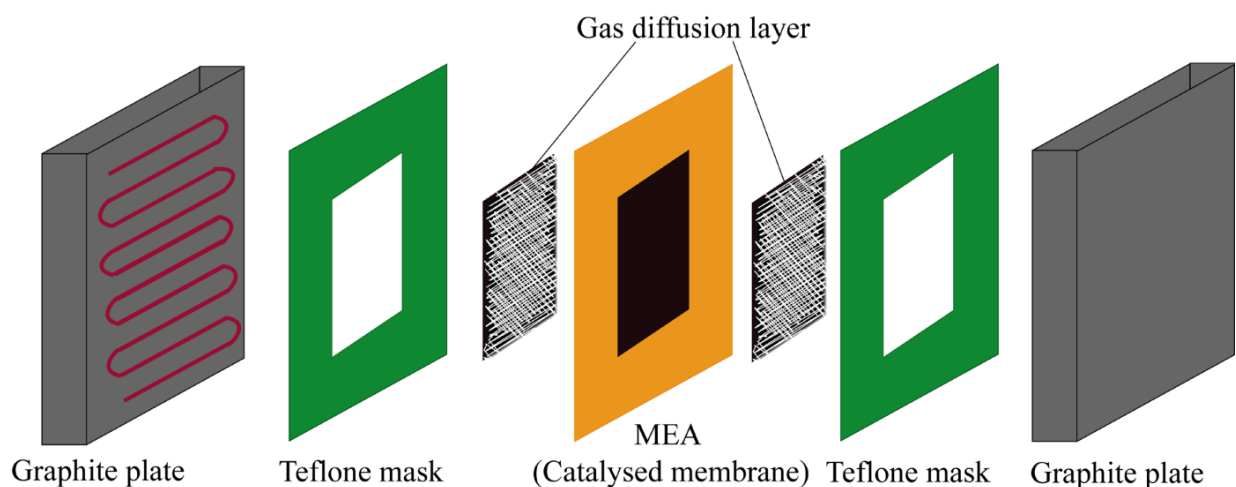
Figure 1.9 Schematic of the single cell hardware.

Table 1.2 PEM fuel cell components

Components	Description	Common examples
Proton exchange membrane	Enable to transfer proton from anode to cathode.	Nafion membrane 112, 115, 117, acid doped PBI, etc.
Catalyst layer	Oxidize the fuel into proton and electron. The proton combines with the oxygen and electron at the cathode and form water.	Platinum deposited on-carbon
Gas diffusion layer	This layer allows the transfer of fuel and oxygen for diffusion to the catalyst layer while collecting electrons.	Carbon cloth or paper
Flow field plates	Distribute the fuel and oxygen to the gas diffusion layer.	Graphite, stainless steel
Gaskets	It prevent the fuel leakage and it help to distribute pressure evenly.	Silicon / Teflon
End plates	It holds the stack layers in place.	Stainless steel, graphite, PVC

1.5.4.2 Role and required properties of proton exchange membrane for PEMFC

The key material for PEMFC, the membrane plays three important roles;

i.   It transport proton from anode to cathode to complete the electrochemical reaction and barrier for the electrons

ii.   It acts as a barrier for the reactant which separates the fuel and oxidant to mix

iii.   It also plays a role of separator between the electrodes (anode and cathode)

For a polymer to use as a membrane in PEMFC, following properties are desired [Hoogers (2003), Gubler (2008)].

✓   High proton conductivity and zero electron conductivity

✓   Long term chemical (*i.e.* good oxidative and hydrolytic stability at elevated temperature), mechanical and thermal stability

✓   Moderate water uptake

✓   Low or zero permeability to fuel or oxygen

✓   Good compatibility with the catalyst layer while fabrication MEA

✓   It should have lower cost and easy process-ability

1.5.4.3 Proton transfer mechanism in PEMFC

There can be two possible mechanisms for proton transfer through the membrane, viz., Grotthus-type and Vehicular-type [Zuo (2012)]. In the Grotthus mechanism, protons are transferred by the hydrogen bonding (formation and breaking of hydrogen bonds). This mechanism is also called as hopping mechanism [Peckham (2010)]. While, in case of Vehicular-type mechanism, protons migrate from one place to another through the medium along with a "vehicle" or solvent, such as, H_3O^+, $H_5O_2^+$ and $H_9O_4^+$ [Peckham (2010)]. In the Nafion based fuel cells, the overall proton conductivity is strongly dependent on the vehicle diffusion rate. The proton conductivity is directly affected by the proton transfer rate [Zuo (2012)]. Normally, in fuel cell, both these mechanisms take part simultaneously and often they make cooperative contributions to proton conductivity in PEMs [Zuo (2012)]. These mechanisms can be pictorially represented as shown in Figure 1.10 and 1.11.

Figure 1.10 Grotthus mechanism of proton transfer.
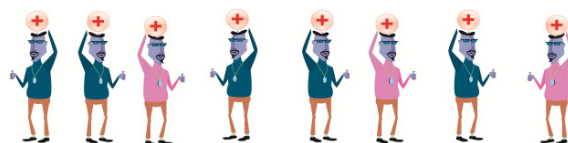
Figure 1.11 Vehicular mechanism of proton transfer.

1.5.4.4 PEM materials

a.   Perfluorosulfonic acid (PFSA) based membrane

The recent well-developed PEMFC technology is based on perfluorosulfonic acid (PFSA) membranes. One of the most widely used one is Nafion, manufactured by DuPont [Broka (1997), Li (2003)]. It is made up of carbon-fluorine backbone with perfluoro side chains containing sulfonic acid group. The Teflon-like molecular backbone gives these materials excellent long-term stability in both oxidative and reductive environments [Li (2003)]. A lifetime of over 60,000 hours under fuel cell conditions has been achieved with Nafion membranes [Li (2003)]. The maximum proton conductivity achieved by Nafion is 0.10 S.cm^{-1} under fully hydrated conditions. Great success has been achieved with the Nafion membranes, even though its cost is

high. Still, there are challenges which need to be addressed to make this technology to reach to the actual commercially available level such as water management, fuel crossover, CO poisoning, thermal balance and heat recovery.

Although several sulfonated aromatic polymers, such as polyimide, polyamides, etc. are evaluated as the alternative materials; none of them show performance as that of Nafion.

Many of the limitations associated with the PEMFC based on PFSA (Nafion) membranes that are usually operated at ~ 80 °C can be avoided by raising the operational temperatures higher than 100 °C. These are summarized as follows [Li (2003), Devanathan (2008)];

✓ The reaction kinetics for the both electrode reactions can be enhanced.

✓ The operation of PEMFCs above the boiling point of water, involves only a single phase of water *i.e.*, the water vapor. Therefore water management can be completely eliminated.

✓ The requirement of cooling system can be simple, increased temperature gradient between the fuel cell stack and the coolant would allow better heat recovery.

✓ The heat management will be easy. The generated steam can be used either for direct heating or steam reforming or for pressurized operation.

✓ The CO tolerance will be enhanced dramatically, from 10-20 ppm of CO at 80 °C, to 1000 ppm at 130 °C, and up to 30,000 ppm at 200 °C.

✓ The feasibility of using nonprecious metal catalysts, avoidance of flooding, simplified cooling system, and ability to recover waste heat.

Including all this factors the overall process will become easy to operate.

b.   Acid-Doped PBI Membranes

Among various possibilities on acid-base polyelectrolyte combinations reported in the literature, H_3PO_4 doped polybenizimidazole (PBI) seems to be a preferred choice. It is a thermoplastic amorphous polymer with a glass transition temperature of 425-436 °C [Li (2003)]. It is known for its good chemical, thermal and mechanical stability and excellent textile fiber properties. Commercially available PBI based MEAs are normally based on PBI-I and ABPBI. They are stable in acid doped as well as in basic condition. They have been doped in acid as well as bases and widely investigated for their use as fuel cell membrane electrolytes at temperatures above 100 °C.

c.   **IL and PIL in PEMFC**

A major challenge towards economically viable PEMFCs is finding an electrolyte that is durable, has good proton conductivity and is able to operate at medium temperatures (above 120 °C). It is already proven that operation of PEMFCs above 120 °C is required for a number of reasons, as given above in section 1.5.4.4.a. ILs and PILs based membranes are gaining wide attention for their applicability in PEMFC due to their high ionic conductivity, good thermal stability and low flammability [Mecerreyes (2015a)]. The doping or impregnation of Nafion, with protic ionic liquids has been investigated extensively [Doyle (2000)]. The anhydrous conductivity values have been achieved in the range of 0.001-0.1 S.cm^{-1} at 100–200 °C. Researcher tried various composites based on ILs while aiming increase in the conductivity, cost reduction, etc. The polymer matrices used are PVDF [Che (2015)], sulfonated poly(aryl ether ketone) (SPAEK) [Sekhon (2009)], sulfonated poly(ether ether ketone) (SPEEK) [Che (2008), (2015)], or sulfonated polyimide (SPI) [Lee (2010a)]. Various composite membranes have been prepared with sulfonated polyimides by embedding the [dema][TfO] as IL. It was reported that [dema][TfO] has appropriate properties for protic electrolyte at medium temperature (~120 °C) in non-humidified condition [Lee (2010a), Yasuda (2012)]. The inorganic fillers have also been tried to enhance the conductivity of IL-polymer electrolyte [Renard (2003)]. Researchers have also proven that the inorganic filler help in ionic liquid retention in PEMFCs [Lin (2010)]. Normally for high temperature (120-200 °C) fuel cell, phosphoric acid PBI membranes have been intensively investigated. It is reported that replacement of phosphoric acid by protic ionic liquids leads to improvement in the proton conductivity as well as it minimizes the corrosive and pollutant electrolyte (H$_3$PO$_4$) [Eguizábal (2013), Ven (2013), Mamlouk (2014)]. It is also reported that the introduction of ordered ionic domains in the PEM membrane can improve the proton conductivity. Kim et al. [2010], have reported that ordered ionic liquid domain in the synthetic block copolymer, poly(styrenesulfonate-b-methylbutylene) increased the proton conductivity. Operation of composite membrane (polyimide/[dema][TfO]) for PEMFC under non-humidified conditions is demonstrated [Lee (2010a), Lee (2010b)]. Recently, diethylamine bisulfate/sulfate IL incorporated into the PBI was evaluated for PEMFC. It was reported that the drag to IL from the membrane (migration from anode to cathode) limits the performance [Mamlouk (2014)]. Subsequently, the retention of IL into the composite membrane is a matter of concern. These issues can be addressed if the IL moiety is located in polymeric backbone, as in

polymeric ionic liquids (PILs). They are anticipated to provide continuous pathway of IL character (which is present on repeat unit of the polymer) and would eliminate the issue of IL drain.

PILs are projected as possible candidate for the application as membrane material for fuel cells (PEMFC). Though the use of PILs in fuel cell seems to be a promising option, it requires considerable research for a complete understanding of the relationship between the molecular structure and their stability in harsh fuel cell conditions at high temperature.

1.5.5 Alkaline Polymer Electrolyte Fuel Cells (APEMFCs)

The alkaline fuel cell, AFC, using aqueous KOH as electrolyte was the first type to be put into practice, at the start of the 20th century [Merle (2011)]. Cheng et al. [Cheng (2007)] explained the efficiency of using a solid polymer electrolyte to replace the liquid electrolyte in AFC (Figure 1.12). Research is focused on the development of an AFC based on anion-conducting polymer electrolytes to replace the KOH solution [Agel (2001), Deavin (2012), Merle (2011), Jheng (2014)].
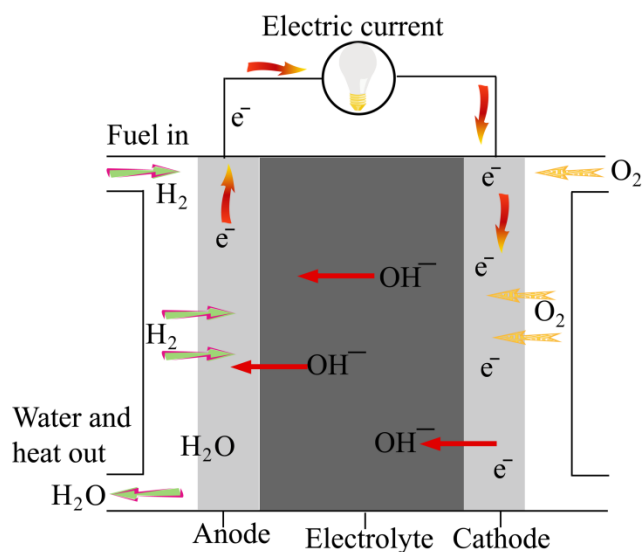
Figure 1.12 Schematic and key feature of anion exchange membrane fuel cell.

1.5.5.1 Basic principles of the anion exchange membrane as polymer electrolyte

The efficiency of fuel cell depends on various parameters such as temperature, pressure, fuel and most importantly, the solid electrolyte, i.e. ion conducting membrane. To use a polymer

for the anion exchange membrane, it should have some specific properties, as summarized below:

- ✓ Good mechanical and thermal stability during manufacturing and operation
- ✓ Good carrier for hydroxyl ion transport or high ionic conductivity
- ✓ Barrier to electrons and to provide effective separation between anode and cathode
- ✓ As thin as possible (50−80 μm) in order to keep good match between mechanical stability and conductivity.
- ✓ Lower cost

1.5.5.2 Mechanism of hydroxide ion transfer

To recognize and explain the transport mechanisms occurring in AEMs, researchers tried to take help of the large amount of literature available on proton exchange membranes (PEMs). In PEMFC also, all the proposed mechanism for proton transfer are based on assumptions [Kreuer (1996), Kreuer (2004), Merle (2011)]. These mechanisms include combinations of the Grotthus mechanism, masse diffusion, migration, surface site hopping along sulfonic acid side chains and convective processes [Kreuer (2004), Weber (2004a), Weber (2004b), Merle (2011)]. The conductivity of any polymer material also depends upon several factors such as temperature, relative humidity and pressure [Hibbs (2009), Grew (2010)].
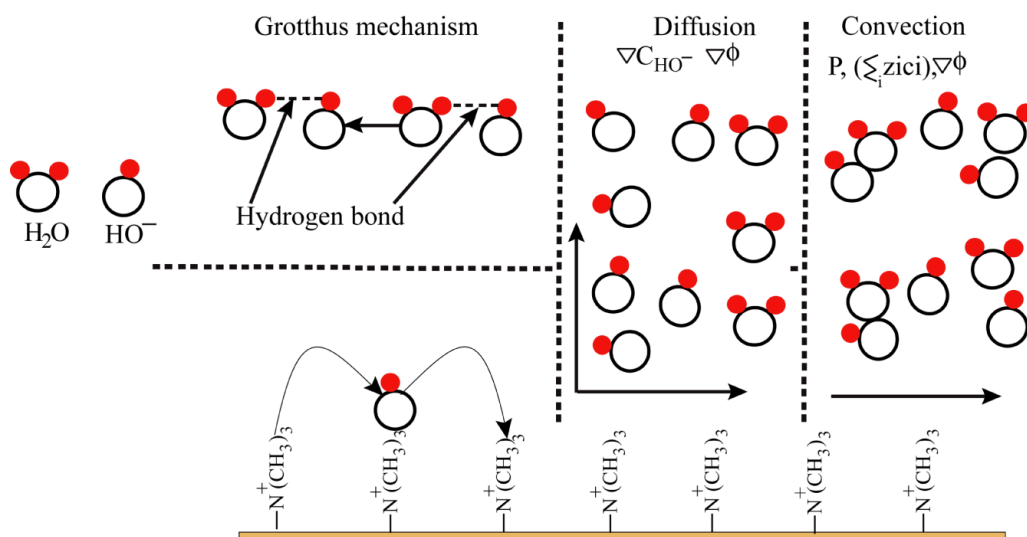
Figure 1.13 Hydroxide transfer mechanism in AEM.

Although the hydroxide conductivity of Nafion is lower than the proton conductivity, it depends on the factors such as temperature and relative humidity [Services (2004), Barbir (2008)]. For hydroxide transport in AEMs, the Grotthus mechanism, diffusion, migration and convection are considered to be the dominant transport mechanisms [Paddison (2002), Choi (2005), Merle (2011)] (Figure 1.13). Diffusive transport occurs in the presence of a concentration and electrical potential gradient across the membrane. In convection transport, it appears that membrane generate a convection flow and drag water molecules with them through the membrane. Hopping of hydroxyl anion can also be possible on the surface site, where quaternary ammonium groups are present on the membrane. This type of transport is thought to be of secondary type across the membrane because the water present in the system acts as a permanent dipole and interacts with the fixed charges of the membrane.

1.5.5.3 PIL in Alkaline Polymer Electrolyte Fuel Cells (APEMFCs)

Alkaline polymer electrolyte fuel cells (APEMFCs) technology can be a potential solution to reduce the cost and weight of current fuel cell technology. The conductivity and the stability of the anion exchange membrane is the key challenge of this technology (due to poor conductivity and low mechanical stability of membranes in alkaline condition). They still have not been commercialized yet [Pan (2014)]. To address these limitations, one proposed approach is to form a morphologically bicontinuous network of an ion-transporting phase and a hydrophobic phase in the membranes in order to provide mechanical strength [Price (2013)]. The second promising solution can be polymeric ionic liquids-based membranes [Deavin (2012), Qiu (2012), Nanwen Li (2013), Lin (2014)]. Lin et al., have prepared alkaly stable PIL membranes by the polymerization of IL monomer, 1-vinyl-3-methylimidazolium iodide ([VMIm][I]). It was photopolymerized in situ with styrene and acrylonitrile in the presence of 2–10 wt% of the divinylbenzene as a cross-linker. After the preparation of PIL membranes, they were converted to their OH^- forms by exchanging the iodide with hydroxide anions [Lin (2010)]. Noonam et al. have reported that the phase separation in the random copolymer, that provides both, the ion transport channels (the imidazolium domain) and a supportive matrix (acrylonitrile domain). They reported the apparent hydroxide ion conductivities above 10^{-2} S.cm^{-1} at room temperature. The prepared membranes exhibited excellent chemical stabilities in high pH media at 60 °C,

which are said to fulfil the basic conductivity and chemical stability requirements [Noonam (2012)].

It has been reported in the literature that imidazolium based PILs can become good candidates for the OH^- transport membranes material in AAEMFC. The stability of these PILs in alkaline condition and low OH^- conductivity still need to be overcome.

1.6   Scope and objectives of this thesis

The overall aim of this work was to enhance an understanding towards physical, gas permeation and ion (proton and hydroxide) transport properties of polymeric ionic liquids (PILs) as membrane materials. Toward this goal, synthesis of PILs possessing partial ionic character and effects of anion variation (while keeping polycation the same) on physical and gas sorption properties became one of the prime objectives. Preparation of blend membrane and synthesis of PILs that would be stable in acidic and alkaline environment was set as the next objective to use PIL membranes in the area of fuel cell.

a)   Effect of partial ionic character in the polymer matrix for gas permeation studies

A structural balance between *N*-substitution and *N*-quaternization could be performed by the controlled *N*-quaternization of PBI-BuI by a bulky group, *4-tert*-butylbenzyl. Partial ionic characters can also be introduced by the blending of PIL (fully *N*-quaternized PBI-BuI) and *N*-substituted PBI-BuI; in order to investigate difference between achieving partial ionic character within the membrane itself (chemical modification) and the one achieved physically (blending). Investigations of physical and gas permeation properties of resulting PILs were planned in order to gain an understanding towards effect of partial ionic character in governing gas permeation properties by both these approaches. Promising PIL candidates bearing halide anion could be chosen for further anion exchange; so that effects on anion on physical and gas permeation properties can be further evaluated.

c)   Effect of amino acid as an anion on PILs

A series of PILs containing amino acid as an anion could be synthesized by the anion exchange method. Investigations of physical and gas sorption properties of resulting PILs were

planned in order to gain an understanding towards specificity of amino acids as an anion in governing CO_2 separation properties.

d)   PIL-PBI blend membranes for PEMFC and AEMFC

Blending of polymeric ionic liquids (PILs) with PBI was planned to evaluate their applicability for high temperature proton exchange membrane fuel cell (HT-PEMFC) as well as anion exchange membrane fuel cell (AEMFC).

A new synthetic methodology was also planned to obtain family of cross-linkable PILs for PEMFC application. Alkali stable PIL membranes based on bulky *N*-substituent could be worthy to evaluate as membranes for AEMFC application.

1.7   Organization of the thesis

The work carried out to meet above objectives is presented in following chapters.

Chapter 1. Introduction, literature survey and scope of the work

This chapter presents a brief overview of gas separation and membrane materials used with an emphasis on ILs and PILs. A brief overview on properties of PILs as membrane material, particularly in gas permeation, PEMFC and AAEMFC are presented.

Scope and objective of the work is illustrated at the end of this chapter, followed by organization of the thesis.

Chapter 2. Experimental

This chapter presents synthesis of various PILs used in the present investigations. These PILs were designed in such a way that obtained polymers can be used for gas separation, proton exchange and anion exchange membranes. PILs were synthesized by modification of PBI (*N*-substitution, followed by partial / complete *N*-quaternization); followed by their halide exchange by promising anions. Characterizations of precursors and resulting PILs were performed by structural elucidation methods, viz., FT-IR, ^{1}H NMR, WAXD, TGA, DSC, DMA, Tensile strength testing, gas permeation, gas sorption, proton conductivity, hydroxide conductivity, MEA preparation etc.

Chapter 3. Polymeric ionic liquids (PILs) possessing partial ionic liquid character: Gas permeation studies
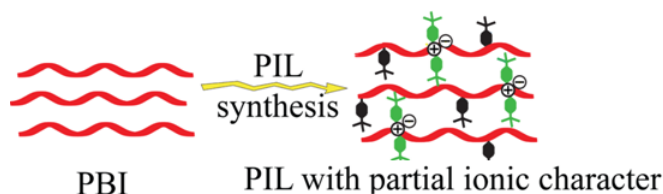
This Chapter is divided into two parts. First part deals with the synthesis of PILs possessing partial ionic character in their backbone. The partial ionic character has been introduced in the membrane during the synthesis of PILs itself. The synthetic aspects of PILs and detailed characterizations, viz., NMR, FT-IR, degree of quaternization, solvent solubility, water sorption, contact angle, mechanical property, density, WAXD, thermal stability and their glassy nature are presented.
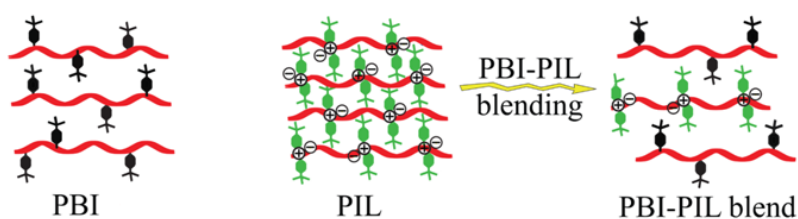
The second part of this chapter deals with an introduction of ionic character in the membranes by external blending of DBzPBI-BuI with a PIL, viz., ([TBzPBI-BuI][Br]$_{88}$). Characterizations followed by gas permeation analysis were performed to compare effect of inducing effect of partial ionic character physically and chemically (as performed above).

Chapter 4. PILs possessing partial ionic liquid character: Effects of anion exchange on their physical and gas permeation properties
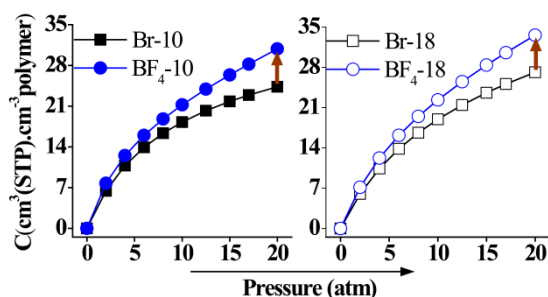
Two PILs, viz., ([TBzPBI-BuI][Br]$_{10}$ and [TBzPBI-BuI][Br]$_{18}$) were chosen from the first part of the above study. The halide anion was exchanged with three chosen anions, Tf$_2$N¯, BF$_4$¯ and Ac¯; based on their CO_2 specific nature. Among formed PILs, the one with BF$_4$¯ anion showed higher CO_2 permeability as well as selectivity while; PILs with Tf$_2$N¯ anion have high permeability with non-interacting gases. This study concludes that combination of partial ionic character and anion variation are crucial in elevating CO_2 permeation properties.

Chapter 5. Amino acid containing polymeric ionic Liquids: gas sorption and physical property investigation
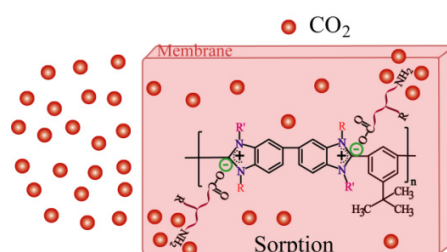
This chapter presents a series of polymeric ionic liquids containing amino acids as anion with an aim to increase CO_2 sorption in PILs. These PILs have been synthesized by *N*-quternization of PBI-BuI and its anion exchange was performed by using sodium salt of amino acids. Their detailed characterization, viz., NMR, FT-IR, degree of quaternization, amount of anion exchange, solvent solubility, density, WAXD and thermal stability are presented in this chapter. The AAPIL with L-Arginate as anion showed higher CO_2 sorption as well as CO_2 based sorption selectivity than that of other anions. This was attributed to the presence effective *N*-sites for CO_2 sorption.

Chapter 6. Blend membranes based on polymeric ionic liquid and polybenzimidazole: Physical and electrochemical properties (PEMFC and AAEMFC)
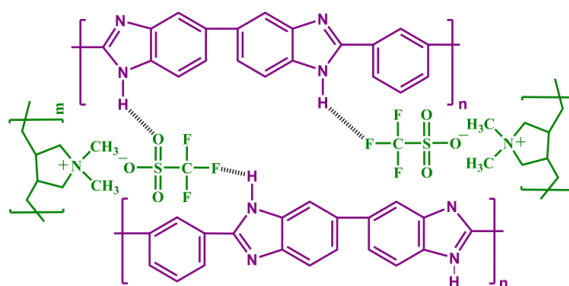
This chapter deals with the blend membrane preparation of the PIL ([PDADMA][TFMS]) and PBI-I for their possible application as fuel cell membranes. These blend membranes are studied for their homogeneous nature by using DSC, FT-IR, WAXD and inherent viscosity. Resultant blend membranes were analyzed for high temperature proton exchange membrane fuel cell (HT-PEMFC) as well as anion exchange membrane fuel cell (AEMFC). The PBI-PIL blend membranes showed significant improvement in the proton conductivity (almost double the performance as that of PBI membranes) as well as hydroxide ion conductivity.

Chapter 7. Novel elegant stable polymeric ionic liquid (PIL) membrane materials for fuel cell (PEMFC and AEMFC)
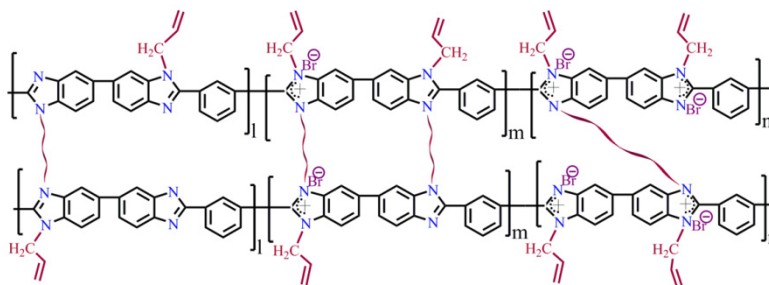
This Chapter is divided into two parts. First part deals with the synthesis of PILs toward their applicability in high temperature conditions for PEMFC. In these PILs, cross linkable (allyl) groups was introduced during synthesis (*N*-quaternization) and were further cross-linked by heating resultant membranes at high temperature. The cross-linking was achieved without use of any external cross-linkers or catalysts. PILs have been characterized by NMR, FT-IR, WAXD, TGA, DSC and conductivity analyses.

The second part of the Chapter presents the study of PILs towards anion exchange membranes. The PILs were synthesized by the partial *N*-quternization of PBI-I and anion (bromide) was introduced in the structure. These PILs were studied further for OH¯ stability test and used as anion exchange membrane in AEMFC. PILs have been characterized by viz., NMR, FT-IR, WAXD, TGA, DSC and conductivity analyses.

Chapter 8. Conclusions of the thesis

This chapter summarizes the conclusions of various approaches studied towards applicability of PILs as a gas separation membrane (esp. for CO_2), proton and anion exchange membrane materials for fuel cells.

Chapter 2

Experimental

2.1 Materials

    3,3′-Diaminobenzidine (DAB), *5-tert*-butylisophthalic acid (BuI), isophthalic acid, sodium hydride (60% dispersion in mineral oil), *N,N′*-dimethylacetamide (DMAc), dry dimethyl sulphoxide (DMSO, 0.01% H_2O), *4-tert*-butylbenzyl bromide (BzBr), allyl bromide (3-bromopropene), sodium tetrafluoroborate ($NaBF_4$), lithium bis(trifluoromethane)sulfonimide ($LiTf_2N$), silver nitrate ($AgNO_3$), aqueous solution of poly(diallyldimethylammonium chloride), P[DADMA][Cl] (20 wt%, average MW: 100-200 kD), silver trifluoromethanesulfonate (> 99%), L-Alanine (L-Ala), L-Arginine (L-Arg), L-Asparagine (L-Asp), L-Histidine (L-His), L-Lysine (L-Lys), L-Phenylalanine (L-Phe) and L-Tryptophane (L-Try) were procured from Aldrich Chemicals; while, sodium salt of Glycine (Gly) was procured from Acros Organics. Polyphosphoric acid (PPA, Ca 84% as phosphorus pentoxide) was procured from Alfa Aesar. Sodium acetate (CH_3COONa), phosphoric acid (PA, 85 wt% aqueous solution) and various solvents viz., chloroform ($CHCl_3$), dichloromethane (CH_2Cl_2), methanol (CH_3OH), toluene, cyclohexanone, acetone, acetonitrile (CH_3CN), *1,4*-dioxane, *N,N*-dimethyl formamide (DMF), dimethyl sulphoxide (DMSO), *N*-methyl-pyrolidinone (NMP), methyl iodide, potassium thiocyanate (KSCN), sodium chloride (NaCl) and sodium hydroxide (NaOH) were procured from Merck. All these chemicals were used without further purification. Dialysis bag (M_w cut of 10 kD) was procured from Aldrich Chemicals. Pure gases viz., He, H_2, N_2 and O_2 (minimum purity of 99.9%) were procured from Vadilal Chemicals Ltd.; while CH_4 and CO_2 (purity of 99.995%) were procured from Air Liquide.

2.2 Synthesis

2.2.1 Synthesis of polybenzimidazole

    Polybenzimidazole (PBI-I and PBI-BuI) was synthesized by polycondensation of DAB and isophthalic acid or *5-tert*-butyl isophthalic acid (BuI) as reported earlier [Kumbharkar (2006)]. A three-necked round bottom flask equipped with a mechanical stirrer, N_2 inlet and $CaCl_2$ drying tube was charged with 1200 g of PPA, 40 g (0.1867 mol) of *3,3′*-diaminobenzidine

(DAB) and the temperature was elevated to 140 ºC. After dissolution of DAB, 0.1867 mol of dicarboxylic acid (isophthalic or *5-tert*-butylisophthalic acid) was added; temperature was slowly raised to 170 ºC and maintained for 5 h under constant flow of N_2. The temperature was further raised to 210 ºC and maintained for 12 h. The polymer was obtained by precipitation in water. It was crushed and thoroughly washed with water in order to remove phosphoric acid. The polymer was kept in 10% $NaHCO_3$ for 16 h, washed with water till the filtrate was neutral to pH, soaked in acetone for 16 h, filtered and dried in vacuum oven at 100 ºC for 7 days. Further purification by dissolving in DMAc (3% w/v) and reprecipitation in water yielded yellow colored fibrous polymer (Scheme 2.1).
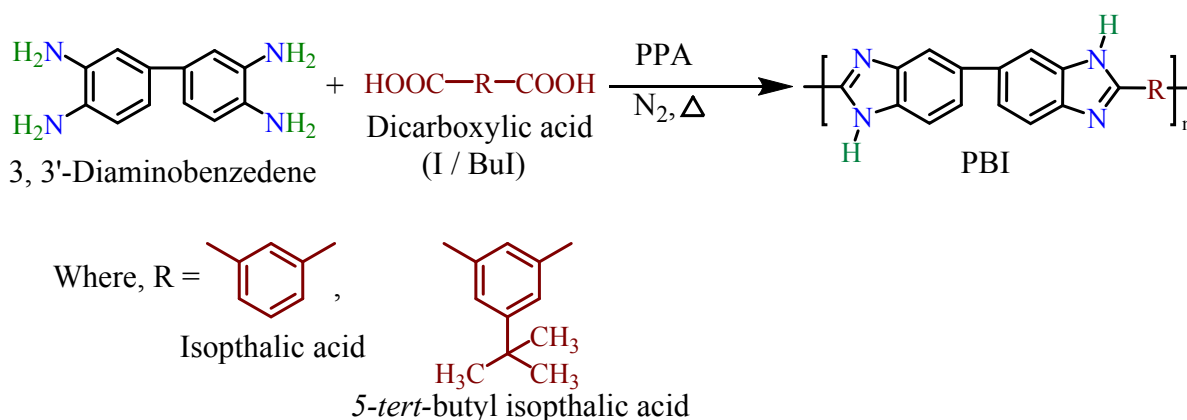
Scheme 2.1 Synthesis of PBI.

2.2.2 Synthesis of *N*-substituted polybenzimidazole (DBzPBI-BuI)

The *N*-substitution of PBI-BuI was carried out in dry DMSO by preparing its sodium salt, followed by addition of the *4-tert*-butylbenzyl bromide. Typically, a three-necked round bottom flask equipped with N_2 balloon was charged with 300 ml of dry DMSO, 10 g (0.0275 mol) of PBI-BuI, 2.1 equivalents (0.058 mol) of NaH and stirred at ambient temperature for 20 h. The reaction mixture was then heated at 80 ºC for 3 h. A deep blood red color developed after the dissolution of PBI. The solution was allowed to cool to the ambient and 2.1 molar equivalents of *4-tert*-butylbenzyl bromide dissolved in 10 ml of dry DMSO was added in a drop wise manner over a period of 15 minutes. The reaction mixture was precipitated indicating formation of the *N*-substituted PBI-BuI, which was stirred further for 12 h in order to achieve complete dissolution. It was slowly poured on to the stirred water. The precipitated polymer was washed several times

with water and dried in a vacuum oven at 100 °C for a week. Synthesized polymers were purified by dissolving in DMAc and reprecipitating in water.
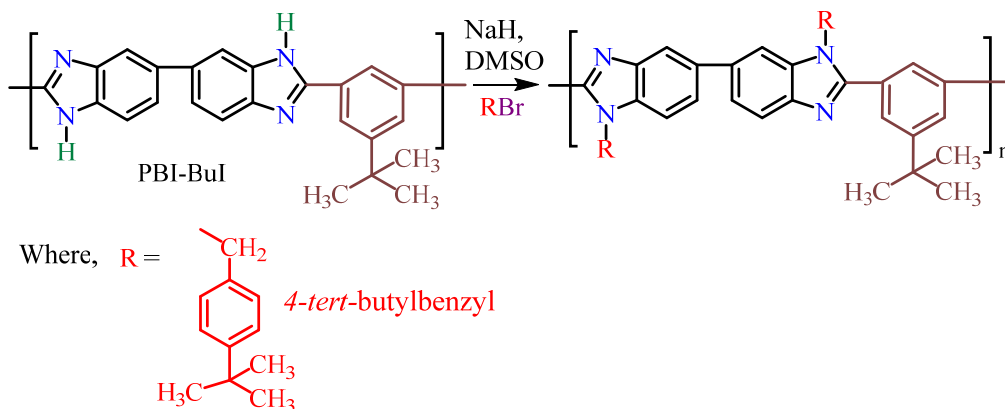
Scheme 2.2 Synthesis of *N*-substituted PBI-BuI (DBzPBI-BuI).

2.2.3 Synthesis of polymeric ionic liquids (PILs) possessing partial ionic character

For obtaining polymeric ionic liquids (PILs) possessing partial ionic character, a PBI (PBI-I or PBI-BuI) was *N*-quaternized in a controlled manner (Scheme 2.3). Typically, a 3-necked RB flask was charged with 160 ml of dry DMSO, 0.0162 mol of a PBI and 1.364 g of NaH (2.1 equivalents, 0.034 mol) while stirring under dry N_2 atmosphere at the ambient temperature. After 3 h, temperature of the reaction mixture was raised to 80 °C and maintained for 2 h. A deep blood red color was developed after complete dissolution of the PBI, which was indicative of its *N*-sodium salt formation. This solution remained homogeneous after cooling it to the ambient temperature. Adequate molar equivalents (calculated for partial *N*-quaternization) of *4-tert*-butylbenzyl bromide were added to the reaction mixture. An immediate precipitate formation after the addition of *4-tert*-butylbenzyl bromide indicated that *N*-substitution of PBI had taken place, as also observed earlier [Rewar (2015)]. The reaction mixture was stirred further for 30 min at ambient temperature and then heated at 80 °C for 20 h in order to obtain a clear solution. The reaction mixture was cooled to the ambient temperature and then precipitated in hexane and toluene (1:1, V/V) mixture. The formed polymer was vacuum dried at 80 ºC for a week. It was purified by dissolving in DMAc, reprecipitating in a mixture of hexane and toluene (1:1, V/V), followed by drying in vacuum oven at 80 ºC for 3 days. The degree of *N*-quaternization (DQ) was calculated by Volhard's method and ^{1}H-NMR, which were closer to

each other. These values were thus averaged and assigned in the parenthesis, while abbreviating the PIL. For example, in the case of [TBzPBI][Br]$_x$, 'x' represents the DQ of that PIL.
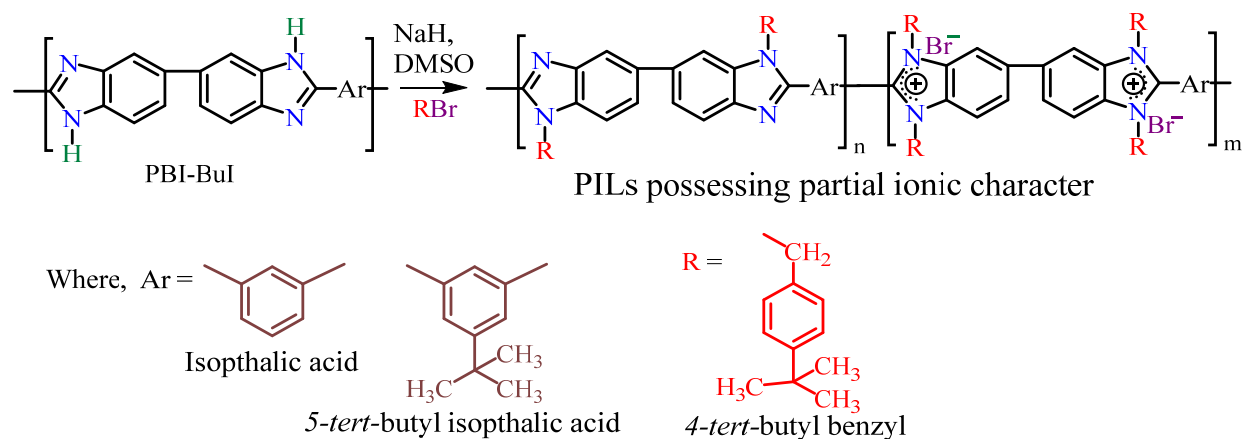
Scheme 2.3 Synthesis of PILs based on partially quaternized PBI.

2.2.4   Anion exchange of PILs possessing partial ionic character

Two PILs, viz., [TBzPBI-BuI][Br]$_{10}$ and [TBzPBI-BuI][Br]$_{18}$ were chosen for the anion exchange. The bromide anion of PILs was exchanged using LiTf$_2$N, NaBF$_4$ and CH$_3$COONa in DMAc (Scheme 2.4). A 3 g (0.0043 mol) of [TBzPBI-BuI][Br]$_{10}$ was dissolved in 100 ml of DMAc while stirring. A 2.35 g (0.0215 mol, 5 eq) of NaBF$_4$ was added and stirred at RT for 48 h. The formed byproducts, LiBr and NaBr, were separated from the polymer solution by precipitating the reaction mixture in water. In order to remove the complete salt from the precipitated polymer, its repeated water washing was done. The same procedure was followed for the exchange of Br$^-$ with Tf$_2$N$^-$ as an anion. In the case of exchange by Ac$^-$ as an anion, different procedure needed to be used due to partial solubility of the polymer in water. The dialysis bags were used to separate the product PILs and byproduct NaBr; owing to the large difference in the molecular weights of these components. The reaction mixture was added in the known quantity of water and then added in to the dialysis bag of MWCO of 10 kD. The bags filled with the reaction mixture were suspended in a beaker containing deionised water. Water from the beaker was removed periodically till 4 days in order to achieve maximum possible removal of NaBr from dialysis bag. In order to confirm that the complete salt has been removed from the PIL solution; dialysis was continued till conductivity of the water (in the beaker) remains to 1 μS.cm^{-1}. The PIL solution from the dialysis bag was concentrated using rotavapor at

60 °C. The PIL solution was poured on glass plate and dried at 80 °C for 24 h, followed by vacuum drying at 80 °C for 1 week. The same procedure was followed for the Br$^-$ exchange of [TBzPBI-BuI][Br]$_{18}$ with the same anions. Obtained PILs were dried at 80 °C for 24 h, followed by vacuum drying at 80 °C for 1 week.
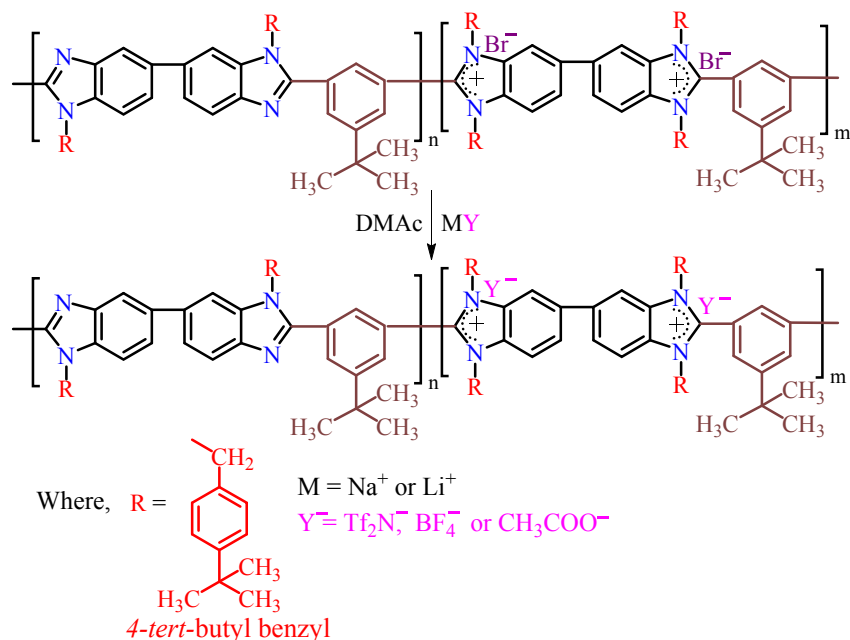
Scheme 2.4 PIL synthesis by anion exchange of partially quaternized PBIs.

2.2.5 Synthesis of asymmetric polymeric ionic liquids
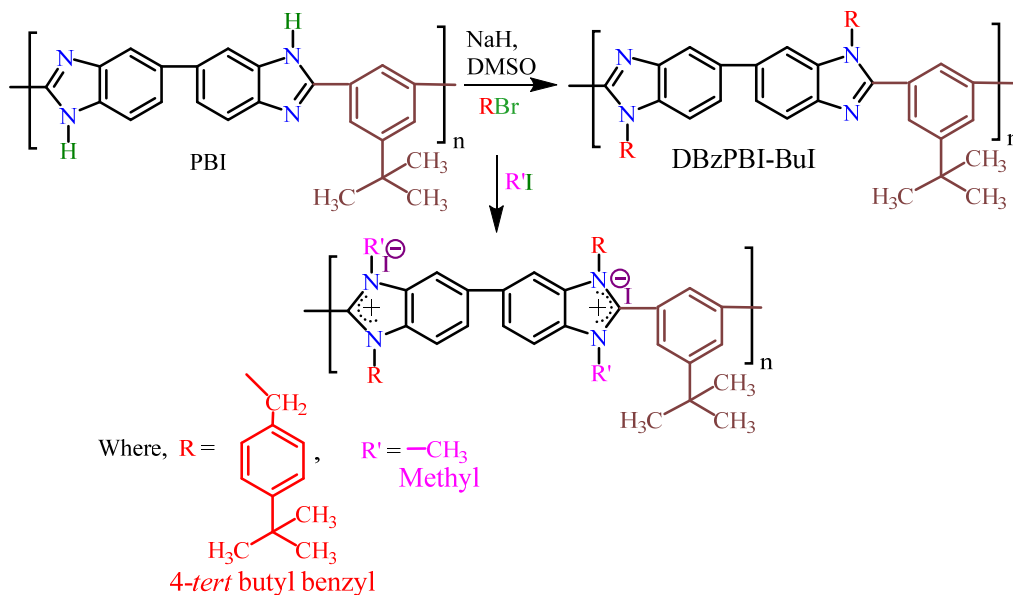
Scheme 2.5 Synthesis of asymmetric polymeric ionic liquids.

The *N*-quaternization of DBzPBI-BuI (synthesis as given in Section 2.2.2) in an asymmetric manner was carried out using methyl iodide. Typically, a 3-necked round bottom flask was charged with 300 ml of dry DMSO, 10 g of *N*-substituted PBI, 2.5 equivalents of methyl iodide and stirred under N_2 atmosphere at the ambient temperature for 12 h. After this, the reaction mixture was further heated at 80 ºC for 12 h in order to achieve quantitative *N*-quternization. After 12 h, the reaction mixture was allowed to cool down to the ambient temperature and then precipitated in a mixture of toluene and acetone (1:1, V/V). The obtained golden yellow fibrous polymer was dried at 80 ºC for 24 h. It was further purified by dissolving in DMF and reprecipitating in the mixture of toluene and acetone (1:1, V/V).

2.2.6 Synthesis of sodium salt of amino acids

Sodium salt of amino acids was synthesized by acid-base neutralization reaction. An 8% solution of amino acid was prepared in water, 1 equivalent of NaOH was added and stirred at ambient for 12 h. The water was evaporated on rotavapor to recover sodium salt of amino acid in a solid form (Scheme 2.6).
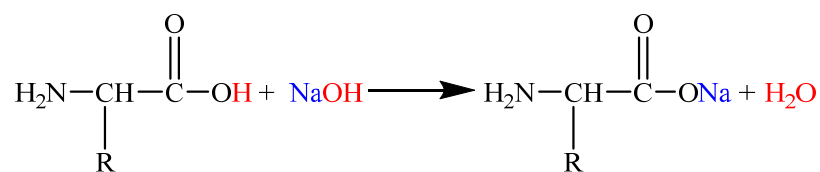
Scheme 2.6 Synthesis of sodium salt of amino acid.

2.2.7 Synthesis of PILs containing amino acids as anions

This family of PILs was synthesized by exchanging the iodide anion of the [DBzDMPBI-BuI][I] by the Na-salt of various amino acids. To a 5% (w/v) solution of PIL, 5 molar equivalent of Na-salt of an amino acid was added and stirred at ambient for 48 h in order to ensure maximum possible exchange of the iodide. The dialysis bag (10 kD) was used to separate the product PILs and byproduct (NaI), since the product PILs (with amino acids as anion) showed partial solubility in water. The detailed procedure is given in Section 2.2.4. The PIL solution was poured on glass plate and dried at 80 °C for 24 h, followed by vacuum drying at 80 °C for 1 week. This process was repeated in order to attain appreciable amount of anion exchange. Formed PIL was further purified by dissolving in DMF (7% w/v) and precipitating in water. These polymers showed partial solubility in water. Thus, the mixture was poured in the dialysis

bag, which was suspended in a beaker containing DI water. The water was repeatedly replaced for 4 days in order to extract the DMF. The solution from the dialysis bag was taken out and water was evaporated. The obtained polymer was dried at 80 ºC in a vacuum oven for 6 days and preserved in desiccator until use.
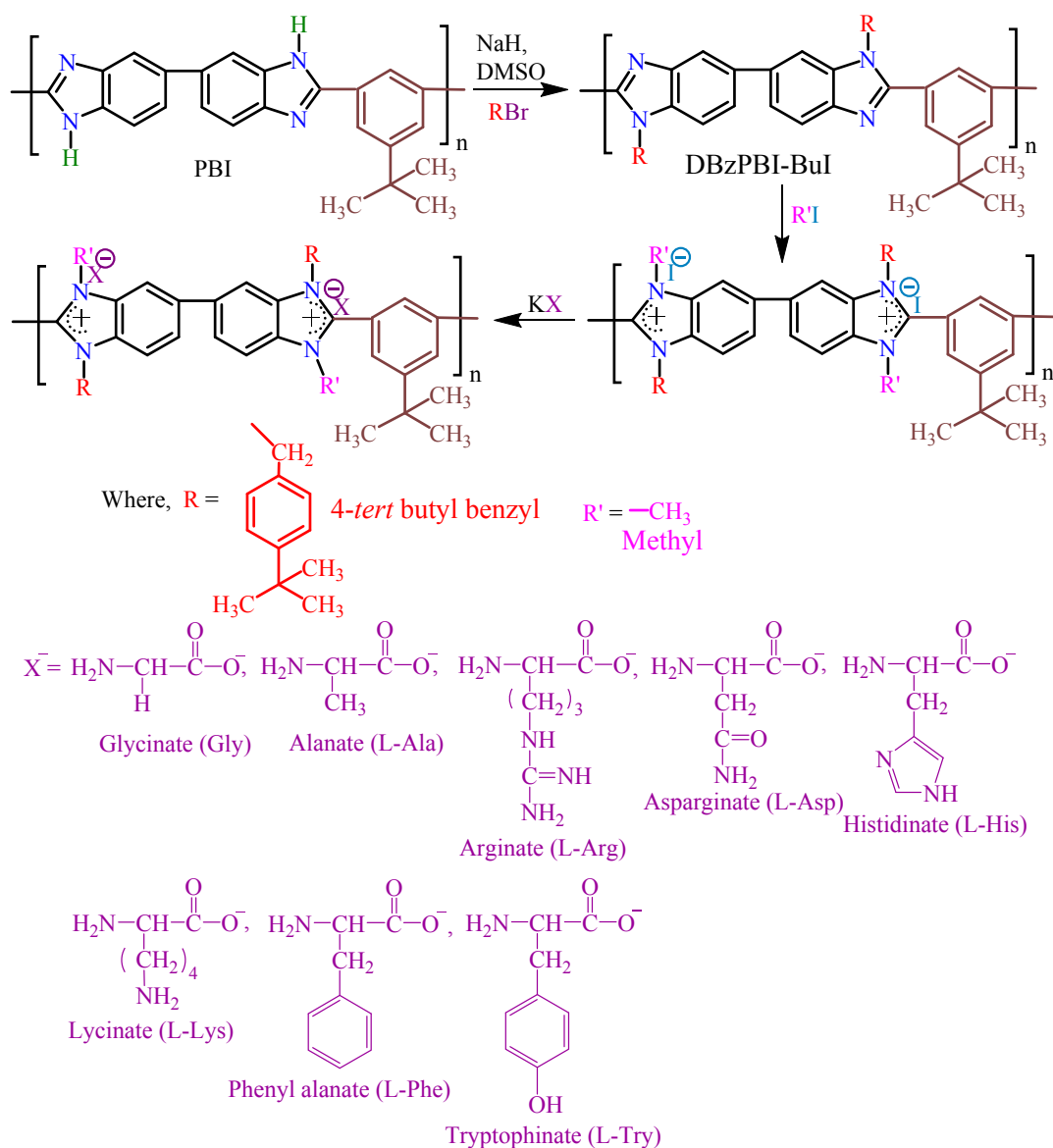
Scheme 2.7 Synthesis of PILs possessing amino acid as anions.

2.2.8 Synthesis of polymeric ionic liquids possessing aliphatic backbone

The aliphatic PIL, viz., P[DADMA][TFMS] was prepared by anion exchange of a commercially available polymer, P[DADMA][Cl] (Scheme 2.8). The 8% (w/v) solution of

P[DADMA][Cl] was prepared in water and an equimolar quantity of Ag salt of trifluoromethanesulphonate was added to the solution while stirring at ambient. As the replacement of Cl⁻ with the anion, TFMS progressed, AgCl precipitated out. In view of polymeric nature of the cation, stirring continued for 24 h in order to ensure maximum possible exchange. The resulting mixture was centrifuged at 12000 rpm for 30 min in order to separate AgCl in a precipitated form. To remove the silver salt, centrifugation was repeated 5 times. In order to recover the product polymer, the supernatant solution was poured on to a flat teflon surface and dried at 60 °C for 24 h and finally in vacuum oven at 60 °C for 7 days.
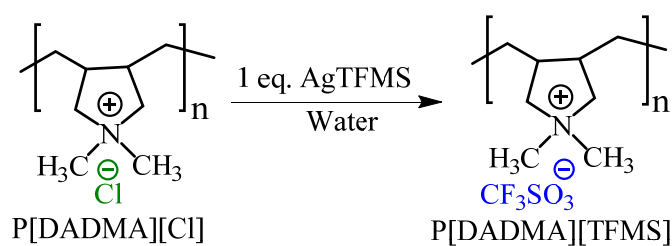
Scheme 2.8 Synthesis of P[DADMA][TFMS].

2.2.9 Synthesis of cross-linkable PILs possessing partial ionic character
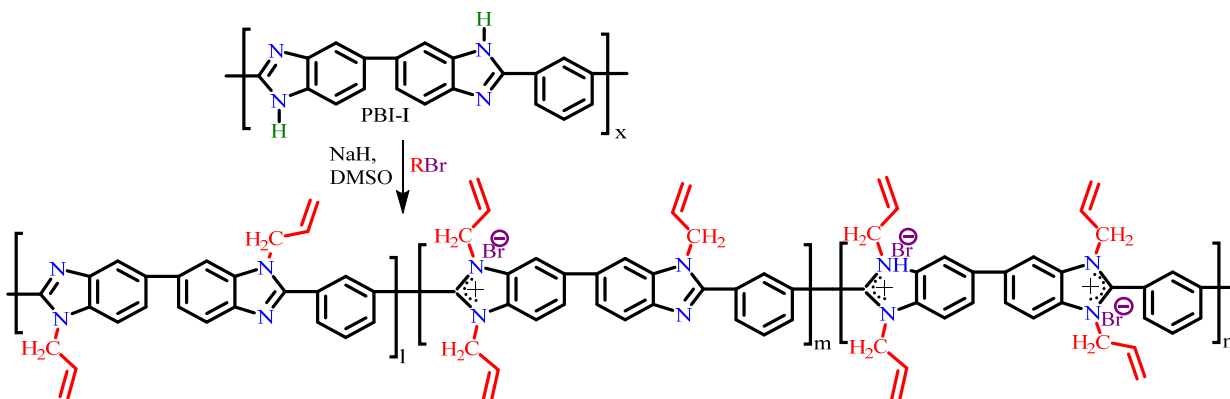
Scheme 2.9 Synthesis of cross-linkable PILs.

In order to induce cross-linking ability in PILs, allyl bromide was used for the *N*-quaternization. The PBI-I based PILs were synthesized by partial *N*-quaternization route. Typically, a 3-necked RB flask was charged with 160 ml of dry DMSO, 5 g (0.0162 mol) of a PBI-I and 1.364 g of NaH (2.1 equivalents, 0.034 mol) while stirring under dry N$_2$ atmosphere at the ambient temperature. After 3 h, temperature of the reaction mixture was raised to 80 °C and

maintained for 2 h. A deep blood red color was developed after complete dissolution of the PBI, which was indicative of its *N*-sodium salt formation. This solution remained homogeneous after cooling it to the ambient temperature. Adequate molar equivalents of allyl bromide (25, 50, 75 and 100 mol %, calculated based on anticipated partial *N*-quaternization) was added to the reaction mixture. An immediate precipitate formation after the addition of allyl bromide indicated that *N*-substitution of PBI-I had taken place. The reaction mixture was stirred further for 20 h at RT in order to obtain a clear solution. The reaction mixture was then precipitated in acetone, filtered and repeatedly washed. The obtained PILs were dried under vacuum at the ambient temperature for a week. The yield of the obtained PILs was > 85% in all the cases, which was a primary indication that the partial *N*-quaternization has occurred, as planned.

2.3   Membrane preparation

2.3.1   Preparation of PBI and PIL membranes

The dense membranes of PBI-I and PILs were prepared by solution casting method (using 3% w/v solution in DMAc) at 80 °C for 18 h under dry atmosphere. The polymer solution after centrifugation at 12000 rpm was poured on to the flat glass surface and heated at 90 °C for 18 h under dry atmosphere. Formed membrane was peeled off and dried in a vacuum oven at 80 °C for a week in order to remove the residual solvent and was then used for subsequent analysis. The PBI-I membrane was further used for electrochemical analyses as described in Chapter 7; while the PIL membranes were used for gas permeation (Chapter 3) as well as for electrochemical analyses (Chapter 8).

2.3.2   Preparation of blend membranes based on [TBzPBI-BuI][Br] and DBzPBI-BuI

The blend membranes were prepared in varying weight ratio of [TBzPBI-BuI][Br] and DBzPBI-BuI and are designated as DBz-TBz$_{x:y}$ as presented in Table 2.1., where 'x' represents the weight percent of [TBzPBI-BuI][Br] in the formed composite membrane. The [TBzPBI-BuI][Br] and DBzPBI-BuI solutions in DMAc (3 wt %) were prepared at 80 °C for 14 h with continuous stirring. The [TBzPBI-BuI][Br] solution was added to the solution of DBzPBI-BuI in requisite proportion and stirred. The dense blend membranes were obtained by solution casting method at 90 °C on a flat glass surface for 20 h under dry atmosphere. Formed film was peeled

off and dried in a vacuum oven at 80 °C for 7 days in order to remove the residual solvent and then used for subsequent analysis, as given in Chapter 5.

Table 2.1 Weight ratio and designation of blend membranes

Proportion of DBzPBI-BuI in blend membrane (Wt %)	Proportion of [TBzPBI-BuI][Br] in blend membrane (Wt %)	Designation of blend membrane
100	0	DBz-TBz$_{100:0}$
90	10	DBz-TBz$_{90:10}$
80	20	DBz-TBz$_{80:20}$
70	30	DBz-TBz$_{70:30}$
55	45	DBz-TBz$_{55:45}$
40	60	DBz-TBz$_{40:60}$
25	75	DBz-TBz$_{25:75}$
10	90	DBz-TBz$_{10:90}$
0	100	DBz-TBz$_{0:100}$

2.3.3   Preparation of PBI-PIL blend membranes

The PBI-PIL blend membranes were prepared by varying their weight ratio and are designated as PBI-PIL$_x$, as presented in Table 2.2, where 'x' represents the weight percent of PIL in the formed composite membrane with PBI. The PBI-I was dissolved in DMAc (3% solution) at 80 °C for 10 h with continuous stirring. A 5 gm of P[DADMA][TFMS] was dissolved in 10 ml of DMSO while stirring at RT for 12 h. A required quantity of PIL solution (based on the proportion, as given in Table 2.2) was added to the solution of PBI-I and stirred for 24 h. The dense blend membranes were obtained by solution casting method at 90 °C on a flat glass surface for 24 h under dry atmosphere. Formed film was peeled off and dried in a vacuum oven at 80 °C for 8 days in order to remove the residual solvent. The average thickness of the membranes was around 70 ($\pm$5) μm. These PBI-PIL blend membranes were used for electrochemical study of proton exchange membrane fuel cell (PEMFC and AEMFC) as described in Chapter 7.

Table 2.2 Weight ratio and designation of PBI and PIL blend membranes

Proportion of PIL in blend membrane (Wt %)	Proportion of PBI in blend membrane (Wt %)	Designation of formed blend membrane
0	100	PBI-I
5	95	PBI-PIL$_5$
15	85	PBI-PIL$_{15}$
25	75	PBI-PIL$_{25}$
35	65	PBI-PIL$_{35}$
45	55	PBI-PIL$_{45}$

2.3.4 Preparation of cross linkable PIL membranes

The dense membranes of cross linkable PILs were prepared by solution casting method. A 3% (w/v) solution of PIL was prepared in DMF while stirring at RT for 18 h under dry atmosphere. The solution after centrifugation at 12000 rpm was poured on to the flat glass surface and heated at 90 °C for 18 h. under inert atmosphere. After initial evaporation of the solvent, formed membrane was peeled off. To ensure cross linking, formed membranes were further heated at 200 °C for 3 h and used for subsequent analysis. The average thickness of the membranes was around 70 ($\pm$5) μm. These cross-linked PIL membranes were used for electrochemical analyses as described in Chapter 8.

2.4 Characterizations

2.4.1 Determination of degree of *N*-quaternization (DQ), solvent solubility, viscosity, density and contact angle

The degree of *N*-quaternization (DQ) of PBI by alkyl halide group was analyzed by ^{1}H-NMR (recorded on Bruker AC-200 using DMSO-d$_6$ as the solvent). The DQ was also obtained by estimating halide content in the formed PIL by Volhard's method [Vogel (1989)]. The extent of halide exchanged by other anion in a PIL was also estimated by titrating formed metal halide (viz., LiX/NaX/AgX) with 0.01 M AgNO$_3$ by Volhard's method. For this, 0.1 g of PIL powder was added in 10 ml of 0.01 M AgNO$_3$ solution and stirred for 24 h. An excess of AgNO$_3$ was

titrated against 0.01 M KSCN, from which, the halide content in the PIL was determined. This halide content is correlated to either DQ or the amount of anion (halide) exchanged.

The solvent solubility of PILs was determined by adding 0.1 g of polymer in 10 ml of a solvent while stirring at ambient for 18 h. In case of insolubility, further heating at 80 °C (or near boiling point, in case of low boiling solvents) was performed for 10 h. Inherent viscosity (η_{inh}) of a PIL solution (conc. = 0.2 g.dL^{-1}) was determined at 35 °C using DMSO as the solvent. The density (ρ) measurement was carried out at 35 °C with ~100 μm thick films using specific gravity bottle and decalin as the solvent that exhibited negligible sorption in present PILs (< 1.4 wt%). Water contact angle of dry membrane surface was determined by the sessile drop method using Digidrop 35 instrument (Kruss, Germany) while placing a water drop on the membrane surface. The measurement was repeated with five different samples prepared by identical conditions and the average value is reported (maximum variation from the average: ± 2.4°).

2.4.2   Determination of spectral, thermal and mechanical properties of membranes

FT-IR spectra of polymers in a thin film (~10 μm) form were recorded initially at the ambient temperature and then at 150 °C on Perkin Elmer Spectrum GX spectrophotometer provided with high temperature assembly of Mettler Toledo make with FP90 central processor. Wide angle X-ray diffraction (WAXD) pattern of polymers in the film form were recorded using Phillips PAnalytical diffractometer in reflection mode using CuKα radiation (λ = 1.5418 Å). The 2θ range from 4 to 40° was scanned with a scan rate of 2.5° min^{-1}. The average intersegmental d-spacing (d_{sp}) for the amorphous peak maxima was calculated using Bragg's equation ($n\lambda$ = $2d\sin\theta$). Thermogravimetric analysis (TGA) was performed using Perkin Elmer TGA-7 in N$_2$ atmosphere with a heating rate of 10 °C.min^{-1}. The glass transition temperature (T_g) was determined using DSC Q-10 (TA instruments, USA) under N$_2$ atmosphere with a heating rate of 10 °C.min^{-1}. A dynamic mechanical thermal analyzer (DMA, Rheometric Scientific) was also employed for determining the glass transition temperature (T_g) of some PILs. The experiment was performed under tensile mode at a frequency of 1 Hz and a heating rate of 10 °C min^{-1}. The scan was recorded up to ~ 20 °C below the IDT of respective PIL. Tensile tests were performed

at ambient temperature on Linkam TST-350 microtensile testing instrument using film samples of 2 x 0.3 x 0.005 cm^3 size at a strain rate of 10 μm.min^{-1}.

2.4.3 Determination of hydrolytic and oxidative stability of membranes

Hydrolytic stability of the membrane samples of 2x1 cm^2 size and ~40-50 μm thickness was evaluated by immersing them in deionised water at 80 °C while shaking. Hydrolytic stability was determined by recording the immersion period required for breaking the film when bent slightly. If the films retained their shape even after folding, it was said to be stable.

The oxidative stability of the membranes was determined by Fenton's test [Yuan (2013)]. The membrane samples of 2x1 cm^2 size and ~40-50 μm thickness were dried, weighed and immersed into a 3% H_2O_2 aqueous solution containing 3 ppm $FeSO_4$ at 80 °C. After specified times, the samples were removed from the oxidizing solution, washed with water, dried and weighed to calculate the weight loss. The observed duration of the experiments was in the range of few hours to weeks, depending on the stability of the resultant membrane.

2.4.4 Determination of water uptake (WU) capacity of membranes

To determine the water uptake capacity of membranes, initially, membrane samples of 2x2 cm^2 size and ~40-50 μm thickness were kept in a vacuum oven at 80 °C for 3 days to ensure the constant weight of the dry membrane (W_d). The membranes then were immersed in deionized water for 48 h at ambient condition. Afterwards, the membranes were taken out and wiped instantly by a tissue paper to remove the adhered water present on the surface of the membrane. Subsequently, the wet membranes were weighed (W_w) and thus, water absorbed inside the membrane was determined. The precise WU capacity was subsequently calculated using following equation,

$$\mathrm{WU(\%)} = \left(\frac{\mathrm{W}_w - \mathrm{W}_d}{\mathrm{W}_d} \right) \times 100 \qquad (2.1)$$

The balance of 0.1 mg accuracy was used and at least three measurements with three different membrane samples were conducted under identical conditions and the values reported are the average of these measurements. The deviation in the measurement was $\pm$ 5 %.

2.4.5   Determination of acid uptake of PIL membranes

The H_3PO_4 uptake was obtained by immersing the PIL membranes in different molarities of H_3PO_4 solution at room temperature for 3 days. After this duration, the PIL membranes were removed from the acid bath, excess of H_3PO_4 was removed with a filter paper and the weight and dimensions were measured. The H_3PO_4 doping of the dried (100 °C, 1 week) membranes was determined by gravimetric method. The following equation [Bhavsar (2010)] was used to calculate the acid uptake:

$$H_3PO_4 \text{ doping level} = \frac{308\,(W_1 - W_2)}{98 \text{ x } W_2} \tag{2.2}$$

where, W_1, and W_2 represent the weight of the doped and undoped membrane respectively. Three membrane samples were doped under exactly identical conditions and the data averaged. The deviation in the measurement was $\pm$ 51.9 mol H_3PO_4/RU.

2.4.6   Determination of acid uptake of blend membranes

The H_3PO_4-doped membranes were obtained by immersing blend membranes in different concentrations of H_3PO_4 solution at room temperature for 3 days. After this duration, the blend membranes were removed from the acid bath, excess of H_3PO_4 was removed with a filter paper and the weight was measured. The H_3PO_4 doping of the dried membranes (100 °C, 1 week) was determined by gravimetric method. The following equation was used to calculate the acid uptake:

$$H_3PO_4 \text{ doping level} = \frac{M_1\,(W_1 - W_2)}{M_2 \text{ x } W_3} \tag{2.3}$$

where, 'W_1' and 'W_2' represent the weight of the doped and undoped membrane, respectively, 'W_3' is the weight fraction of PBI in the undoped membrane; while 'M_1' and 'M_2' are the molecular weight of PBI repeat unit (308) and that of H_3PO_4 (98), respectively. The H_3PO_4 doping level of the composite membranes is plotted with reference to its PIL content.

2.4.7   Determination of hydroxide stability of membranes

In order to determine the stability of membranes prepared with different degree of quaternization (DQ) in alkaline condition. The membrane samples of 2x1 cm^2 size and ~40-50

µm thickness in bromide form were immersed in KOH solution of different molarity for few days at room temperature. The stability was determined by recording the immersion period required for breaking the film when bent slightly. If the films retained their shape even after folding, it was said to be stable. Based on this study, the alkaline concentration for dipping the membrane was decided and used for further analyses.

2.5   Gas permeation and sorption

The variable volume method [Stern (1963)] was used for the determination of gas permeability. A schematic and photograph of the permeation equipment used are shown in Figure 2.1 and 2.2, respectively.
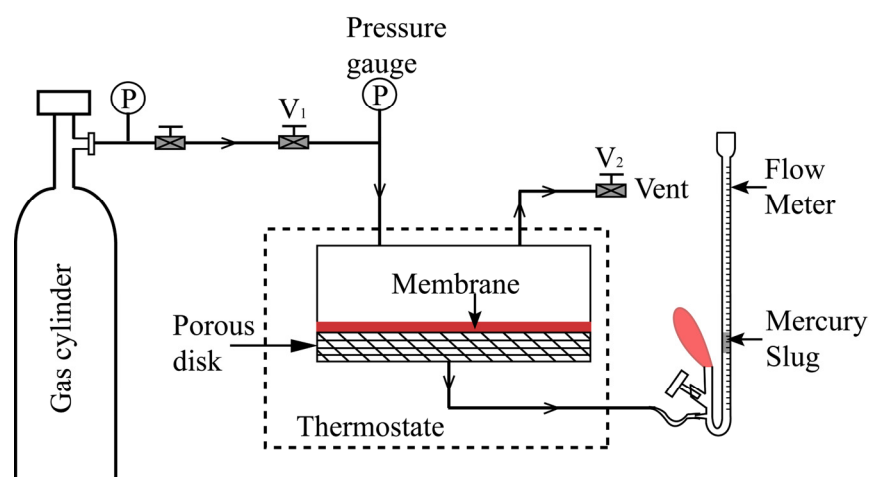
Figure 2.1 Schematic of gas permeation equipment.
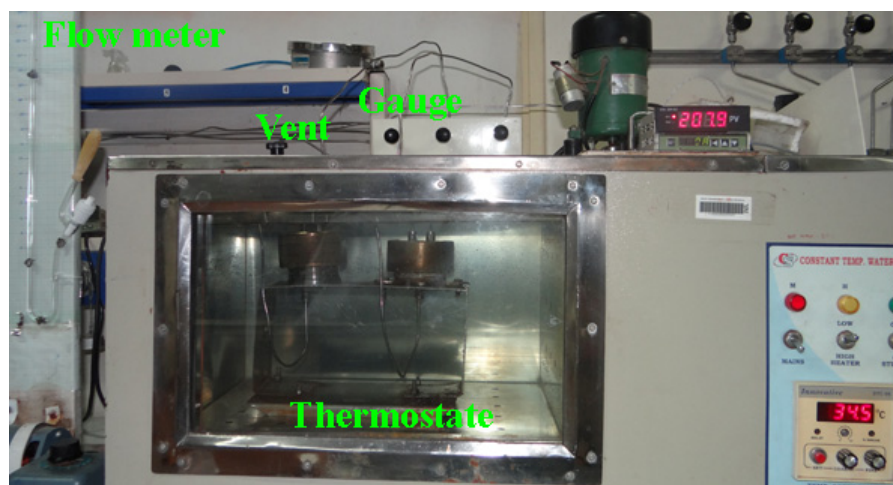
Figure 2.2 Photograph of gas permeation equipment.

One end of the feed side of the cell was connected through valve V_1 to the feed gas cylinder outlet and a pressure gauge (0-550 psi range). The valve V_2 was vent and used to control the feed pressure. On the permeate side of the cell, a calibrated borosilicate glass capillary (I.D. = either 1.0 or 1.5 mm) containing a small mercury slug (~ 4-6 mm in length) was connected. The membrane cell assembly was kept in a thermostat. Before pressurizing a particular gas, the whole system was fluxed 8 times and then the pressure was hold in the cell. Displacement of the mercury slug was monitored against time.

The pure gas permeability measurement using He, H_2, N_2, O_2, CH_4 and CO_2 (in the same sequence) was carried out at upstream gas pressure of 20 atm and at 35 °C, while maintaining the permeate side at the atmospheric pressure. The vacuum dried membrane samples of either 5 cm or 7.5 cm diameter and ~ 35 μm (±3) thickness were used. The permeability was determined using the Eq. 2.4;

$$P = \frac{N \cdot l}{(p_1 - p_2)} \tag{2.4}$$

where 'P' is the permeability coefficient expressed in Barrer, 'p_1' and 'p_2' are the permeate side and feed side pressure (cm Hg), respectively; 'l' is the membrane thickness (cm) and 'N' is the steady-state gas flux ($cm^3.cm^{-2}.sec^{-1}$). The permeation measurements were repeated with at least 3 different membrane samples prepared under identical conditions. The variation in permeability measurement was up to ~ 10%, depending upon the gas analysed. The ideal selectivity, P_A/P_B was calculated as the ratio of pure gas permeability.
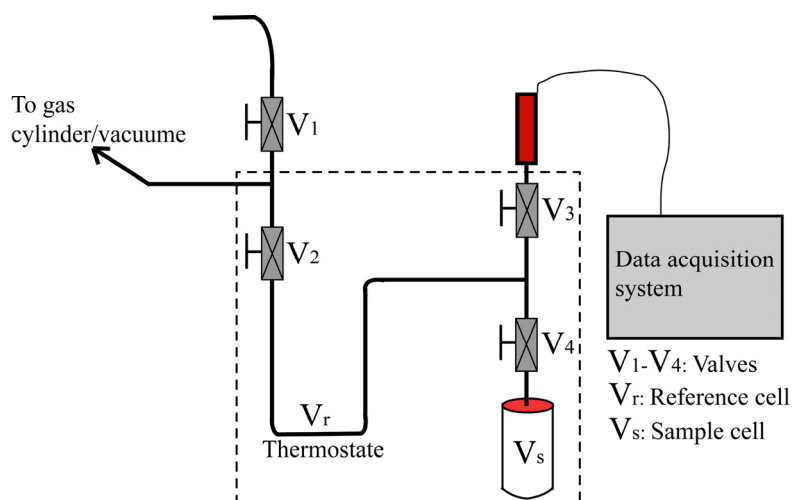
Figure 2.3 Schematic of gas sorption equipment.
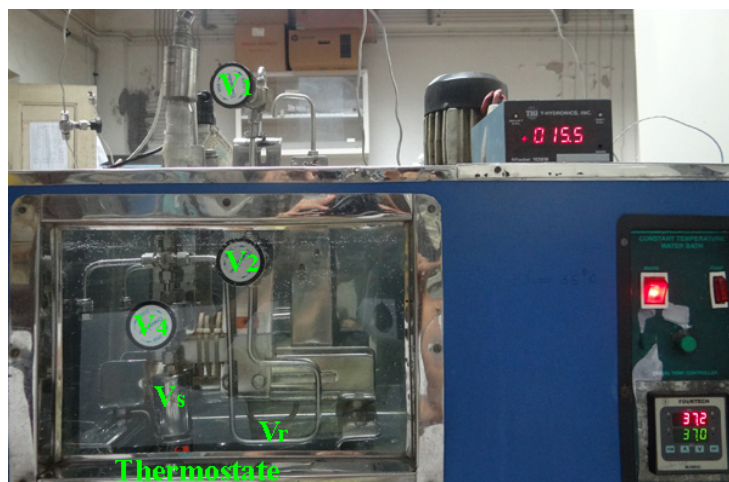
Figure 2.4 Photograph of gas sorption equipment.

Pure gases (H_2, N_2, CH_4 and CO_2, in the same sequence) were used for the analysis of gas sorption in PILs at 35 °C and at incremental pressures up to 20 atm. The gas sorption equipment consisted of dual-volume single-transducer set up based on the pressure decay method [Koros (1976), Karadkar (2007)]. The schematic and photograph of sorption equipment is given in Figure 2.3 and 2.4 respectively. The design of the sorption cell, specifications, material of construction, etc. is discussed elsewhere [Karadkar (2007), Kumbharkar (2006)].

The polymer sample in film form was placed in the sorption cell, evacuated and flushed with the gas several times. The system was then evacuated to 0.00001 mbar using oil diffusion pump. The gas was introduced rapidly and initial pressure recorded. As the sorption proceeds, the pressure starts decreasing and ultimately remains constant after the equilibrium is established. Incremental rise in pressure of the equilibrated system until about 20 atm was attained. The amount of gas sorbed in the sample at each equilibrium pressure was determined from the initial and final pressures.

The gas solubility coefficient (S), for a gas in these glassy polymers is described by the dual-mode model [Vieth (1976)]. The dual mode sorption parameters (k_D, b and C'_H) were determined by non-linear regression analysis of the experimentally determined data at varying pressures.

$$S_A = \frac{C}{p} = k_D + \frac{C'_H \, b}{(1 + bp)} \qquad (2.5)$$

where, 'C' is the gas concentration in polymer, 'p' is the applied gas pressure, 'K_D' is the Henry's solubility coefficient, 'C'_H' is the Langmuir saturation constant and 'b' is the Langmuir affinity constant.

The diffusivity coefficient (D_A) was obtained from the experimentally determined permeability and solubility coefficient (S_A) using the following equation.

$$P_A = D_A S_A \tag{2.6}$$

2.6 Electrochemical analysis of PIL membranes

The proton and hydroxide conductivity (σ) measurements of the PIL membranes were carried out by two-probe and four-probe AC impedance analyzer (BioLogic Science Instruments), respectively.

2.6.1 Conductivity measurement by two probe method

In two probe conductivity cell, the electrolyte films were sandwiched between symmetrical gold coated stainless-steel electrodes of diameter 1.3 cm having thickness in the range of 50-250 micron and connected to the analyzer by Pt wires. The impedance measurements were performed over the frequency range from 10 Hz to 1 MHz with an amplitude of 10 mV at different temperatures in the range of 30–150 °C. The frequency response was analyzed using EC-lab software.
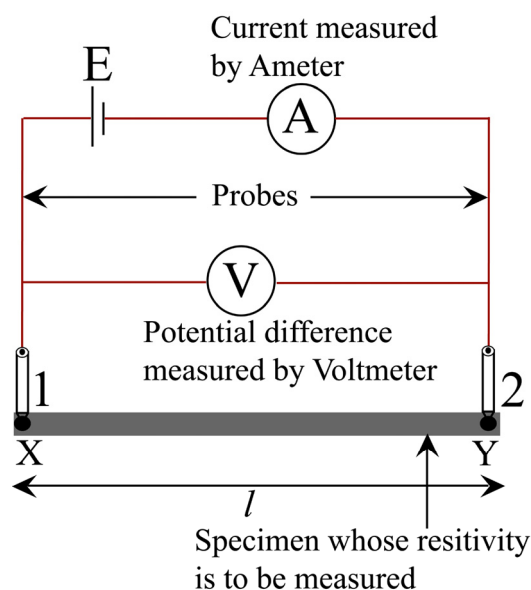
Figure 2.5 Schematic of two-probe method of measuring resistivity of a specimen.

The measurements were performed in a thermo-controlled cell under anhydrous conditions. The conductivity (σ) was calculated as follows:

$$\sigma = \frac{L}{RA} \tag{2.7}$$

where, L, R, and A are the measured thickness, resistance and cross-sectional area of the membrane, respectively.

2.6.2   Conductivity measurement by four-probe method
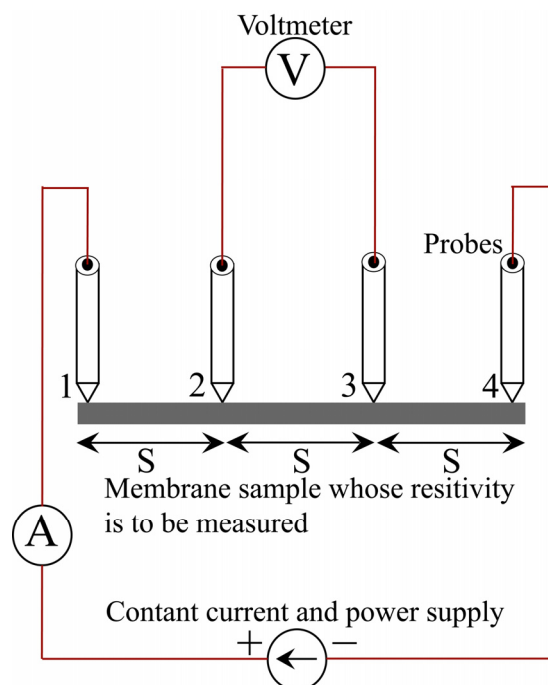
Figure 2.6 Schematic of four-probe method of measuring resistivity of a specimen.

The alkaline conductivity (σ) measurements of the membranes were carried out by a four-probe AC impedance analyzer (BioLogic Science Instruments) with a cell, consists of four equally spaced platinum metal tips with finite radius. Each tip is supported by a spring at the end to minimize sample damage during probing. The four metal tips are part of an auto mechanical stage which travels up and down during measurement. A high impedance current source is used to supply current through the outer two probes; a voltmeter measures the voltage across the inner two probes to determine the sample resistivity. Typical probe spacing is ~1 mm.

These inner probes draw no current because of high input impedance voltmeter in the circuit. Thus unwanted voltage drop (IR drop) at point 2 and 3 caused by contact resistance

between probes and the sample is eliminated from the potential measurements. Since these contact resistance are very sensitive to pressure and to surface condition (such as oxidation of either surface), error with the conventional two-electrode technique (in which potential measuring contact passes a current) can be quite large. The measurements were performed in a thermo-controlled cell under 90% humidity conditions. The resistance (R) in terms of bulk resistivity (ρ), was calculated by equation 2.8.

$$R = \frac{\rho\, l}{A} = \frac{\rho\, l}{W\, T} \tag{2.8}$$

where, **A** is the cross-sectional area perpendicular to the current flow, (which in this case, is sample width (W) x thickness (T)) and l is the distance in the direction of ion flow, between voltage measurements. The resistivity, ρ, can be calculated by equation 2.9.

$$\rho = \frac{R\, W\, T}{l} \tag{2.9}$$

Conductivity, σ, is the inverse of resistivity, as shown in equation 2.10.

$$\sigma = \frac{1}{\rho} = \frac{l}{R\, W\, T} \tag{2.10}$$

2.6.3 Determination of activation energy for ion transport

The activation energy (E_a) for ion transport was calculated from the slope of the plot corresponding to proton or hydroxide conductivity in a logarithmic scale *vs*. inversed Kelvin temperature by using the Arrhenius equation (Eq. 2.11).

$$\sigma = \sigma_o \exp\left(\frac{-E_a}{RT}\right) \tag{2.11}$$

where, σ is the ion (proton or hydroxide) conductivity in $S.cm^{-1}$, σ_o is the pre-exponential factor, E_a is the activation energy in $kJ.mol^{-1}$, R is the universal gas constant ($8.314\ J.mol^{-1}.K^{-1}$) and T is the absolute temperature in K.

2.6.4 Membrane-electrode assembly (MEA) fabrication and cell polarization

2.6.4.1 MEA preparation, polarization study and impedance measurement for PEMFC

Membrane electrode assemblies (MEAs) were prepared as follows: first, a gas diffusion layer (GDL) was prepared by coating a mixture of Vulcan XC-72 carbon and PTFE in

cyclohexane on teflonized carbon paper after sonicating for 2 min on a 30 sec on/off basis using a probe sonicator. The carbon loading was maintained as 1.5 mg.cm^{-2}. The GDL was pressed at 0.25 ton.cm^{-2} for 2 min followed by sintering at 350 °C for 30 min. The catalyst ink was made by mixing 40 wt% Pt/C, Nafion and isopropyl alcohol in an appropriate ratio and sonicating for 2 min. This ink was coated on the GDL to prepare the electrode with a Pt loading of 1 mg.cm^{-2}, which was chosen in order to avoid variation in performance due to the catalyst layer. The electrode was then cut into 3x3 cm^2 pieces and hot-pressed uniaxially with phosphoric acid doped membrane at 130 °C and at a pressure of 0.5 ton.cm^{-2} for 3 min in order to fabricate the MEA.

The polarization measurements were carried out in a test cell of 9 cm^2 active area comprising serpentine type gas flow field. The cell was operated at 160 °C through a pair of external electrical heating elements. Arbin fuel cell test station (Model: Arbin-001 MITS Pro-FCTS 5.0-FCTS) was used to do the polarization measurement under dry conditions. After the conditioning, the polarization measurements were carried out. The H$_2$ and O$_2$ flow rates were maintained constant at 1.18 and 0.88 slpm, respectively.

MEA impedance measurements were performed on a frequency response analyzer (Autolab PGSTAT 30 with FRA software) in the frequency range 100 kHz to 100 mHz with an AC signal of 10 mV amplitude. The measurements were performed with the MEAs of the membranes at 160 °C.

2.6.4.2 MEA preparation and polarization study of AAEMFC

MEA of alkaline anion exchange membrane (AAEMs) was prepared as given below. Required amount of the Vulcan XC-72R carbon powder dispersed in cyclohexane and then mixed with polytetrafluoroethylene (15 wt% PTFE) to prepare the slurry subsequently the solution were coated on Teflonized Toray paper until the loading of 1.5 mg.cm^{-2} is reached to form gas diffusion layer. For the preparation of the catalyst ink, the carbon-supported catalyst (40% Pt) was dispersed in de-ionized water followed by the addition of fix amount of Fumion (FAA-3) (polyaromatic polymer with quaternary ammonium ions, bromide counter-ion and NMP) (10 wt%) in ethanol while ultrasonic vibration for 30 min. After the preparation of the catalyst ink, it was then coated on the gas diffusion layer to make the electrode. The required Pt metal loading was kept similar, *i.e.*, 0.5 mg.cm^{-2}, for both the anode and cathode. Consequently,

to exchange the binder to OH¯ form, the electrodes were dipped in KOH solution (1.0 mol.L^{-1}). The MEA was formed after sandwiching the membrane in between the above two electrodes at 80 °C for 3 min at a pressure of 15-20 kg.cm^{-2}. The MEA was then placed in a single-cell assembly with parallel serpentine flow-field machined on graphite plates. The polarization measurements were carried out in a test cell of 4 cm^2 active area comprising serpentine type gas flow field. Measurements of the cell potential as a function of current density and power density were carried out galvanostatically by using electronic load (Model-LCN4-25-24/ LCN 50-24) from Bitrode Instruments (US) with humidified H$_2$ and O$_2$ flowing at 200 mL.min^{-1}.

Chapter 3

Polymeric ionic liquids (PILs) possessing partial ionic liquid character: Gas permeation studies

3.1 Preamble

PILs demonstrated in the literature for gas permeation analysis are tested at lower pressures of ~ 2 bar, as discussed in Chapter 1. Although reports on analyzing PILs membranes at 5-10 bar are emerging now, this literature is scanty [Li (2010)]. There are enough evidences in the literature to conclude that the aliphatic backbone of demonstrated PILs is responsible for their poor film forming ability [Tang (2005a), Hu (2006), Bhavsar (2014a), Bhavsar (2014b)]. To mitigate this issue, we have recently demonstrated a new methodology of synthesizing tough, film forming PIL based on fully aromatic, rigid backbone. These PILs were obtained by N-quaternization of PBI using methyl iodide, followed by metathesis (anion exchange reaction) by anions that are known to elevate CO_2 sorption in RTILs [Kumbharkar (2014), Bhavsar (2014a), Bhavsar (2014b), Bhavsar (2014c)]. Although gas permeation properties (especially selectivity performance) of these PILs were highly promising, there is a need for elevating their permeability coefficient, so that this new family of materials can be projected for CO_2 separation. The gas permeability of these PILs was lower in comparison to merely N-substituted (but not N-quaternized) PBIs reported earlier [Kumbharkar (2010)]. As an example, N-substituted DMPBI-BuI exhibited H_2 and CO_2 permeability of 13.06 and 5.62 Barrer, respectively [Kumbharkar (2010)]. On the other hand, permeability for these gases in N-quaternized [TMPBI-BuI][I] was only 6.3 and 1.84 Barrer, respectively [Bhavsar (2014c)]. This reduction in permeability caused by the dense chain packing in PIL matrix (due to ionic interactions in fully quaternized PBI) can be conveniently mitigated by reducing ionic character and increasing content of merely N-substitution. Li et $al.$ have observed that with increasing content of IL monomer, resulting co-polyimides exhibited gradual reduction in the gas permeability [Li (2010)]. These findings suggest that in the case of PBI based PILs, a systematic structural balance between N-substitution of PBI (in order to enhance permeability) and its N-quaternization leading to ionic character (to enhance gas solubility, especially that of CO_2) can be of specific interest for obtaining high

permeability and selectivity, simultaneously. With this as an objective, present chapter deals with introducing ionic character in PILs in a controlled manner. Two pathways for this proposition are evaluated. In the first part of this chapter, *N*-quaternization of PBI-BuI by a bulky group (*4-tert*-butylbenzyl) was performed. Obtained film forming PILs were investigated for physical and gas permeation properties. In second part of the chapter, blending of PIL and PBI was evaluated as a methodology to evaluate the hypothesis of simultaneous combination of *N*-substitution and *N*-quaternization for elevating their gas permeation properties.

Part A: Polymeric ionic liquids based on partial *N*-quaternization of PBI-BuI: Gas permeation studies

3.2a Synthesis

3.2.1a Synthesis of PBI-BuI and PILs

The experimental details including PBI and PIL synthesis, their physical and gas permeation characterization methods are given in Chapter 2. The PBI-BuI was selected for *N*-quaternization based on its good gas permeation and sorption properties than that of other members of the PBI family [Kumbharkar (2006)]. It was anticipated that PBI-BuI backbone would be helpful in offering high gas permeation properties of resulting PILs possessing partial ionic character. Another reason in selecting PBI-BuI was its better solvent solubility than that of PBI-I.

PBI-BuI was synthesized by solution polycondensation in PPA, which acts as both, condensation agent as well as polymerization solvent [Mader (2008)]. The ratio of DAB:PPA was taken as 1:30 w/w and sequential rise in temperature after the addition of the 5-*tert*-butylisophthalic acid (170 °C and then 200 °C) was based on our previous investigations [Kumbharkar (2009)]. The time of reaction at 200 °C was 12 h. The PBI-BuI purified by dissolving in DMAc (3% w/v) and reprecipitation in water yielded a yellow colored fibrous polymer. Purified PBI-BuI was used further for PIL synthesis. The PBI-BuI was synthesized with high enough inherent viscosity of 1.3 dL.g^{-1} that offered a tough film by the solution casting method. The partial *N*-quaternization of PBI-BuI was successfully performed in a single step by in-situ preparation of its Na-salt, followed by *N*-substitution by *4-tert*-butylbenzyl bromide in various proportions, as given in Table 3.1a.

Table 3.1a Degree of PBI-BuI *N*-quaternization in PILs.

Degree of quaternization, DQ (%)				Designation of resulting PILs
Planned (Molar equivalent of BzBr)	Observed			
	By NMR	By Volhard's method	Average	
7 (2.14)	7.7	8.3	8.0	[TBzPBI-BuI][Br]$_8$
10 (2.2)	11.3	9.5	10.4	[TBzPBI-BuI][Br]$_{10}$
15 (2.3)	13.4	12.8	13.1	[TBzPBI-BuI][Br]$_{13}$
20 (2.4)	19.1	17.9	18.0	[TBzPBI-BuI][Br]$_{18}$
40 (2.8)	40.0	42.2	41.1	[TBzPBI-BuI][Br]$_{41}$
60 (3.2)	54.5	57.1	55.8	[TBzPBI-BuI][Br]$_{56}$
80 (3.6)	71.3	74.9	73.1	[TBzPBI-BuI][Br]$_{73}$
100 (4)	86.0	89.5	87.8	[TBzPBI-BuI][Br]$_{88}$

The *N*-substitution of a PBI do occur by the reaction between its Na-salt and an alkyl halide [Kumbharkar (2009)], while it's further quaternization takes place due to the availability of an excess of alkyl halide. Yield of the obtained polymers was > 90% in all cases, which was a primary indication that the partial *N*-quaternization had occurred as planned. The quantitative estimation of the degree of quaternization (DQ) was performed by two independent methods as discussed below.

3.2.2a Estimation of the degree of quaternization (DQ)

In ^{1}H-NMR spectra of the PILs, the peak for 'N-H' protons were absent (that appeared at δ 13.2 in the case of unsubstituted PBI-BuI, Figure 3.1a). This indicated that almost all of the imidazole N-H groups were substituted by the *4-tert*-butylbenzyl group. A quantitative analysis of *N*-quaternization was performed by comparing the integration of *tert*-butyl protons of the substituent group with that of aromatic protons of PBI-BuI. Obtained values of DQ for different PILs are given in Table 3.1a. Another way of determining DQ is to estimate amount of bromide present as an anion in a particular PIL. This was determined by Volhard's method, as given in Chapter 2. For the particular PIL, obtained value of DQ by this method was closer to that obtained by ^{1}H-NMR, as given in Table 3.1a. Therefore, values obtained by both the methods were averaged and assigned in the parenthesis, while abbreviating the PIL. For example, in the case of [TBzPBI-BuI][Br]$_x$, 'x' represents the DQ of that PIL.
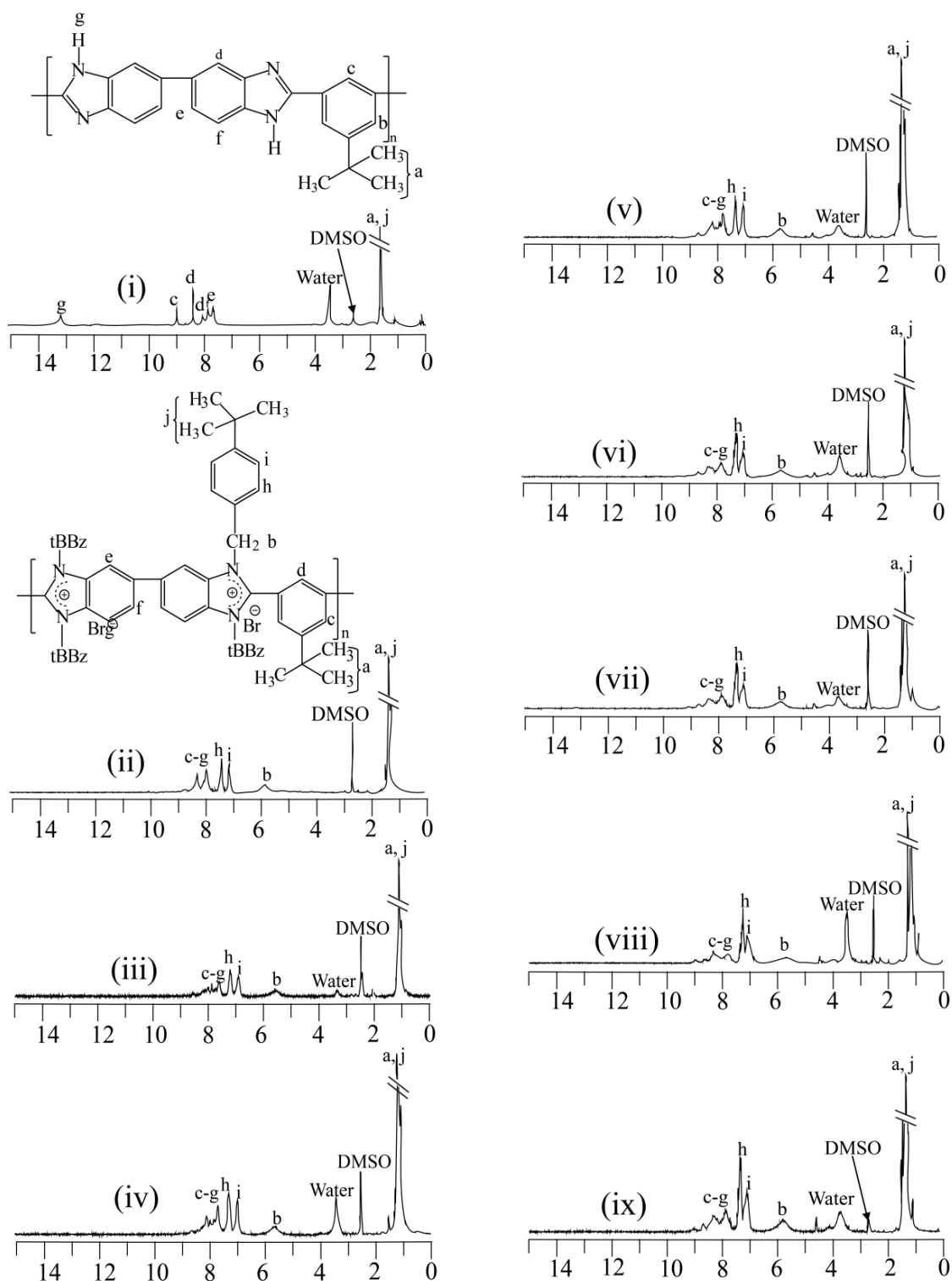
Figure 3.1a ^{1}H-NMR spectra of (i) PBI-BuI and present PILs: (ii) [TBzPBI-BuI][Br]$_8$, (iii) [TBzPBI-BuI][Br]$_{10}$, (iv) [TBzPBI-BuI][Br]$_{13}$, (v) [TBzPBI-BuI][Br]$_{18}$, (vi) [TBzPBI-BuI][Br]$_{41}$, (vii) [TBzPBI-BuI][Br]$_{56}$, (viii) [TBzPBI-BuI][Br]$_{73}$ and (ix) [TBzPBI-BuI][Br]$_{88}$.

3.3a Physical properties

3.3.1a Solvent solubility and viscosity

As could be seen from Table 3.2a, all PILs were soluble in DMF, DMAc, NMP and DMSO; in which PBI-BuI and disubstituted DBzPBI-BuI are also known to be soluble [Kumbharkar (2009)]. The DBzPBI-BuI was also soluble in chloroform. This peculiarity of solubility in CHCl$_3$ was followed further till DQ of 56% (Table 3.2a). PILs with the higher DQ showed only swelling in CHCl$_3$. Interestingly, increase in DQ improved solubility of the PILs in the polar solvents like acetonitrile and methanol.

Table 3.2a Solvent solubility of PILs.

PILs	DMF	DMAc	DMSO	NMP	CHCl$_3$	CH$_3$OH	Acetone	H$_2$O	Aceto-nitrile
[TBzPBI-BuI][Br]$_8$	++	++	++	++	++	−	−	−	−
[TBzPBI-BuI][Br]$_{10}$	++	++	++	++	++	−	−	−	−
[TBzPBI-BuI][Br]$_{13}$	++	++	++	++	++	−	−	−	±
[TBzPBI-BuI][Br]$_{18}$	++	++	++	++	++	±	−	−	±
[TBzPBI-BuI][Br]$_{41}$	++	++	++	++	++	++	−	−	±
[TBzPBI-BuI][Br]$_{56}$	++	++	++	++	++	++	−	−	+
[TBzPBI-BuI][Br]$_{73}$	++	++	++	++	±	++	−	−	+
[TBzPBI-BuI][Br]$_{88}$	++	++	++	++	±	++	−	−	+

++: Soluble at ambient temperature, +: soluble after heating at 80 ºC (reflux in case of acetone and acetonitrile), ±: partially soluble or swelling, −: insoluble.

This enhanced solubility behavior could be attributed to their high ionic character. It may be noted that PBI-BuI and DBzPBI-BuI are found to be insoluble in these volatile solvents. Such improvement in solubility of methylated PILs based on PBI-BuI was noted recently [Bhavsar (2014a)]. This aspect of PIL's solubility in lower boiling solvents could be useful in transforming them into a film form for a desired application, such as membranes.

Interestingly, most of these PILs remained hydrophobic in nature in spite they possessed distinct ionic character. This was indicated by their higher water contact angle (89 to 94 º) as given in Table 3.3a. This peculiarity could be attributed to their aromatic nature, as well as presence of the bulky aralkyl substituent, *4-tert*-butylbenzyl. It could be seen from Table 3.3a that inherent viscosity (η_{inh}) of PILs is in the range of 3.2-4.1 dL.g^{-1}. Higher η_{inh} of these PILs than that of parent PBI-BuI (η_{inh}= 1.3 dL.g^{-1}) was attributable to their polyelectrolyte nature.

Such behavior was also observed earlier for PBI based methylated PILs [Bhavsar (2014a)]. It may be noted that this crucial behavior shown by the present PILs is not really dependant on their DQ. This peculiarity could be useful in applications where polyelectrolyte behavior with low ionic content is desirable.

Table 3.3a Physical properties of PILs.

| PILs | η_{inh}[a] (dL/g) | d_{sp}[b] (Å) | ρ[c] (g/cm^3) | TGA | | Mechanical properties | | | Water contact angle (º) |
				IDT[d] (°C)	W_{900}[e] (%)	Tensile strength (MPa)	Modulus (MPa)	Elongation at break (%)	
[TBzPBI-BuI][Br]$_8$	3.2	5.18	1.092	291	47	104	2469	6.8	94
[TBzPBI-BuI][Br]$_{10}$	3.3	5.27	1.089	267	45	98	2224	7.4	90
[TBzPBI-BuI][Br]$_{13}$	3.3	5.35	1.087	252	44	89	2161	7.1	92
[TBzPBI-BuI][Br]$_{18}$	3.6	5.27	1.154	242	39	87	2253	7.7	90
[TBzPBI-BuI][Br]$_{41}$	4.1	5.24	1.158	235	37	85	2291	7.1	89
[TBzPBI-BuI][Br]$_{56}$	3.4	5.21	1.157	231	34	83	2192	9.9	89
[TBzPBI-BuI][Br]$_{73}$	3.4	5.18	1.173	227	29	80	2308	11.5	92
[TBzPBI-BuI][Br]$_{88}$	3.5	5.12	1.175	213	27	87	2136	6.7	93

[a]: Inherent viscosity determined using 0.2 g.dL^{-1} PIL solution in DMSO at 35 ºC, [b]: d-spacing obtained from WAXD pattern, [c]: density measured at 35 ºC, [d]: initial decomposition temperature, [e]: char yield at 900 °C.

3.3.2a FTIR, WAXD and density

FTIR spectra of PILs showed bands in the range of ~3600-3300 cm^{-1} attributable to the absorbed moisture (Figure 3.2aa). It was disappeared when the scan was recorded again at 180 ºC (Figure 3.2ab). This indicated that the present PILs, in spite of being hydrophobic in nature (as revealed by their high contact angle), absorb moisture due to their ionic character. For unsubstituted PBI-BuI, a broad band at ~ 3400-2400 cm^{-1} originating from N-H stretching was observed [Kumbharkar (2009)]. In the present cases (Figure 3.2ab), this band was disappeared as a result of *N*-substitution. The characteristic bands for benzimidazole in the range of 1650-1500 cm^{-1} is attributable to C=C/C=N stretching vibrations and ring modes [Musto (1993)].
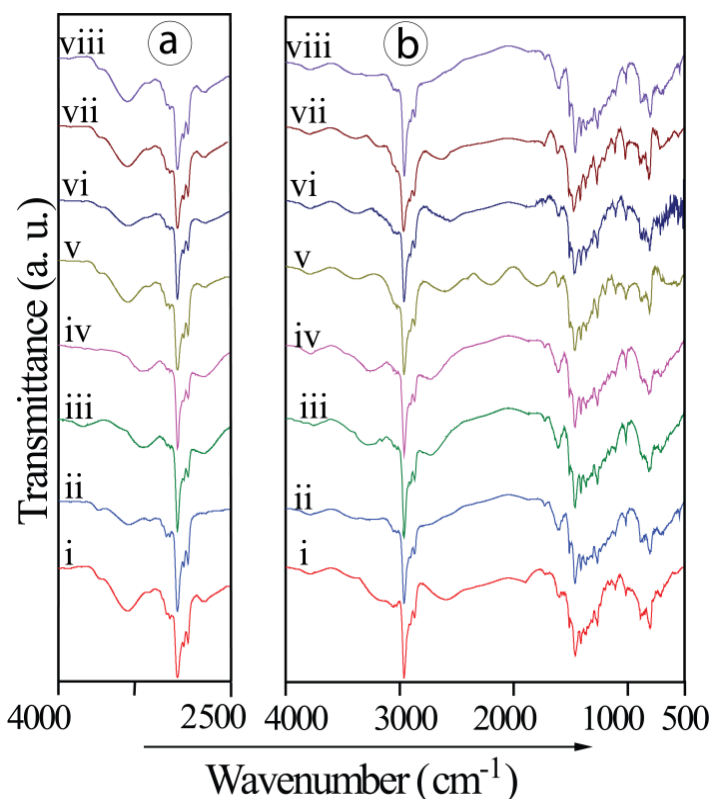
Figure 3.2a FT-IR spectra of PILs at (a) ambient and (b) 180 °C: (i) [TBzPBI-BuI][Br]$_8$,
(ii) [TBzPBI-BuI][Br]$_{10}$, (iii) [TBzPBI-BuI][Br]$_{13}$, (iv) [TBzPBI-BuI][Br]$_{18}$,
(v) [TBzPBI-BuI][Br]$_{41}$, (vi) [TBzPBI-BuI][Br]$_{56}$, (vii) [TBzPBI-BuI][Br]$_{73}$
and (viii) [TBzPBI-BuI][Br]$_{88}$.

The X-ray diffraction analysis and density were used to understand the chain packing in PIL membrane matrix. The WAXD measurements were used to determine the average intersegmental *d*-spacing (d$_{sp}$) of the PIL membranes. The WAXD pattern of these PILs (Figure 3.3a) indicated their amorphous nature, in spite they possessed ionic character. It may be noted that some of the PILs having aliphatic backbone possess some crystallinity [Bhavsar (2012), Pan (2009)]. The present PILs remained amorphous, which could be due to their fully aromatic and rigid backbone. Moreover, they have bulky aralkyl substituent on their backbone, which would inhibit ordered chain packing. The *d*-spacing (d$_{sp}$) of PILs corresponding to the amorphous peak maxima in the respective WAXD pattern are given in Table 3.3a. The d$_{sp}$ increased with an increase in DQ of PIL till 13%. This is attributable to the added bulk of *4-tert*-butylbenzyl group. Beyond this DQ, the d$_{sp}$ decreases, as shown in Figure 3.4a. This behavior showed that attractive

interactions due to the increased ionic character became dominant than the repulsive effect caused by an added bulky *4-tert*-butylbenzyl group. The variation in d_{sp} was also qualitatively supported by the variation in density that exhibited minima at DQ of ~13% (Figure 3.4a). The density of present PILs decreased till 13% DQ and beyond this, the density started increasing with DQ. Both these analyses revealed that the chain packing density is lowered at DQ of 13%. It would have been beneficial to determine fractional free volume (FFV) of these PILs, but it could not be estimated due to unavailability of vander Waal's volume of 'quaternary N' group. Any speculation made further on 'microvoids' or the 'unrelaxed volume' present in these PILs is based on the observations of d_{sp} and density variations.
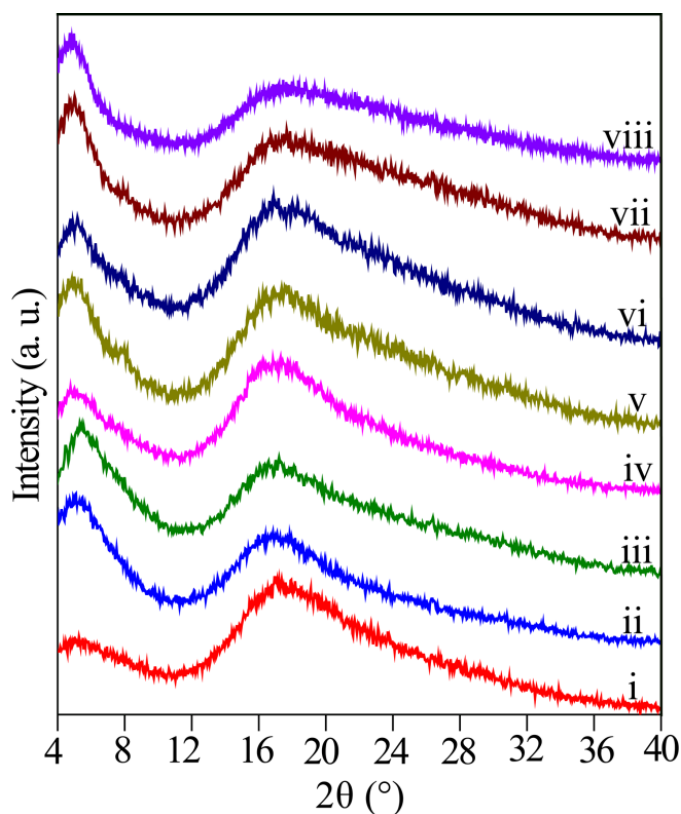
Figure 3.3a WAXD pattern of PILs: (i) [TBzPBI-BuI][Br]$_8$, (ii) [TBzPBI-BuI][Br]$_{10}$, (iii) [TBzPBI-BuI][Br]$_{13}$, (iv) [TBzPBI-BuI][Br]$_{18}$, (v) [TBzPBI-BuI][Br]$_{41}$, (vi) [TBzPBI-BuI][Br]$_{56}$, (vii) [TBzPBI-BuI][Br]$_{73}$ and (viii) [TBzPBI-BuI][Br]$_{88}$.
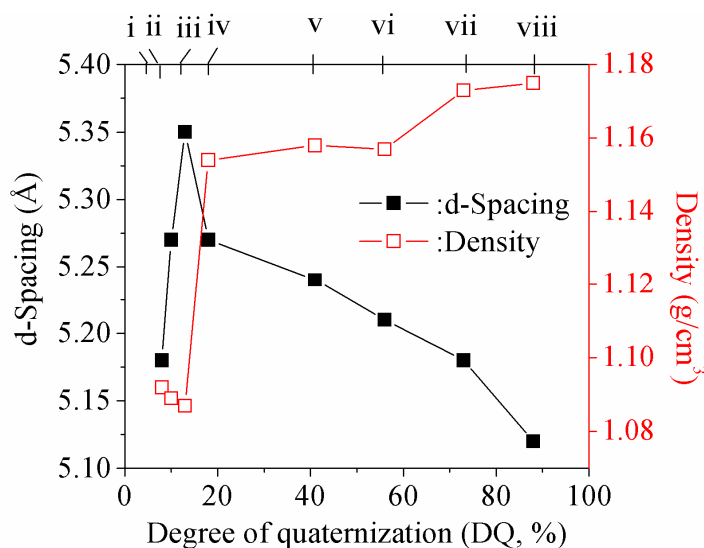
Figure 3.4a Variation in the d-spacing and density of PILs with degree of quaternization: (i) [TBzPBI-BuI][Br]$_8$, (ii) [TBzPBI-BuI][Br]$_{10}$, (iii) [TBzPBI-BuI][Br]$_{13}$, (iv) [TBzPBI-BuI][Br]$_{18}$, (v) [TBzPBI-BuI][Br]$_{41}$, (vi) [TBzPBI-BuI][Br]$_{56}$, (vii) [TBzPBI-BuI][Br]$_{73}$ and (viii) [TBzPBI-BuI][Br]$_{88}$.

3.3.3a Thermo-mechanical properties of the PILs

The TGA curves of the present PILs are shown in Figure 3.5a, which showed multistep degradation. This type of degradation behaviour could be attributed to the ionic nature of PILs. At 50 ºC, some of the PILs showed a small weight loss that might be ascribed to the absorbed moisture. Initial decomposition temperature (IDT) of the present PILs varied from 213 to 290 °C (Table 3.3a), which is considerably lower than that of PBI-BuI or DBzPBI-BuI (525 and 370 °C, respectively [Kumbharkar (2006), Kumbharkar (2009)]. As the DQ increased, a consistent decrease in IDT was observed. Such a lowering in the thermal stability of quaternized polymers than their unquaternized counterparts is known [Bhavsar (2014a), Chen (2012)]. Li et. al., also have reported that with increasing amount of the RTIL monomer, thermal stability of the resulting copolyimides was decreased [Li (2010)]. The glass transition temperature of these PILs could not be detected in DSC thermogram even after repeated cycles of heating and cooling.
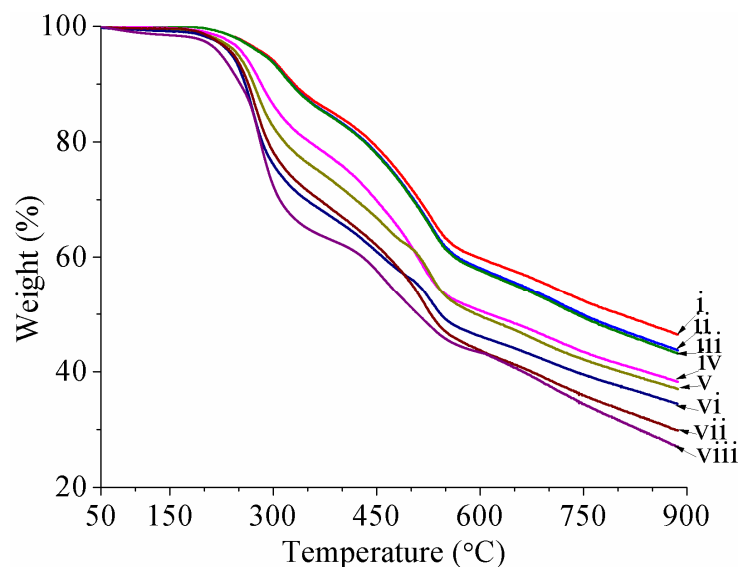
Figure 3.5a TGA curves of PILs: (i)[TBzPBI-BuI][Br]$_8$, (ii) [TBzPBI-BuI][Br]$_{10}$, (iii) [TBzPBI-BuI][Br]$_{13}$, (iv) [TBzPBI-BuI][Br]$_{18}$, (v) [TBzPBI-BuI][Br]$_{41}$, (vi) [TBzPBI-BuI][Br]$_{56}$, (vii) [TBzPBI-BuI][Br]$_{73}$ and (viii) [TBzPBI-BuI][Br]$_{88}$.

Figure 3.6a Stress-strain curves of PILs:(i) [TBzPBI-BuI][Br]$_8$, (ii) [TBzPBI-BuI][Br]$_{10}$, (iii) [TBzPBI-BuI][Br]$_{13}$, (iv) [TBzPBI-BuI][Br]$_{18}$,(v) [TBzPBI-BuI][Br]$_{41}$, (vi) [TBzPBI-BuI][Br]$_{56}$, (vii) [TBzPBI-BuI][Br]$_{73}$ and (viii) [TBzPBI-BuI][Br]$_{88}$.

Figure 3.6a presents stress-strain curves of the PIL films, while Table 3.3a summarizes their mechanical properties. It could be seen that the mechanical strength of the PILs was considerably lower than that of PBI-BuI (stress-strain curve of PBI-BuI is given as the inlay of

Figure 3.6a). The tensile strength of PBI-BuI was 128 MPa; while in case of the PILs, it was in the range of 78-104 MP (which decreased with increasing the DQ). This reduction in mechanical strength could be attributed to the absence of H-bonding in the PILs (which was present in their precursor, PBI-BuI).

3.4a Permeation properties

3.4.1a Gas permeability and selectivity

Table 3.4a Permeability coefficient (P)[a] of PILs

PILs	P_{He}	P_{H_2}	P_{O_2}	P_{N_2}	P_{CH_4}	P_{CO_2}
[TBzPBI-BuI][Br]$_8$	35.3	48.3	5.2	1.31	0.85	15.1
[TBzPBI-BuI][Br]$_{10}$	38.4	58.6	7.6	1.90	1.87	29.4
[TBzPBI-BuI][Br]$_{13}$	94.2	128.3	15.9	5.59	5.31	37.8
[TBzPBI-BuI][Br]$_{18}$	37.4	56.4	7.0	1.76	1.52	27.1
[TBzPBI-BuI][Br]$_{41}$	25.1	31.2	3.0	0.79	0.98	16.7
[TBzPBI-BuI][Br]$_{56}$	23.5	28.3	2.6	0.70	0.77	13.7
[TBzPBI-BuI][Br]$_{73}$	24.8	27.3	2.3	0.63	0.65	10.1
[TBzPBI-BuI][Br]$_{88}$	17.3	22.2	2.3	0.69	0.49	9.6

[a]: Expressed in Barrer (1 Barrer = 10^{-10} cm^3.(STP).cm.cm^{-2}.s^{-1}.cm Hg^{-1}).
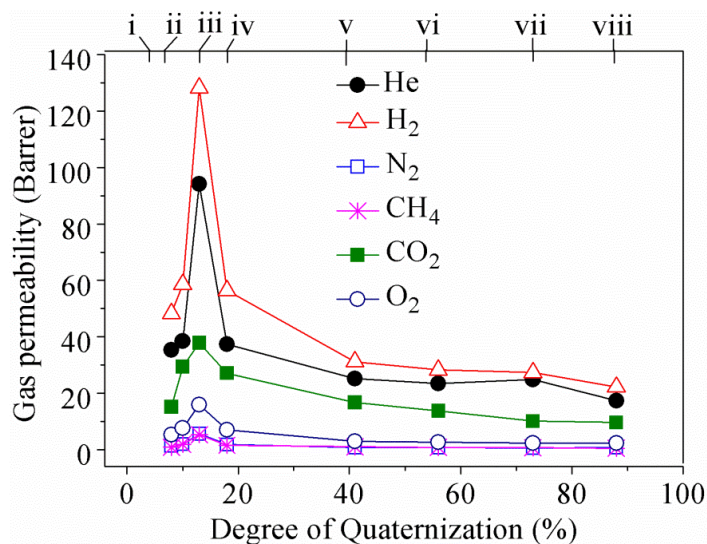
Figure 3.7a Variation in gas permeability with DQ of PILs: (i) [TBzPBI-BuI][Br]$_8$, (ii) [TBzPBI-BuI][Br]$_{10}$, (iii) [TBzPBI-BuI][Br]$_{13}$, (iv) [TBzPBI-BuI][Br]$_{18}$, (v) [TBzPBI-BuI][Br]$_{41}$, (vi) [TBzPBI-BuI][Br]$_{56}$, (vii) [TBzPBI-BuI][Br]$_{73}$ and (viii) [TBzPBI-BuI][Br]$_{88}$.

The permeability of He, H_2, N_2, O_2, CH_4 and CO_2 in the present PILs are given in Figure 3.7a. With change in DQ, remarkable variations in the gas permeation properties were observed. The permeability for all the gases increased with an increase in the DQ till 13%. Beyond this DQ, permeability starts decreasing with further increase in DQ (Table 3.4a). This is in accordance with the fact that the chain packing at DQ of 13% is looser (as indicated by the density and d_{sp} variations) than that of the PILs with either lower or higher DQ. At lower DQ, incorporation of bulky 'Bz' group would effectively loosen the chain packing, especially when all the N-H groups of PBI-BuI are already substituted with 'Bz' group and any further addition of this group by virtue of PBI-quaternization would further impose restrictions in the chain packing. At lower DQ, the ionic groups would remain incapable of inducing attractive effects, since they are localized. After certain DQ is attained (> 13%), the introduction of the ionic groups probably supersedes (in creating attractive interaction and bring chains closer) than the repulsive effect caused by bulky 'Bz' group. In other words, at higher DQ, effects of the ionic groups in inducing attractive nature are more dominant than the repulsive effects caused by similar number of bulky groups. This ultimately led to reduction in the gas permeability. The CO_2 permeability in $[TBzPBI-BuI][Br]_{13}$ is 5.6-6.8 time higher than that of common gas separation membrane materials such as Matrimid [Tin (2003)], polysulphone [McHattie (1990)] and polycarbonate [Hellums (1989)].

Table 3.5a Permselectivity (P_A/P_B) of PILs possessing partial ionic character.

PILs	P_{He}/P_{N_2}	P_{He}/P_{CH_4}	P_{H_2}/P_{N_2}	P_{H_2}/P_{CO_2}	P_{H_2}/P_{CH_4}	P_{O_2}/P_{N_2}	P_{CO_2}/P_{N_2}	P_{CO_2}/P_{CH_4}
$[TBzPBI-BuI][Br]_8$	27.0	41.5	36.9	3.2	56.8	4.0	11.5	17.8
$[TBzPBI-BuI][Br]_{10}$	20.2	20.5	30.8	2.0	31.3	4.0	15.5	15.7
$[TBzPBI-BuI][Br]_{13}$	16.9	17.7	23.0	3.4	24.2	2.8	6.8	7.1
$[TBzPBI-BuI][Br]_{18}$	21.3	24.6	32.1	2.1	37.1	4.0	15.4	17.8
$[TBzPBI-BuI][Br]_{41}$	31.8	25.6	39.5	1.9	31.8	3.8	21.1	17.0
$[TBzPBI-BuI][Br]_{56}$	33.6	30.5	40.4	2.1	36.8	3.7	19.6	17.8
$[TBzPBI-BuI][Br]_{73}$	39.4	38.2	43.3	2.7	42.0	3.7	16.0	15.5
$[TBzPBI-BuI][Br]_{88}$	25.1	35.3	32.2	2.3	45.3	3.3	13.9	19.6

Present series of the PILs followed conventional trade-off relationship, wherein [TBzPBI-BuI][Br]$_{13}$ possessing highest permeability and lowest selectivity than that of other PILs (Table 3.5a). The permeability of CO_2 and its selectivity over other gases (P_{CO_2}/P_{N_2} and P_{CO_2}/P_{CH_4}) were appreciable, especially at the middle values of DQ; in comparison to He or H_2 based selectivity. At higher DQ, the permeability of larger gases (N_2, CH_4 and CO_2) varied to a larger extent than the permeability of He and H_2, as usually observed by introduction of polar groups in glassy polymer families [Xiao (2005), Guiver (2002)].

3.4.2a Gas sorption

The gas sorption analysis in present PILs was performed in order to understand effects of incremental variations in DQ. Equilibrium gas sorption isotherms of H_2, N_2, CH_4 and CO_2 were determined at 35 °C and are shown in Figure 3.8a. These isotherms showed a typical dual-mode nature, as usually observed for glassy polymers [Kumbharkar (2006), Koros (1976)]. Gas solubility coefficients and sorption selectivity for various gas pairs was calculated at 20 atm and are given in Table 3.6a. The gas sorption coefficient in a given PIL increased in the sequence: $H_2 < N_2 < CH_4 < CO_2$. This follows the trend of increasing order of inherent condensability of these gases [Kumbharkar (2010)]. In the case of [TBzPBI-BuI][Br]$_{13}$, the CO_2 sorption was considerably higher than that of other PILs in this series. It may be noted that along with higher CO_2 sorption in [TBzPBI-BuI][Br]$_{13}$, the S_{CO_2}/S_{H_2} selectivity is also slightly higher than that of other PILs. In comparison to DBzPBI-BuI, the S_{CO_2}/S_{H_2} selectivity of this PIL exhibited ~ 31% enhancement, which is noteworthy. These observations convey synergistic balance between the bulky group substitution (responsible for free volume) and an ionic character in the PIL (responsible for enhancing CO_2 sorption) at this particular DQ. It is known that gas sorption properties of the PILs were affected by both, free volume as well as the ionic character [Bhavsar (2014c)].
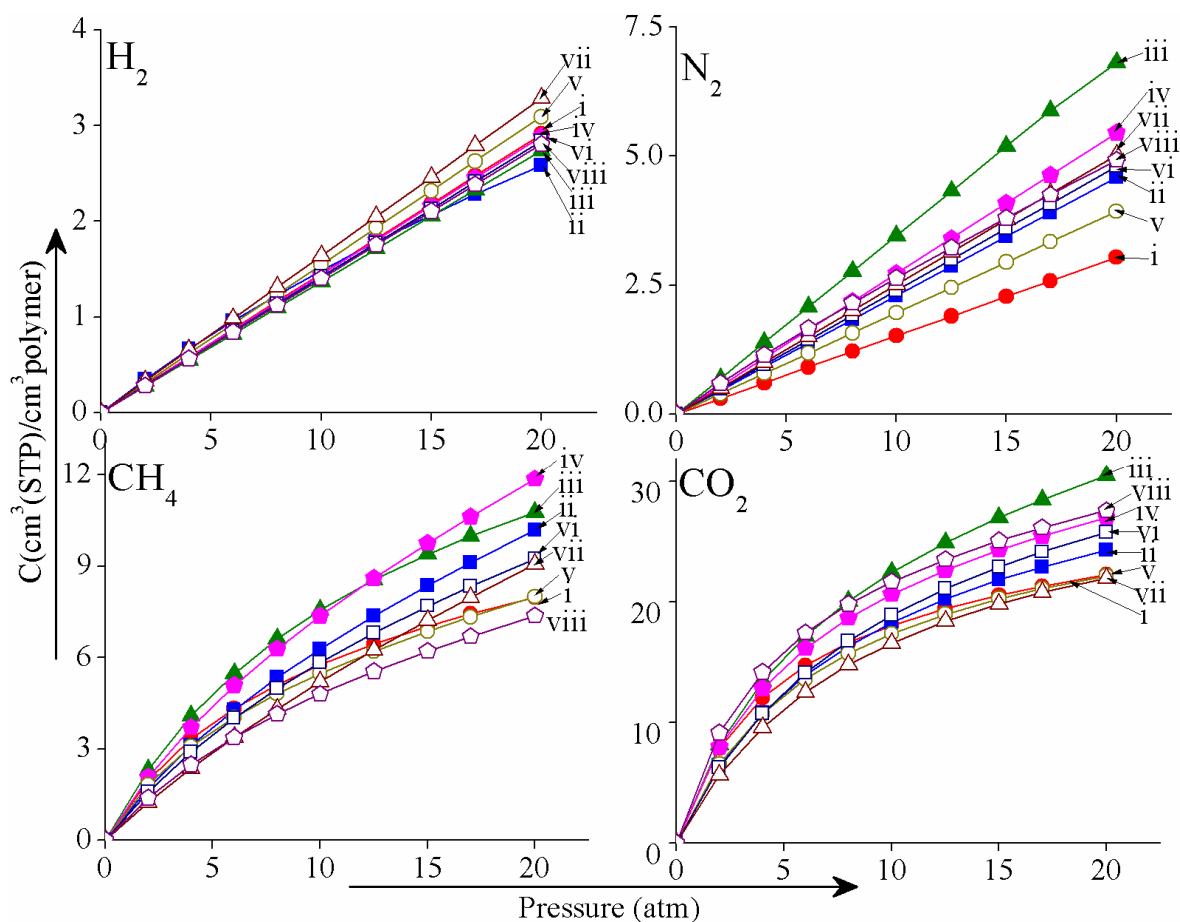
Figure 3.8a Gas sorption of PILs: (i) [TBzPBI-BuI][Br]$_8$, (ii) [TBzPBI-BuI][Br]$_{10}$, (iii) [TBzPBI-BuI][Br]$_{13}$, (iv) [TBzPBI-BuI][Br]$_{18}$, (v) [TBzPBI-BuI][Br]$_{41}$, (vi) [TBzPBI-BuI][Br]$_{56}$, (vii) [TBzPBI-BuI][Br]$_{73}$ and (viii) [TBzPBI-BuI][Br]$_{88}$.

Table 3.6a Solubility coefficient (S)[a] and solubility selectivity (S$_A$/S$_B$) of the PILs at 20 atm.

PILs	S_{H_2}	S_{N_2}	S_{CH_4}	S_{CO_2}	S_{N_2}/S_{CH_4}	S_{CO_2}/S_{H_2}	S_{CO_2}/S_{N_2}	S_{CO_2}/S_{CH_4}
[TBzPBI-BuI][Br]$_8$	0.15	0.15	0.40	1.11	0.38	7.20	7.33	2.79
[TBzPBI-BuI][Br]$_{10}$	0.13	0.23	0.51	1.22	0.45	9.43	5.29	2.39
[TBzPBI-BuI][Br]$_{13}$	0.14	0.35	0.54	1.53	0.64	11.14	4.41	2.84
[TBzPBI-BuI][Br]$_{18}$	0.14	0.27	0.59	1.35	0.46	9.37	4.95	2.28
[TBzPBI-BuI][Br]$_{41}$	0.15	0.20	0.40	1.11	0.49	7.18	5.65	2.77
[TBzPBI-BuI][Br]$_{56}$	0.14	0.24	0.46	1.29	0.52	9.08	5.37	2.79
[TBzPBI-BuI][Br]$_{73}$	0.16	0.25	0.45	1.10	0.55	6.69	4.37	2.43
[TBzPBI-BuI][Br]$_{88}$	0.14	0.25	0.37	1.38	0.68	9.86	5.52	3.73

[a]: Expressed in cm^3(STP)/cm^{3}polymer.atm.

3.4.3a Gas sorption parameters

Gas sorption parameters (k_D, C'_H and b) for the present PILs obtained (using Eq. 5 as given in chapter 2) are presented in Table 3.7a.

Table 3.7a Dual-mode sorption parameters[a] for PILs.

Polymer	H_2			N_2			CH_4			CO_2		
	k_D	C'_H	b	k_D	C'_H	B	k_D	C'_H	b	k_D	C'_H	b
[TBzPBI-BuI][Br]$_8$	0.14	1.8	9.2×10^{-5}	0.15	0.85	5.2×10^{-5}	0.086	8.6	0.13	0.12	24.3	0.23
[TBzPBI-BuI][Br]$_{10}$	0.13	1.6	7.2×10^{-4}	0.23	0.73	7.4×10^{-4}	0.26	7.7	0.09	0.13	30.0	0.13
[TBzPBI-BuI][Br]$_{13}$	0.14	0.23	1.4×10^{-3}	0.35	3.8	4.7×10^{-5}	0.26	14.9	0.09	0.36	30.5	0.16
[TBzPBI-BuI][Br]$_{18}$	0.14	0.93	9.2×10^{-5}	0.27	4.7	1.2×10^{-4}	0.32	8.0	0.11	0.23	28.7	0.18
[TBzPBI-BuI][Br]$_{41}$	0.15	0.53	1.1×10^{-4}	0.20	2.3	3.0×10^{-4}	0.15	6.5	0.15	0.06	28.2	0.15
[TBzPBI-BuI][Br]$_{56}$	0.14	1.12	2.7×10^{-4}	0.24	0.10	1.9×10^{-3}	0.17	9.8	0.07	0.13	34.0	0.11
[TBzPBI-BuI][Br]$_{73}$	0.16	0.48	4.6×10^{-5}	0.25	0.43	1.2×10^{-4}	0.26	7.2	0.05	0.01	32.0	0.11
[TBzPBI-BuI][Br]$_{88}$	0.14	1.30	7.0×10^{-4}	0.21	1.03	0.09	0.13	7.2	0.09	0.25	27.7	0.23

[a]: k_D is expressed in $cm^3(STP).cm^{-3}polymer.atm^{-1}$, C'_H is expressed in $cm^3(STP).cm^{-3}polymer$, b is expressed in atm^{-1}.

It could be seen that the Henry's solubility coefficient 'k_D', ascribed to gas dissolution in the rubbery state was low for all the gases (Table 3.7a), which is attributable to the glassy nature of these PILs. The Langmuir affinity constant b is the ratio of rate constants of sorption and desorption processes and characterizes the sorption affinity for particular gas-polymer system [Vieth (1976), Kanehashi (2005)]. It was low for H_2 and N_2, than that of CH_4 and CO_2. The C'_H is the hole-filling constant or the capacity parameter, which represents the maximum amount of penetrant sorbed into microvoids or free volume of the polymer matrix [Vieth (1976), Kanehashi (2005)]. For all PILs, C'_H was higher for CO_2 than that of other gases. Both, C'_H and 'b' increased with the increasing order of gas condensability for any particular PIL. As could be seen from Figure 3.8a, the sorption isotherm of hydrogen and nitrogen seems linear, in spite they following the dual mode sorption isotherm.

3.4.4a Gas diffusivity

The pure gas diffusivity (D) for H_2, N_2, CH_4 and CO_2 was determined by using Eq. 2.6 as given in chapter 2) and diffusivity selectivity for various gas pairs are given in Table 3.8a. It could be seen that the gas diffusivity for all the gases was increased with increase in DQ up to

13%. Beyond this DQ, diffusivity started lowering with further increase in DQ. This variation in gas diffusivity was very similar to that observed in gas permeability as given in Section 3.4.1a. These variations with respect to DQ are considerably higher than those observed in solubility coefficient (Table 3.6a). In other words, systematic variation in DQ has its profound effect on gas diffusivity, rather than the gas sorption. This is indicative that glassy nature of the present PILs would be more dominating in governing gas permeation properties than their IL–character.

Table 3.8a Diffusivity coefficient (D)[a] of the PILs.

PILs	D_{H_2}	D_{N_2}	D_{CH_4}	D_{CO_2}	D_{H_2}/D_{N_2}	D_{H_2}/D_{CO_2}	D_{N_2}/D_{CH_4}	D_{CO_2}/D_{N_2}	D_{CO_2}/D_{CH_4}
[TBzPBI-BuI][Br]$_8$	237.6	6.6	1.6	10.3	36.2	23.0	4.1	1.6	6.4
[TBzPBI-BuI][Br]$_{10}$	345.3	6.3	2.8	18.4	55.0	18.8	2.3	2.9	6.6
[TBzPBI-BuI][Br]$_{13}$	711.9	12.3	7.5	18.8	58.0	37.8	1.6	1.5	2.5
[TBzPBI-BuI][Br]$_{18}$	297.4	4.9	2.0	15.3	60.6	19.5	2.5	3.1	7.8
[TBzPBI-BuI][Br]$_{41}$	153.5	3.1	1.9	11.4	50.2	13.4	1.6	3.7	6.1
[TBzPBI-BuI][Br]$_{56}$	151.6	2.2	1.3	8.1	68.4	18.8	1.8	3.7	6.4
[TBzPBI-BuI][Br]$_{73}$	126.4	1.9	1.1	7.0	66.3	18.1	1.8	3.7	6.4
[TBzPBI-BuI][Br]$_{88}$	120.5	2.1	1.0	5.3	57.5	22.8	2.1	2.5	5.3

[a]: Expressed in 10^{-8} cm^2.s^{-1}.
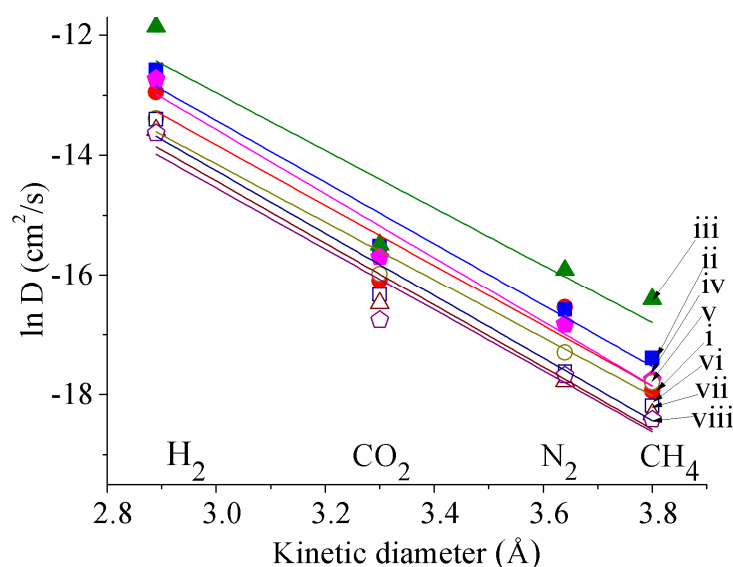
Figure 3.9a Correlation of kinetic diameter of gases with diffusion coefficient in PILs:
(i)[TBzPBI-BuI][Br]$_8$, (ii) [TBzPBI-BuI][Br]$_{10}$, (iii) [TBzPBI-BuI][Br]$_{13}$,
(iv) [TBzPBI-BuI][Br]$_{18}$, (v) [TBzPBI-BuI][Br]$_{41}$, (vi) [TBzPBI-BuI][Br]$_{56}$,
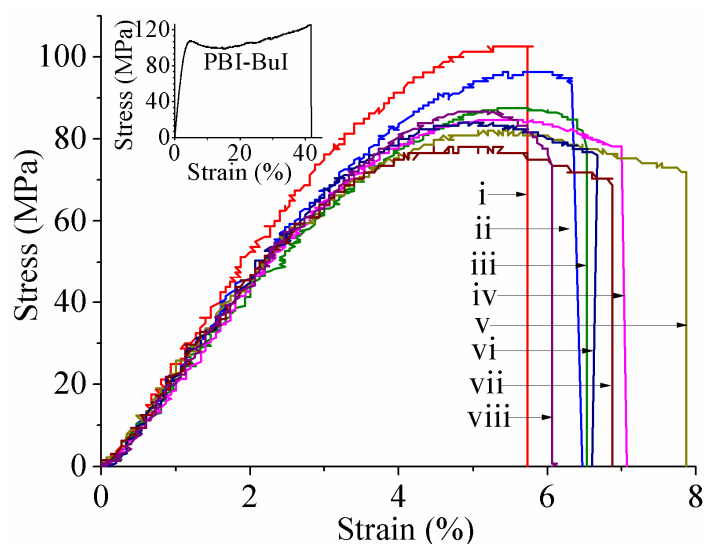(vii) [TBzPBI-BuI][Br]$_{73}$ and (viii) [TBzPBI-BuI][Br]$_{88}$.

As could be seen from Figure 3.9a, the diffusivity coefficient correlated well with the kinetic diameter of gases. It was observed that most of the PILs exhibited higher gas diffusivity than their parent PBI-BuI, as studied earlier [Bhavsar (2014b), Koros (1976)]. The diffusivity of H_2 in PIL with 13% DQ was 27.6 times higher than of PBI-BuI. This conveys that the path followed (systematic variation in DQ) could lead to assertive effects on the permeation properties. This increase in diffusivity was associated with decrease in the diffusivity selectivity.

3.5a Conclusions

The degree of PBI-quaternization (DQ) in a series of the PILs was systematically varied in order to study concurrent effects of bulk of the substituent and induced ionic liquid (IL) character on their physical and gas permeation properties. A substitution by bulky *4-tert-*butylbenzyl group led to lowering in packing density till DQ of merely 13%, beyond which, the induced ionic content took precedence in governing the packing density of the polymer matrix. A sluggish solvent solubility of PBI was enhanced at higher DQ (IL character), wherein these PILs became soluble even in methanol and acetonitrile. Owing to induced ionic character, thermal stability of these PILs was lower than that of their parent PBI-BuI. Variations observed in packing density were reflected in the gas permeation properties. At lower DQ of 13%, the gas diffusivity and permeability were higher than that of other members of the family. With variation in DQ, effects of induced ionic content on CO_2 sorption though were promising; variations in diffusivity were more prominent. The present work indicates that there is a need to enhance free volume in the polymer as well as IL character, simultaneously, in order to obtain their better benefits in improving CO_2 permeation characteristics in the PILs.

Part B: Blend membranes based on polymeric ionic liquid and DBzPBI-BuI: Gas permeation studies

3.2b Synthesis and blend preparation

3.2.1b Synthesis of DBzPBI-BuI and [TBzPBI-BuI][Br]

The details on synthesis of PBI-BuI and [TBzPBI-BuI][Br][88] are given in Chapter 2. The synthesis of DBzPBI-BuI was successfully performed in a single step by in-situ preparation of its Na-salt, followed by *N*-substitution by 2 equivalent *4-tert*-butylbenzyl bromide. The *N*-substitution of a PBI-BuI does occur by the reaction between its Na-salt and *4-tert*-butylbenzyl bromide [Kumbharkar (2009)]. Yield of the obtained polymers was > 90%, which was a primary indication that the *N*-substitution had occurred as planned. The quantitative estimation of the degree of substitution was performed by ^{1}H-NMR methods as discussed in section 3.2.2b. Obtained spectra have been shown in Figure 3.1b.

3.2.2b Degree of *N*-substitution of PBI-BuI

In ^{1}H-NMR spectra of the DBzPBI-BuI, the peak for 'N-H' protons were absent (that appeared at δ 13.2 in the case of unsubstituted PBI-BuI, Figure 3.1b). This indicated that almost all of the imidazole N-H groups were substituted by the *4-tert*-butylbenzyl group. A quantitative analysis of *N*-substitution was performed by comparing the integration of *tert*-butyl protons of the substituent group with that of aromatic protons of PBI-BuI.
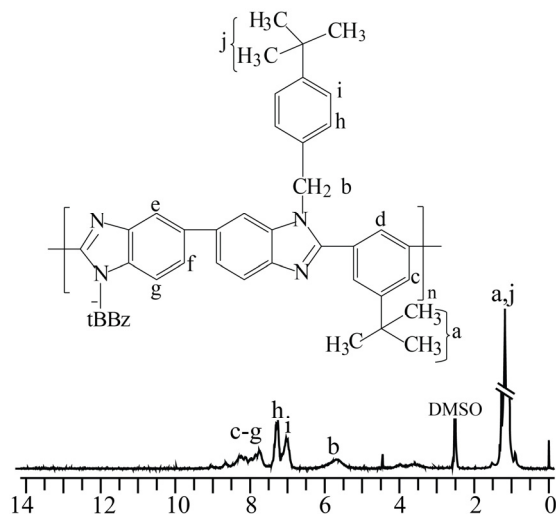
Figure 3.1b NMR of DBzPBI-BuI.

3.2.3b Preparation of blend membranes

The blend membranes possessing varying content of [TBzPBI-BuI][Br]$_{88}$ and DBzPBI-BuI have been prepared by solution casting method in DMAc solvent; wherein the free-standing yellowish transparent films were obtained. The ratio of [TBzPBI-BuI][Br]$_{88}$ and DBzPBI-BuI were varied as 100:0, 90:10, 75:25, 60:40, 45:55, 30:70, 20:80, 10:90, and 0:100. The formed blend membranes appeared transparent, without any phase separation.

3.3b Physical properties

3.3.1b Solvent solubility and viscosity

The DBzPBI-BuI was soluble in DMF, DMAc, NMP and DMSO and even in chloroform as described by Kumbharkar et. al. [Kumbharkar (2009)]. The TBzPBI-BuI was also soluble in DMF, DMAc, NMP and DMSO but not in chloroform as described in part A. This PIL showed only swelling in CHCl$_3$. Consequently, blend membranes were casted in DMAc.

3.3.2b FTIR spectra of blend membranes

The FTIR spectra of all the blend membranes exhibited typical bands corresponding to benzimidazole of PBI (1430, 1600 and 1620 cm^{-1}) (Figure 3.2b) which are attributable to C=C/C=N stretching vibrations and ring modes [Musto (1992)]. FT-IR analysis showed bands, at $\sim$ 3300 and $\sim$ 3600 cm^{-1} (Figure 3.2b). The nature of these bands was different than the broad band appeared at 2400–3500 cm^{-1} for unsubstituted PBI, attributable to N-H stretching. In case of substituted PBI, the band appearing at $\sim$3300 cm^{-1} could be attributed to the sorbed moisture, which could be assigned to hydrogen bonding between imidazole 'N' and water molecules [Kumbharkar (2009)]. The presence of water was also supported by a band at $\sim$3600 cm^{-1}, observed for all the polymers, attributable to the O-H stretching of absorbed water. In the FTIR spectra, all the bands were present related to both the polymer. However, the structure of DBzPBI-BuI and [TBzPBI-BuI][Br]$_{88}$ are very much similar. Thus, it could not possible to define the miscibility and homogenous nature of blend membranes by just FTIR analysis.
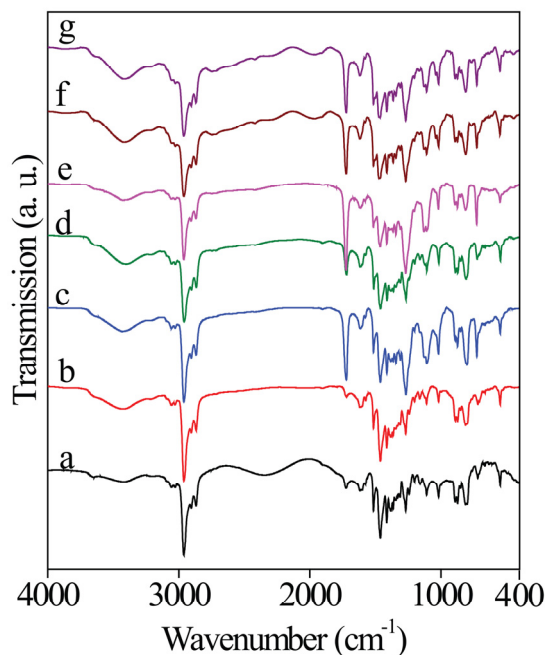
Figure 3.2b FTIR spectra of the blend membranes.

3.3.3b WAXD pattern and density of blend membranes

The X-ray diffraction spectra and density estimation were used to understand the chain packing in blend membrane matrix. The d_{sp} of PILs corresponding to the amorphous peak maxima in the respective WAXD pattern are given in Table 3.1b. The WAXD pattern of these PILs (Figure 3.3b) indicated their amorphous nature; in spite them possessing ionic character. All the blend membranes were found amorphous in nature and the value of d_{sp} was also very close to each other. This could be because both the precursor polymers, DBzPBI-BuI and [TBzPBI-BuI][Br]$_{88}$ were amorphous in nature and possess almost similar d_{sp}. Moreover, the d_{sp} of DBzPBI-BuI was 5.22 [Kumbharkar (2010)], while the d_{sp} of [TBzPBI-BuI][Br]$_{88}$ was 5.12 [Table 3.3a], both the values being close to each other. The density of blend membranes was determined in decaline, as it showed very low sorption (< 0.01 % after 1 hr) in the membrane samples. The obtained density values are given in Table 3.1b. The density of membranes increased with a gradually increase of PIL content in the blend. This could be due to the increased ionic character in the blend as [TBzPBI-BuI][Br]$_{88}$ has higher density than that of DBzPBI-BuI. It could be seen from Table 3.1b that the inherent viscosity (η_{inh}) of blends is in the range of 2.0-3.5 dL.g^{-1}. This higher viscosity of the blend as compared to DBzPBI-BuI could be

due to the PIL component. The high viscosity of PBI based PILs than their non-quternized counterpart was observed previously due to their polyelectrolyte nature [Bhavsar (2014a)].
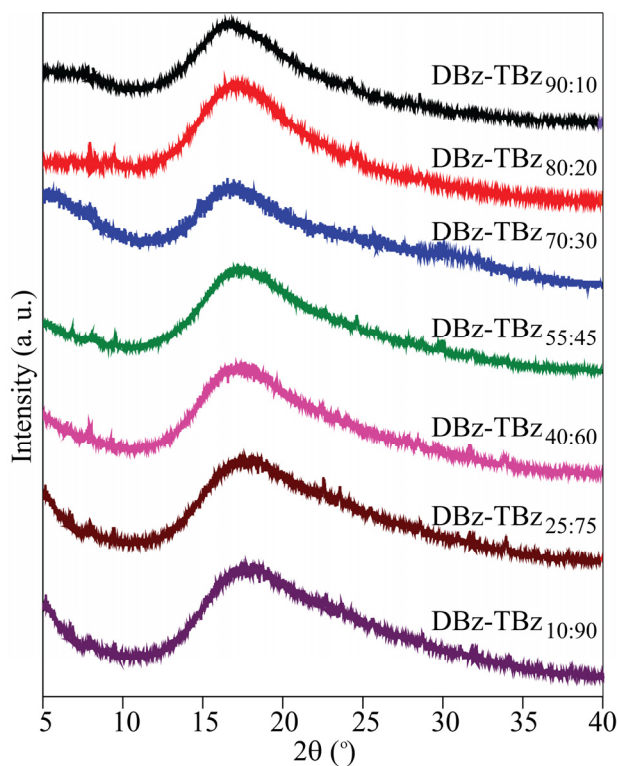
Figure 3.3b WAXD patterns of the blend membranes.

Table 3.1b Physical properties of blend.

| Blend membranes | η_{inh}^{a} (dL.g^{-1}) | d_{sp}^{b} (Å) | ρ^{c} (g/cm^3) | TGA | | T_g^{f}(°C) |
				IDT^{d} (°C)	W$_{900}^{e}$ (%)	
^{g}DBz-TBz$_{100:00}$	2.0	5.22	1.097	370	53	370
DBz-TBz$_{90:10}$	2.6	5.27	1.124	365	51	305
DBz-TBz$_{80:20}$	2.9	5.21	1.134	360	50	287
DBz-TBz$_{70:30}$	2.6	5.24	1.144	270	45	285
DBz-TBz$_{55:45}$	2.5	5.15	1.149	260	40	272
DBz-TBz$_{40:60}$	2.7	5.21	1.152	255	37	298
DBz-TBz$_{25:75}$	2.3	5.15	1.156	240	34	265
DBz-TBz$_{10:90}$	2.8	5.03	1.165	237	30	260
^{h}DBz-TBz$_{00:100}$	3.5	5.12	1.175	213	27	-

^{a}: Inherent viscosity determined using 0.2 g.dL^{-1} blend membrane solution in DMSO at 35 ºC, ^{b}: d-spacing obtained from WAXD pattern, ^{c}: density measured at 35 ºC, ^{d}: initial decomposition temperature, ^{e}: char yield at 900 °C, ^{f}: T$_g$ obtained by DMA ^{g}: Kumbharkar (2010), ^{h}: taken from Section 3.3a.

3.3.4b Thermal properties of blend membranes

The TGA curves of the present blend membranes are shown in Figure 3.4b. A multistep degradation pattern was observed. This type of degradation behaviour could be attributed to the ionic nature of PIL present in the blend membranes. Initial decomposition temperature (IDT) of blend membranes varied from 237 to 365 °C (Table 3.1b), which is considerably lower than that of DBzPBI-BuI, but was higher than that of [TBzPBI-BuI][Br]$_{88}$ (370 and 213 °C, respectively [Kumbharkar (2009) and part A]. As the amount of PIL increased in the blend, a consistent decrease in the IDT was observed. This type of variation in the thermal stability was also observed in PILs possessing partial ionic character [Section 3.3.3a].
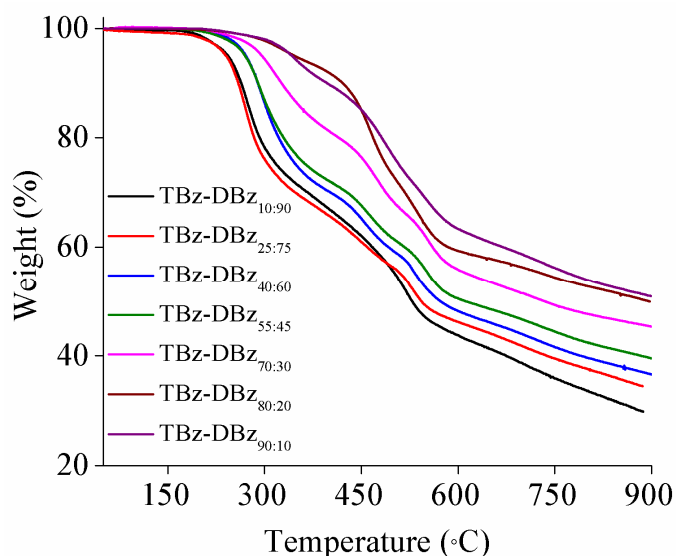
Figure 3.4b TGA curves of the blend membranes.

The glass transition temperature (T$_g$) of these PILs could not be detected in DSC thermogram, even after repeated cycles of heating and cooling. Thus, dynamic mechanical analysis (DMA) was employed to determine the T$_g$. Variation in tan δ with temperature is shown in Figure 3.5b. All the blend membranes showed T$_g$ in the range of 260-305 °C (Table 3.1b). A gradual decrease in T$_g$ was observed with increasing amount of PIL content in the blend membrane. It is worth to note that all the blends showed single T$_g$, which indicated the miscibility of both the components.
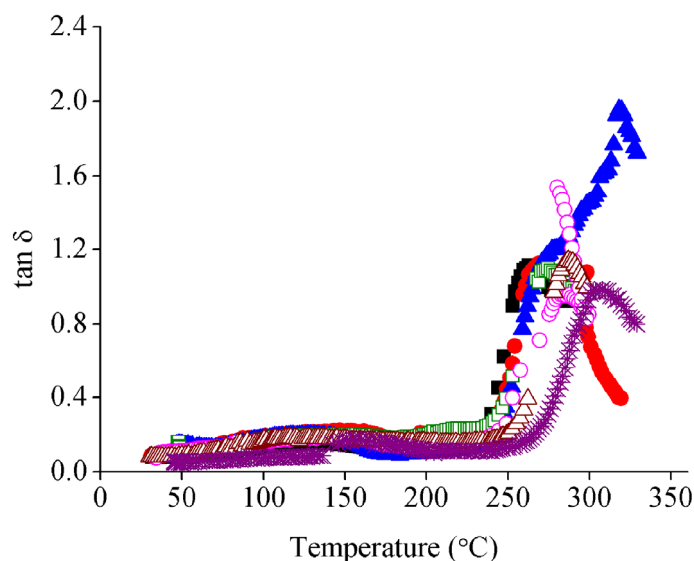
Figure 3.5b DMA curves of the blend membranes.

3.4b Gas permeation of blend membranes

The permeability of He, H_2, N_2, O_2, CH_4 and CO_2 in the present blend membranes are given in Table 3.2b and Figure 3.6b.

Table 3.2b Permeability coefficient (P)[a] of blend membranes.

Blend membranes	P_{He}	P_{H_2}	P_{O_2}	P_{N_2}	P_{CH_4}	P_{CO_2}
[b]DBz-TBz$_{100:00}$	38.3	46.5	6.3	1.5	1.37	21.3
DBz-TBz$_{90:10}$	51.3	69.1	10.4	2.6	2.2	30.8
DBz-TBz$_{80:20}$	49.8	64.5	9.8	2.5	1.9	28.7
DBz-TBz$_{70:30}$	37.8	52.2	6.9	1.7	1.2	20.5
DBz-TBz$_{55:45}$	39.9	55.4	6.9	1.7	1.4	18.7
DBz-TBz$_{40:60}$	35.3	44.3	5.4	1.6	1.34	16.5
DBz-TBz$_{25:75}$	35.3	47.5	5.1	1.6	1.32	14.9
DBz-TBz$_{10:90}$	31.9	43	4.6	1.4	1.19	13.5
[c]DBz-TBz$_{00:100}$	17.3	22.2	0.69	2.3	0.49	9.6

[a]: Expressed in Barrer (1 Barrer = 10^{-10} cm^3.(STP).cm.cm^{-2}.s^{-1}.cm Hg^{-1}), [b]: Kumbharkar (2010), [c]: taken from part A.

With the increasing amount of PIL in the blend, significant variations in the gas permeation properties were observed. The permeability coefficient (P) for all the gases increased with an increase in the PIL content in the blend till only 10%. This can be better visualized from

Figure 3.6b. Beyond this amount of PIL content, permeability starts decreasing with further increase of PIL in the blend.
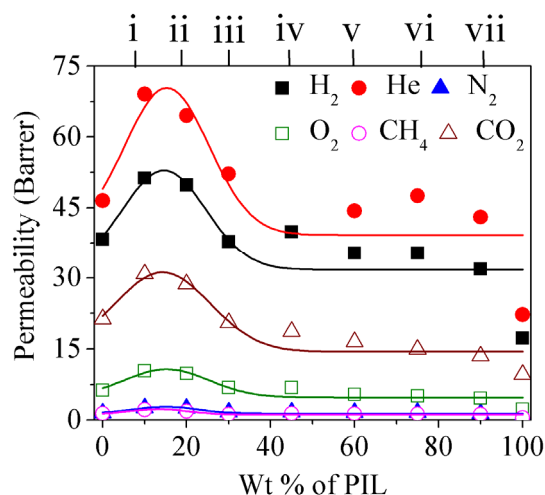
Figure 3.6b Variation in gas permeability with PIL [TBzPBI-BuI][Br]$_{88}$ in the blend membranes.

The higher gas permeability in DBz-TBz$_{90:10}$ could be because of loosening in the chain packing density, as also supported by its higher d$_{sp}$ and low density. This is in accordance with the earlier observation, wherein PILs possessing partial ionic character (part A) possessed similar behaviour. In case of PILs possessing partial ionic character, the highest permeability was observed at 13% DQ, than that of the PILs with either lower or higher DQ. This further confirms the hypothesis that at lower amount of PIL content in the blend, chain packing would loosen effectively. At lower PIL content in the blend, the ionic groups would remain incapable of inducing attractive effects, since they are localized. After certain amount of loading of PIL in the blend is attained (~ 10%), the introduction of the ionic groups probably supersedes (in creating attractive interaction and bring chains closer) than the repulsive effect caused by Bz groups. In other words, at higher loading of PIL in the blend, attractive nature is more dominant due to more ionic groups. This ultimately led to reduction in the gas permeability coefficient. This study revealed similar result of variation in gas the permeation as observed in case of PILs possessing partial ionic character (Section 3.4a); although the extent of variation in GP was high in earlier case. This could be because of distribution of Bz group and ionic species in the first case occurred more symmetrically which could not be possible in blend membrane.

Table 3.3b Permselectivity (P_A/P_B) of blend membranes.

Blend membranes	P_{He}/P_{N_2}	P_{He}/P_{CH_4}	P_{H_2}/P_{N_2}	P_{H_2}/P_{CO_2}	P_{H_2}/P_{CH_4}	P_{O_2}/P_{N_2}	P_{CO_2}/P_{N_2}	P_{CO_2}/P_{CH_4}
[b]DBz-TBz$_{100:00}$	5.36	28.0	30.8	2.2	33.9	4.2	14.1	15.6
DBz-TBz$_{90:10}$	9.73	23.3	26.6	2.2	31.4	4.0	11.9	14.0
DBz-TBz$_{80:20}$	9.92	26.2	25.8	2.3	34.0	3.9	11.5	15.1
DBz-TBz$_{70:30}$	2.24	31.5	30.7	2.6	43.5	4.1	12.1	17.1
DBz-TBz$_{55:45}$	3.47	28.5	32.6	3.0	39.6	4.1	11.0	13.4
DBz-TBz$_{40:60}$	2.06	26.3	27.7	2.7	33.1	3.4	10.3	12.3
DBz-TBz$_{25:75}$	2.06	26.7	29.7	3.2	36.0	3.2	9.3	11.3
DBz-TBz$_{10:90}$	2.79	26.8	30.7	3.2	36.1	3.3	9.6	11.3
[c]DBz-TBz$_{00:100}$	5.07	35.3	32.2	2.3	45.3	3.3	13.9	19.6

Present series of the blend membranes showed good permeability and appreciable selectivity (Table 3.3b). The selectivity of DBz-TBz$_{70:30}$ was appreciable, especially with CO_2 and H_2 over other gases (P_{CO_2}/P_{N_2}, P_{CO_2}/P_{CH_4} and P_{H_2}/P_{CO_2}, P_{H_2}/P_{CH_4}).

3.5b Conclusions

Seven blend membranes were prepared with different blend ratio of DBzPBI-BuI and [TBzPBI-BuI][Br]$_{88}$ in order to study effect of blending of PBI and PIL (inducing ionic character externally). The viscosity increased with increasing ionic content in the blend. The thermal stability of these blend membranes was lower than that of DBzPBI-BuI. All the blend components showed single T_g, which support the homogenous blend formation. The maximum gas permeability was observed at 10% loading of [TBzPBI-BuI][Br]$_{88}$ in the blend. This could be due to lowering in packing density of this blend, as was observed by increase in d_{sp}. This work supports the results which were observed in case of PILs possessing partial ionic character [part A].

Chapter 4

PILs possessing partial ionic liquid character: Effects of anion exchange on their physical and gas permeation properties

4.1 Preamble

A family of PILs possessing varying degree of quaternization (DQ) of PBI-BuI exhibited interesting variations in their permeation properties, due to concurrent effects of increasing bulk and ionic character [Chapter 3]. Gas permeability showed maxima at PBI-degree of quaternization (DQ) of just 13%, but the selectivity of various gas pairs were lowest within the series, as could be anticipated. The two immediate neighboring PILs possessing 10 and 18% DQ, (viz., [TBzPBI-BuI][Br]$_{10}$ and [TBzPBI-BuI][Br]$_{18}$, respectively) exhibited good combination of permeability and selectivity. These PILs possessed bromide as an anion. It is well known that by variation of anion, CO_2 permeation (especially sorption) properties can be improved in PILs [Mecerreyes (2011), Bhavsar (2012, 2014c), Yuan (2013), Shaligram (2015)]. It is thus worth to examine effects of variation in anion in PILs possessing partial ionic character (esp. [TBzPBI-BuI][Br]$_{10}$ and [TBzPBI-BuI][Br]$_{18}$) on their selectivity performance (especially CO_2 based), and became the objective of this study. Anions (Tf$_2$N$^-$, BF$_4$$^-$ and Ac$^-$) that are known to improve CO_2 sorption characteristics in PILs [Mecerreyes (2011), Yuan (2013), Bhavsar (2012, 2014c)] were chosen for bromide exchange of [TBzPBI-BuI][Br]$_{10}$ and [TBzPBI-BuI][Br]$_{18}$. Investigations towards physical, CO_2 sorption and permeation properties of resulting PILs are presented.

4.2 Anion exchange

PILs with high degree of anion exchange could be obtained in both the cases, viz., [TBzPBI-BuI][Br]$_{10}$ and [TBzPBI-BuI][Br]$_{18}$ using Tf$_2$N$^-$, BF$_4$$^-$ and Ac$^-$ as anion. The solvent used for metathesis (anion exchange reaction) was DMAc. The potential of using Tf$_2$N$^-$ and BF$_4$$^-$ as anion towards improving CO_2 sorption is well established [Mecerreyes (2011), Yuan

(2013), Bhavsar (2014c), Shaligram (2015)]; while Ac¯ was chosen based on its excellent sorption characteristics observed in our previous study on PILs [Bhavsar (2012)]. In order to achieve maximum possible exchange of Br¯ by the chosen anion, 5 molar equivalents of the respective salt was used. Formed byproduct, LiBr and NaBr could be easily separated from the polymer by just precipitating the reaction mixture in water. Obtained PILs were designated based on their structural features (cation and anion), as presented in Table 4.1 The obtained anion exchange was appreciable ($\geq$ 95%), as confirmed by Volhard's analysis (Table 4.1).

Table 4.1 Physical properties of PILs.

PILs	Bromide exchange (%)	η_{inh}[a] $(dL.g^{-1})$	d_{sp}[b] (Å)	ρ[c] $(gm.cm^{-3})$	Thermal properties		
					IDT[d] (°C)	W_{900}[e] (%)	T_g (°C)[f]
[TBzPBI-BuI][Tf$_2$N]$_{10}$	96	3.4	5.35	1.084	409	25	278
[TBzPBI-BuI][BF$_4$]$_{10}$	95	3.6	5.32	1.154	377	33	290
[TBzPBI-BuI][Ac]$_{10}$	97	1.8	5.19	1.108	265	51	-
[TBzPBI-BuI][Tf$_2$N]$_{18}$	95	3.4	5.38	1.110	411	50	280
[TBzPBI-BuI][BF$_4$]$_{18}$	96	3.8	5.31	1.140	291	47	270
[TBzPBI-BuI][Ac]$_{18}$	97	2.9	5.32	1.126	244	41	-

[a]: Inherent viscosity determined using 0.2 $g.dL^{-1}$ solution in DMSO at 35 °C, [b]: d-spacing obtained from WAXD, [c]: density measured at 35 °C, [d]: initial decomposition temperature, [e]: char yield at 900 °C, [f]: T_g obtained from DMA.

4.3   Physical properties

4.3.1   Solvent solubility, spectral characterizations and density

Table 4.2 Solvent solubility of PILs.

PILs	DMF	DMAc	DMSO	NMP	CHCl$_3$	CH$_3$OH	Acetone	H$_2$O	Aceto-nitrile
[TBzPBI-BuI][Tf$_2$N]$_{10}$	+	+	+	+	+	−	−	−	±
[TBzPBI-BuI][BF$_4$]$_{10}$	+	+	+	+	+	−	±	−	−
[TBzPBI-BuI][Ac]$_{10}$	+	+	+	+	+	−	−	±	±
[TBzPBI-BuI][Tf$_2$N]$_{18}$	+	+	+	+	+	−	±	−	±
[TBzPBI-BuI][BF$_4$]$_{18}$	+	+	+	+	+	−	−	−	−
[TBzPBI-BuI][Ac]$_{18}$	+	+	+	+	+	−	−	±	−

+: Soluble at ambient, ±: partially soluble or swelling, −: insoluble at 80 °C while stirring for 8 h (reflux in case of acetone and acetonitrile).

All PILs were found to be soluble in DMF, DMAc, NMP and DMSO (Table 4.2). Moreover, these PILs were also soluble in CHCl$_3$. Such a high solubility of present PILs in lower boiling solvents could be useful in transforming them easily into a film form for the desired application, such as membranes. It could be seen from Table 4.1 that inherent viscosity (η_{inh}) of PILs is in the range of 1.8-3.8 dL.g^{-1}. The high η_{inh} suggests their polyelectrolyte nature, as also observed previously for PBI-based PILs [Bhavsar (2014a), Chapter 3].

FTIR spectra of PILs scanned at ambient temperature showed a broad band at ~3610 cm^{-1} attributable to the sorbed moisture (Figure 4.1a). Intensity of this band was generally higher for PILs with Ac$^-$ as the counterion and was lower for those with hydrophobic BF$_4^-$ or Tf$_2$N$^-$ as the counter anion. This band was disappeared when the IR scans were recorded at 180 °C (Figure 4.1b) owing to the elimination of moisture at higher temperature.

Figure 4.1 FT-IR spectra of PILs recorded at (a) ambient and (b) 180 °C;
(i) [TBzPBI-BuI][Tf$_2$N]$_{10}$, (ii) [TBzPBI-BuI][BF$_4$]$_{10}$, (iii) [TBzPBI-BuI][Ac]$_{10}$,
(iv) [TBzPBI-BuI][Tf$_2$N]$_{18}$, (v) [TBzPBI-BuI][BF$_4$]$_{18}$ and (vi) [TBzPBI-BuI][Ac]$_{18}$.

In present cases, the band at ~ 2400-3400 cm^{-1} originating from N-H stretching was disappeared, conveying '*N*-substitution' has taken place almost quantitatively. The characteristic bands for benzimidazole backbone in the range of 1500-1650 cm^{-1} attributable to C=C/C=N stretching vibrations and ring modes are observed [Bhavsar (2014a), Chapter 3]. For PILs with BF$_4^-$ as the counterion, a band at ~1060 cm^{-1} was seen, which was attributed to the B-F

stretching vibrations [Suarez (1996), Bhavsar (2014a)]. In case of PILs with Tf_2N^- as the counterion, bands at ~1330 cm^{-1} and 612 cm^{-1} were seen. These could be attributed to the asymmetric stretching and bending vibrations of sulfone group, respectively [Pennarun (2005), Bhavsar (2014a)]. In these spectra, a band at 1130-1240 cm^{-1}, attributable to the symmetric stretching vibrations of C-F bond was also seen [Choi (2005), Pennarun (2005), Bhavsar (2014a)]. In a spectrum of PILs with acetate as anion, a typical C=O stretching (belonging to the acid group) at 1651 cm^{-1} was observed. The appearance of bands attributable to a particular anion confirms the formation of PILs with that anion.

Figure 4.2 WAXD pattern of PILs; (i) [TBzPBI-BuI][Tf_2N]$_{10}$, (ii) [TBzPBI-BuI][BF_4]$_{10}$, (iii) [TBzPBI-BuI][Ac]$_{10}$, (iv) [TBzPBI-BuI][Tf_2N]$_{18}$, (v) [TBzPBI-BuI][BF_4]$_{18}$ and (vi) [TBzPBI-BuI][Ac]$_{18}$.

The WAXD patterns of these PILs indicated their amorphous nature (Figure 4.2). This is in line with the amorphous nature of rigid PBI-based PILs as we have reported recently [Bhavsar (2014a), Shaligram (2015)]. It is known that PILs possessing aliphatic backbone exhibit some crystallinity [Pan (2009), Bhavsar (2012)]. Present series of PILs further signify the necessity of rigid PBI-based backbone for rendering amorphous nature of PILs that is better suited for the

membrane application. The d-spacing (d_{sp}) of present PILs (Table 4.1) varied marginally, conveying that the effect of anion is secondary and the repulsive effects caused by *N*-substitution on PBI predominates in governing the d_{sp}. It may be noted that in case of PILs with fully quaternized PBI, the effect of anion on governing d_{sp} was distinctly observed [Bhavsar (2014a)]. The density of these PILs varied in the narrow range (1.126-1.084 Å), since all PILs have less amount of ionic character and chain packing in the polymer matrix is majorly governed by the *N*-substitution.

4.3.2 Thermal stability of PILs

Figure 4.3 TGA curves of PILs; (i) [TBzPBI-BuI][Tf$_2$N]$_{10}$, (ii) [TBzPBI-BuI][BF$_4$]$_{10}$, (iii) [TBzPBI-BuI][Ac]$_{10}$, (iv) [TBzPBI-BuI][Tf$_2$N]$_{18}$, (v) [TBzPBI-BuI][BF$_4$]$_{18}$ and (vi)[TBzPBI-BuI][Ac]$_{18}$.

The TGA curves of present PILs are given in Figure 4.3. Initial decomposition temperature (IDT) of PILs is given in Table 4.1. For a particular DQ (10 and 18%), PILs with Tf$_2$N$^-$ anion had higher IDT than those possessing BF$_4$$^-$ and Ac$^-$ as anions. The parent brominated PIL as given in Chapter 3, has lower IDT than those with Tf$_2$N$^-$ and BF$_4$$^-$ as anions ([TBzPBI-BuI][Br]$_{10}$: 267 °C and [TBzPBI-BuI][Br]$_{18}$: 242 °C). This behavior was observed in both the series of DQ (10 and 18%). As also could be seen from thermograms (Figure 4.3), while keeping the polycation same and varying the anion, thermal stability of PILs decreased with the

order of anions as $Tf_2N^- > BF_4^- > Ac^-$. The similar variation of the thermal stability of PILs with varying anions was observed in our earlier study [Bhavsar (2012)]. From present observations, it could be inferred that anion played a significant role in determining thermal stability of PILs, even at lower DQ of PBI based PILs. Since T_g could not be observed in DSC thermogram, dynamic mechanical analysis (DMA) was used to determine it. All the present PILs showed T_g in the range of 272-290 °C (Table 4.1 and Figure 4.4, except for PILs based on Ac^- anion,), conveying their glassy nature.

Figure 4.4 DMA curve of PILs; ■ [TBzPBI-BuI][Br]$_{10}$, ● [TBzPBI-BuI][Tf$_2$N]$_{10}$, ▲ [TBzPBI-BuI][BF$_4$]$_{10}$, □ [TBzPBI-BuI][Br]$_{18}$, ○ [TBzPBI-BuI][Tf$_2$N]$_{18}$ and [TBzPBI-BuI][BF$_4$]$_{18}$, ⊕ [TBzPBI-BuI][Ac]$_{10}$, × [TBzPBI-BuI][Ac]$_{18}$.

4.4   Gas permeation properties

4.4.1   Effect of anion variation on gas permeability and selectivity

The permeability of pure gases of interest and permselectivity for various gas pairs in the present PILs are given in Table 4.3 and 4.4 respectively. The permeation properties of parent PILs with Br^- as anion (Chapter 3), are also reproduced in Table 4.3 for convenience. For a particular DQ, the CO_2 (interacting gas) permeability in PILs varied with the variation of anion as: $BF_4^- > Tf_2N^- > Br^- > Ac^-$.

Table 4.3 Gas permeation properties of PILs.

PILs	Permeability coefficient (P)[a]				
	P_{He}	P_{H_2}	P_{N_2}	P_{CH_4}	P_{CO_2}
[TBzPBI-BuI][Tf$_2$N]$_{10}$	41.5	60.2	1.91	1.73	28.1
[TBzPBI-BuI][BF$_4$]$_{10}$	35.3	41.4	1.87	1.60	29.8
[TBzPBI-BuI][Ac]$_{10}$	41.1	59.7	1.76	1.64	26.6
[TBzPBI-BuI][Br]$_{10}$[b]	38.4	58.6	1.90	1.87	29.4
[TBzPBI-BuI][Tf$_2$N]$_{18}$	41.4	58.8	1.90	1.70	30.2
[TBzPBI-BuI][BF$_4$]$_{18}$	30.6	39.8	1.79	1.58	31.5
[TBzPBI-BuI][Ac]$_{18}$	30.3	44.0	1.30	1.24	23.2
[TBzPBI-BuI][Br]$_{18}$[b]	37.4	56.4	1.76	1.52	27.1

[a]: Expressed in Barrer (1 Barrer = 10^{-10} cm^3.(STP).cm.cm^{-2}.s^{-1}.cmHg^{-1}),

[b]: Taken from Chapter 3.

Table 4.4 Gas permeation properties of PILs.

PILs	Permselectivity (P_A/P_B)							
	P_{He}/P_{N_2}	P_{He}/P_{CH_4}	P_{H_2}/P_{He}	P_{H_2}/P_{N_2}	P_{H_2}/P_{CO_2}	P_{H_2}/P_{CH_4}	P_{CO_2}/P_{N_2}	P_{CO_2}/P_{CH_4}
[TBzPBI-BuI][Tf$_2$N]$_{10}$	21.7	24.0	1.5	31.6	2.2	34.9	14.7	16.2
[TBzPBI-BuI][BF$_4$]$_{10}$	18.9	22.1	1.2	22.1	1.4	25.9	15.9	18.6
[TBzPBI-BuI][Ac]$_{10}$	23.4	25.1	1.5	33.9	2.2	36.4	15.1	16.2
[TBzPBI-BuI][Br]$_{10}$[a]	20.2	20.5	1.5	30.8	2.0	31.3	15.5	15.7
[TBzPBI-BuI][Tf$_2$N]$_{18}$	21.8	24.4	1.4	31.0	2.0	34.6	15.9	17.8
[TBzPBI-BuI][BF$_4$]$_{18}$	17.1	19.4	1.3	22.2	1.3	25.2	17.6	19.9
[TBzPBI-BuI][Ac]$_{18}$	23.3	24.4	1.5	33.9	1.9	35.5	17.9	18.7
[TBzPBI-BuI][Br]$_{18}$[a]	21.3	24.6	1.5	32.1	2.1	37.1	15.4	17.8

[b]: Taken from Chapter 3.

For non-interacting gases, (He, H$_2$, N$_2$) the permeability was highest in PIL possessing Tf$_2$N$^-$ anion. This was true for both the series, possessing 10 and 18% DQ. It is noteworthy that the CO$_2$ permeability as well as CO$_2$ related permselectivities (CO$_2$/N$_2$ and CO$_2$/CH$_4$) was found to be higher in PILs possessing BF$_4$$^-$ as an anion in both the series, as shown in Figure 4.5. This could be due to CO$_2$ specific nature of BF$_4$$^-$ anion. Such anion specificity in governing CO$_2$ permeation properties was also observed previously for PBI-based PILs possessing BF$_4$$^-$ anion [Bhavsar (2014c)]. It is evident that anion of the PILs does indeed affect CO$_2$ permeability, even with lower DQ of 10 and 18%. However, this effect may not be as pronounced as for PILs having higher ionic character [Bhavsar (2014c)]. In both the series of polycations, Tf$_2$N$^-$ containing PILs exhibited higher gas permeation (except for CO$_2$) than that of PILs with other

anion. Although the variation in d_{sp} was not significant, this could be correlated to the higher Vander wall volume of Tf_2N^- (88.5 cm^3/mol=143 Å^3) anion than that of BF_4^- (30.1 m^3/mol=48 Å^3) and Ac^- (~ 28.87 m^3/mol=46.3.1 Å^3) [Bondi (1964), Park (1997), Koch (1998)] that would ultimately affect the chain separation in polymer matrix. Anion variation affecting chain packing is further supported by the lower density of PILs with Tf_2N^- as an anion, than that of PILs possessing other anions.
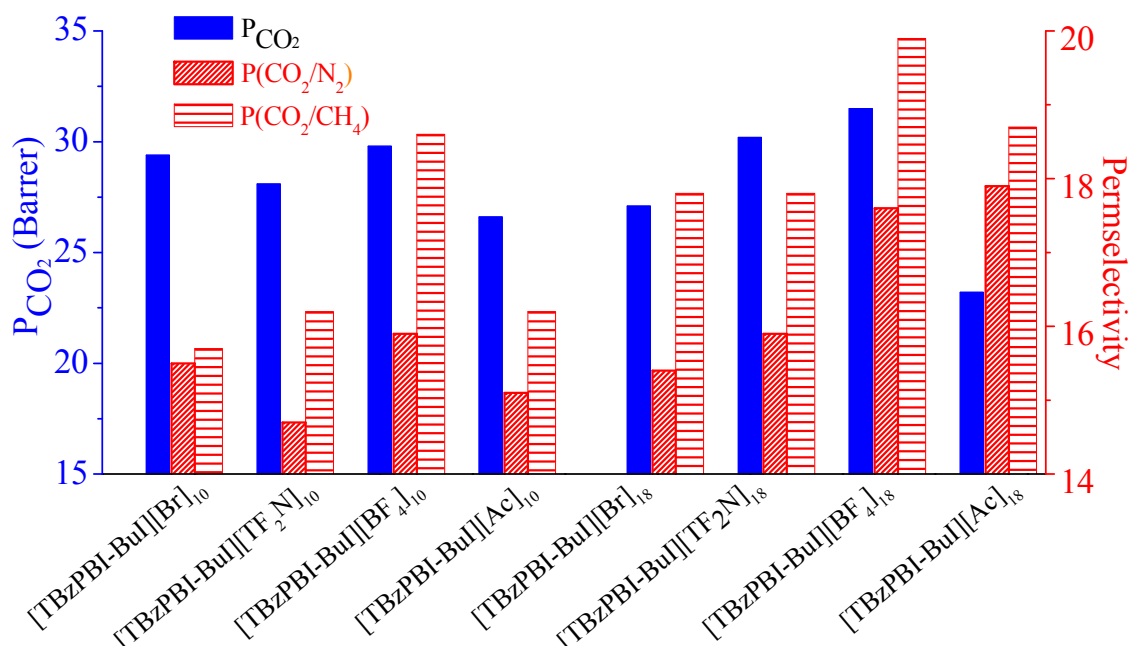
Figure 4.5 CO_2 permeability and related permselectivities of PILs.

A close look to the gas permeability of non-interacting gases (He, H_2, N_2 and CH_4) for a PILs with a particular anion, but varying DQ conveys that permeability is generally higher for those with 10% DQ than that of 18% DQ. On the contrary, order of CO_2 permeability is reverse (i. e., higher for PILs with 18% DQ). This allows to speculate that the permeability of CO_2 in PILs possessing 18% DQ is majorly governed by its PIL nature. Although an increase in *N*-quaternization helps to improve permeability of CO_2, such increased ionic interactions would bring chains closer and thus lower the permeability of non-interacting gases (He, H_2, N_2 and CH_4). In order to understand role of anion on governing CO_2 sorption in PILs possessing partial ionic character, CO_2 sorption analysis was performed as discussed below.

4.4.2 Gas sorption

Figure 4.6 shows the CO_2 sorption isotherms and Table 4.5 shows sorption parameters and solubility coefficients.

Table 4.5 Dual-mode sorption parameters, solubility coefficient (S_{CO_2}) and diffusivity coefficient (D_{CO_2})[a] of CO_2 in present PILs.

PILs	k_D	C'_H	b	S_{CO_2}	D_{CO_2}
[TBzPBI-BuI][Tf$_2$N]$_{10}$	0.28	27.6	0.16	1.32	16.2
[TBzPBI-BuI][BF$_4$]$_{10}$	0.67	21.3	0.22	1.54	14.4
[TBzPBI-BuI][Ac]$_{10}$	0.18	31.6	0.12	1.30	15.6
[TBzPBI-BuI][Br]$_{10}$[b]	0.13	30.0	0.13	1.22	18.4
[TBzPBI-BuI][Tf$_2$N]$_{18}$	0.22	28.4	0.11	1.44	15.9
[TBzPBI-BuI][BF$_4$]$_{18}$	0.05	32.0	0.15	1.68	14.3
[TBzPBI-BuI][Ac]$_{18}$	0.10	35.0	0.09	1.35	14.0
[TBzPBI-BuI][Br]$_{18}$[b]	0.23	28.7	0.18	1.35	15.3

[a]: Expressed in 10^{-8} cm^2.s^{-1}, k_D is expressed in cm^3(STP).cm^{-3}polymer.atm^{-1}, C'_H is expressed in cm^3(STP).cm^{-3}polymer, b is expressed in atm^{-1}, S_{CO_2} is expressed in cm^3(STP)cm^{-3}polymer.atm^{-1} at 20 bar, [b]: Taken from Chapter 3.
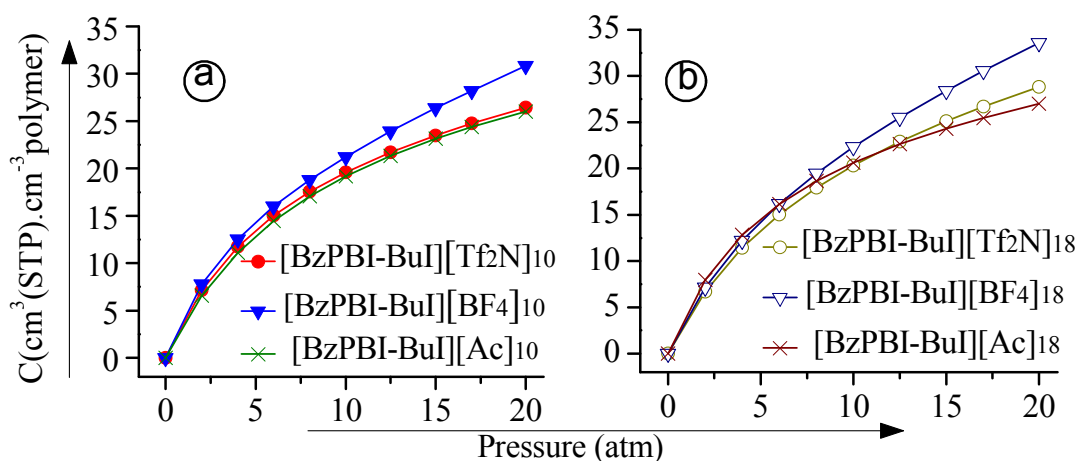
Figure 4.6 CO_2 sorption isotherms of PILs at 35 °C, (a) PILs with 10% ionic character and (b) PILs with 18% ionic character.

The sorption isotherm showed a typical dual-mode nature, usually observed for glassy polymers [Veith (1976), Kumbharkar (2010)]. The CO_2 sorption increased with the pressure and its rate slowed down with an increase in pressure, as a typical behavior of dual mode sorption in

glassy polymers. It was observed that for a particular series of PIL (based on either 10 or 18% DQ), CO_2 solubility coefficients generally increased in the order of their anion variation as, BF_4^- > Tf_2N^- > Ac^- > Br^- (Table 4.5). The highest sorption in PILs with BF_4^- as an anion probably led to the higher observed permeability in these PILs, in comparison to their counter parts possessing other anions. It is known that the PILs with BF_4^- as an anion show higher CO_2 sorption than that of PILs with halide or Tf_2N^- anion [Tang (2009), Mecerreyes (2011), Bhavsar (2012), Yaun (2013)]. This peculiarity indicated that even at less DQ in the present PILs, anion played a significant role in governing their CO_2 sorption, and thus permeation properties. Table 4.5 lists gas sorption parameters (k_D, b and C'_H) for present PILs (obtained by using Eq. 3.5 described in Chapter 2). The Henry's solubility constant is low for present PILs owing to their glassy nature. On the other hand, the Langmuir saturation 'C'_H' was higher than that of PSF (polysulphone): 16.63, PH (polyhydroxyether): 8.89 [Barbari (1988)] indicating favorable interactions of present PILs with the CO_2.

The CO_2 diffusivity coefficient was estimated using Eq. 3.6 (Chapter 2) and are given in Table 4.5 for different PILs. It could be seen that the CO_2 diffusivity coefficient varied in a narrow range. It is worth to note that PILs with BF_4^- anion although exhibited high CO_2 permeability and CO_2 based selectivity, they possessed lower diffusivity than that of their counterparts with other anions. This allows to speculate that there is a room for structural modification in PILs that would elevate CO_2 diffusivity. The path followed in present family (partial *N*-quaternization of PBI followed by anion exchange) may not be enough by itself, to reach to this goal and need to be supplemented by other methodologies of structural variations.

4.5 Conclusions

Polymeric ionic liquids (PILs) were prepared by a simple anion exchange method based on PILs possessing partial ionic character ([TBzPBI-BuI][Br]$_{10}$ and [TBzPBI-BuI][Br]$_{18}$) as a precursor. For anion exchange, selected anions (viz., Tf_2N^-, BF_4^- and Ac^-) have been chosen based on their CO_2 specific nature. The lithium and sodium salts of anions were used for anion exchange of PILs and ~ 95% anion exchange were achieved. Concurrent effects of variation in anion were analyzed for physical and gas permeation properties of the resulting PILs. PILs were glassy in nature and thermally stable (degradation temperature: ≥ 250 °C). The thermal stability of PILs decreased with the order of anions as Tf_2N^- > BF_4^- > Ac^-. PILs with BF_4^- anion

showed higher CO_2 permeation as well as CO_2 based selectivity than their counter parts possessing other anions. This proves the CO_2 specific nature of BF_4^- anion. While with non-interacting gases Tf_2N^- showed higher gas permeation; this is due to higher Vander wall volume of this anion. This study concludes that anion played a significant role in governing the physical and gas permeation properties even at lower DQ.

Chapter 5

Effect of amino acid as an anion on physical and gas sorption properties of PBI based Polymeric ionic liquids

5.1 Preamble

Amino acids as an anion in room temperature ionic liquids (RTILs) have offered very interesting results towards CO_2 sorption. These ionic liquids are further termed as amino acid ionic liquids (AAIL). Davis and co-worker have reported CO_2 chemisorption by using an amino-functionalized IL, in which, 0.5 mol of CO_2 was captured per mol of IL under ambient pressure [Bates (2002)]. Subsequently, functionalization of ILs with amino group has received great interest, as this group interacts with CO_2 by Lewis acid-base interaction [Wang (2011), Wang (2012)]. It is reported that the nature of the anion has the most significant influence on the CO_2 solubility, regardless of whether the cation was imidazolium, pyrrolidinium, or tetraalkylammonium [Anthony (2005)]. Amino acid can be a good candidates as an anion since it has at least one NH_2 group in their structure. Lot of reports on ILs composed of amino acid as anions were reported and the results are highly impressive. High CO_2 sorption capacity of ~ 0.5-1 mol CO_2 per mol of IL is reported [Yu (2009), Wang (2011)].

PILs were shown to exhibit higher CO_2 absorption capacity than those of monomeric room temperature ionic liquids (RTILs) or commonly used ILs [Tang (2005a), Yuan (2013)]. Furthermore, they are shown to exhibit faster CO_2 absorption and desorption rate than that of ILs [Mecerreyes (2011)]. It would be worth to investigate CO_2 sorption in PBI based PILs possessing different amino acid as anion and became the objective of this part of the work. The cation of these PILs was obtained from a common asymmetric *N*-quaternized polybenzimidazole, PBI-BuI. The *N*-substituents chosen were methyl and *t*-butylbenzyl (Bz), owing to high permeability of resulting PIL, viz., [DBzDMPBI-BuI][I]. It's iodide anion was exchanged with various amino acid based anions (viz., sodium glycinate, sodium L-alanate, sodium L-arginate, sodium L-asparginate, sodium L-histidinate, sodium L-lycinate, sodium L-phenyl alanate and sodium L-tryptophinate). The chosen amino acids contain varying length of alkyl group in them, presence of other functional groups and are commercially available.

5.2   Synthesis

5.2.1   Polybenzimidazole (PBI-BuI)

The polybenzimidazole based on *3,3′*-diaminobenzidene and *t*-butylisophthalic acid, PBI-BuI, was synthesized in polyphosphoric acid (PPA) as described previously (Chapter 2, Section 2.2.1) with inherent viscosity of 1.3 dL.g^{-1}. Initially, PBI-BuI was disubstituted by *4-tert*-butylbenzyl group via formation of Na-salt of a PBI-BuI. The *N*-substituted polymer was isolated, purified by dissolving in DMF followed by reprecipitation in acetone. The degree of substitution was assessed by ^{1}H-NMR spectroscopy, as discussed below. It was then quaternized by methyl iodide in the next step to obtain PIL ([DBzDMPBI-BuI][I]) containing iodide anion. The detail of this two stage synthesis methodology of obtaining 'asymmetrically substituted' PILs is given in Chapter 2, Section 2.2.5.

5.2.2   Estimation of the degree of *N*-substitution and *N*-quaternization (DQ)
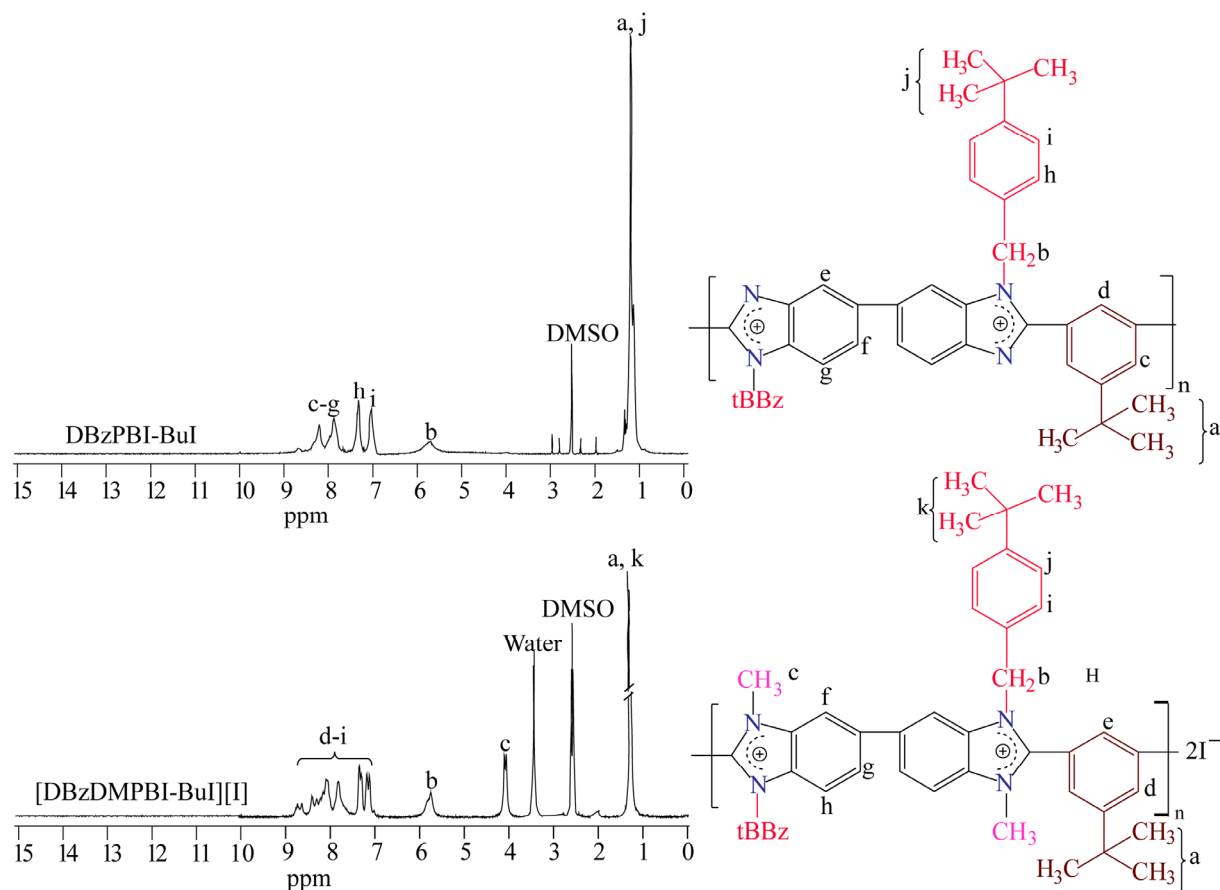
Figure 5.1 ^{1}H-NMR spectra of DBzPBI-BuI and PIL.

A broad peak in the spectra of PBI-BuI appearing at δ 13-14 (corresponds to the proton belonging to N-H of imidazole) has disappeared completely after the *N*-substitution reaction by *tert*-butyl benzyl group. This indicated that the *N*-substitution reaction has taken place almost quantitatively. After the *N*-quaternization by methyl iodide, DQ was estimated by comparing integration of protons belonging to the methyl group (appearing in the range δ 4-4.5) with that of aromatic protons of the precursor PBI (appearing in the range of δ 7.5-9.5, Figure 5.1). The DQ obtained by this method was 93%. The DQ was also determined by Volhard's method (estimation of iodide content), which was found to be 92%. The DQ obtained by both methods (^{1}H-NMR and Volhard's) were in good agreement and are appreciably high.

5.2.3   Synthesis of sodium salt of amino acids

Sodium salts of amino acid were successfully synthesized by acid-base neutralization reaction (Chapter 2, Scheme 2.6). An 8% solution of amino acid was prepared in water, equimolar amount of sodium hydroxide was added and kept for continuous stirring for 8 h at the ambient temperature. This method has an advantage that the byproduct is only water. The sodium salt of amino acid in the solid form (white powder) was easily removed by the evaporation.

5.2.4   Anion exchange of PIL by amino acids

Iodide exchange of [DBzDMPBI-BuI][I] was performed using sodium salts of amino acids in DMF. For iodide exchange, 5 molar equivalents of Na salts were used. The excess amount was taken since use of Na salt is anticipated to offer reversible anion exchange. Formed anion exchanged PILs were found to be partially soluble in water. Thus, dialysis bags were used in order to separate the formed byproduct, NaI. The detailed procedure of use of dialysis bag is given in Chapter 2, Section 2.2.4. The process of anion exchange was repeated twice in order to achieve an appreciable exchange of iodide by an anion of amino acid in resulting PILs. Volhard's analysis (estimation of remainder iodide) showed that exchange in all cases of PILs was almost quantitative, as given in Table 5.1. Obtained amino acid containing polymeric ionic liquids (AAPILs) are designated based on their respective anion, as given in Table 5.1.
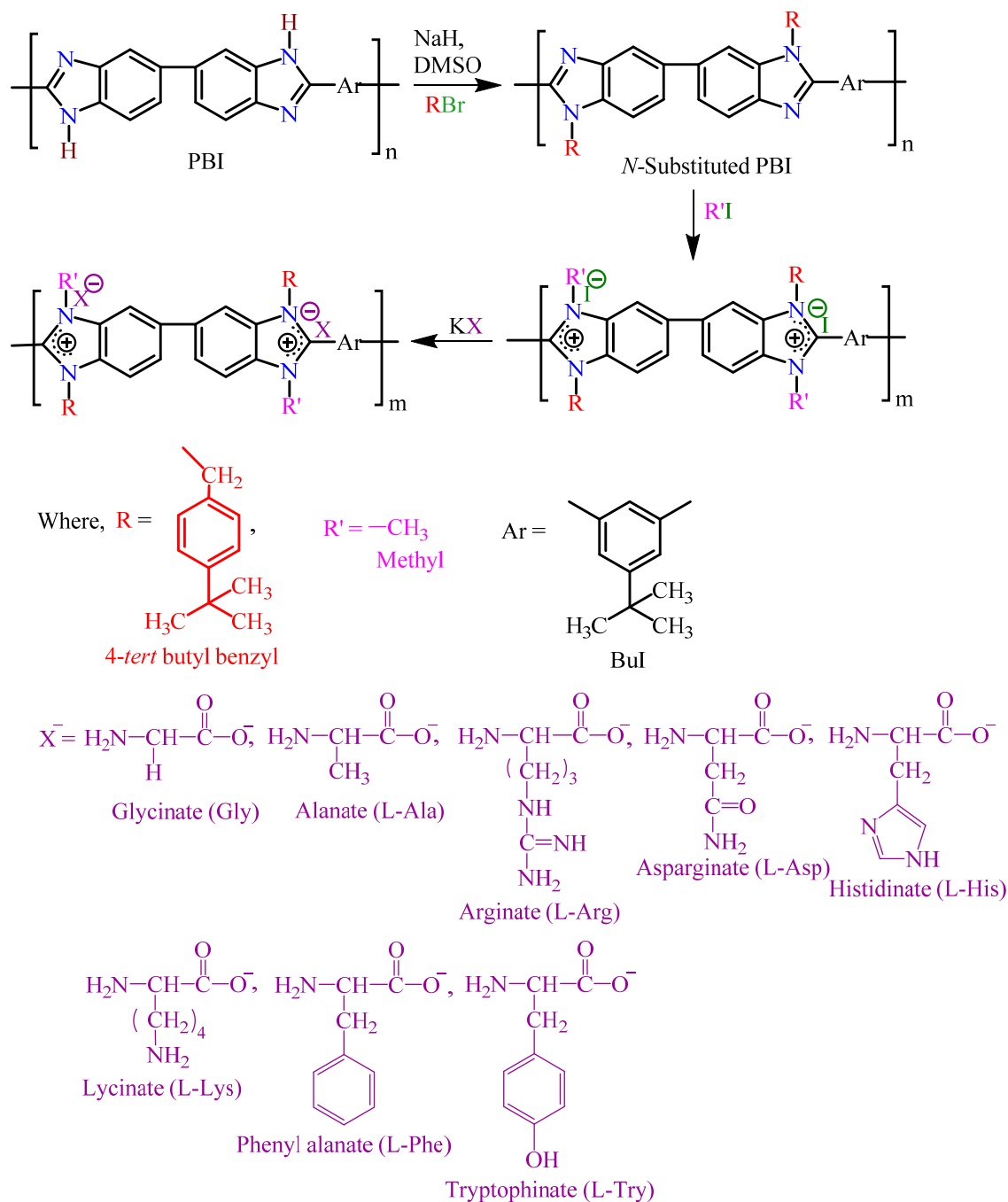
Scheme 5.1 Synthesis of PILs.
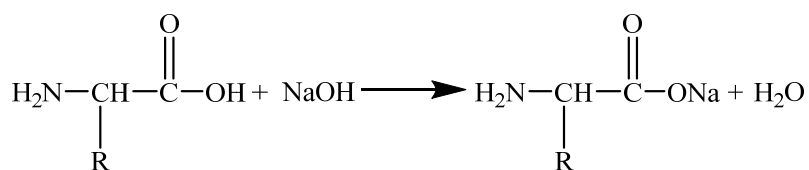
Scheme 5.2 Synthesis of sodium salt of amino acid.

Table 5.1 Physical properties of PILs.

PILs	Anion exchange (%)	η_{inh}^a (dL.g^{-1})	ρ^b (gm.cm^{-3})	d_{sp}^c (Å)	TGA	
					IDT^d (°C)	W$_{900}^e$ (%)
[DBzDMPBI-BuI][I]	-	4.1	1.399	4.92	222	29
[DBzDMPBI-BuI][Gly]	82	2.9	1.132	4.87	226	35
[DBzDMPBI-BuI][L-Ala]	80	1.6	1.188	4.69	230	39
[DBzDMPBI-BuI][L-Arg]	88	3.3	0.999	4.98	160	38
[DBzDMPBI-BuI][L-Asp]	78	1.7	1.142	5.09	284	41
[DBzDMPBI-BuI][L-His]	83	2.3	1.087	5.01	225	39
[DBzDMPBI-BuI][L-Lys]	82	0.8	1.044	4.92	224	24
[DBzDMPBI-BuI][L-Phe]	81	3.0	1.212	4.84	279	35
[DBzDMPBI-BuI][L-Try]	87	2.7	1.118	5.03	232	37

^{a}: Inherent viscosity determined using 0.2 g.dL^{-1} DMSO solution at 35 °C, ^{b}: density measured at 35 °C, ^{c}: d-spacing obtained from WAXD pattern, ^{d}: initial decomposition temperature, ^{e}: char yield at 900 °C.

5.3   Physical properties

5.3.1   Solvent solubility, spectral characterizations and density

AAPILs were soluble in low boiling solvents such as CHCl$_3$, CH$_2$Cl$_2$, acetone and methanol as given in Table 5.2. This shows that PILs with amino acid as anions improved solvent solubility than that of parent PIL, [DBzDMPBI-BuI][I]. All the AAPILs were partially soluble in water.

Table 5.2 Solvent solubility of PILs.

PILs	DMF	DMAc	DMSO	NMP	CHCl$_3$	CH$_2$Cl$_2$	CH$_3$OH	Acetone	H$_2$O
[DBzDMPBI-BuI][I]	+	+	+	+	−	−	−	−	−
[DBzDMPBI-BuI][Gly]	+	+	+	+	+	+	+	+	±
[DBzDMPBI-BuI][L-Ala]	+	+	+	+	+	+	+	+	±
[DBzDMPBI-BuI][L-Arg]	+	+	+	+	+	+	+	+	±
[DBzDMPBI-BuI][L-Asp]	+	+	+	+	±	±	±	+	±
[DBzDMPBI-BuI][L-His]	+	+	+	+	+	+	+	+	±
[DBzDMPBI-BuI][L-Lys]	+	+	+	+	+	+	+	+	±
[DBzDMPBI-BuI][L-Phe]	+	+	+	+	+	+	+	+	±
[DBzDMPBI-BuI][L-Try]	+	+	+	+	+	+	+	+	±

+: Soluble at ambient temperature, ±: partially soluble or swelling, −: insoluble at ambient temperature.

For all the PILs, FTIR spectra scanned at ambient temperature showed a broad band at ~3610 cm^{-1}, which could be attributed to the sorbed moisture (Figure 5.2). For unsubstituted PBI, a band at ~ 3400-2400 cm^{-1} originating from N-H stretching is well reported [Musto (1993), Brook (1993)]. In present cases, this band has disappeared, which confirms that the *N*-substitution has taken place almost quantitatively. The band observed in the range of 1650-1500 cm^{-1} is attributable to the C=C/C=N stretching vibrations and ring modes, which is a characteristic band for benzimidazole [Musto (1993)]. All AAPILs absorbs strongly near 1600-1590 cm^{-1} and weakly near 1400 cm^{-1}. These bands are attributable to the asymmetric and symmetric stretching of (C=O), respectively, originating from the carboxylate group of amino acid.
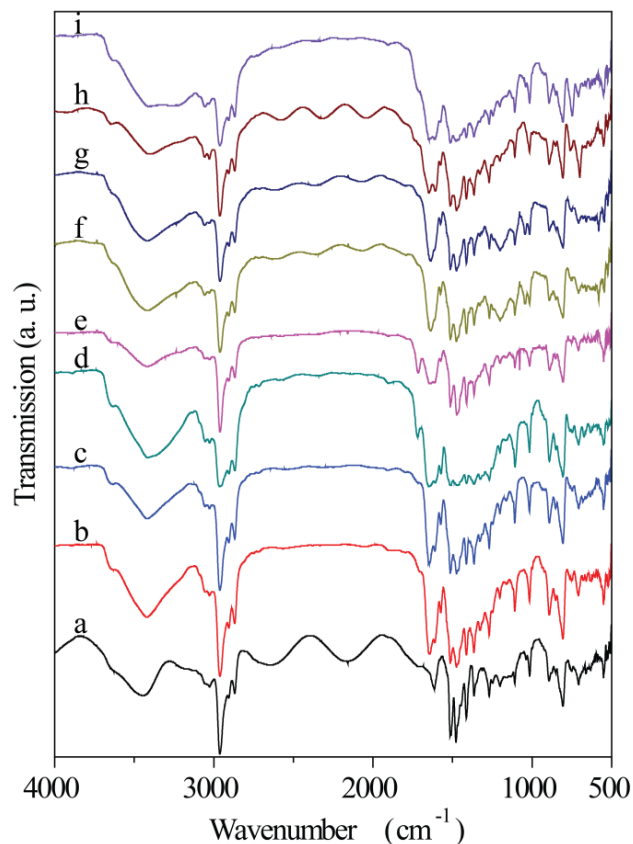
Figure 5.2 FT-IR spectra of PILs at ambient
(a) [DBzDMPBI-BuI][I], (b) [DBzDMPBI-BuI][Gly], (c) [DBzDMPBI-BuI][L-Ala],
(d) [DBzDMPBI-BuI][L-Arg], (e) [DBzDMPBI-BuI][L-Asp], (f) [DBzDMPBI-BuI][L-His],
(g) [DBzDMPBI-BuI][L-Lys], (h) [DBzDMPBI-BuI][L-Phe] and (i) [DBzDMPBI-BuI][L-Try].

WAXD spectra of these PILs (Figure 5.3) indicated their amorphous nature. This could be due to their structural peculiarity, wherein, the rigid aromatic PBI backbone would inhibit ordered packing arrangement in the polymer matrix. The *d*-spacing (d_{sp}) of AAPIL corresponding to the amorphous peak maxima in the respective WAXD spectra are given in Table 5.1, which varied in the range of 4.69-5.09 Å. Although the variation in d_{sp} is not large, the nature of anion seems to have its own effect on governing this parameter. The PILs with L-arginate, L-asparginate, L-histidinate and L-tryptophinate as an anion exhibited higher d_{sp} than that of iodide as an anion. This might be because of their asymmetric structure, which helps in disturbing chain packing than in PILs with glycinate, L-alanate and L-phenyl alanate as anions. The later AAPILs showed lower d_{sp}, which might be due to more symmetric structure of their anion. The anions, viz., Gly, L-Ala and L-Phe possess nonpolar aliphatic side chains and don't have any other functional group in their side chain structure [Sistla (2015)]. This may be a reason for lower d_{sp} of PILs possessing these anions.
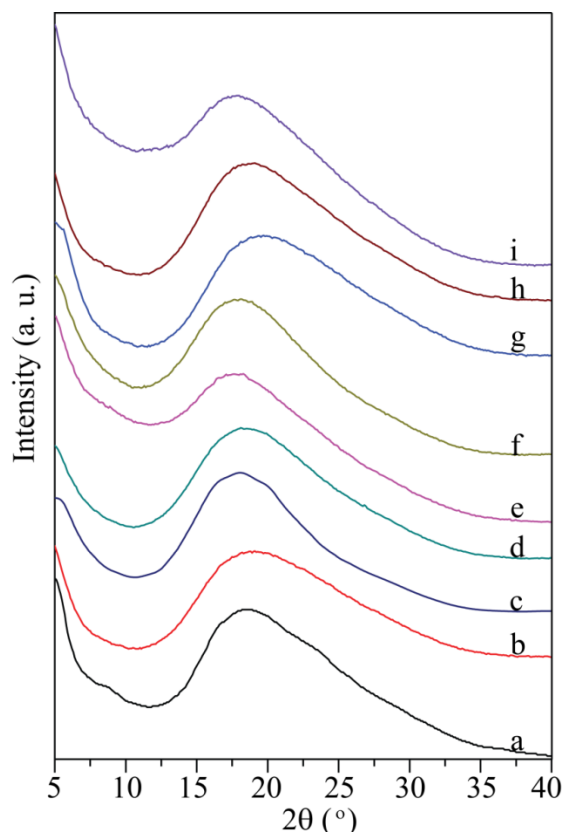
Figure 5.3 WAXD patterns of PILs
(a) [DBzDMPBI-BuI][I], (b) [DBzDMPBI-BuI][Gly], (c) [DBzDMPBI-BuI][L-Ala],
(d) [DBzDMPBI-BuI][L-Arg], (e) [DBzDMPBI-BuI][L-Asp], (f) [DBzDMPBI-BuI][L-His],
(g) [DBzDMPBI-BuI][L-Lys], (h) [DBzDMPBI-BuI][L-Phe] and (i) [DBzDMPBI-BuI][L-Try].

The density of AAPILs determined using specific gravity bottle is given in Table 5.1. For all AAPILs, it was lower than their parent *N*-quaternized PBI containing iodide anion ([DBzDMPBI-BuI][I]). This qualitatively supports the finding of WAXD analysis, wherein loser chain packing was concluded owing to the bulky nature of anion present in these AAPILs.

5.3.2 Thermal stability of PILs

Initial decomposition temperature (IDT) of AAPILs is given in Table 5.1. Their thermal stability was higher than that of their parent, [DBzDMPBI-BuI][I]. This increase in thermal stability as compared to the parent PIL could be attributed to the added interaction due to amino acid groups. It is noteworthy that in the case of amino acids as anion, many of them contain functional groups in their side chain such as carboxyl, hydroxyl, etc. This implies some intra- and inter-molecular interaction responsible for increased thermal stability. The nature of anions was also responsible for governing the thermal stability of these PILs. As could be seen from Table 5.1 and thermograms (Figure 5.4) given below, thermal stability of PILs decreased (backbone cation remaining the same) with the order of anions as L-asp > L-phe > L-try ~ L-ala ~ L-his ~ gly ~ L-lys ~ I > L-arg.
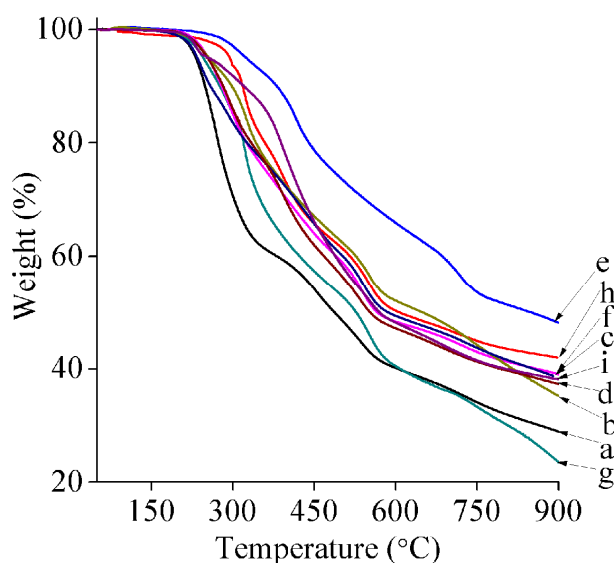
Figure 5.4 TGA curve of PILs
(a) [DBzDMPBI-BuI][I], (b) [DBzDMPBI-BuI][Gly], (c) [DBzDMPBI-BuI][L-Ala],
(d) [DBzDMPBI-BuI][L-Arg], (e) [DBzDMPBI-BuI][L-Asp], (f) [DBzDMPBI-BuI][L-His],
(g) [DBzDMPBI-BuI][L-Lys], (h) [DBzDMPBI-BuI][L-Phe] and (i) [DBzDMPBI-BuI][L-Try].

The variation in thermal stability of PILs could also be explained based on the pK_a of anion. The amino acids are characterised by two pK_as : pK_a1 and pK_a2 for the carboxylic acid and the amine, respectively. The average pK_a of amino acid will be halfway between, or the average of these two pK_as, *i.e.* pI or $pK_a = 1/2 (pK_a1 + pK_a2)$ [Bhutani (2010)]. The alkyl group of amino acids also play an important role in determining the pK_a value of those amino acids. Other functional group present on the alkyl chain may also contribute to it. The electron withdrawing groups increases its acidity, while electron donating groups do the reverse. It could be seen from Figure 5.5 that the thermal stability of present AAPILs decreased with increasing pK_a of its anion, as also observed previously for various types of organic and inorganic anions [Bhavsar (2014a)]. The role of other polymer properties (e.g. packing density) would also have its own role in governing thermal stability.

Table 5.3 pK_a value of amino acids.

PILs	$pK_a (COOH)^a$	$pK_a (NH_3+)^a$	$pK_a (R)^a$	pK_a^a
[DBzDMPBI-BuI][I]	-	-	-	10
[DBzDMPBI-BuI][Gly]	2.34	9.60		5.97
[DBzDMPBI-BuI][L-Ala]	2.35	9.69		6.02
[DBzDMPBI-BuI][L-Arg]	2.17	9.04	12.48	10.76
[DBzDMPBI-BuI][L-Asp]	2.02	8.8	-	5.41
[DBzDMPBI-BuI][L-His]	1.82	9.17	6.0	7.59
[DBzDMPBI-BuI][L-Lys]	2.18	8.95	10.53	9.74
[DBzDMPBI-BuI][L-Phe]	1.83	9.13	-	5.48
[DBzDMPBI-BuI][L-Try]	2.38	9.39	-	5.89

[a]: [S. P. Bhutani (2010)]
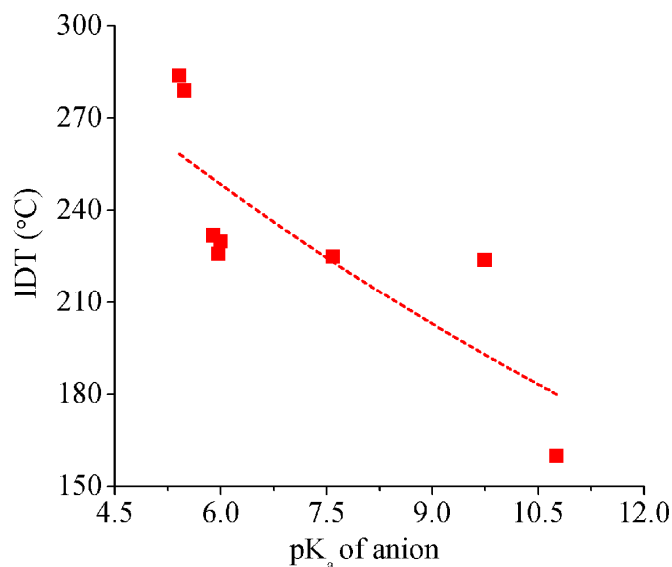
Figure 5.5 Variation of IDT with pK_a of AAPILs.

5.4 Gas sorption properties

5.4.1 Gas sorption coefficient

Table 5.4 Solubility coefficient (S)[a] and solubility selectivity (S_A/S_B) of PILs at 20 atm.

PILs	S_{H_2}	S_{N_2}	S_{CH_4}	S_{CO_2}	S_{N_2}/S_{CH_4}	S_{CO_2}/S_{H_2}	S_{CO_2}/S_{N_2}	S_{CO_2}/S_{CH_4}
[DBzDMPBI-BuI][I]	0.37	0.37	0.44	1.14	0.85	3.08	3.04	2.58
[DBzDMPBI-BuI][Gly]	0.27	0.32	0.50	1.52	0.63	5.71	4.78	3.03
[DBzDMPBI-BuI][L-Ala]	0.21	0.26	0.49	1.35	0.53	6.40	5.17	2.77
[DBzDMPBI-BuI][L-Arg]	0.15	0.19	0.57	1.58	0.34	10.47	8.32	2.80
[DBzDMPBI-BuI][L-Asp]	0.16	0.25	0.37	1.14	0.68	6.95	4.61	3.13
[DBzDMPBI-BuI][L-His]	0.31	0.38	0.45	1.27	0.85	4.14	3.34	2.84
[DBzDMPBI-BuI][L-Lys]	0.18	0.25	0.48	1.48	0.53	8.35	5.81	3.09
[DBzDMPBI-BuI][L-Phe]	0.27	0.35	0.57	0.90	0.61	3.29	2.58	1.58
[DBzDMPBI-BuI][L-Try]	0.24	0.28	0.39	1.23	0.71	5.08	4.48	3.16

[a]: Expressed in $cm^3(STP).cm^{-3}polymer.atm^{-1}$.

The films of AAPILs were brittle in nature as shown in Figure 5.6. Even if the cation remains as the PBI backbone, PILs based on acid as an anion were found to be brittle [Bhavsar (2012)]. In view of film forming inability, only gas sorption analysis could be analysed for the

present AAPILs. Equilibrium sorption isotherms of H_2, N_2, CH_4 and CO_2 in them exhibited typical dual-mode nature (Figure 5.7), as usually observed for glassy polymers [Koros (1976), Kumbharkar (2010), Bhavsar (2012)].

Figure 5.6 Photographs of PILs (a) [DBzDMPBI-BuI][I], (b) [DBzDMPBI-BuI][Gly],
(c) [DBzDMPBI-BuI][L-Ala], (d) [DBzDMPBI-BuI][L-Arg],
(e) [DBzDMPBI-BuI][L-Asp], (f) [DBzDMPBI-BuI][L-His], (g) [DBzDMPBI-BuI][L-Lys],
(h) [DBzDMPBI-BuI][L-Phe] and (i) [DBzDMPBI-BuI][L-Try].

Table 5.4 presents the solubility coefficient (S) and solubility selectivity (S_A/S_B) for different PILs at 20 atm. The solubility coefficient for different gases in all PILs at 20 atm decreased in the order: $CO_2 > CH_4 > N_2 \geq H_2$; which followed the order of increasing inherent condensability of these gases [Li (2009), Kumbharkar (2010)]. This order of gas sorption is obeyed by the glassy polymers [Barbari (1988), Koros (1988), Karadkar (2007)]. As could be seen from Table 5.4, the solubility coefficient for AAPILs was higher than that of parent PIL containing iodide (with an exception of [DBzDMPBI-BuI][L-Phe]). The effect of pressure on the gas solubility expressed in mol (gas)/mol (AAPIL) is shown in Figure 5.7. The order of CO_2 sorption in AAPILs with different anion was L-Arg > L-Lys > L-His > L-Try > L-Ala ~ Gly > L-Asp > I > L-Phe. Among the studied AAPILs, L-Arg, L-Lys, L-His and L-Try belong to the

same category (i.e., amino acid with polar and basic side chains). Therefore, the acid–base interaction between CO_2 and PILs possessing these amino acids is expected to be stronger as compared with the other AAPILs in the series [Sistla (2015)].
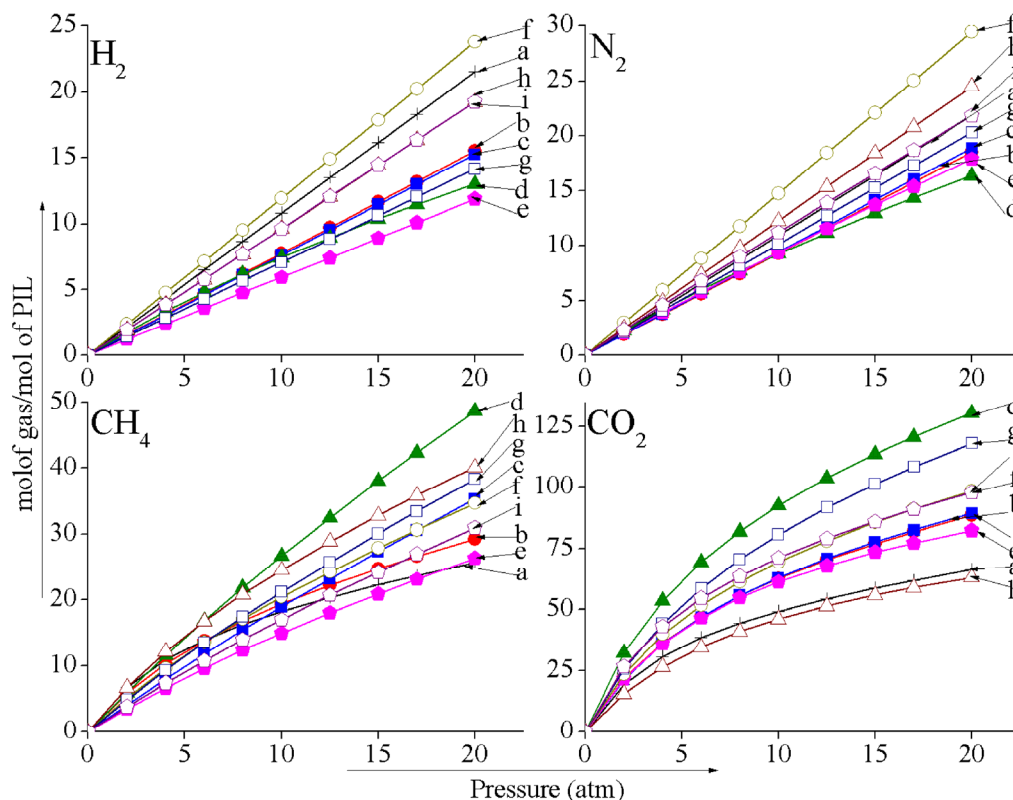
Figure 5.7 Gas sorption isotherms of PILs
(a) [DBzDMPBI-BuI][I], (b) [DBzDMPBI-BuI][Gly], (c) [DBzDMPBI-BuI][L-Ala],
(d) [DBzDMPBI-BuI][L-Arg], (e) [DBzDMPBI-BuI][L-Asp], (f) [DBzDMPBI-BuI][L-His],
(g) [DBzDMPBI-BuI][L-Lys], (h) [DBzDMPBI-BuI][L-Phe] and (i) [DBzDMPBI-BuI][L-Try].

Among all the AAPILs, the maximum CO_2 sorption was found in the case of [DBzDMPBI-BuI][L-Arg]. The L-Arg is encompassed of two primary and two secondary amine groups. Thus, there are more chances for CO_2 to interact with these available *N*-sites. This could result in higher CO_2 sorption capacity in [DBzDMPBI-BuI][L-Arg]. The L-Lys anion has two primary amine groups; therefore, [DBzDMPBI-BuI][L-Lys] has more CO_2 sorption than that of [DBzDMPBI-BuI][L-His] (Figure 5.7). The lower CO_2 sorption capacity for [DBzDMPBI-BuI][L-His] could be explained based on one primary and one secondary amine functional groups present in the anion, L-His (the secondary amine group is associated with steric

hindrance). The CO_2 sorption of [DBzDMPBI-BuI][L-Try] appears at fourth place. The L-Try has one primary amine and one secondary hydroxyl group and hydroxyl group is less effective than that of amine group (Table 5.5).

Table 5.5 Functional group present in anion and CO_2 sorption capacity (mol of CO_2/mol of PIL) of PILs.

Amino acids containing PILs	Groups present (number of groups in brackets)	CO_2 sorption capacity (mol of CO_2/mol of PIL)
[DBzDMPBI-BuI][Gly]	NH_2 (1)	0.89
[DBzDMPBI-BuI][L-Ala]	NH_2 (1)	0.89
[DBzDMPBI-BuI][L-Arg]	NH_2 (2) & NH (2)	1.31
[DBzDMPBI-BuI][L-Asp]	NH_2 (1) & NH_2 (amide)	0.82
[DBzDMPBI-BuI][L-His]	NH_2 (1), NH (1) & N (1)	0.99
[DBzDMPBI-BuI][L-Lys]	NH_2 (2)	1.18
[DBzDMPBI-BuI][L-Phe]	NH_2 (1)	0.63
[DBzDMPBI-BuI][L-Try]	NH_2 (1) & OH (1)	0.97
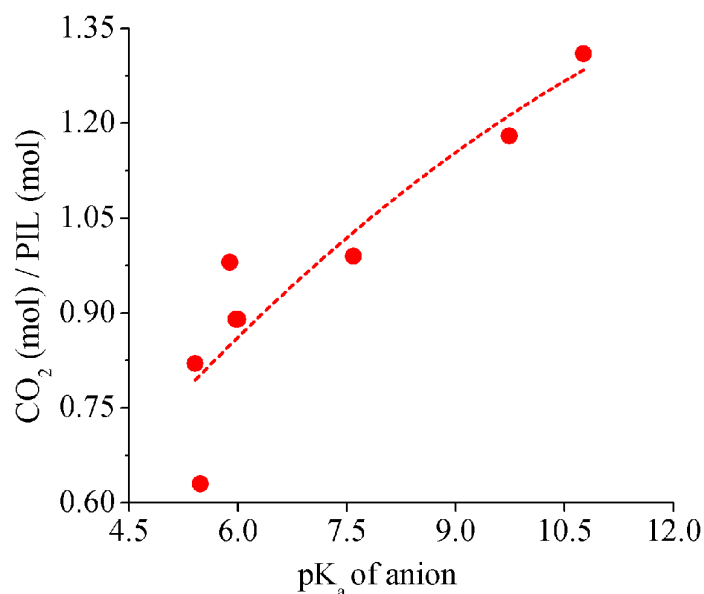
Figure 5.8 Variation of sorption in mol (CO_2) / mol (PIL) with pK_a of AAPILs.

Rest of the amino acids ([Gly], [L-Ala] and [L-Phe]) belong to the category of nonpolar aliphatic side chains consisting of only one primary amine functional group. All these AAPILs show slight variations in the CO_2 sorption capacities, which could be because of the differences in their alkyl chain length. The effect of the basicity of present AAPILs on CO_2 sorption is

shown in Figure 5.8. It was found that the sorption capacity of CO_2 was significantly affected by the basicity of anions of these AAPILs. The CO_2 sorption of [DBzDMPBI-BuI][L-Arg] and [DBzDMPBI-BuI][L-Lys] was 1.31 and 1.18 mol CO_2/mol of AAPIL respectively; these values are significantly higher than the CO_2 sorption in case of normally reported AAILs (amino acid based ionic liquids). Hong Yu et. al., have studied various amino acid based ionic liquids (AAILs) by the combination of different tetraalkylammonium cations with four amino acid anions ([Gly], [L-Ala], [b-Ala] and [Val]). They found that the mole uptake of CO_2 per mole of IL with alanine as an anion (e.i. [N_{2224}][L-Ala], [N_{2221}][L-Ala], [N_{2222}][L-Ala], [N_{2222}][b-Ala]) was approaching to 0.5 mol/mol of IL of CO_2 [Yu (2009)]. Wang et. al., have synthesized a functionalized amino acid ionic liquid [C_4mim]Gly by a low cost easy-preparation method and found that the maximum CO_2 sorption was ~ 0.5 mol of CO_2 per mol of IL [Wang (2011)]. The higher CO_2 sorption of AAPILs than that of AAIL could be explained based on their polymeric nature as they possess free volume in addition (vis-s-vis ILs) present in polymer matrix that would elevate the gas sorption. It is reported that the polymers obtained from ionic liquid monomers possessed higher CO_2 absorption capacity than their room temperature ionic liquid monomers [Tang (2005a), Mecerreyes (2011)]. Most importantly, the CO_2 absorption and desorption of PILs are much faster than those of ionic liquids, and the sorption/desorption is completely reversible. These poly(ionic liquid)s are thus very promising as sorbent and membrane materials for CO_2 separation [Tang (2005a), Mecerreyes (2011)].

It could be anticipated that changing the basicity of an anion could affect its interaction with CO_2. This change in acid-base interaction would in turn influence the CO_2 sorption in PILs. The solubility coefficient them was generally increased with increasing pK_a of anion as shown in Figure 5.8. The solubility coefficient of non-interacting gases was much lower and no correlation was found with pK_a. Similar behaviour was seen in case of solubility selectivity. It was observed that CO_2 sorption in room temperature ionic liquids (RTILs) vary with pK_a of conjugate acid of an anion [Wang (2011)]. Figure 5.9 shows that S_{CO_2}/S_{H_2} and S_{CO_2}/S_{N_2} increased with increasing pK_a of conjugate acid of the anion; while the selectivity of non-interacting gases (S_{N_2}/S_{CH_4}) was significantly lower and was not affected by the variation in pK_a. It could be thus concluded that the pK_a of conjugate acid of anion has a significant role in governing sorption of CO_2 of PILs.
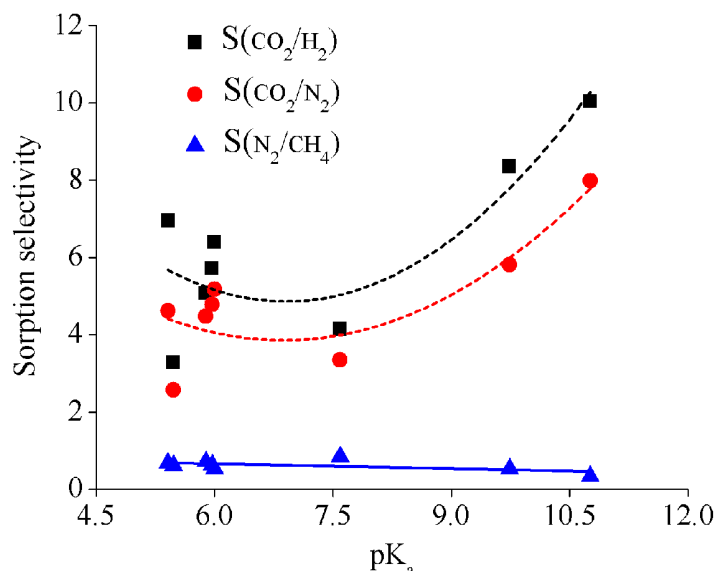
Figure 5.9 Variation of CO_2 based sorption selectivity with pK_a of different PILs.

5.4.2 Sorption parameters

Table 5.6 Dual-mode sorption parameters for PILs.

PILs	H₂			N₂			CH₄			CO₂		
	k_D	C'_H	b	k_D	C'_H	b	k_D	C'_H	b	k_D	C'_H	B
[DBzDMPBI-BuI][I]	0.37	3.4	0.001	0.37	5.0	0.001	0.17	6.8	0.20	0.33	20.1	0.21
[DBzDMPBI-BuI][Gly]	0.27	2.6	0.0015	0.3	5.0	0.004	0.19	9.0	0.11	0.47	27.7	0.15
[DBzDMPBI-BuI][L-Ala]	0.21	2.9	0.001	0.26	4.1	0.001	0.34	7.8	0.03	0.39	26.1	0.14
[DBzDMPBI-BuI][L-Arg]	0.09	4.3	0.05	0.19	2.4	0.066	0.4	6.7	0.05	0.36	23.1	0.2
[DBzDMPBI-BuI][L-Asp]	0.13	2.0	1.2E-05	0.18	2.1	0.0005	0.18	8.8	0.04	0.16	27.0	0.13
[DBzDMPBI-BuI][L-His]	0.31	4.0	0.0003	0.38	6.0	0.0001	0.27	5.9	0.08	0.28	25.0	0.14
[DBzDMPBI-BuI][L-Lys]	0.18	4.4	9.4E-05	0.25	5.6	0.0001	0.33	6.0	0.05	0.48	28.2	0.12
[DBzDMPBI-BuI][L-Phe]	0.27	3.2	0.0008	0.35	5.9	0.0004	0.31	7.8	0.10	0.13	22.0	0.12
[DBzDMPBI-BuI][L-Try]	0.24	1.2	0.002	0.24	2.6	0.021	0.24	7.0	0.04	0.36	22.0	0.19

k_D is expressed in $cm^3(STP)cm^{-3}polymer.atm^{-1}$, C'_H is expressed in $cm^3(STP)cm^{-3}polymer$, b is expressed in atm^{-1}.

The gas sorption parameters (k_D, b and C'_H) are given in Table 5.6. For all AAPILs, C'_H was higher for CO_2 than for other gases. This is in accordance with the gas sorption behaviour observed for most of the common glassy polymers [Barbari (1988), McHattie (1992), Kumbharkar (2006), Karadkar (2007)], possessing higher C'_H for CO_2 than for other gases owing to higher condensability of this gas [Kanehashi (2005)]. The Langmuir affinity constant 'b' is the ratio of rate constants of sorption and desorption processes and characterizes the

sorption affinity of a particular gas-polymer system [Kanehashi (2005)]. This parameter was negligible for H_2, N_2 and CH_4, but was considerably higher in case of CO_2. The C'_H values of present PILs are higher than for conventional glassy polymers.

5.5   Conclusions

A series of PILs containing amino acids as an anion (AAPILs) have been synthesized by anion exchange method. Selected amino acids were chosen based on their length of alkyl group and presence of other functional groups in them. The sodium salts of amino acids were used for the anion exchange; which was prepared by acid-base neutralization reaction. Considerably high anion exchange was achieved (~ 90%) using modified protocol. Concurrent effects of variation in amino acids were analyzed for physical and gas sorption properties of the resulting AAPILs. All of them exhibited good solvent solubility (soluble even in low boiling solvents viz., $CHCl_3$, CH_2Cl_2, acetone, methanol etc) and were amorphous in nature. Owing to the presence of interactions due to amino acid groups, thermal stability of these AAPILs was higher than that of parent PIL containing iodide anion. Thermal stability of PILs decreased with the order of anions as L-Asp > L-Phe > L-Try ~ L-Ala ~ L-His ~ Gly ~ L-Lys ~ I > L-Arg. The order of CO_2 sorption in AAPILs with different anion was L-Arg > L-Lys > L-His > L-Try > L-Ala > Gly > L-Asp > I > L-Phe. AAPIL with L-Arg anion showed higher CO_2 sorption as well as CO_2 based sorption selectivity than that of other anions because of presence of more effective and number of *N*-sites for CO_2 sorption. The CO_2 sorption in AAPILs was found to depend upon the pK_a, which is a function of number and type of primary and secondary amine group present in the anion. This study concludes that amino acids as an anion could be a promising option for synthesizing PILs for CO_2 sorption.

Chapter 6

PIL-PBI blend membranes: Physical and electrochemical evaluations towards their applicability as membranes for PEMFC and AEMFC

6.1 Preamble

This work presents an approach of blending polymeric ionic liquids (PILs) with PBI for applicability of resultant membranes as high temperature proton exchange membrane fuel cell (PEMFC) as well as anion exchange membrane fuel cell (AEMFC). Recently, ionic liquids (ILs) have attracted considerable attention in electrochemical applications. They are non-volatile and are composed of organic cations and organic or inorganic anions. Use of proton-conducting ionic liquids (PCILs) was proposed in order to ensure high anhydrous proton conductivities while maintaining sufficient thermal stability. The membranes based on PBI-IL blends have been reported to exhibit high proton conductivity at high temperatures [Ye (2008), Wang (2011), Shen (2012), Mishra (2014)]. However, addition of IL in PBI decreased mechanical properties of resulting PBI-IL composite membranes [Wang (2011), Shen (2012)]. Moreover, ILs tends to leach out from the membrane after prolonged usage [Mishra (2012), Mishra (2014)]. Most of these issues can be addressed if the IL moiety is located in polymeric backbone, viz., polymeric ionic liquids (PILs). They are anticipated to provide continuous pathway of IL character due to their polymeric nature and would also eliminate the issue of IL drain. PILs also hold some of the unique properties of IL (e.g. ionic conductivity, thermal stability, tunable solution properties and chemical stability), which are combined with intrinsic polymer properties [Mecerreyes (2011), Yuan (2013)]. Such amalgamation is anticipated to offer better benefits than simple ILs. Possibilities of tuning cation-anion pair further allow their property variations [Green (2009)].

Present work deals with preparation and analysis of blend membranes obtained from a PIL, poly(diallyldimethylammonium trifluoromethanesulfonate) (P[DADMA][TFMS]) in varying proportions with PBI. Their physicochemical (spectral, thermal, mechanical, chemical, H_3PO_4 doping) and electrochemical (proton conductivity, single cell testing) properties were examined in order to validate the proposed approach of blending PIL rather than IL in the membrane matrix. These membranes were evaluated for proton as well as hydroxide ion transport.

6.2 Synthesis of PBI and PIL

PBI-I was synthesized by solution polycondensation in PPA (Scheme 2.1, as given in Chapter 2, Section 2.2.1). The obtained PBI-I was purified by dissolving in DMAc (3% w/v) and reprecipitation in water, yielding a yellow colored fibrous polymer. The inherent viscosity of purified PBI was 1.24 g/dL.

PIL was prepared by anion exchange method in an aqueous medium using commercially available polyelectrolyte precursors, P[DADMA][Cl]. It's quaternary nitrogen is a part of a five-membered cyclic ring that contributes to the polymer chain backbone (Scheme 2.8, as given in Chapter 2). For anion exchange, Ag salt of trifluoromethanesulfonate (TFMS) was used. The advantage of using silver salt was that during the anion exchange, precipitation of silver chloride takes place in an aqueous medium. This makes the anion exchange an irreversible reaction. Moreover, separation of the formed AgCl can be done by simple centrifugation. The obtained PIL was estimated for residual chloride content by Volhards method (as given in Chapter 2, Section 2.4.1). It was found that the amount of chloride anion exchanged with TFMS was 97%, which is appreciably high.

6.3 PBI-PIL blend membranes

Blend membranes possessing varying content of PIL: (P[DADMA][TFMS]) in PBI were made by solution casting method; where free-standing yellowish-brown transparent films were obtained till 45 wt% of PIL in PBI (Figure 6.1). Beyond this concentration of PIL, though free standing films without any inhomogeneity could be successfully prepared, they became fragile in H_3PO_4 (15M) during the doping process and thus were not investigated further.
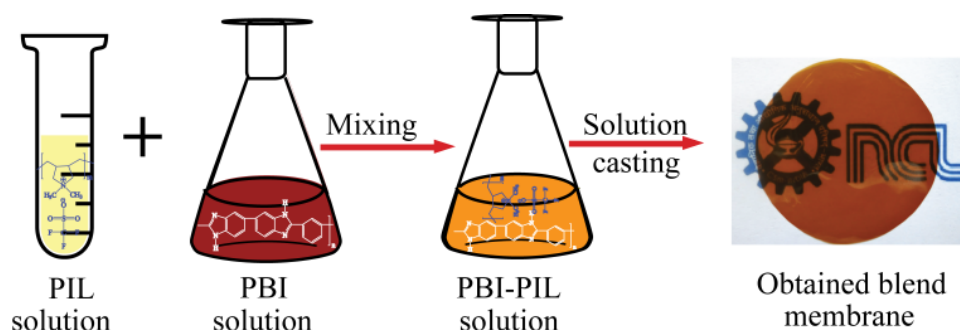
Figure 6.1 Preparation of PBI-PIL blend membranes.
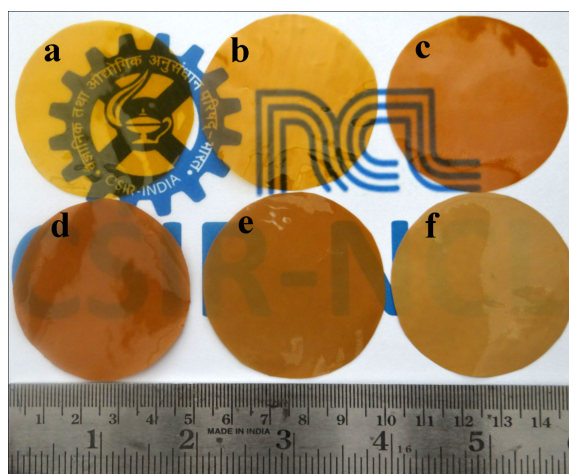
Figure 6.2 Photographs of PBI-PIL blend membranes (a) PBI, (b) PBI-PIL$_5$, (c) PBI-PIL$_{15}$, (d) PBI-PIL$_{25}$, (e) PBI-PIL$_{35}$, (f) PBI-PIL$_{45.}$
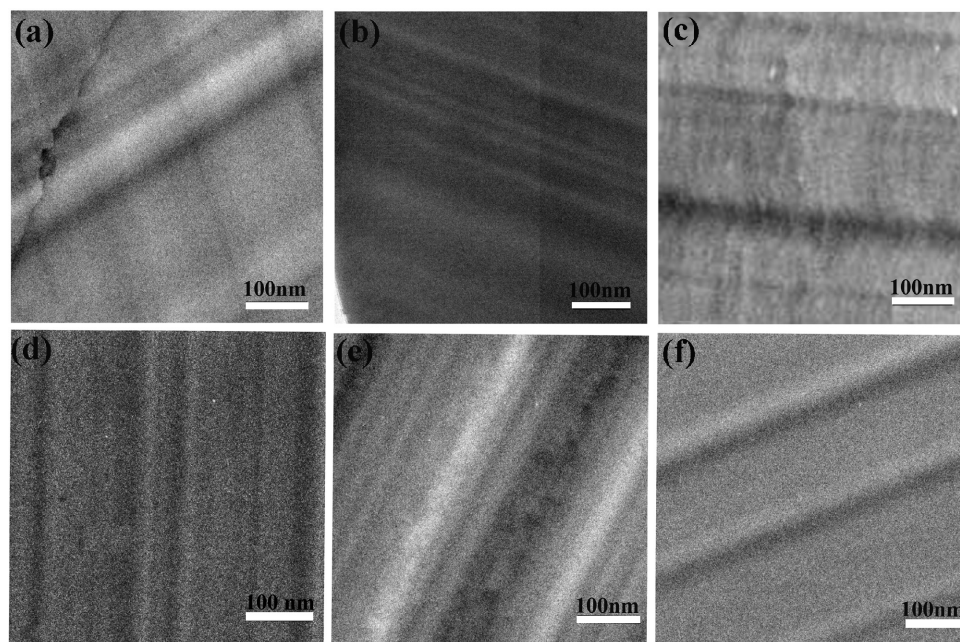
Figure 6.3 TEM images of PBI-PIL blend membranes (a) PBI, (b) PBI-PIL$_5$, (c) PBI-PIL$_{15}$, (d) PBI-PIL$_{25}$, (e) PBI-PIL$_{35}$, (f) PBI-PIL$_{45}$.

The photographs (Figure 6.2) of blend membranes visually convey homogeneity of the formed membranes, which was further ascertained by TEM images (Figure 6.3). The formed

blend membranes were thoroughly investigated for requisite physical characterizations, which proved blend formation.

6.4 Spectral and physicochemical characterization

6.4.1 FTIR spectra of blend membranes

The FTIR spectra of all the PBI-PIL blend membranes exhibited typical bands corresponding to benzimidazole of PBI (1430, 1600 and 1620 cm^{-1}) as well as the sulfone group (1030 cm^{-1}) of PIL (Figure 6.4).
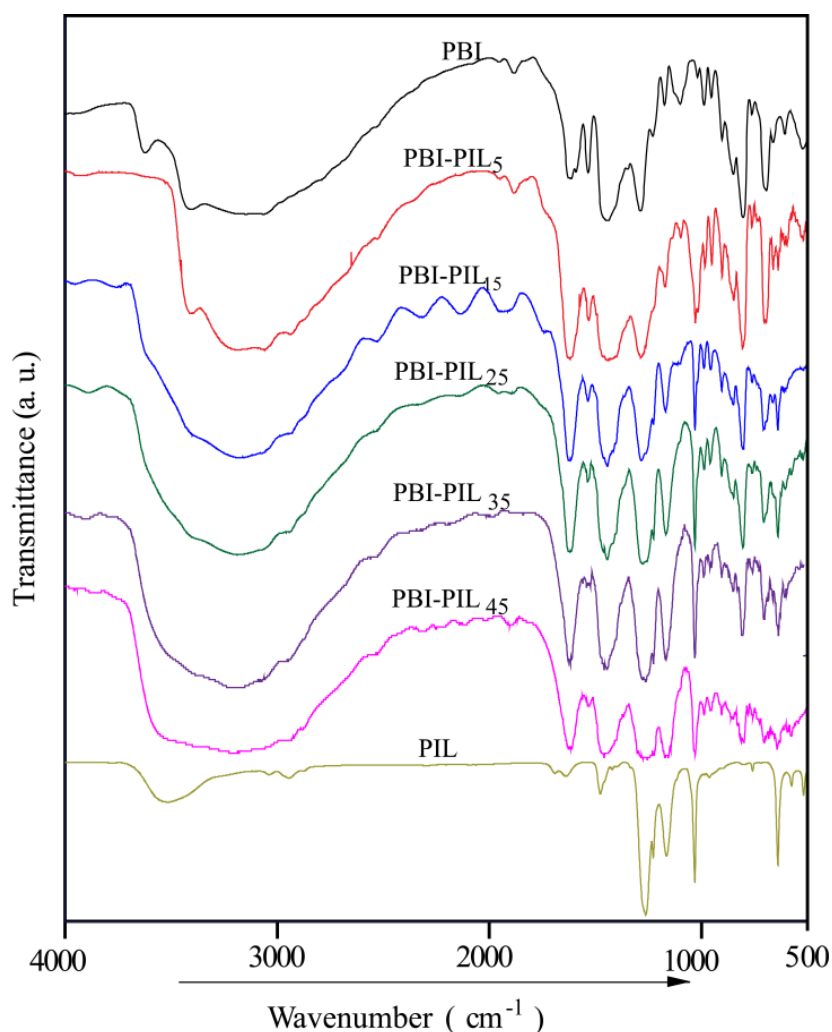
Figure 6.4 FTIR spectra of PBI-PIL blend membranes.

From Figure 6.4, it is evident that with increasing PIL content in the blend, the free non-hydrogen bonded N-H stretching band at 3434 cm^{-1} present in pristine PBI showed a substantial

broadening and displacement to lower frequencies. The red shift and the peak broadening after the blending are indicative of interactions between the PBI with PIL. It can thus be concluded that interactions of imidazole N-H of PBI and ionic nature of PIL is responsible for offering miscible blends. Similar shift in IR bands was seen in the blends of PBI with poly(vinylidene fluoride) [Arunbabu (2008)] and poly(4-vinyl pyridine) [Makhija (1990)]. The elucidation of hydrogen bonding interaction in PBI and PIL is showing in Figure 6.5.
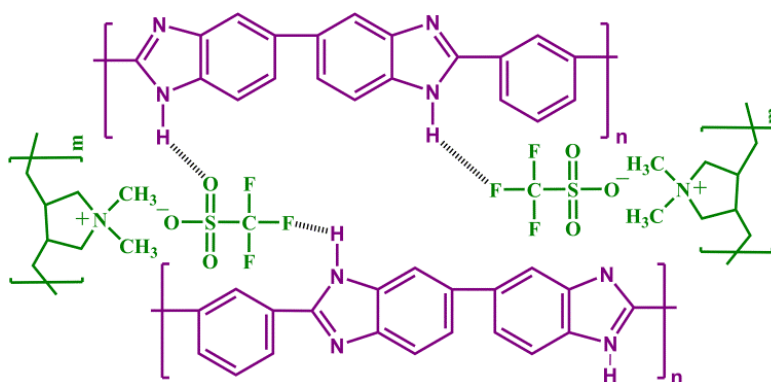
Figure 6.5 Probable interactions between PBI and PIL.

6.4.2 Thermal properties of blend membranes

Thermal properties of the blend were studied by TGA and DSC under N_2 atmosphere (Figure 6.6 and 6.7). It could be seen that the decomposition temperature of PBI and PIL are ~600 °C and ~375 °C, respectively.
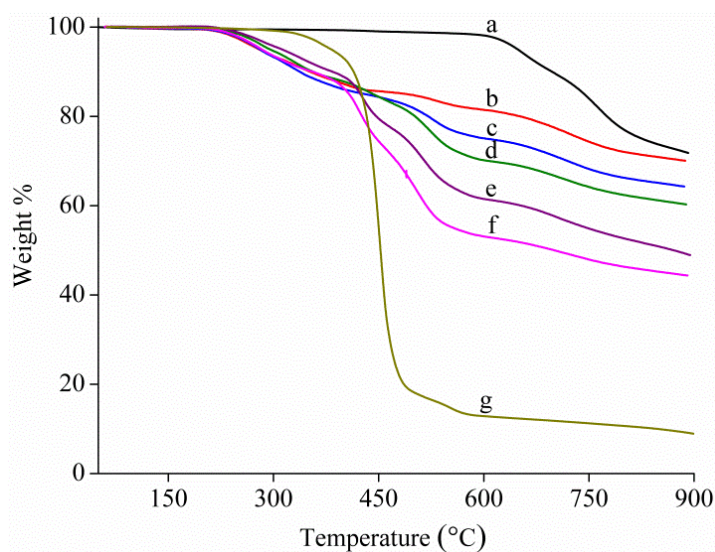
Figure 6.6 TGA curve of PBI-PIL blend membranes (a) PBI, (b) PBI-PIL$_5$, (c) PBI-PIL$_{15}$, (d) PBI-PIL$_{25}$, (e) PBI-PIL$_{35}$, (f) PBI-PIL$_{45}$, (g) PIL.

119

For the blend membranes, two-step degradation pattern was observed (Figure 6.6). The first degradation beginning at ~240 °C corresponds to ~15% weight loss. This temperature is far below than the IDT of either of the precursor polymers. Since these samples were dried at 100 °C in vacuum oven for 7 days prior to the analysis and were again subjected to the temperature up to 150 °C before recording the TGA, it is unlikely that the observed degradation with 15% wt loss can be ascribed to the presence of water. It may be possible that anions of PIL became more labile due to interactions with PBI's N-H group and became responsible for the weight loss. The second abrupt degradation starts at > 400 °C, can be correlated to the degradation of PIL backbone. Similar two stage degradation is reported for the blends of PBI and poly(4-vinylpyridine) [Arunbabu (2008)]. The char yield of the blend membrane at 900 °C decreased with increase in the amount of PIL, as anticipated; since the char yield of PIL is much lower than that of PBI (Table 6.1). This qualitatively correlates to the amount of PIL present in the blend. Although, the thermal stability of the blend membranes decreased in comparison to the parent PBI, it was high enough ($\geq$ 240 °C) for their applicability as the membrane for HT-PEMFC.

Table 6.1 Physical properties of PBI-PIL blend membranes.

Membrane	$d_{sp}{}^a$(Å)	Thermal analysis			Permeability coefficient $(P)^c$		Oxidative stability		H_3PO_4 uptake (Wt %)	Hydrolytic Stability
		IDT^b (°C)	Char yield (%)	T_g(°C)	$P(H_2)$	$P(O_2)$	Weight loss after 12 h (%)	Weight loss after 18 h (%)		Weight loss after 15 days (%)
PBI	3.63	600	72	416	0.63^d	0.015^d	0.091	1.12	308	0.76
PBI-PIL$_5$	4.0	530	70	405	0.47	0.008	9.25	10.97	323	0.56
PBI-PIL$_{15}$	3.89	528	64	370	0.63	0.025	13.20	14.50	324	0.66
PBI-PIL$_{25}$	4.35	449	60	345	0.64	0.026	15.83	Break	330	0.69
PBI-PIL$_{35}$	4.10	417	49	337	0.81	0.028	21.20	Break	355	0.63
PBI-PIL$_{45}$	4.14	407	44	327	0.90	0.046	37.03	Break	413	0.70
PIL	5.12	375	9	114	-	-	Break	Break	-	-

^{a}: d-Spacing obtained from WAXD pattern, ^{b}: initial decomposition temperature, ^{c}: expressed in Barrer (1 Barrer = 10^{-10} cm^3.(STP).cm/cm^2.s.cm Hg), ^{d}: [Kumbharkar (2006)].

The DSC thermograms of PBI, PIL and their blends with different compositions are shown in Figure 6.7. A single T_g of a blend, which lies in between the glass transition temperature of individual components (PBI and PIL) further confirms the miscible blend

fomration. It is understood that in a binary polymer blend, presence of a single T_g is indicative of a miscible blend formation [Foldes (2000), Pu (2003)]. It could also be seen from Figure 6.8 that with increasing amount of PIL in the blend, T_g was decreased. This could be anticipated based on the considerably lower T_g of PIL than that of PBI (Table 6.1). These results also indicate that the T_g of the blends are controlled by the strength of interactions between the blend components. As a result of such interactions, PIL chains start their segmental motion at much higher temperature than their individual T_g.
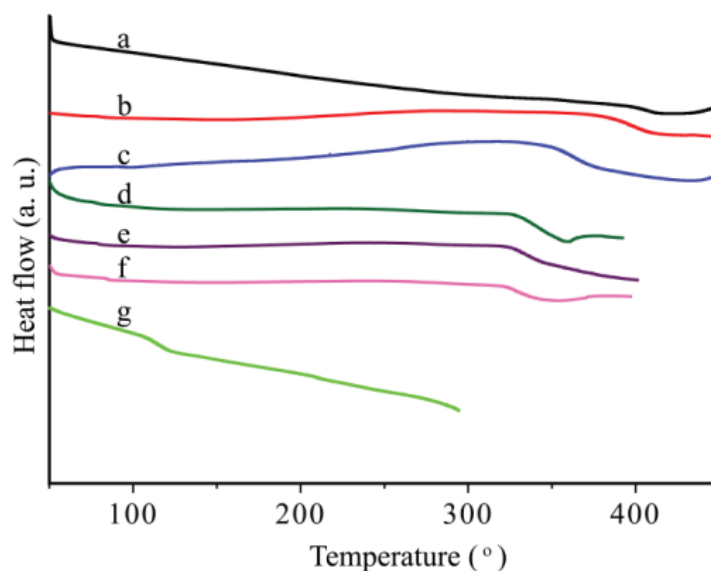
Figure 6.7 DSC curves of blend membranes (a) PBI, (b) PBI-PIL$_5$, (c) PBI-PIL$_{15}$, (d) PBI-PIL$_{25}$, (e) PBI-PIL$_{35}$, (f) PBI-PIL$_{45}$, (g) PIL.

For miscible polymeric blends, the Fox equation (6.1)is extensively used to describe their glass transition temperature [Foldes (2000)]:

$$\frac{1}{T_g} = \frac{W_1}{T_{g_1}} + \frac{W_2}{T_{g_2}}$$

(6.1)

where W_1 and W_2 are the mass fractions, T_g is the glass transition temperature of the blends, T_{g1} and T_{g2} represent the glass transition temperature of the pure components (PBI and PIL, respectively). As could be seen from Figure 6.8, the experimental values are placed well above than the predicted values obtained by the Fox equation. This suggests that the interactions between PBI and PIL are quite strong and represents a good miscibility of PBI and PIL in the blend membranes.
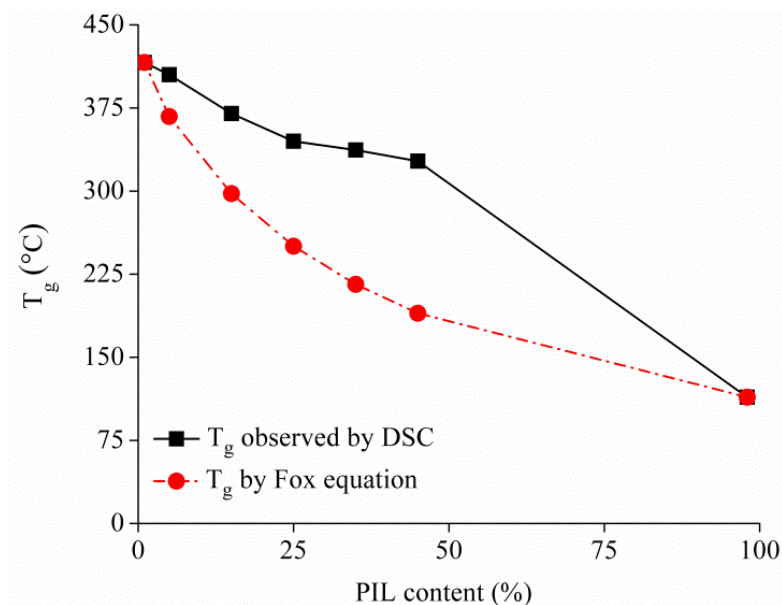
Figure 6.8 Composition dependence of the T_g determined by DSC (—■—) and that calculated by the Fox equation (⋯◆⋯).

6.4.3 Inherent viscosity and WAXD pattern of blend membranes

The inherent viscosity (η_{inh}) of blends was increased with increasing amount of PIL in them, as shown in Figure 6.9.
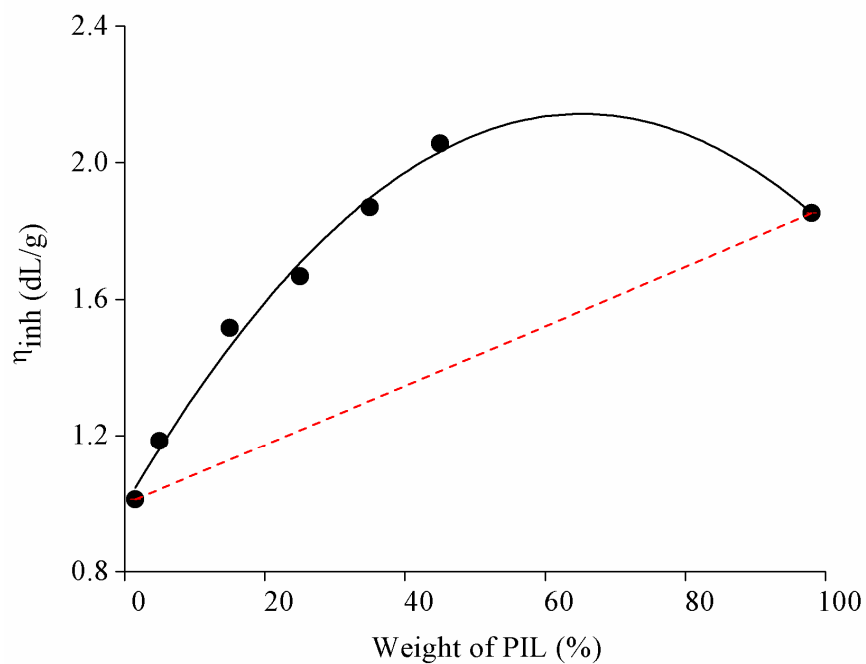
Figure 6.9 Variation in inherent viscosity of PBI-PIL blend membranes with composition.

The obtained viscosity of a particular blend composition was higher than the one calculated based on the additivity rule (a dotted line joining viscosity of pure PBI and PIL). This positive deviation of experimental observation reflects increasing PBI-PIL interactions with increasing PIL content in the blend. Such as increase in viscosity due to the miscible blend formation is known for poly(vinylidene fluoride)-poly(methyl methacrylate) and poly(vinylidene fluoride)-polystyrene blend systems [Soria (1994)]. This positive deviation could be ascribed to the favorable interactions among blend components. In the present case, an elevation in viscosity suggests that molecular level interactions of PBI and PIL are highly favorable, leading to homogeneous blend formation.

The WAXD pattern of PBI showed a completely amorphous broad peak, while PIL shows sharper peaks indicating its crystalline nature (Figure 6.10). All blend membranes exhibited amorphous nature, where crystalline peaks corresponding to the PIL are completely absent (Figure 6.10). This result further ascertains that the PIL has lost its individual crystalline identity in the formed blend membranes due to strong interactions between PBI and PIL; offering well miscible blend system.
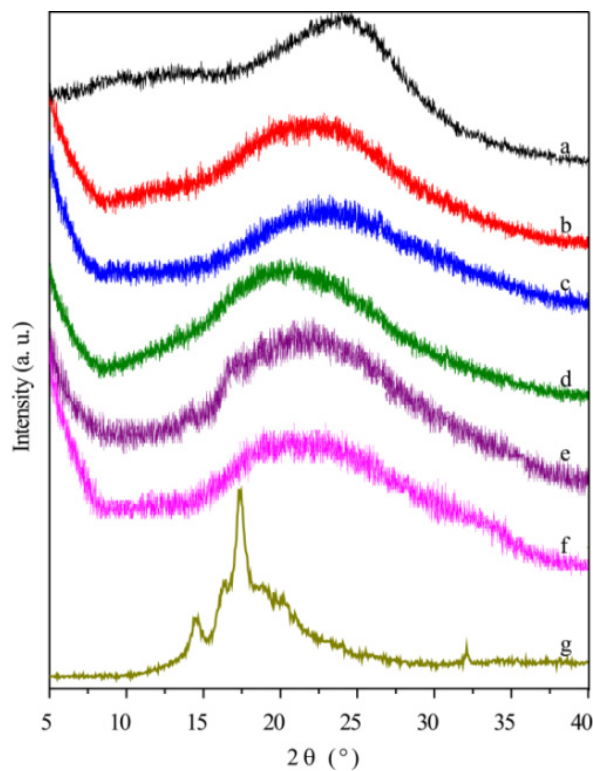
Figure 6.10 WAXD patterns of PBI-PIL blend membranes (a) PBI, (b) PBI-PIL$_5$, (c) PBI-PIL$_{15}$, (d) PBI-PIL$_{25}$, (e) PBI-PIL$_{35}$, (f) PBI-PIL$_{45}$, (g) PIL.

6.4.4   Gas permeability, oxidative and hydrolytic stability of blend membranes

In view of possible applicability of these blend membranes in PEMFC, permeability of H_2 and O_2 was measured (Table 6.1). It can be seen that the blend membranes have comparable H_2 and O_2 permeability as that of PBI. This result suggests that all the blend membranes having low gas permeability can be used as membranes for PEMFC/AEMFC, without a serious threat of fuel crossover. It is a crucial phenomenon, where fuel supply at the anode intersects over into the cathode catalyst layer, which adversely affects the overall fuel cell performance [Li (2009), Sprague (2010)] and need to be minimized to the possible extent.

The oxidative stability of the membrane is critical for its application in PEMFC and AAEMFC. It is generally evaluated by the Fenton's test [Li (2003), Borup (2007), Brujin (2007)]. For this study, the blend membranes were soaked in 3% H_2O_2 containing 3 ppm $FeSO_4$ at 80 °C and the weight loss was recorded as given in Table 6.1. In comparison with the PBI membrane, blend membranes exhibit inferior resistance to oxidation. This could be due to the weak bond energy of the C–H in PILs. Oxidative stability decreased with the increasing content of PIL in the blend membrane (i.e. PBI > PBI-PIL$_5$ > PBI-PIL$_{15}$ > PBI-PIL$_{25}$ > PBI-PIL$_{35}$ > PBI-PIL$_{45}$). It is well known that during operation of the fuel cell, peroxide radicals may be produced. The radical oxidation-induced polymer degradation has been identified to be one of the main reasons that cause deterioration of the proton exchange membrane [Soria (1994)]. It is said that the radicals (eg $HO^\bullet$ and $HOO^\bullet$) are responsible for the degradation of membranes during fuel cell operation [Borup (2007), Bruijn (2007)]. It is greatly desirable to investigate oxidative stability of new materials to be used as membranes for PEMFC/AEMFC.

All blend membranes were hydrolytically stable for > 2 weeks. It was also observed that all the membranes remain flexible when they were bent even after such a prolonged water treatment. After treatment for 2 week, weight of dried membrane (dried at 100 °C in vaccum oven for 3 days) was measured and it was observed that the weight for all the blend membranes was almost similar before and after treatment (Table 6.1). There was a very small weight loss that could be an artifact.

6.4.5   Acid doping of blend membranes

Figure 6.11 shows that with increasing bath concentration of H_3PO_4, doping level of the blend membranes increased progressively, as anticipated.
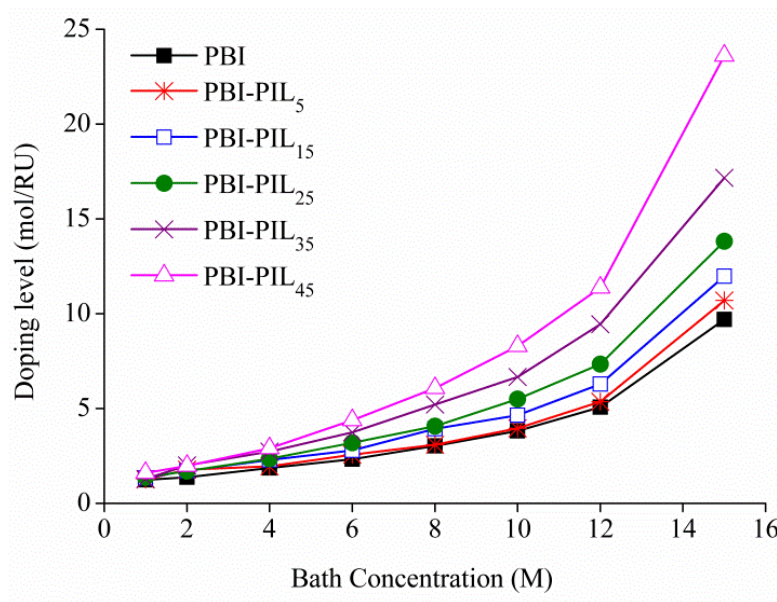
Figure 6.11 Variation in the doping level of PBI-PIL blend membranes with bath concentration.

The acid uptake in the blend membranes is more than that of pristine PBI membranes in all the range of bath concentrations. It is encouraging to note that the formed blend membranes are stable and no coloration was observed even in 15M H_3PO_4. This is particularly important when we had observed complete dissolution of PIL (P[DADMA][TFMS]) in 15M H_3PO_4, offering pale yellow color to the resulting PIL solution. It could thus be said that the PIL chains were well blended with the PBI and did not leach out during the doping by H_3PO_4. Owing to this excellent stability, conductivity analysis and single cell MEA experiments for PEMFC were performed using membranes doped with 15 M H_3PO_4.

6.4.6   Alkaline stability of blend membranes

In view of possible applicability of these blend membranes in alkaline anion exchange membrane fuel cell (AAEMFC), stability of blend membranes in alkaline condition was evaluated. The long-term stability of AEMs is of concern due to well-known degradation pathways for tetra alkyl ammonium ions under alkaline conditions. Variation degradation mechanisms include beta-hydrogen Hofmann elimination [Iojoiu (2006), Cheng (2015)], direct nucleophilic substitution at an alpha-carbon [Couture (2011), Cheng (2015)], or nitrogen ylide formation [Cope (1963), Cheng (2015)]. The alkaline stability of the present blend AEMs was determined by observing changes in flexibility with time in 1 M, 2 M and then in 3 M KOH

solution at RT for 7 days. All of the membranes remained tough and flexible throughout these tests, which confirms the stability of the miscible blend membranes in alkaline condition.

6.4.7 Ion exchange capacity of blend membranes

Ion exchange capacity (IEC) of these blend membranes is an important property for their applicability as an anion exchange membrane for fuel cell (AEMFC). The IEC was determined based on the theoretical value of TFMS anions present in the blend membrane. The method experimental determination of IEC is described in Chapter 2. The ion exchange capacity is basically number of ion present per mol of polymer [Thomas (2011), Karas (2014)], which increased with increasing amount of PIL in the present blend membranes (Table 6.2).

Table 6.2 Ion exchange capacity and water uptake capacity of blend membranes.

Membrane	Ion exchange capacity $(meq.g^{-1})$	Water uptake capacity (Wt %)
PBI	0	12.45
PBI-PIL$_5$	0.16	13.33
PBI-PIL$_{15}$	0.50	13.76
PBI-PIL$_{25}$	0.83	14.15
PBI-PIL$_{35}$	1.18	14.37
PBI-PIL$_{45}$	1.54	16.08

6.4.8 Water uptake capacity of the blend membranes

Water uptake (WU) of AEMs is an important parameter for their IEC, ionic conductivity, mechanical strength and membrane electrode compatibility. The WU was evaluated at RT for 24 h dip time. Table 6.2 compares the IEC and water uptake. Generally, the water uptake of membranes increased with IEC value (or PIL content). The highest water uptake was 16.08 wt % at RT for the membrane PBI-PIL$_{45}$ (IEC = 1.54 meq.g^{-1}).

6.4.9 Mechanical properties of blend membranes

One of the important requirements of the membrane for PEMFC application is its good mechanical stability. Figure 6.12 and 6.13 show mechanical properties of the PBI-PIL blend membranes in undoped and doped conditions, respectively. The tensile strength and Young's modulus of the undoped membrane decreased with increasing amount of PIL, while elongation increased with increasing amount of PILs (Table 6.3). These observations suggest that the PIL

may be acting as a plasticizer to make the PBI backbone more flexible. This could be anticipated based on its lower glass transition temperatures (T_g).
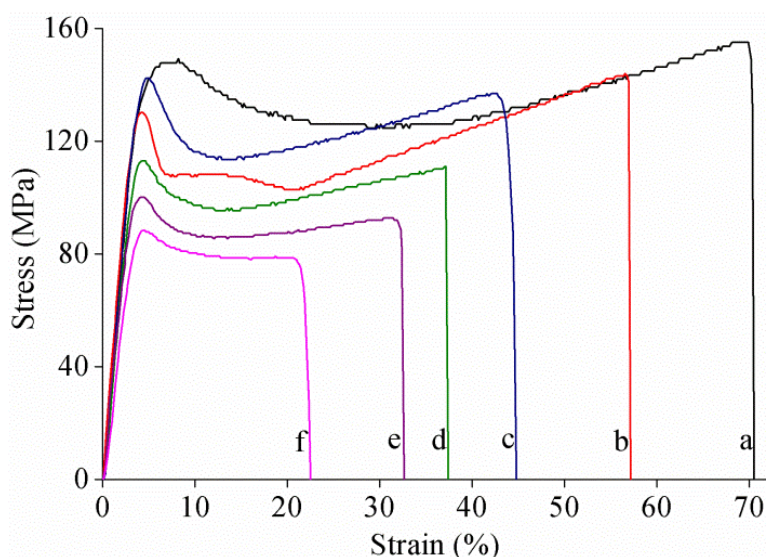
Figure 6.12 Stress-strain curve of undoped PBI-PIL blend membranes (a) PBI, (b) PBI-PIL$_5$, (c) PBI-PIL$_{15}$, (d) PBI-PIL$_{25}$ (e) PBI-PIL$_{35}$, (f) PBI-PIL$_{45}$.
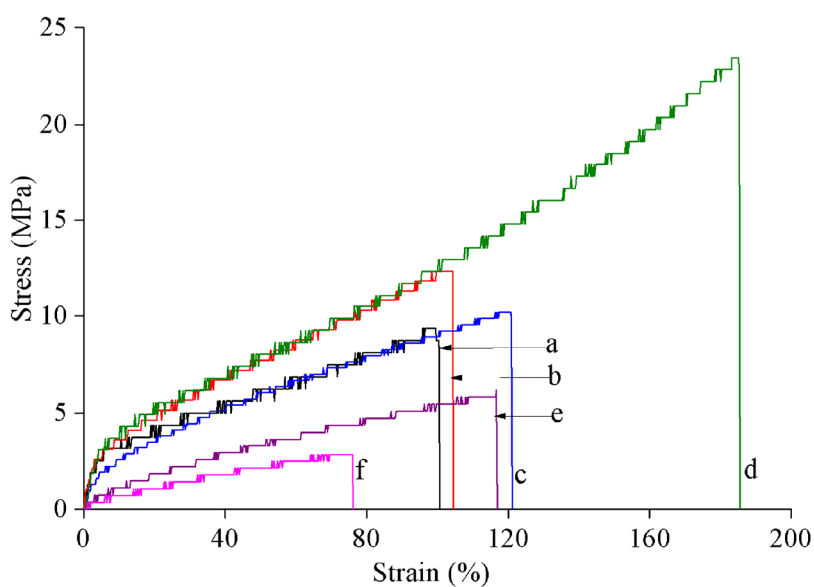
Figure 6.13 Stress-strain curve of doped PBI-PIL blend membranes (a) PBI, (b) PBI-PIL$_5$, (c) PBI-PIL$_{15}$, (d) PBI-PIL$_{25}$ (e) PBI-PIL$_{35}$, (f) PBI-PIL$_{45}$.

The stress-strain curve (Fig. 6.12) shows that all the undoped membranes exhibited glassy nature. After doping, these membranes exhibited stress-strain curves which are typical of rubbery

127

nature (Fig. 6.13). This is due to the uptake of H_3PO_4. It is known that the glassy PBI after doping with H_3PO_4 exhibit rubbery nature [Li (2009), Kumbharkar (2009)]. We have measured the proton conductivity of PA doped blend membrane by varying the temperature from 30 to 150 °C in dry condition.

Table 6.3 Mechanical properties of PBI-PIL blend membranes.

Membrane	Before H_3PO_4 doping			After H_3PO_4 doping		
	Modulus (GPa)	Tensile strength (MPa)	Elongation (%)	Modulus (MPa)	Tensile strength (MPa)	Elongation (%)
PBI	3.7	155.1	70.5	80.7	9.4	100.7
PBI-PIL$_5$	3.8	144.0	57.2	78.1	12.4	104.5
PBI-PIL$_{15}$	3.5	115.0	34.5	70.6	10.2	121.1
PBI-PIL$_{25}$	3.5	107.3	41.9	74.1	23.8	188.1
PBI-PIL$_{35}$	3.2	97.2	38.8	20.4	5.0	99.0
PBI-PIL$_{45}$	2.7	88.3	22.5	3.9	2.8	76.5

6.5 Electrochemical analysis of blend membranes

6.5.1 Electrochemical property analysis for PEMFC

The proton conductivity is a highly significant property of a membrane towards its applicability as for fuel cell. The proton conductivity of PBI-PIL blend membranes as a function of temperature is shown in Figure 6.14.
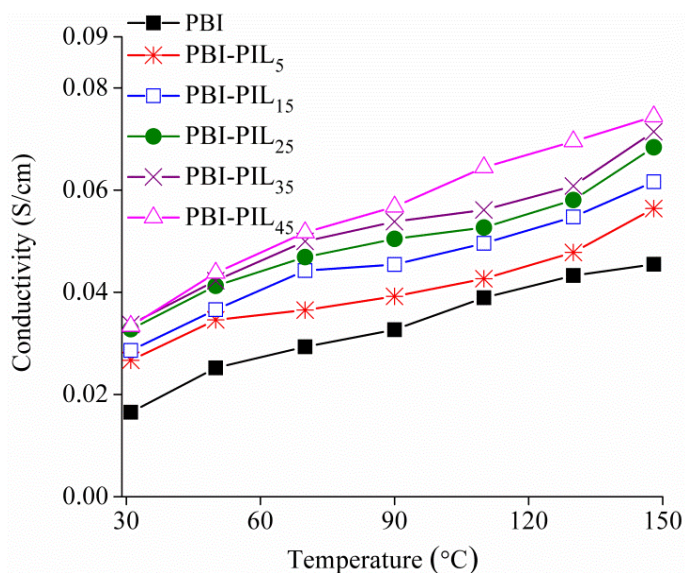
Figure 6.14 Proton conductivity of blend membranes as a function of temperature.

128

It was found that conductivity increased with increasing temperature as well as with the PIL content. The proton conductivity of the PBI membrane was 0.04 S.cm^{-1} at 150 °C, which further increased up to 0.07 S.cm^{-1} for PBI-PIL$_{45}$ at the same temperature.

In order to further elucidate the effects of PIL in the blend membranes, the activation energy (E$_a$) for proton transport was calculated from the slope of the plot corresponding to proton conductivity in a logarithmic scale *vs* inverse of temperature (1/K) by using the Arrhenius equation (Figure 6.15) [Lin (2010), Sannigrahi (2011)].
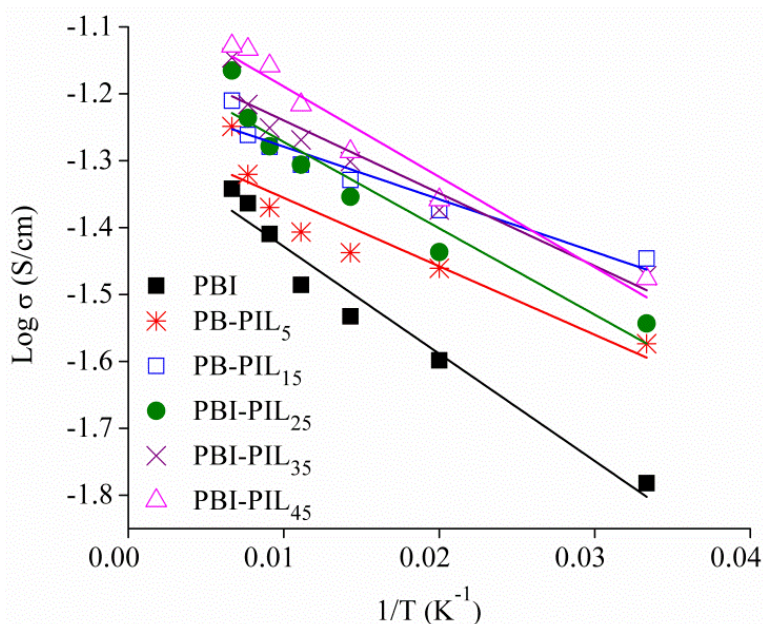
Figure 6.15 Arrhenius curve of proton conductivity of PBI-PIL blends membrane at different temperatures.

The fitting curve used to calculate the E$_a$ values had temperature boundary conditions of 30 and 150 °C. The values determined are presented in Figure 6.16. This curve shows that the activation energy decreased with increasing the PIL content in the blend up to a loading of PIL corresponding to 25%. The activation energy became almost stable with further increase in the amount of PIL in the blend membranes. The calculated E$_a$ values (12.5-13.4 kJ.mol^{-1}) of all the blend membranes are lower than that of the PBI membrane reported in the literature (13-25 kJ.mol^{-1}) [Asensio (2003), Carollo (2006), Xu (2009), Xu (2011), Daletou (2014)], but are higher than that of Nafion membrane (9-11 kJ.mol^{-1}) [Silva (2004), Tay (2008), Sadrabadi (2010)]. On the basis of the E$_a$ values, it can be concluded that PBI-PIL blend led to a lower E$_a$ than that of

PBI due to the presence of additional internal conducting channels provided by PIL chains involved in the transport process. By comparing the E_a values, it can also be concluded that the proton transport of this type of blend based membranes might have occurred predominantly by the Grotthuss mechanism.
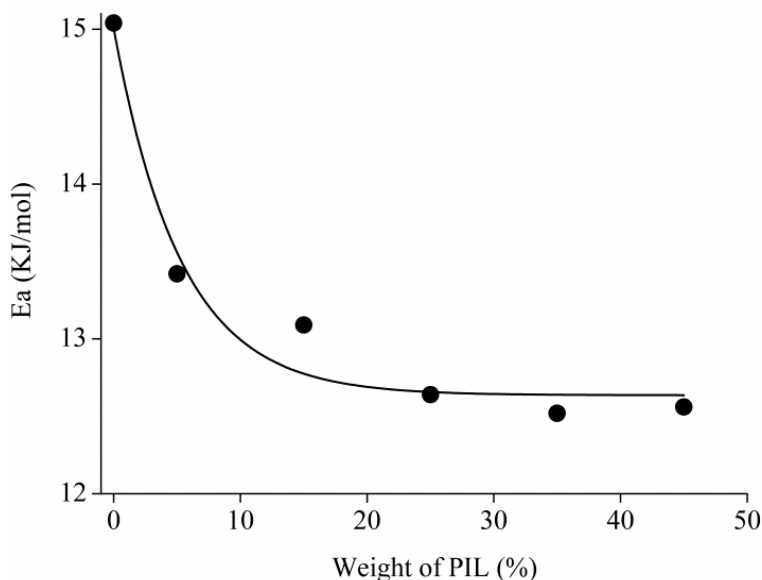
Figure 6.16 Activation energy of PBI-PIL blends membrane with weight percent of PIL.

Figure 6.17 shows the single cell performance of PBI-I, PBI-PIL$_{15}$, PBI-PIL$_{25}$ and PBI-PIL$_{35}$ as the membrane electrolyte at an operating temperature of 160 °C. The performance assessment was done on a 9 cm^2 MEA prepared by using the blend membrane (~200 μm thick) and Pt/C (40 wt.% Pt supported on active carbon) as the catalyst. The Pt loading of 1 mg.cm^{-2} was used on both the electrodes.

The open circuit potentials (OCPs) and power densities of these MEAs at 160 °C were found to be 0.88, 0.94, 0.96, 0.98 V and 277, 364, 512, 440 mW.cm^{-2}, respectively. The higher OCP is an indication of the absence of fuel crossover from anode to cathode through the membrane. The maximum current density obtained in these experiments was 1261, 1467, 1632 and 1478 mA.cm^{-2}, respectively. As shown in Figure 6.17, PIL content in the membrane improved the cell performance as compared to that of PBI-I. The performance was highest for PBI-PIL$_{25}$ blend composition. At current densities below 1.4 A.cm^{-2}, the curves PBI-PIL$_{15}$ and PBI-PIL$_{35}$ were overlapping, despite differences in the proton conductivity, which should lead to variations in ohmic losses. This behavior is likely to be a result of the important contribution of

the interfacial resistance to the ohmic loss. Indeed, no optimizations of the membrane electrode assembly were undertaken at this stage.
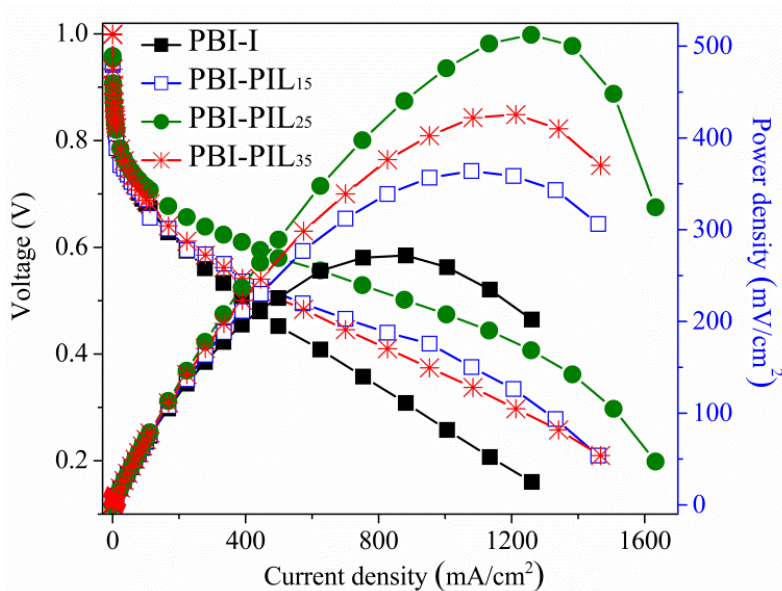
Figure 6.17 Polarization curve of PBI-I, PBI-PIL$_{15}$, PBI-PIL$_{25}$ and PBI-PIL$_{35}$ blend membranes.

In order to understand the fuel cell performance and examine the ohmic resistance of the single cells of the blend membranes (PBI-PIL$_{15}$ and PBI-PIL$_{35}$), electrochemical impedance spectroscopy was carried out at OCV and 0.6 V, Figure 6.18 shows the Nyquist plots of PBI-PIL$_{15}$ and PBI-PIL$_{35}$ blend membranes.
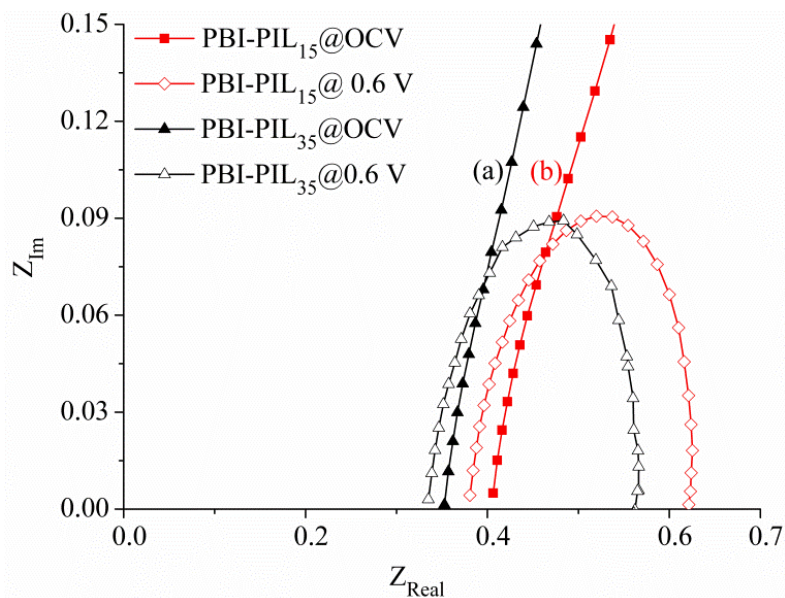
Figure 6.18 MEA impedance curves of PBI-PIL$_{35}$ and PBI-PIL$_{15}$ blend membranes.

At 0.6 V, the Nyquist plots were semi-circular; the left point of intersection with the *x*-axis corresponds to the ohmic resistance and the diameter of the semi-circle to the charge transfer resistance. By comparing Figure 6.18a and b, it is observed that with increasing content of PIL, ohmic resistance decreases. From the point of intersecting with the real axis of the high frequency limit, the internal resistance (ESR, equivalent series resistance) of the single cells for PBI-PIL$_{15}$ and PBI-PIL$_{35}$ was estimated as 0.41 and 0.35 Ω cm^{-1} at OCV and 0.38 and 0.33 Ω cm^{-1} at 0.6 V, respectively. In the AC impedance measurement, the oxygen electrode served as the working electrode and hydrogen electrode as the counter electrode. The counter electrode also served as the reference with its negligible over potential for the hydrogen oxidation or evolution reaction. Thus, the charge transfer resistance obtained through the AC impedance study primarily could be attributed to the oxygen reduction reaction. The charge transfer resistance of the single cells of PBI-PIL$_{15}$ and PBI-PIL$_{35}$ MEAs are almost same (0.23 Ω cm^{-1} and 0.22 Ω cm^{-1}).

6.5.2 Electrochemical property analysis for AEMFC

Hydroxide conductivity is a critical performance for AEMs. The conductivity of the present blend membranes was determined in the fully hydrated state with varying temperature are listed in Table 6.4. Figure 6.19 illustrates the in-plane ionic conductivity of all the membranes at different temperatures.
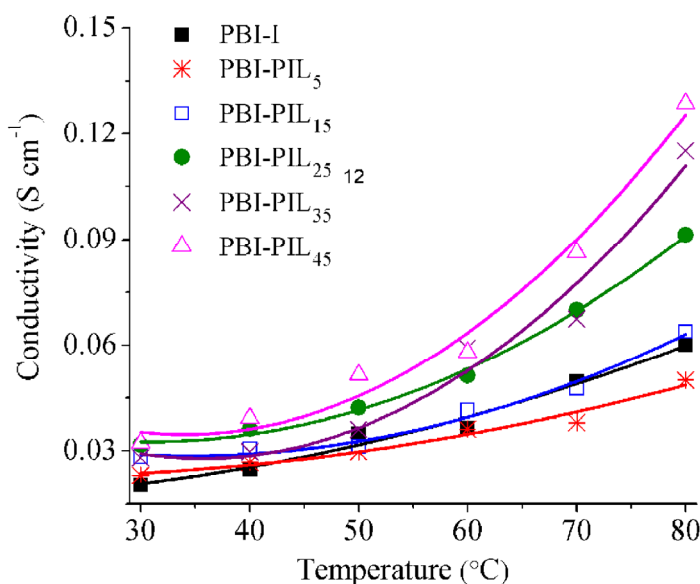
Figure 6.19 Hydroxide conductivity of PBI-PIL blends membrane at different temperatures.

The conductivity of blend increased with increasing temperature as well as increasing PIL content in the blend membrane. This could be due to increased ion exchange capacity of blend membrane with increasing PIL content, as shown in figure 6.20. AEMFC has a drawback compared to PEMFC that the hydroxide ion has a lower diffusion coefficient than that of the protons. Consequently, it turns out to be difficult to reach conductivity similar to that of proton conducting membranes. Besides, there are no anion-exchange membranes (AEM) as efficient as Nafion is for the proton conducting fuel cells. This is because of the alkaline environment that dictates the AEM stability. Here the achieved conductivity is better than that of proton conductivity, which could be attributed to its in plane measurement.
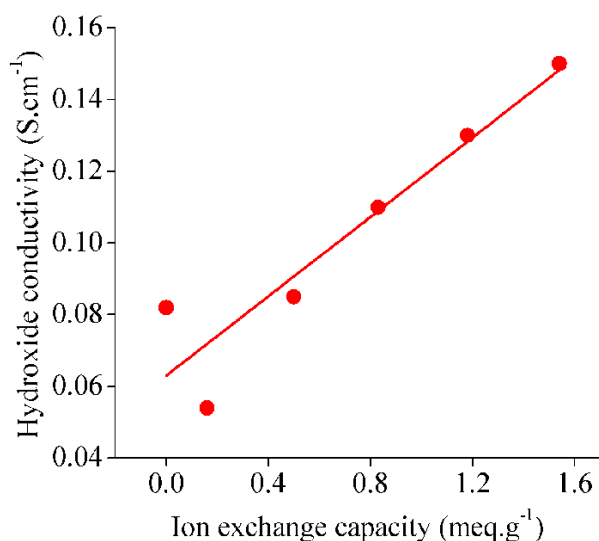
Figure 6.20 Variation in hydroxide conductivity with ion exchange capacity of PBI-PIL blend membranes.

Table 6.4 Hydroxide ion conductivity, activation energy and open circuit potential (OCV) of blend membranes.

Membrane	Hydroxide conductivity at 80 °C (S.cm^{-1})	Activation energy (KJ.mol^{-1})	Open circuit potential (Volt)
PBI	0.082	-	-
PBI-PIL$_5$	0.054	8.21	0.97
PBI-PIL$_{15}$	0.085	9.38	0.98
PBI-PIL$_{25}$	0.11	5.78	0.985
PBI-PIL$_{35}$	0.13	5.43	0.995
PBI-PIL$_{45}$	0.15	5.16	1.01

Table 6.4 shows the OCV value of single cell MEAs at 80 °C for different blend membranes. Single cell performance of different blend membrane/KOH as anion electrolyte at 80 °C in H_2-O_2 fuel cell was evaluated. It was found that the OCV of the cell was close to 1.0 V as shown in Table 6.4, which was higher than the corresponding value of conventional H_2-O_2 AEMFC. Unfortunately, the OCV value reduced exponentially when the load was applied and no current was flown through the cell. At this stage, the voltage was around -2.9-3.6 V which is very less. Further analyses could not be completed and at this stage polarization curve could not be recorded.

6.6 Conclusions

We have prepared novel polymer blend membranes based on polymeric ionic liquid P[DADMA][TFMS] and PBI. The DSC and IR results of blend membranes suggest that PBI and PIL exhibited good miscibility in all attempted proportions. The T_g of all blend membranes was higher than predicted by the Fox equation, indicating presence of strong interactions in individual blend components. As the temperature increased, conductivity of PBI-PIL blends doped with H_3PO_4 increased. The PBI-PIL blend membranes have shown a significant improvement in the proton conductivity as compared to the pristine PBI membrane. The maximum proton conductivity of the PBI-PIL$_{45}$ blend membrane was 0.07 S/cm at 150 °C under anhydrous condition. These membranes also have enough mechanical and thermal stability. Single cell evaluations have been successfully demonstrated by using H_2/O_2 at temperature of 160 °C under nonhumidified conditions and a current density of 1632 mA cm^{-2} has been achieved for PBI-PIL$_{25}$ composition. The polymeric ionic liquid based blend membrane is found to be a possible candidate for HT-PEMFC to work at elevated temperatures.

The blend membranes prepared for the proton transfer were also found to be good carrier for OH as well. All the blends membranes showed good hydroxide stability up to 3M KOH concentration for 7 days. The maximum hydroxide conductivity was found 0.15 Scm^{-1} at 80 °C with PBI-PIL$_{45}$. During single cell evaluations, the value to open circuit potential (OCV) was found around 1 V, however the current flow was not observed when the load was applied.

Chapter 7

New polymeric ionic liquids (PILs) as membrane materials for fuel cell (PEMFC and AEMFC)

Part A. Cross-linked PIL membranes based on polybenzimidazole: Evaluations on physical and electrochemical properties for HT-PEMFC

7.1a Preamble

This work presents an approach towards use of pure polymeric ionic liquids (PILs) as membrane materials for high temperature proton exchange membrane based fuel cell (HT-PEMFC). Previous chapter discussed that ionic liquids (ILs) and proton-conducting ionic liquids (PCILs) have attracted considerable attentions in electrochemical applications due to their high ionic conductivity and good thermal stability. These IL based membranes have disadvantages towards their long term use, which can be avoided by replacing them by polymeric form of ionic liquids (PILs). In the previous chapter, polymer blend membranes based on PIL (P[DADMA][TFMS]) and PBI-I (polybenzimidazole) were investigated. These PBI-PIL blend membranes showed significant improvement in the proton conductivity as compared to the pristine PBI membrane. The conductivity of the blend membranes generally increased with increasing amount of the PIL. Based on this result, it was thought that, it would be worth investigating membranes based on pure PILs. The conductivity of acid undoped PILs is poor for the practical application in HT-PEMFC. Moreover, their films are not stable in acid doped conditions. To conquer these issues, it was decided to cross-link the PIL backbone. For this purpose, allyl bromide, propargyl chloride and vinyl benzyl chloride groups are incorporated in the backbone of PIL. The basic PBI-I backbone was selected for the partial *N*-quaternization owing to its high mechanical, chemical, and thermal stability [Kumbharkar (2009), Antolini (2010)]. It was thought that by performing partial *N*-quternization of PBI-I, some of the imidazole sites of the PBI will be left free for the acid doping. This way, their conductivity can be increased for PEMFC application. By adopting this methodology, polymer chains bearing ionic character as well as capability to hold doped acid would offer better physical stability as well as proton conductivity. The double bond containing alkyl halides have been introduced as

an alkyl group since they can be cross-linked after the membrane formation. Systematic investigations on physical and electrochemical properties of such membranes are carried out and presented in this chapter.

7.2a Synthesis

7.2.1a Synthesis of PBI-I and PILs

The fundamental thought behind the cross-linking was to increase the stability of PIL membranes in acid (H_3PO_4) doped condition to use them in HT-PEMFC application. Initially three different cross-linkers (allyl bromide, propargyl chloride and vinyl benzyl chloride) were selected for the in situ cross-linking of the PIL membranes.

PBI-I was synthesized with high enough inherent viscosity of 1.24 dL.g^{-1} that offered a tough film by solution casting method (Scheme 2.1, as given in Chapter 2, Section 2.2.1). The polymer was same as described in Chapter 6. The partial *N*-quaternization of this PBI-I was done in a single step by in-situ preparation of its Na-salt, followed by *N*-substitution by cross-linkers (allyl bromide, propargyl chloride or vinyl benzyl chloride). The *N*-substitution of a PBI occurs by the reaction between its Na-salt and an allyl bromide, while its further quaternization takes place due to the availability of an excess of allyl bromide [Bhavsar (2014a)]. Formed PILs were dried in vacuum oven at RT for 7 days. The yield of the obtained PILs was > 90% in all the cases, which was a primary indication that the partial *N*-quaternization has occurred as planned.

The prepared PILs with three different pendent alkyl groups were soluble in DMF, DMAc and DMSO. It was observed that after cross-linking (heating at 250 °C for 3h); PIL membranes were stable in DMSO even after heating at 80 °C. These results indicated that the PILs lost their solubility in DMSO due to cross-linking. For the proton conductivity analysis, these membranes were further doped with H_3PO_4 of different molar concentration. It was observed that the membranes which were cross-linked with propargyl chloride and vinyl benzyl chloride were brittle in H_3PO_4, even at lower concentration, as shown in Figure 7.1a; while the membranes which were cross-linked with allyl bromide were stable even in 15 M H_3PO_4 concentration. On the basis of these results, the PIL membranes cross-linked with allyl bromide were selected for the further study.
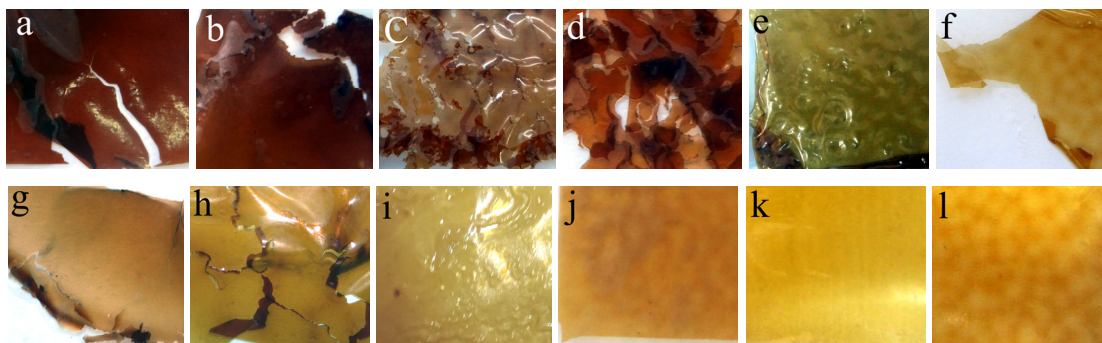
Figure 7.1a Photographs of PIL membranes doped in 5M H_3PO_4: (a) [TPPBI-I][Cl]$_{25}$, (b) [TPPBI-I][Cl]$_{50}$, (c) [TPPBI-I][Cl]$_{75}$, (d) [TPPBI-I][Cl]$_{100}$, (e) [TVBPBI-I][Cl]$_{25}$, (f) [TVBPBI-I][Cl]$_{50}$, (g) [TVBPBI-I][Cl]$_{75}$, (h) [TVBPBI-I][Cl]$_{100}$, (i) [TAPBI-I][Br]$_{25}$, (j) [TAPBI-I][Br]$_{50}$, (k) [TAPBI-I][Br]$_{75}$, (l) [TAPBI-I][Br]$_{100}$.

PILs were prepared using allyl bromide (3-bromopropene) as a cross-linker in various proportions (25%, 50%, 75% and 100%) and investigated further as described below. The quantitative estimation of the degree of quaternization (DQ) was performed by two independent methods as discussed below.

7.2.2a Estimation of the degree of *N*-quaternization (DQ)

In ^{1}H-NMR spectra of the PILs, the peak for 'N-H' protons were absent (that appeared at δ 13.2 in the case of unsubstituted PBI-I, Figure 7.2a). This indicated that almost all of the imidazole N-H groups were substituted by the allyl group. A quantitative analysis of *N*-quaternization was performed by comparing the integration of allyl protons (appeared at δ 4.5-5.5) of the substituent group with that of aromatic protons of PBI-I (appeared at δ 7.5-8.5). Obtained values of DQ for different PILs are given in Table 7.1a. Another way of determining DQ is to estimate the amount of bromide present as an anion in a particular PIL. This was determined by Volhard's method, as given in Chapter 2, Section 2.4.1. For the particular PIL, the obtained value of DQ by this method was closer to that obtained by ^{1}H-NMR, as given in Table 7.1a. Therefore, values obtained by both the methods were averaged and assigned in the parenthesis, while abbreviating the PIL. For example, in the case of [TAPBI-I][Br]$_x$, 'x' represents the DQ of that PIL.
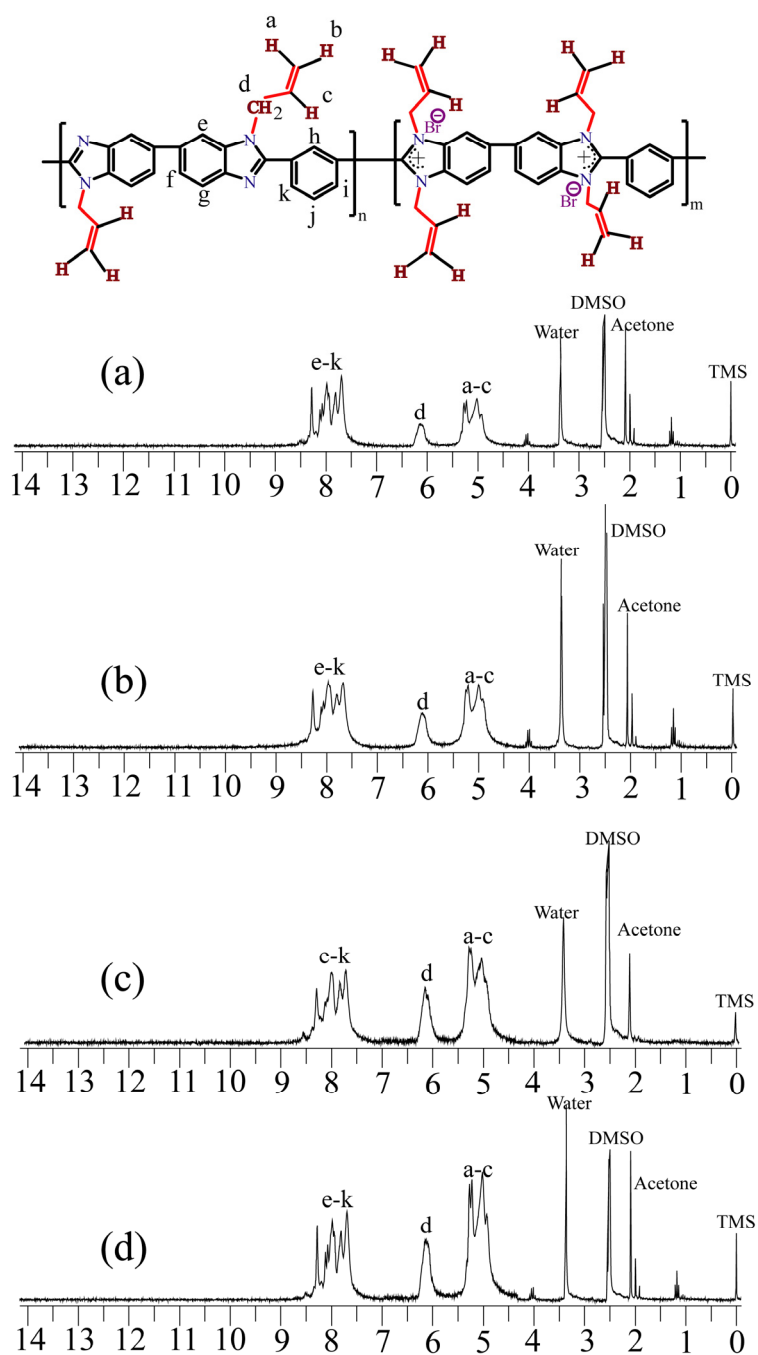
Figure 7.2a ^{1}H-NMR spectra of PILs: (a) [TAPBI-I][Br]$_{23}$,
(b) [TAPBI-I][Br]$_{43}$, (c) [TAPBI-I][Br]$_{67}$, (d) [TAPBI-I][Br]$_{84}$.

Table 7.1a Degree of PBI-I quaternization in PILs.

Degree of *N*-quaternization, DQ (%)				Designation of resulting PILs
Planned (Molar equivalent of ABr)	Observed			
	By NMR	By Volhard's method	Average	
25 (2.5)	23	22	23	[TAPBI-I][Br]$_{23}$
50 (3)	41	45	43	[TAPBI-I][Br]$_{43}$
75 (3.5)	65	69	67	[TAPBI-I][Br]$_{67}$
100 (4)	82	86	84	[TAPBI-I][Br]$_{84}$

7.3a Post cross-linking of PIL membranes

The PIL membranes were prepared in DMF by solution casting method. The thermal cross-linking of unsaturated sites after the membrane preparation was performed by heating at 250 °C for 3 h. A schematic of the cross-linking procedure by post-treatment is shown in Scheme 7.1a. After the heat treatment process, the membranes are visually homogeneous and insoluble in DMF, DMAc and DMSO, even at 80 °C for 8 h. This loss in solubility concludes that the cross-linking has been accomplished. These membranes were used for further physical and electrochemical analyses.
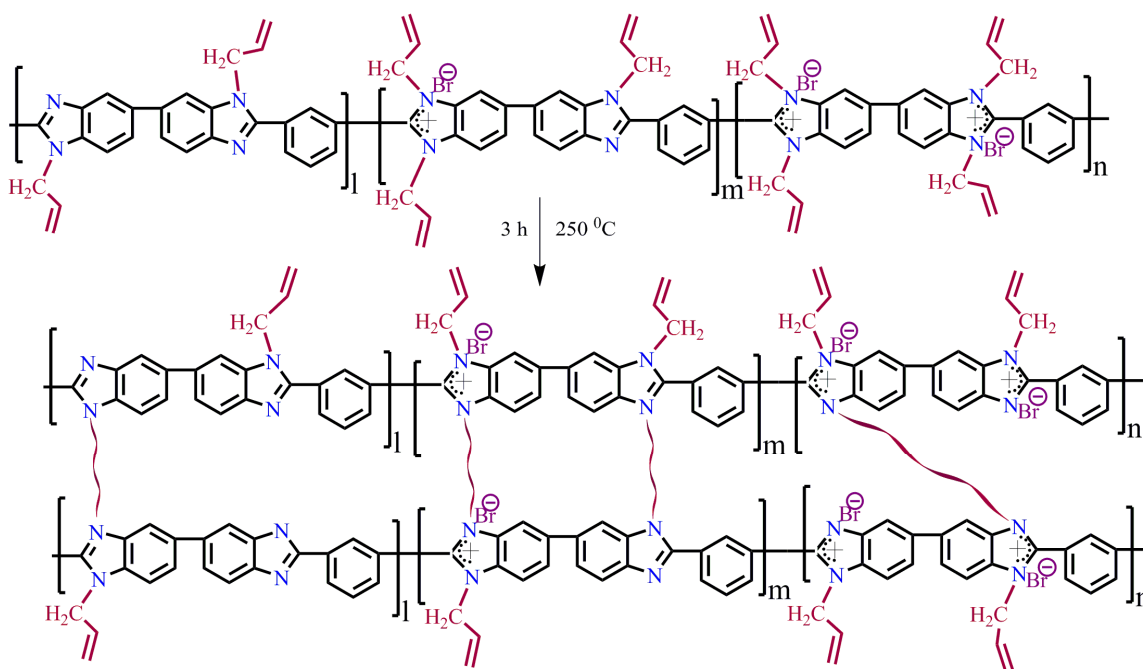
Scheme 7.1a. Schematic of PIL cross-linking by post heat treatment.

7.4a Physical properties

7.4.1a Solvent solubility and viscosity

All PILs before heat treatment were soluble in DMF, DMAc, NMP and DMSO (Table 7.2a), in which, PBI-I is also known to be soluble [Kumbharkar (2009)]. These PILs were also found to be soluble in acids such as H_3PO_4 and H_2SO_4. They were not soluble in low boiling point solvents (*i.e.* $CHCl_3$, acetone and alcohols).

Table 7.2a Solvent solubility of PILs.

PILs	DMF	DMAc	DMSO	NMP	CHCl$_3$	CH$_3$OH	Acetone	H$_2$O	Aceto-nitrile	H$_3$PO$_4$
[TAPBI-I][Br]$_{23}$	+	+	+	+	−	−	−	−	−	+
[TAPBI-I][Br]$_{43}$	+	+	+	+	−	−	−	−	−	+
[TAPBI-I][Br]$_{67}$	+	+	+	+	−	−	−	−	−	+
[TAPBI-I][Br]$_{84}$	+	+	+	+	−	−	−	−	−	+

+: soluble after heating at 80 ºC (reflux in case of low boiling solvents), −: insoluble.

After the heat treatment (at 250 °C for 3 h), these membranes lost the solubility in various solvents as described above. Their film retained integrity even in 15 M H_3PO_4.

Table 7.3a Physical properties of PILs.

PILs	η_{inh}[a] (dL.g^{-1})	d_{sp}[b] (Å)	ρ[c] (gm.cm^{-3})	TGA	
				IDT[d] (°C)	W$_{900}$[e] (%)
PBI-I	1.0	3.63	1.4	600	72
[TAPBI-I][Br]$_{23}$	5.2	4.13	1.157	251	63
[TAPBI-I][Br]$_{43}$	6.2	3.96	1.204	232	57
[TAPBI-I][Br]$_{67}$	9.1	3.85	1.241	220	56
[TAPBI-I][Br]$_{84}$	9.7	3.86	1.329	210	52

[a]: Inherent viscosity determined using 0.2 g.dL^{-1} PIL solution in DMSO at 35 ºC, [b]: d-spacing obtained from WAXD pattern, [c]: density measured at 35 ºC, [d]: initial decomposition temperature, [e]: char yield at 900 °C.

It could be seen from Table 7.3a that inherent viscosity (η_{inh}) of PILs is in the range of 5.2-9.7 dL.g^{-1}. A dramatic increase in the viscosity was observed with increasing DQ. This behavior was probably due to the strong inter-chain associations, which form large aggregates with increase in DQ. At lower DQ, the chains had little chance of interacting intermolecularly

with one another. However, as the polymer DQ was increased, intermolecular associations could be more probable, giving rise to a network structure of polymer chains and, consequently, high solution viscosity. These network structures contributed significantly to the thickening behavior of this associative polymer [Sharkh (2003)]. Such a polyelectrolyte behavior was observed earlier for PBI based PILs (methylated and *tert*-butyl benzylated) [Bhavsar (2014a), Chapter 3]. It may be noted that this crucial behavior shown by the present PILs is dependent on their DQ. This peculiarity could be useful in applications where polyelectrolyte nature with low ionic or moderate ionic character with good mechanical strength is required.

7.4.2a FTIR, WAXD and density analysis

FTIR spectra of PILs showed bands in the range of ~ 3600-3300 cm^{-1}, attributable to the absorbed moisture. For unsubstituted PBI-I, a broad band at ~ 3400-2400 cm^{-1} originating from N-H stretching was observed [Kumbharkar (2009)]. In the present cases (Figure 7.3a), this band was disappeared as a result of *N*-substitution. The characteristic bands for benzimidazole in the range of 1650-1500 cm^{-1} is attributable to C=C/C=N stretching vibrations and ring modes [Musto (1992)]. The band in the range of 1200-800 cm^{-1} is attributable to C-C stretching vibrations while the band 1250-1010 cm^{-1} is responsible for C-N stretching coupled with the stretching of the adjacent bonds in the PIL.
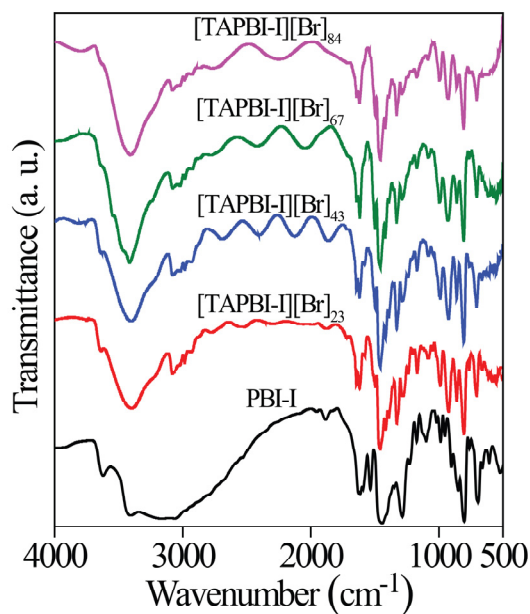
Figure 7.3a FTIR spectra of cross-linked PIL membranes.

The X-ray diffraction and density analysis were used to understand the chain packing in the PIL membrane matrix. The WAXD pattern of these PIL films (Figure 7.4a) indicated their amorphous nature in spite they possessed ionic character. It was reported that some of the PILs having aliphatic backbone possess crystallinity [Bhavsar (2012), Pan (2009)]. The present PILs remained amorphous, which could be due to their fully aromatic and rigid backbone. Moreover, they have alkyl substituent on their backbone, which would inhibit ordered chain packing. The d_{sp} of PILs corresponding to the amorphous peak maxima in the respective WAXD pattern are given in Table 7.3a. The d_{sp} decreased with an increase in DQ of PIL. The density of PILs was lower than that of PBI-I, as anticipated.
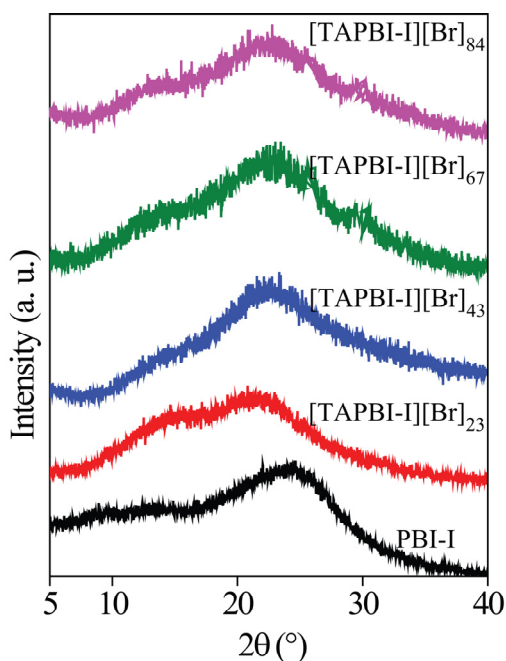
Figure 7.4a WAXD pattern of cross-linked PIL membranes.

7.4.3a Thermal, oxidative and hydrolytic stability of the PIL membranes

The TGA curves of the present PILs are shown in Figure 7.5a, which showed multistep degradation. This type of degradation behaviour could be attributed to the ionic nature of PILs. At 50 ºC, some of the PILs showed a small weight loss (~ 3%) that might be ascribed to the absorbed moisture. Initial decomposition temperature (IDT) of the present PILs varied from 210 to 251 °C (Table 7.3a), which is considerably lower than that of PBI-I [Kumbharkar (2006)]. As the DQ increased, a consistent decrease in IDT was observed. Such a lowering in the thermal

stability of quaternized polymers than their unquaternized counterparts is known [Bhavsar (2014a), Chen (2012)]. Li et. al., also have reported that with increasing amount of the RTIL monomer, thermal stability of the resulting copolyimides was decreased [Li (2010)]. In previous study, we found the similar results, where increasing DQ (ionic liquid character) in PILs resulted in lowering of the thermal stability [Chapter 3]. The glass transition temperature of these PILs could not be detected in DSC as well as DMA thermograms even after repeated cycles of heating and cooling.
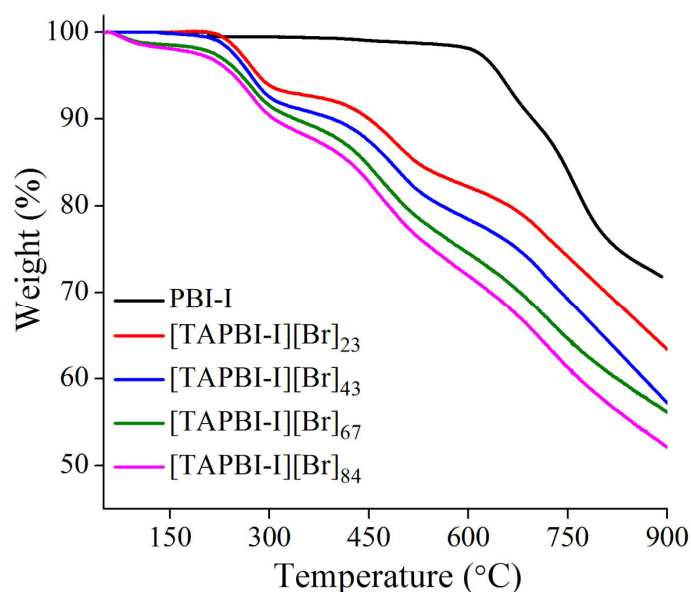
Figure 7.5a TGA curves of cross-linked PILs.

Table 7.4a Mechanical properties of PIL membranes.

Membrane	Modulus (GPa)	Tensile strength (MPa)	Elongation (%)
PBI-I	3.66	155	70.5
[TAPBI-I][Br]$_{23}$	0.70	128	18.0
[TAPBI-I][Br]$_{43}$	0.62	125	12.2
[TAPBI-I][Br]$_{67}$	0.61	116	7.1
[TAPBI-I][Br]$_{84}$	0.46	68	6.0

Figure 7.6a presents the stress-strain curves of the cross-linked PIL films, while Table 7.4a summarizes their mechanical properties. It could be seen that the mechanical strength of the PILs was considerably lower than that of PBI-I. The tensile strength of PBI-I was 155 MPa, while in case of the PILs, it was in the range of 68-128 MP (which decreased with increasing the

DQ). This reduction in mechanical strength could be attributed due to the absence of H-bonding in the PILs (which was present in their precursor, PBI-I). It could be seen that these PILs shown higher mechanical strength than that of the earlier reported PILs based on PBI [Bhavsar (2014a), Chapter 3], which could be attributed to their cross-linked nature.
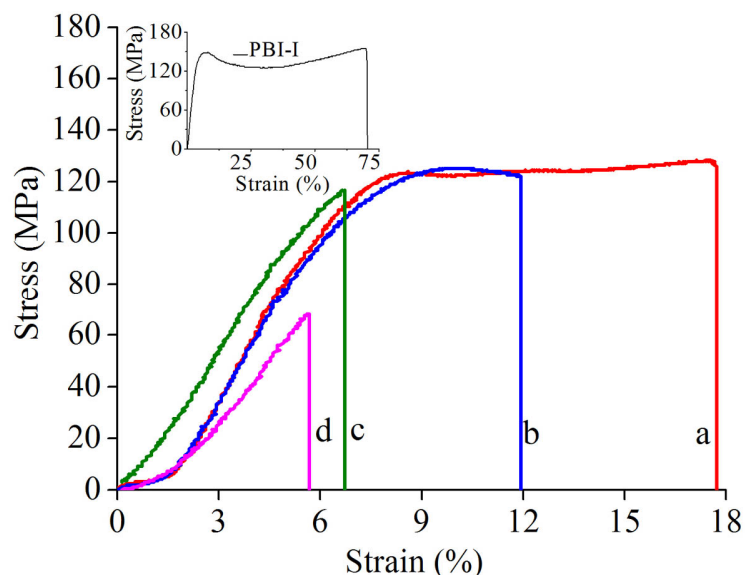
Figure 7.6a Stress-strain curves of cross-linked PIL membranes: PBI-I,
(a) [TAPBI-I][Br]$_{23}$, (b) [TAPBI-I][Br]$_{43}$, (c) [TAPBI-I][Br]$_{67}$,(d) [TAPBI-I][Br]$_{84}$.

The oxidative stability of the membrane is critical for its application in PEMFC and can be evaluated by the Fenton's test. In this study, the cross-linked PIL membranes were soaked in 3% H_2O_2 containing 3 ppm $FeSO_4$ at 80 °C and the weight loss was recorded (Table 7.5a). In comparison with the PBI-I membranes, the PIL membranes exhibit inferior resistance to Fenton oxidation. Oxidative stability decreased with the increasing DQ of PIL (Table 7.5a). The oxidative stability of these cross-linked PIL membranes was higher than that of the blend membranes containing same amount of ionic liquid character [Chapter 6]. This could be due to cross-linking of these PIL membranes that provides additional stability.

All cross-linked PILs membranes were hydrolytically stable for > 2 weeks. It was observed that all the membranes remain flexible when they were bent even after so long duration. After the treatment for 2 weeks, the weight of the dried membrane (dried at 100 °C in vacuum oven for 3 days) was measured and it was observed that the weight for all the cross-linked PIL membranes was almost similar before and after the treatment.

Table 7.5a Oxidative stability and electrochemical properties of PIL membranes.

Membrane	Oxidative stability[a]			Doping level (H_3PO_4/RU)	Electrochemical properties	
	Weight loss after 6 h (%)	Weight loss after 12 h (%)	Weight loss after 18 h (%)		Proton conductivity ($S.cm^{-1}$)	Activation energy ($KJ.mol^{-1}$)
PBI-I[b]	0.06	0.091	1.12	5.6	0.04	15.2
[TAPBI-I][Br]$_{23}$	1.0	1.5	1.9	5.3	0.0156	23.68
[TAPBI-I][Br]$_{43}$	1.2	2.4	3.2	4.0	0.0110	19.45
[TAPBI-I][Br]$_{67}$	11	12.0	12.7	3.6	0.0039	16.10
[TAPBI-I][Br]$_{84}$	13.2	14.3	15.3	2.2	0.0013	14.57

[a]: 3 ppm Fe^{+2}, 3% H_2O_2 at 80 °C, [b]: Chapter 6.

7.5a Electrochemical properties of PIL membranes

7.5.1a Acid doping and proton conductivity

As given above, all the cross-linked PIL membranes were stable in 15 M H_3PO_4. Although, they became soft, it was an indication of doping. For performing conductivity analysis of the PIL membranes, 10 M concentration of H_3PO_4 was maintained for the doping. The doping level of PIL membranes decreased with increasing DQ. This could be due to the decrease in the availability of free N with increasing DQ.
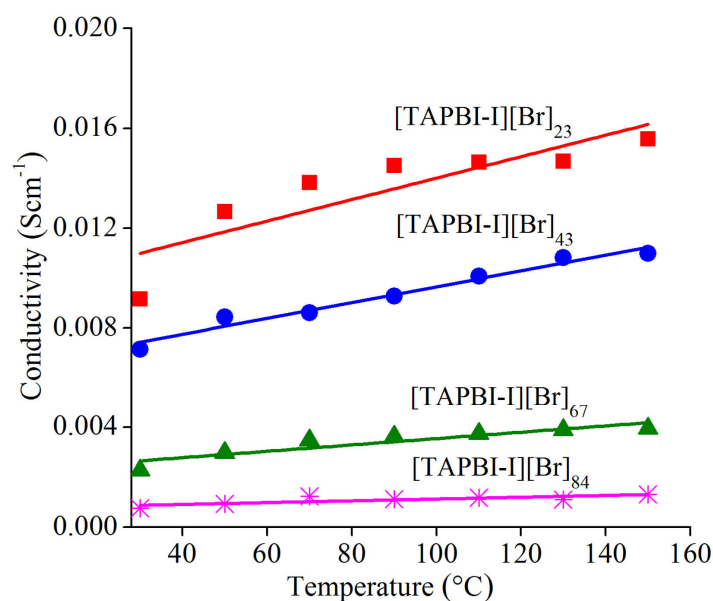
Figure 7.7a Proton conductivity of the PIL membranes as a function of temperature.

The proton conductivity of the membrane is one of the most important parameters which determine the performance of the PEM fuel cell. It is reported that the PA-doped PBI has a zero osmotic drag coefficient for proton conduction [Mader (2008)]. The proton conductivity of the PIL membranes as a function of temperature is shown in Figure 7.7a. It was found that the conductivity decreased with increasing DQ while, increased with increasing temperature. The maximum proton conductivity of the PIL membrane was 0.015 S.cm^{-1} at 150 °C with [TAPBI-I][Br]$_{23}$, which could be attributed to the higher doping level of PIL with this DQ (Table 7.5a).

Generally, the proton conductivity of the doped membranes is directly related to the doping level of the polymers. In these partial ionic PILs, free nitrogen would help in H$_3$PO$_4$ doping to obtain high proton conduction without losing their mechanical strength, which is a key issue in case of pure polymeric ionic liquids. When the DQ increases, amount of free nitrogen would be reduced and subsequently, the doping level will also get decreased. This leads to reduction in the conductivity as shown in Figure 7.8a and Table 7.5a. This is not surprising, as the total number of charge carriers get reduced with increasing DQ in accordance with the lower phosphoric acid uptake compared to the PIL membrane with lower DQ.
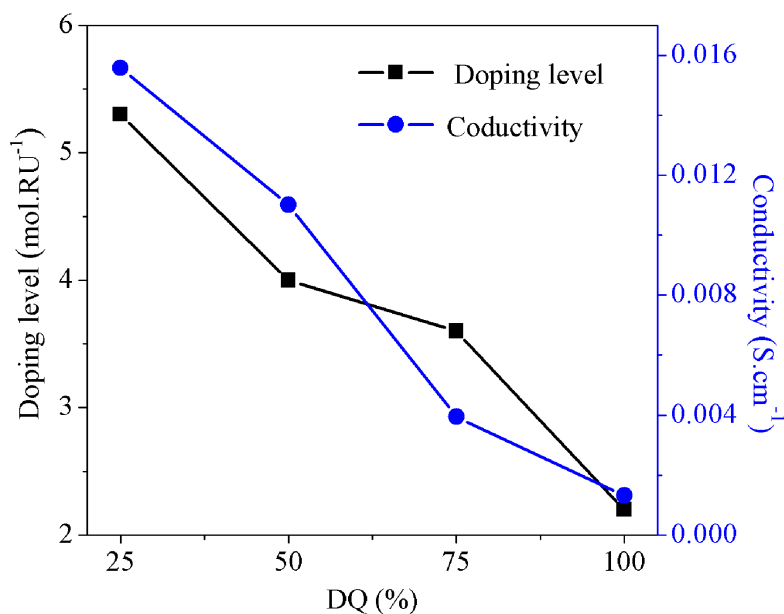
Figure 7.8a Effect of DQ on proton conductivity and doping level of cross-linked PIL membrane.

Unfortunately, in these PILs, presence of IL content seems to be less predominant for the proton conduction than the presence of H$_3$PO$_4$. This might be due to less number of Br^{-} anion

than that of H_3PO_4 and secondly, it was also expected that Br^- anion is less favorable for proton transfer than that of H_3PO_4. Thus, proton conductivity of this type of PIL could be further improved by employing suitable anion exchangers such as TFMS (trifluromethanesulfonate), MS (methanesulfonate) and PTS (*p*-toluenesulfonate), as these anions having acidic moiety in their structure. There are various reports where, sulphonate containing compounds have been used as proton transport agents [Shen (2012), Wang (2011), Oliveira (2013)].
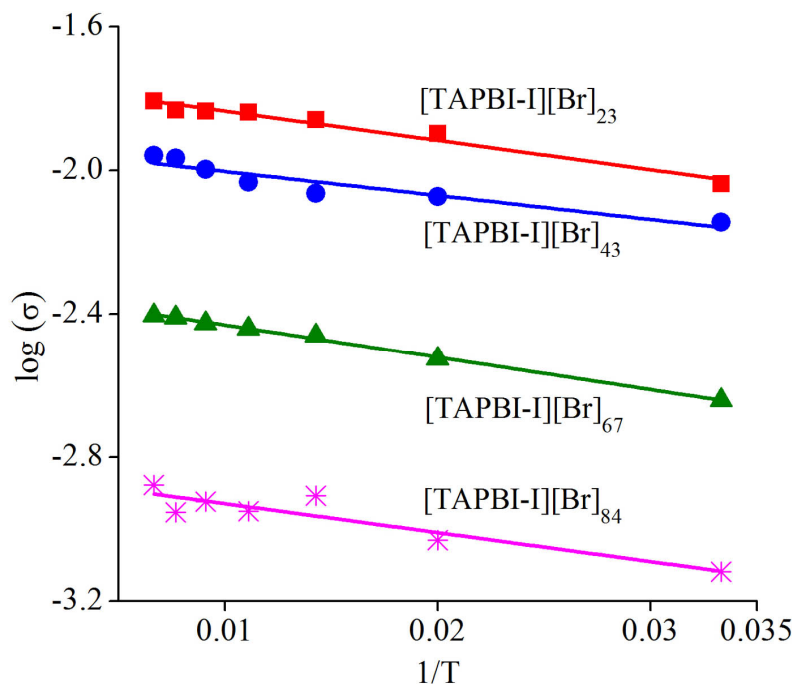
Figure 7.9a The Arrhenius plots of 1/T versus log of conductivity of PIL membranes.

Figure 7.9a shows typical Arrhenius behavior. The ion transport activation energies (E_a) of PIL membranes obtained by the Arrhenius equation are presented in Table 7.4a. The values show that, with increasing DQ, the E_a decreases. [TAPBI-I][Br]$_{84}$ showed the lowest E_a value (14.57 kJ.mol^{-1}) in the present series. On the basis of the measured E_a values, it can be anticipated that the anion of quaternized PILs is helping in maintaining proton transportation. The E_a values of all the PIL membranes were higher than or equal to that of the acid doped PBI membrane (14-16 kJ.mol^{-1}), which indicates that the proton transfer needs more energy in the PIL membranes. On the basis of higher E_a values, it can be concluded that the proton transport in these PIL membranes mainly occurred by Grotthuss mechanism which required more energy for the transportation of the proton.

7.6a Conclusions

This section covers a new route for the synthesis of cross-linked PILs membranes for proton transfer without the need for any external cross-linkers or catalyst. The soluble PILs bearing flexible side chains, with alkene pendant groups were synthesized *via* the *N*-quaternization of PBI-I. The cross-linked derivatives were then prepared by the thermal cross-linking of the unsaturated side chains after the membrane preparation. DQ in a series of the PILs was systematically varied in order to study the concurrent effects induced by the ionic liquid (IL) character as well as cross-linking on their physical and electrochemical properties. All the PILs were amorphous in nature and have good solvent solubility in polar aprotic solvents. Owing to the induced ionic character, thermal stability and mechanical strength of these PILs were lower than that of their parent PBI-I. The viscosity investigations of the PIL solutions suggested their typical polyelectrolyte behavior. The PILs membranes were stable in H_3PO_4 and were doped in 10 M H_3PO_4 for their electrochemical analysis. The doping level decrease with increasing DQ due to reduced amount of free nitrogen in PILs with increasing DQ. The cross-linked PILs membranes showed conductivity in the range of 0.0013-0.016 S.cm^{-1}. The present work indicates that there is a need to enhance doping level as well as favorable IL character in the polymer, so that their better in improving electrochemical performance can be obtained.

Part B. PIL membranes based on polybenzimidazole: Physical and electrochemical properties for AEMFC

7.1b Preamble

Recently, alkaline polymer electrolyte fuel cells (APEFCs) using anion exchange membranes (AEM) have received a great attention [Zhao (2010)]. APEFCs have apparent advantages over their acidic polymer electrolyte counterparts (Proton Exchange Membrane Fuel Cells, PEMFCs) such as, the fuel oxidation and oxygen reduction kinetics exhibit inherently faster in the high pH environments in APEFCs. Thus, the use of nonprecious metal catalysts is permitted (e.g., nickel and manganese oxides) [Ran (2012)] in the case of APEFCs. To date, most commonly studied AAEMs contain quaternary ammonium (QA) cationic groups and are prepared *via* post functionalization of polymer films [Ran (2012), Varcoe (2004), Wang (2011), Hibbs (2009)]. The low alkali thermochemical stabilities of QA-type AAEMs limit their long term durability in APEFCs. This poor stability of AEM in alkaline conditions arrives from the strong nucleophilicity of the OH$^-$ anions. It induces displacement (SN^2, or *via* ylide intermediates) and Hofmann elimination reactions [Ye (2011), Chempath (2008), Makosza (2002)]. To enhance the stability of AEMs, alternative cationic groups including guanidinium [Wang (2010), Zhang (2010)], stabilized phosphonium [Gu (2009), Gu (2010)] and imidazolium [Lin (2010), Zhang (2011), Li (2011), Thomas (2011)] have been investigated. These membranes suggested good stability in alkaline condition; however, these guanidinium and phosphonium based AAEMs are higher in cost due to use of expensive functional reagents (pentamenthylguanidine and tris(2,4,6- trimethoxyphenyl)phosphine). With the aim to develop AEM with a balance between cost effectiveness and high performance, PILs based on *N*-quaternization of PBI-I have been synthesized in present study and evaluated for their physical and electrochemical characterization. In order to study the effect of ionic content for AEM, we have synthesized a series of PILs with increasing order of ionic character in them by increasing the DQ (degree of *N*-quaternization).

7.2b Synthesis and related characterizations

7.2.1b Synthesis of PILs

The *N*-quaternization of PBI-I was carried out while aiming at varying degrees of partial ionic character in the resulting PILs (as given in Chapter 2, Section 2.2.3 and Scheme 2.3).

Typically, a 3-necked flask was charged with 160 ml of dry DMSO, 5.0 g (0.0162 mol) of PBI-I and 1.364 g of NaH (2.1 equivalents, 0.0340 mol) while stirring under dry N_2 atmosphere at the ambient temperature. After 3 h, temperature was raised to 80 °C and maintained for 2 h in order to obtain a clear solution. A deep blood red color was developed after complete dissolution of PBI-I, indicating formation of its *N*-sodium salt. The solution remained homogeneous after cooling it to the ambient temperature. Adequate molar equivalent of *4-tert*-butylbenzyl bromide (as given in Table 7.1b) was added to the reaction mixture. An immediate precipitate formation was observed, indicating the *N*-substitution of PBI-I has taken place. The reaction mixture was stirred for 30 min at RT and then heated at 80 °C for 20 h in order to obtain a clear solution. The reaction mixture was precipitated in hexane:toluene (1:1) as the nonsolvent. The formed polymer was vacuum dried at 80 ºC for a week. It was purified by dissolving in DMAc, reprecipitating in hexane:toluene (1:1), followed by drying in vacuum oven at 80 ºC for 3 days. The yield of obtained PILs was > 90% in all the cases, which was a primary indication that the partial *N*-quaternization has occurred as planned. The quantitative estimation of the degree of quaternization (DQ) was performed by two independent methods as discussed below.

7.2.2b Estimation of the degree of quaternization (DQ)

The degree of quaternization (DQ) of PBI-I by *4-tert*-butylbenzyl group was analyzed by ^{1}H-NMR (recorded on Bruker AC-200 using DMSO-d_6 as the solvent, Figure 7.1b). Obtained values of DQ for different PILs are given in Table 7.1b. In ^{1}H-NMR spectra of the PILs, the peak for 'N-H' protons were absent (that appeared at δ 13.2 in the case of unsubstituted PBI-I). This indicated that almost all of the imidazole N-H groups were substituted by the *4-tert*-butylbenzyl group. A quantitative analysis of *N*-quaternization was performed by comparing the integration of *tert*-butyl protons of the substituent group appeared in δ 0.5-1.5 with that of aromatic protons of PBI-I appeared in δ 7.5-8.5. Another way of determining DQ is to estimate the amount of bromide present as an anion in a particular PIL. This was determined by Volhard's method, as given in Chapter 2. For the particular PIL, obtained value of DQ by this method was closer to that obtained by ^{1}H-NMR, as given in Table 7.1b. Therefore, values obtained by both the methods were averaged and assigned in the parenthesis, while abbreviating the PIL as described in Section 7.2.2a. For example, in the case of [TBzPBI-I][Br]$_x$, 'x' represents the DQ of that PIL.

PILs possessing partial ionic character

Where, Ar = ... R Br = ... m+n = 1

PBI:PBI-I

tert-butylbenzyl
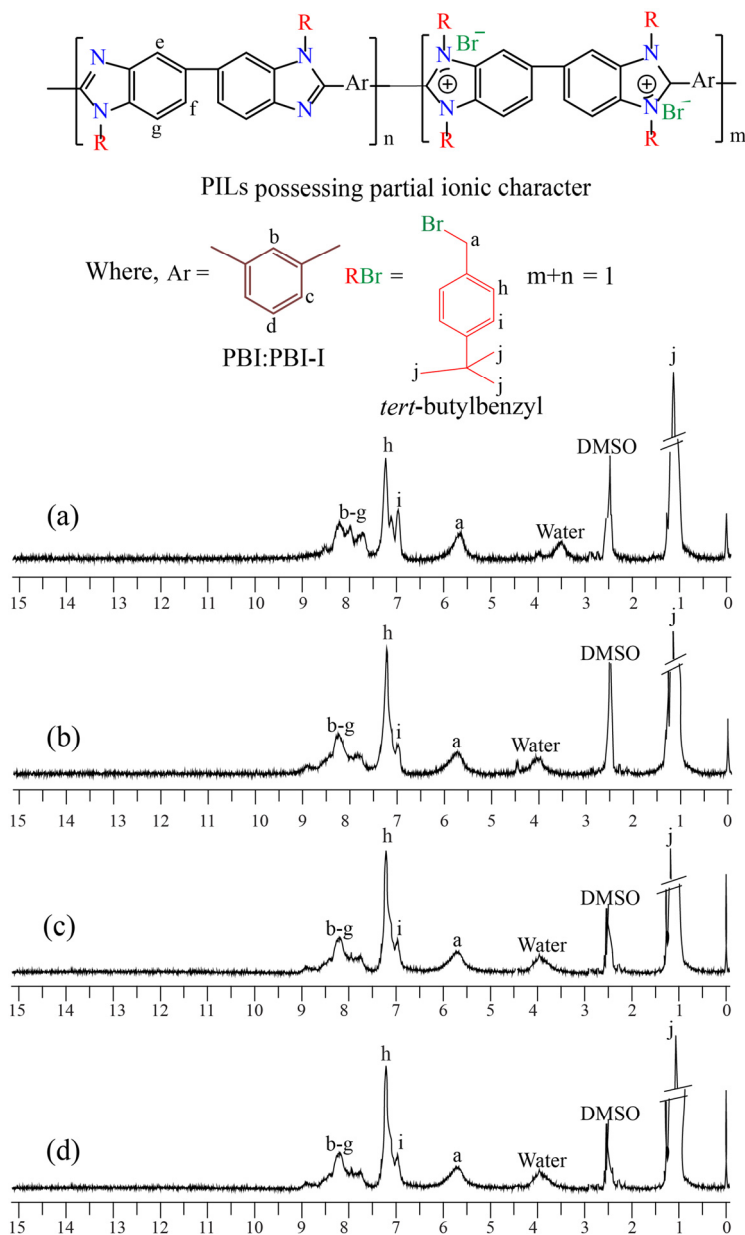
Figure 7.1b ^{1}H-NMR spectra of PILs: (a) [TBzPBI-I][Br]$_{24}$,
(b) [TBzPBI-I][Br]$_{47}$, (c) [TBzPBI-I][Br]$_{69}$, (d) [TBzPBI-I][Br]$_{87}$.

Table 7.1b Degree of quaternization in PILs.

Degree of quaternization, DQ (%)				Designation of resulting PILs
Planned (Molar equivalent of BzBr)	Observed			
	By NMR	By Volhard's method	Average	
25 (2.5)	23	24	24	[TBzPBI-I][Br]$_{24}$
50 (3)	45	48	47	[TBzPBI-I][Br]$_{47}$
75 (3.5)	68	70	69	[TBzPBI-I][Br]$_{69}$
100 (4)	85	89	87	[TBzPBI-I][Br]$_{87}$

7.3b Physical and electrochemical properties of PIL membranes

7.3.1b Solvent solubility

As could be seen from Table 7.2b, all PILs were soluble in DMF, DMAc, NMP and DMSO; in which PBI-I is also known to be soluble [Kumbharkar (2009)]. They were not soluble in low boiling point solvent (*i.e.* CHCl$_3$, acetone and alcohols).

Table 7.2b Solvent solubility of PILs.

PILs	DMF	DMAc	DMSO	NMP	CHCl$_3$	CH$_3$OH	Acetone	H$_2$O	Aceto-nitrile
[TBzPBI-I][Br]$_{24}$	+	+	+	+	−	−	−	−	−
[TBzPBI-I][Br]$_{47}$	+	+	+	+	−	−	−	−	−
[TBzPBI-I][Br]$_{69}$	+	+	+	+	−	−	−	−	−
[TBzPBI-I][Br]$_{87}$	+	+	+	+	−	−	−	−	−

+: soluble after heating at 80 ºC (reflux in case of lower boiling solvents), −: insoluble.

7.3.2b FTIR, WAXD and density analysis

FTIR spectra of PILs scanned at the ambient temperature are given in Figure 7.2b. FTIR spectra of PILs showed bands in the range of ~3600-3300 cm^{-1} attributable to the absorbed moisture (Figure 7.2b).
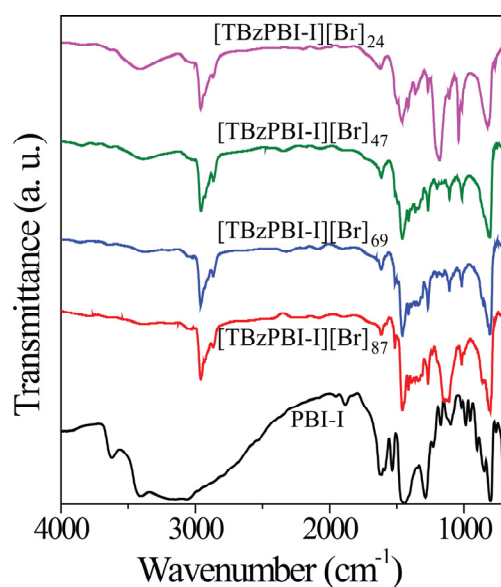
Figure 7.2b FTIR spectra of the PIL membranes.

For unsubstituted PBI-I, a broad band at ~ 3400-2400 cm^{-1} originating from N-H stretching was observed [Kumbharkar (2009)]. In the present cases (Figure 7.2b), this band was disappeared as a result of *N*-substitution. The band appeared in the range of 2800-3000 cm^{-1} for CH$_3$ group of substituent tBz (*tert*-butylbenzyl) which was absent in case of pristine PBI-I [Kumbharkar (2006)]. The characteristic bands for benzimidazole in the range of 1650-1500 cm^{-1} is attributable to the C=C/C=N stretching vibrations and ring modes [Musto (1992)].

The X-ray diffraction analysis and density were used to understand the chain packing in the PIL membrane matrix. The WAXD pattern of these PILs (Figure 7.3b) indicated their amorphous nature; in spite they possessed ionic character.
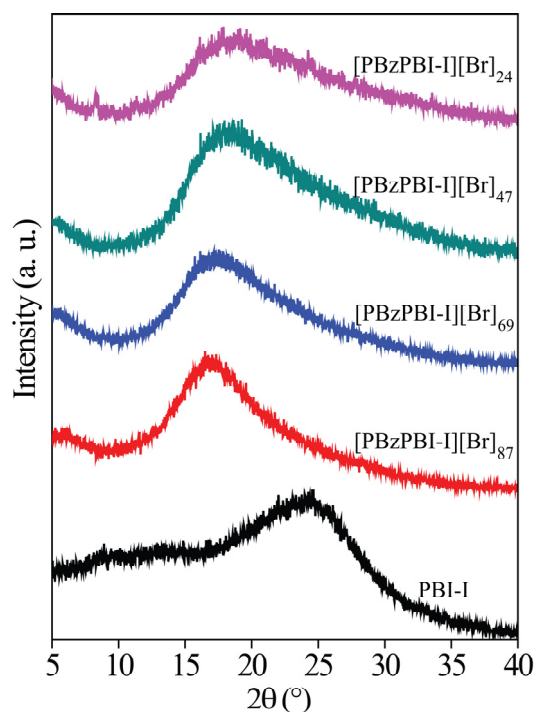
Figure 7.3b WAXD patterns of PIL membranes.

The present PILs remained amorphous, which could be due to their fully aromatic and rigid backbone. The *d*-spacing (d$_{sp}$) of PILs corresponding to the amorphous peak maxima in the respective WAXD pattern are given in Table 7.3b. The d$_{sp}$ of PILs possessing partial ionic character are more than that of PBI-I. This could be bulky *tert*-butylbenzyl (Bz) substituent on their backbone, which would inhibit ordered chain packing. The d$_{sp}$ of all PILs decreased with increasing DQ, this could be due to increased population of the ionic groups with increasing DQ leading to increase in attractive interaction that supersedes repulsive interactions due to added

'Bz' groups. This ultimately resulted into better chain packing (as indicated by d-spacing). The density of PILs was lower than PBI-I as it is known that the precursor PBI-I has more closely packed structure as described in part a. The d_{sp} increased with an increase in DQ of PIL. The maximum density was found in case of [TBzPBI-I][Br]$_{87}$. This is attributable to the added bulk of *tert*-butylbenzyl bromide group.

Table 7.3b Physical properties of PILs.

PILs	d_{sp}^a (Å)	ρ^b (gm.cm^{-3})	TGA		Oxidative stability		
			IDT^c (°C)	W_{900}^d (%)	Weight loss after 6 h (%)	Weight loss after 12 h (%)	Weight loss after 18 h (%)
PBI-I^e	3.63	1.4	600	72	0.06	0.091	1.12
[TBzPBI-I][Br]$_{24}$	5.39	1.108	300	50	0.35	1.09	1.28
[TBzPBI-I][Br]$_{47}$	5.33	1.137	280	42	1.08	1.13	1.61
[TBzPBI-I][Br]$_{69}$	5.27	1.150	250	40	3.19	3.85	4.94
[TBzPBI-I][Br]$_{87}$	5.12	1.238	213	27	6.95	8.26	8.70

^{a}: d-spacing obtained from WAXD pattern, ^{b}: density measured at 35 °C, ^{c}: initial decomposition temperature, ^{d}: char yield at 900 °C, ^{e}: Kumbharkar (2009).

7.3.3b Thermo-mechanical, oxidative and hydrolytic stability of the PIL membranes

The TGA curves of the present PILs showed multistep degradation (Figure 7.4b). This type of degradation behavior could be attributed to the ionic nature of PILs. A small initial weight loss (max 3%) at 150 °C is attributable to the absorbed moisture. Initial decomposition temperature (IDT) of PILs was decreased from 300 to 213 °C (Table 7.3b), with an increased DQ. The IDT of first PIL in series (i.e.[TBzPBI-I][Br]$_{24}$) is 300 °C, which is considerably lower than that of PBI-I or DBzPBI-I (600 and 330 °C, respectively) [Kumbharkar (2006), Kumbharkar (2010)]. This suggests that an introduction of ionic content in even rigid polymer like PBI significantly lowers the IDT than the parent polymer. Such a lowering in the thermal stability of quaternized polymers than their unquaternized counterparts is well reported [Bhavsar (2014a), Chapter 3]. The thermal stability is high enough to operate AEMFC. The thermal stability of PBI-I based PILs was higher than that of PBI-BuI based PILs as described in Chapter 3. This higher thermal stability was further worthy for use them in fuel cell application. The glass transition temperature of these PILs could not be detected in DSC thermograms even after repeated cycles of heating and cooling.
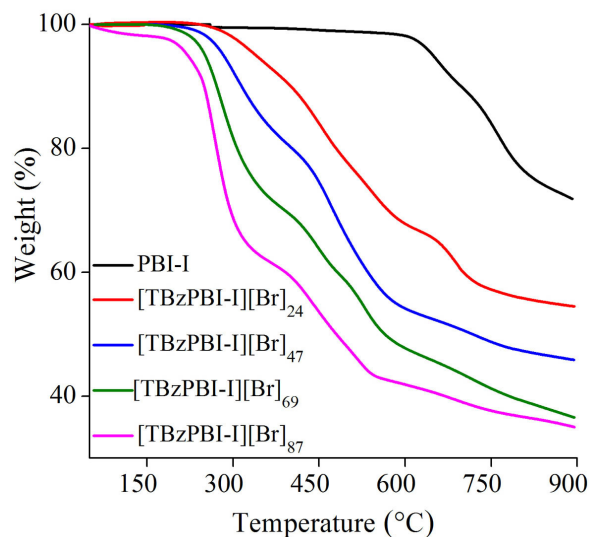
Figure 7.4b TGA curves of PIL membranes.
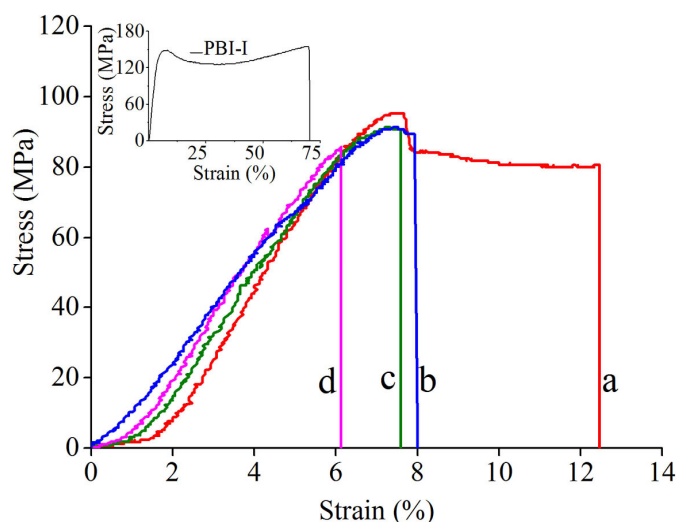
Figure 7.5b Stress-strain curves of PIL membranes: PBI-I, (a) [TBzPBI-I][Br]$_{24}$, (b) [TBzPBI-I][Br]$_{47}$, (c) [TBzPBI-I][Br]$_{69}$, (d) [TBzPBI-I][Br]$_{87}$.

Figure 7.5b presents stress–strain curves of the PIL films, while Table 7.4b summarizes their mechanical properties. It could be seen that the mechanical strength of PILs was considerably lower than that of PBI-I. Although the introduction of alkyl during *N*-quaternization decreased the mechanical properties to some extent (Table 7.4b), the PILs still had sufficiently high mechanical properties. The tensile strength of PBI-I was 154 MPa; while in case of the PILs, it was in the range of 75.7-95.3 MPa (which decreased with increasing the DQ). This

reduction in mechanical strength could be attributed to the absence of H-bonding in these PILs (which was present in their precursor, PBI-I). These results indicate that the PIL membranes were tough and flexible after *N*-quaternization as AEMs.

Table 7.4b Mechanical properties of PIL membranes.

PILs	Modulus (GPa)	Tensile strength (MPa)	Elongation (%)
[TBzPBI-I][Br]$_{24}$	1.84	95.3	12.5
[TBzPBI-I][Br]$_{47}$	1.74	91.7	8.0
[TBzPBI-I][Br]$_{69}$	1.66	85.9	7.6
[TBzPBI-I][Br]$_{87}$	1.45	75.7	6.2

The oxidative stability of the membrane is critical for its application in AEMFC also and can be evaluated by the Fenton's test as described in Part A of the chapter. In comparison with the pristine PBI-I membrane, the PIL membranes exhibited inferior resistance to Fenton oxidation. This could be due to the weak bond energy of the C–H in PILs. Oxidative stability decreases with the increasing DQ of PIL in the order: [TBzPBI-I][Br]$_{24}$>[TBzPBI-I][Br]$_{47}$>[TBzPBI-I][Br]$_{69}$>[TBzPBI-I][Br]$_{87}$ (Table 7.3b).

All PILs membranes were hydrolytically stable for > 2 weeks. It was observed that all the membranes are flexible when they were bent even after so long treatment. After treatment for 2 weeks, weight of the dried membrane (dried at 100 °C in vacuum oven for 3 days) was measured and it was observed that the weight for all the PIL membranes was almost similar before and after the treatment. There was a very small weight loss observed, that could be owing to the solvent loss.

7.3.4b Alkaline stability of PIL membranes

In view of possible applicability of these PILs membranes in alkaline anion exchange membrane fuel cell (AAEMFC), alkaline stability has been performed. The alkaline stability of the PIL AEMs was determined by observing changes in flexibility with time in 1M, 2M and 3M KOH solutions at RT for 7 days. These PILs membranes are stable in alkaline condition upto 3M KOH for a week. The long-term stability of AEMs is of concern due to the well-known degradation pathways for tetra alkyl ammonium ions under alkaline conditions. All of the membranes remained tough and flexible throughout the test which confirms the stability of the

PIL membranes in alkaline condition. These membranes were showing higher alkaline stability than that of the reported quaternized polymers for OH¯ transport. This could be due to the bulky (*tert*-butylbenzyl) substitution on the nitrogen atom of the imidazole ring, which prevents the nucleophilic attack of the OH¯ at the quaternary nitrogen group. The *N*-quaternized polybenzimidazole have also been synthesized for ion exchange membranes by O. D. Thomas et. al. by using methyl iodide as an alkyl halide; however, these membranes were found brittle in KOH solution. They found that, decomposition and possible ring-opening of the imidazole moiety is occurring, resulting in possible cleavage of the polymer chain [Thomas (2011)]. After this, the same group has synthesized new Mes-PBI (mesitylene-polybenzimidazole) and they have quaternized this by again using the same reagent methyl iodide. They have found that the installation of adjacent bulky groups would hinder nucleophilic attack by OH¯, thus, improving the stability of the hydroxide form [Thomas (2012)]. In the area of chemical stability, many mechanistic and experimental studies have been reported. It has been proved that, major degradation paths are Hofmann elimination, ylide formation and nucleophilic substitution in alkaline anion exchange membranes [Ran (2012)].

7.3.5b Ion exchange capacity (IEC) of PIL membranes

Ion exchange capacity of these PIL membranes is an important property for use them as an AEMFC which affects most of the other property of the membranes such as water uptake and hydroxide conductivity. The ion exchange capacity was determined based on the theoretical value of the bromide anion present in the PIL membrane by the Volhard's titration. The detailed method has been described in Chapter 2. The ion exchange capacity basically represents the number of ions present in per mol of the polymer, which increases with increasing the amount of the ion in the polymer membrane [Karas (2014), Thomas (2011)].

IEC= No of ionic moiety in one mole of the polymer/molecular weight of the polymer

The ion exchange capacity increases with increasing DQ of PIL as the number of ions increases in the membrane as mentioned in Table 7.5b. The IEC has been observed in the range of 0.7-1.9 meq.g^{-1} which has been considered as a good range for the ion transport in AEM. The IEC of the membranes must be high enough to allow for good anion transport, but it should not swell much in aqueous solution. A very high IEC often reduces the strength of the membrane and

such membranes break after immersion in water. A good IEC of quaternary ammonium has been found in the range of 0.9-1.4 meq.g^{-1} [Soo (2013)].

Table 7.5b Ion exchange capacity and water uptake capacity of PIL membranes.

PILs	Ion exchange capacity (meq.g^{-1})	Water uptake capacity (Wt %)	Hydroxide conductivity (S.cm^{-1})	Activation Energy (KJ.mol^{-1})
[TBzPBI-I][Br]$_{24}$	0.70	4.7	0.028	12.23
[TBzPBI-I][Br]$_{47}$	1.2	11.3	0.033	11.77
[TBzPBI-I][Br]$_{69}$	1.6	13.7	0.049	9.17
[TBzPBI-I][Br]$_{87}$	1.9	21.9	0.067	8.26

7.3.6b Water uptake capacity of PIL membranes

Water uptake (WU) of AEMs is an important parameter for IEC, ionic conductivity, mechanical strength and membrane electrode compatibility. The water uptake capacity was determined at RT for 24 h dip condition. Table 7.5b compares the water uptake of PIL membranes. Generally, the water uptake of membranes increased with the IEC value. The water uptake capacity increased with increasing DQ due to increased hydrophilicity. The highest water uptake was 21.9 wt % at RT for the highest IEC membrane TBzPBI-I (1.9 meq.g^{-1}).

7.3.7b Hydroxide ion conductivity of the PIL membranes
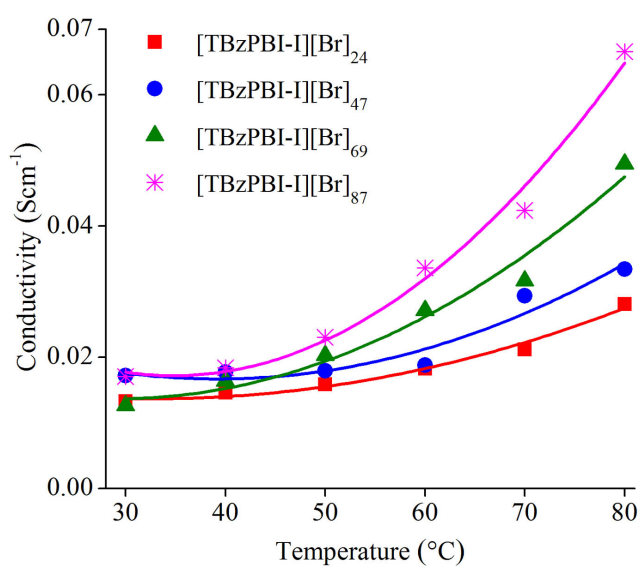
Figure 7.6b Variation in hydroxide ion conductivity of PILs membranes with temperature.

The ionic conductivities of the AEMs were measured in the hydroxide (OH⁻) anion form by dipping the PIL membranes in OH⁻ solution (3 M KOH) for 24 h before measuring the conductivity. The conductivity of the PIL membranes was determined in the fully hydrated state with varying temperature are listed in Table 7.5b. Figure 7.6b illustrates the hydroxide ion conductivity of all the PILs membranes under hydrous conditions within the plane of sample (in-plane direction). The conductivity increased with increasing DQ of the PIL membranes. This could be due to the increased IEC and water uptake. It is known that with increasing DQ, hydrophilicity increases owing to the increased ionic character. It is clearly seen in Figure 7.7b that the hydroxide conductivity increased with DQ as well as with IEC due to the increased number of ions in the PILs. The conductivity of PIL membranes was also increased with increasing temperature. Hydroxide ion shows lower conductivity as compared to proton due to low transport number for the hydroxide ion than that of proton as the hydroxide ion is bigger in size. Preliminary measurements show that the conductivity falls in the range of 0.03-0.07 S cm⁻¹ which was higher than that of the blend membrane of quaternized mesitylene-containing PBI and pristine PBI-I mentioned by Thomas *et. al*. The conductivity of these PILs was also found to be higher than that of the quaternary ammonium-substituted poly(aryl ether sulfone) [Yan (2010)], Nafion based anion-exchange membranes [Jung (2011), Salerno (2012)], and ionic-liquid-derived membranes [Ye (2011)].
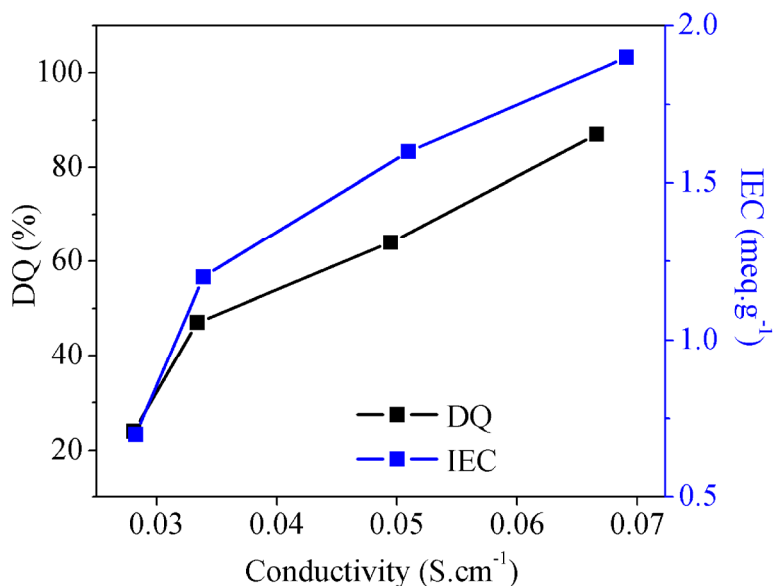
Figure 7.7b Variation in the hydroxide ion conductivity with DQ and IEC of the PILs membranes.

The conductivity of these PILs was not showing the Arrhenius behavior with temperature as shown in Figure 7.8b. Consequently; the activation energy of the hydroxide ion transport was not calculated.
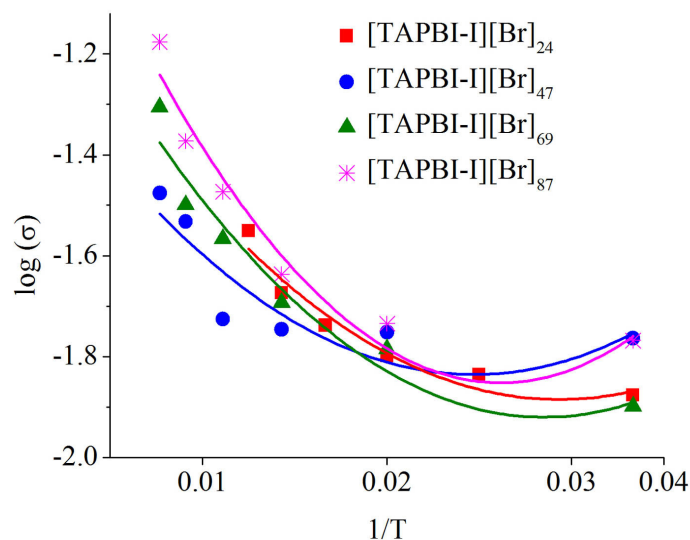
Figure 7.8b Variation in log of conductivity with inverse of temperature (1/T).

7.4b Conclusions

This Chapter reports PILs membranes possessing partial ionic character in their backbone for hydroxide transport. The soluble PILs bearing flexible side chains, with *tert*-butylbenzyl pendant groups, were synthesized *via* the *N*-quaternization of PBI-I. DQ in a series of the PILs was systematically varied in order to study the concurrent effects induced by the ionic liquid (IL) character as on their physical and electrochemical properties. All the PILs were amorphous in nature and having good solvent solubility in polar aprotic solvents. Owing to the induced ionic character, even though thermal stability and mechanical strength of these PILs was lower than that of their parent PBI-I, it was high enough to operate these PILs for AEMFC. The PILs membranes were stable in alkaline condition and were doped in 3 M KOH to use further as a membrane in alkaline fuel cell. The IEC and water uptake capacity increase with increasing DQ due to the increased ionic character in PILs with increasing DQ. The PIL membranes were showing conductivity in the range of 0.03-0.07 S.cm^{-1}. These AEMs exhibit high hydroxide ion conductivity while retaining good mechanical strength, making them very exciting candidates for fuel cell applications.

Chapter 8

Conclusions

This work deals with the investigation of new families of polymeric ionic liquids (PILs) and their applicability in gas separation and fuel cell area. Effects of structural variation by introducing partial ionic character in their backbone, blending of a PIL, viz., [TBzPBI-BuI][Br] with DBzPBI-BuI and anion exchange of [DBzDMPBI-BuI][I] with CO_2 specific anion were analyzed for physical and gas permeation properties. Towards evaluating applicability of PILs for PEMFC/AEMFC, their structural variations by introducing partial ionic character in their backbone, blending of a PIL, viz., [PDADMA][TFMS] with PBI and cross-linking performed.

Initially, partial ionic character was introduced in the polymer matrix during the synthesis of PIL by varying the systematic degree of *N*-quaternization (DQ) in PBI-BuI. A substitution by bulky *4-tert*-butylbenzyl group led to lowering in packing density till DQ of merely 13%, beyond which, the induced ionic content took precedence in governing the closer packing density of the resulting polymer matrix. The solubility of resulting PILs was increased and thermal stability decreased than that of parent PBI-BuI. At lower DQ of 13%, the gas diffusivity and permeability were higher than that of other members of this family. With variation in DQ, effects of induced ionic content on CO_2 sorption though were promising; variations in diffusivity were more prominent. As a result, overall permeability decreased with increase in DQ. The present work indicates that there is a need to enhance free volume in a polymer as well as IL character, simultaneously; so that better benefits of introducing IL character in a polymer can be drawn for improving CO_2 permeation properties.

In order to understand effects of physically introducing ionic character, blending of a PIL ([TBzPBI-BuI][Br]$_{88}$) with DBzPBI-BuI was performed in various blend compositions. The maximum gas permeability was observed at 10% loading of [TBzPBI-BuI][Br]$_{88}$ in the blend. This supported above finding of IL character becoming predominant in governing overall chain packing in the matrix and thus gas permeation properties.

In the next study, effects of variation of anion in PILs possessing partial ionic character were examined towards selectivity performance (especially CO_2 based). The [TBzPBI-BuI][Br]$_{10}$ and [TBzPBI-BuI][Br]$_{18}$ were chosen for bromide exchange based on their good combination of

permeability and selectivity, as studied earlier. For bromide exchange, three anions, viz., Tf_2N^-, BF_4^- and Ac^- were chosen based on their CO_2 specific nature. PILs with BF_4^- anion showed higher CO_2 permeation as well as CO_2 based selectivity than their counter parts possessing other anions. PILs with Tf_2N^- anion showed higher permeability for non-interacting gases. This could be due to higher Vander wall volume of this anion.

Next study was focused on PILs with amino acids as an anion. The cation of these PILs was obtained by asymmetric *N*-quaternization of PBI-BuI by methyl and *t*-butylbenzyl (Bz) groups. Variation in the length of alkyl group, presence of other functional groups and are commercial availability were the criteria for choosing amino acids. Obtained AAPILs exhibited good solvent solubility, were amorphous in nature, but lowered thermal stability. AAPIL with L-Arginate anion showed higher CO_2 sorption as well as CO_2 based sorption selectivity than its counterpart with other amino acid as anion. The CO_2 sorption in these AAPILs was found to depend upon the pK_a, which is a function of number and type of primary and secondary amine group present in them.

In the next part of the work, blend membranes were prepared using a PILs, viz., P[DADMA][TFMS] and PBI-I for evaluating them as high temperature proton exchange membrane fuel cell (HT-PEMFC) as well as anion exchange membrane fuel cell (AEMFC). The DSC and IR results suggested that PBI and PIL exhibited good miscibility in all attempted proportions. As the temperature increased, conductivity of PBI-PIL blends doped with H_3PO_4 increased. The maximum proton conductivity of the PBI-PIL$_{45}$ blend membrane was found to be 0.07 S/cm at 150 °C under anhydrous condition. Single cell evaluations have been successfully demonstrated by using H_2/O_2 at temperature of 160 °C under nonhumidified conditions. Highest current density of 1632 mA cm^{-2} was obtained for PBI-PIL$_{25}$, which was almost double than that of PBI-I obtained under same conditions. The blend membranes were also found to be good carrier for OH^- anion as well. All the blends membranes showed good hydroxide stability up to 3M KOH concentration for 7 days. The maximum hydroxide conductivity was found 0.15 Scm^{-1} at 80 °C with PBI-PIL$_{45}$.

In the second scheme of evaluating electrochemical applicability of PILs, pure PILs membranes were prepared for HT-PEMFC. Here, a facile new route for the synthesis of self-cross-linked PILs membranes for proton transfer without the need for any cross-linkers or catalysts was employed. Solvent soluble PILs bearing alkene pendant groups were synthesized

via the *N*-quaternization of PBI-I. After their film formation, cross-linking was performed by just heating. DQ in this series of the PILs was systematically varied in order to study concurrent effects of induced ionic liquid (IL) character and cross-linking on their physical and electrochemical properties. The H_3PO_4 doping level decreased with increasing DQ due to reduced amount of free nitrogen in PILs. The cross-linked PILs membranes showed conductivity in the range of 0.0013-0.016 S.cm^{-1}.

In the next part of the work, soluble PILs bearing flexible side chains (*tert*-butylbenzyl as pendant groups) were synthesized via the *N*-quaternization of PBI-I for OH⁻ transport study. DQ in a series of the PILs was varied systematically. Formed PILs membranes were stable in alkaline condition and were doped in 3 M KOH to use further as a membrane in alkaline fuel cell. The IEC and water uptake increased with increasing DQ due to increased ionic character in PILs. These membranes showed conductivity in the range of 0.03-0.07 S.cm^{-1}. These AEMs exhibited high hydroxide ion conductivity, while retaining good mechanical strength, making them promising candidates for AEMFC.

In summary, present work opens a new approach of utilizing PILs as membrane material for gas separation, PEMFC and AEMFC.

References

Aaron D. and Tsouris C., *Sep. Purif. Technol*, **2005**, 40, 321–348.

Adewolea J. K., Ahmad A. L., Ismail S., Leo C. P., *Int. J. Greenhouse Gas Control*, **2013**, 17, 46–65.

Agel E., Bouet J., Fauvarque J. F., *J. Power Sources*, **2001**, 101, 267-274.

Albo J., Santos E., Neves L. A., Simeonov S. P., Afonso C. A. M., Crespo J. G., Irabien A., *Sep. Purif. Technol.*, **2012**, 97, 26–33.

Alessandro D. M., Smit B. and Long J. R., *Angew. Chem. Int. Ed.*, **2010**, 49, 6058 – 6082.

Almantariotis D., Gefflaut T., Pa´dua A. A. H., Coxam J. Y., and Costa Gomes M. F., *J. Phys. Chem. B*, **2010,** 114*,* 3608–3617.

Anderson J. L., Dixon J. K. and Brennecke J. F., *Acc. Chem. Res.,* **2007**, 40*,* 1208–1216.

Anderson S. and Newell R., *Annu. Rev. Environ. Resour.*, **2004,** 29, 109–142.

Anthony J. L., Anderson J. L., Maginn E. J. and Brennecke J. F., *J. Phys. Chem. B,* **2005**, 109, 6366-6374.

Antolini E., Gonzalez E. R., *J. Power Sources*, **2010**, 195, 3431–3450.

Arunbabu D., Sannigrahi A. and Jana T., *J. Phys. Chem. B*, **2008**, 112, 5305-5310.

Asensio J. A., Borros S. and Gomez-Romero P., *Electrochem. Commun.*, **2003**, 5, 967-972.

Baltus R. E., Counce R. M., Culbertson B. H., Luo H., DePaoli D. W., Dai S. and Duckworth D. C., *Sep. Sci. Technol.*, **2005**, 40, 525–541.

Bara J. E., Carlisle T. K., Gabriel C. J., Camper D., Finotello A., Gin D. L., and Noble R. D., *Ind. Eng. Chem. Res.,* **2009a,** *48,* 2739–2751.

Bara J. E., Gabriel C. J., Hatakeyama E. S., Carlisle T. K., Lessmann S., Noble R. D., Gin D. L., *J. Membr. Sci.,* **2008b**, 321, 3–7.

Bara J. E., Gin D. L. and Noble R. D., *Ind. Eng. Chem. Res.* **2008d,** 47*,* 9919–9924.

Bara J. E., Hatakeyama E. S., Gabriel C. J., Zeng X., Lessmann S., Gin D. L., Noble R. D., *J. Membr. Sci.,* **2008c**, 316, 186-191.

Bara J. E., Hatakeyama E.S., Gin D. L. and Noble R. D., *Polym. Adv. Technol.,* **2008a**, 19, 1415–1420.

Bara J. E., Lessmann S., Gabriel C. J., Hatakeyama E. S., Noble R. D. and Gin D. L., *Ind. Eng. Chem. Res.*, **2007**, 46, 5397-5404.

Bara J. E., Noble R. D. and Gin D. L., *Ind. Eng. Chem. Res.,* **2009b**, 48, 4607–4610.

Barbari T. A. and Conforti R. M., *Polym. Adv. Technol.*, **1994**, 5, 698-707.

Barbari T. A., Koros W. J. and Paul D. R., *J. Polym. Sci., Part B: Polym. Phys.*, **1988**, 26, 729-744.

Barbir F. and Yazici S., *Int. J. Energy Res.*, **2008**, 32:369–378.

Bates E. D., Mayton R. D., Ntai I., and Davis J. H., Jr., *J. Am. Chem. Soc.,* **2002**, 124, 926-927.

Bernardo P., Drioli E. and Golemme G., *Ind. Eng. Chem. Res.*, **2009**, 48, 4638–4663.

Bhavsar R. S., "Polymeric Ionic Liquids (PILs): Synthetic Approaches and Gas Permeation Studies with an Emphasis on CO_2 Separation", *PhD dissertation*, **2014a**, 195 pages AcSIR, National Chemical Laboratory (NCL) India.

Bhavsar R. S., Kumbharkar S. C., Kharul U. K., *J. Membr. Sci.,* **2012**, 389305– 315.

Bhavsar R. S., Kumbharkar S. C., Kharul U. K., *J. Membr. Sci.*, **2014c**, 470, 494–503.

Bhavsar R. S., Kumbharkar S. C., Rewar A. S. and Kharul U. K., *Polym. Chem.*, **2014b**, 5, 4083–4096.

Bhavsar R. S., Nahire S. B., Kale M. S., Patil S. G., Aher P. P., Bhavsar R. A. and Kharul U. K., Journal of Applied Polymer Science, **2011**, 120, 1090–1099.

Bondi A., *J. Phys. Chem.*, **1964**, 68, 441–451.

Borup R., Meyers J., Pivovar B., Kim Y. S., Mukundan R., Garland N., Myers D., Wilson M., Garzon F., Wood D., Zelenay P., More K., Stroh K., Zawodzinski T., Boncella X. J., McGrath J. E., Inaba M., Miyatake K., Hori M., Ota K., Ogumi Z., Miyata S., Nishikata A., Siroma Z., Uchimoto Y., Yasuda K., Kimijima K. and Iwashita N., *Chem. Rev.,* **2007**, 107, 3904-3951.

Brooks N. W., Duckett R. A., Rose J. and Ward I. M., Polymer, **1993**, 34, 4038-4042.

Bruijn F. A. de, Dam V. A. T. and Janssen G. J. M., *Fuel Cells*, **2008**, 08, 3-22.

Buzzeo M. C., Evans R. G. and Compton R. G., *Chem. Phys. Chem.*, **2004**, 5, 1106 - 1120.

Cadena C., Anthony J. L., Shah J. K., Morrow T. I., Brennecke J. F. and Maginn E. J., *J. Am. Chem. Soc.,* **2004**, 126, 5300-5308.

Calleja E. T., Skinner J. and Tauste D. G., *Hindawi Publishing Corporation Journal of Chemistry*, **2013**, 473584-473599.

Camper D., Bara J., Koval C. and Noble R., *Ind. Eng. Chem. Res.,* **2006**, 45, 6279-6283.

Carlisle T. K., Bara J. E., Gabriel C. J., Noble R. D. and Gin D. L., *Ind. Eng. Chem. Res.,* **2008**, *47,* 7005–7012.

Carlisle T. K., Bara J. E., Lafrate A. L., Gin D. L., Noble R. D., *J. Membr. Sci.,* **2010***, 359, 37–43.

Carlisle T. K., Nicodemus G. D., Gin D. L., Noble R. D., *J. Membr. Sci.,* **2012**, 397– 398, 24–37.

Carlisle T. K., Wiesenauer E. F., Nicodemus G. D., Gin D. L. and Noble R. D., *Ind. Eng. Chem. Res.*, **2013**, 52, 1023−1032.

Carollo A., Quartarone E., Tomasi C., Mustarelli P., Belotti F., Magistris A., Maestroni F., Parachini M., Garlaschelli L., Righetti P. P., *J. Power Sources*, **2006**, 160, 175-180.

Che Q., Sun B. and He R., *Electrochim. Acta*, **2008**, 53, 4428–4434.

Che Q., Zhou L., Wang J., *J. Mol. Liq.*, **2015**, 206, 10–18.

Chempath S., Boncella J. M., Pratt L. R., Henson N. and Pivovar B. S., *J. Phys. Chem. C*, **2010**, 114, 11977–11983.

Chen C., Hess A. R., Jones A. R., Liu X., Barber G. D., Mallouk T. E., Allcock H. R. *Macromolecules*, **2012**, 45, 1182–1189.

Cheng J., He G., Zhang F., *Int. J. Hydrogen Energy*, **2015**, 40, 7348-7360.

Chi W. S., Hong S. U., Jung B., Kang S. W., Kang Y. S., Kim J. H., *J. Membr. Sci.,* **2013**, 443, 54–61.

Choi P., Jalani N. H. and Datta R., *J. Electrochem. Soc.*, **2005**, 152 ~3 E123-E130.

Cope A. C. and Mehta A. S., *J . Am. Chcm.* Soc., **1963**, 85, 1949-1952.

Couture G., Alaaeddine A., Boschet F., Ameduri B., *Prog. Polym. Sci.*, **2011**, 36, 1521– 1557.

Cserjesi P., Nemestothy N., Bako K. B., *J. Membr. Sci.,* **2010**, 349, 6–11.

Cserjesi P., Nemestothy N., Vass A., Csanadi Zs., Bako K. B., *Desalination*, **2009**, 246, 370–374.

Daletou M. K., Geormezi M., Vogli E., Voyiatzis G. A. and Neophytides S. G., *J. Mater. Chem. A*, **2014**, 2, 1117-1127.

Deavin O. I., Murphy S., Ong A. L., Poynton S. D., Zeng R., Hermanac H. and Varcoe J. R., *Energy Environ. Sci.*, **2012**, 5, 8584-8597.

Devanathan R., *Energy Environ. Sci.*, **2008**, 1, 101–119.

Domanska U. and Rekawek A., *J. Solution Chem.*, **2009**, 38, 739–751.

Dong G., Li H. and Chen V., *J. Mater. Chem. A*, **2013**, 1, 4610-4630.

Doyle M., Choi S. K., and Proulx G., *J. Electrochem. Soc.,* **2000**, 147 (1) 34-37.

Dupont J. and Scholten J. D., *Chem. Soc. Rev.*, **2010**, 39, 1780–1804.

Earle M. J. and Seddon K. R., *Pure Appl. Chem.*, **2000**, 72, 1391–1398, 2000.

Eguizábal A., Lemus J., Pina M. P., *J. Power Sources*, **2013**, 222, 483-492.

Fang W., Luo Z. and Jiang J., *Phys. Chem. Chem. Phys.,* **2013**, 15, 651-658.

Fernandez F. J. H., Rıos A. P., Rubio M., Alonso F. T., G´omez D., V´ıllora G., *J. Membr. Sci.*, **2007**, 293, 73–80.

Foldes E., Fekete E., Karasz F. E. and Pukanszky B., *Polymer*, **2000**, 41, 975-983.

George S. C. and Thomas S., *Prog. Polym. Sci.,* **2001**, 26, 985-1017.

Goodrich B. F., de la Fuente J. C., Gurkan B. E., Lopez Z. K., Price E. A., Huang Y., and Brennecke J. F., *J. Phys. Chem. B*, **2011b**, 115, 9140–9150.

Goodrich B. F., de la Fuente J. C., Gurkan B. E., Zadigian D. J., Price E. A., Huang Y., and Brennecke J. F., *Ind. Eng. Chem. Res.,* **2011a,** *50,* 111–118.

Green O., Grubjesic S., Lee S. and Firestone M. A., *J. Macromol. Sci. Polymer. Rev.*, **2009**, 49, 339–360.

Grew K. N. and Chiu W. K. S., *J. Electrochem. Soc.,* **2010***,* B327-B337.

Gu S., Cai R., Luo T., Chen Z., Sun M., Liu Y., He G., and Yan Y., *Angew. Chem. Int. Ed.*, **2009**, 48, 6499 –6502.

Gu S., Cai R., Luo T., Jensen K., Contreras C., and Yan Y., *Chem Sus Chem*, **2010**, 3, 555 – 558.

Gubler L. and Scherer G. G., *Adv. Polym. Sci,.* **2008**, 215, 1–14.

Guiver M. D., Robertson G. P., Dai Y., Bilodeau F., Kang Y. S., Lee K. J., Jho J. Y., Won J., *J. Polym. Sci. Part A: Polym. Chem.*, **2002**, 40, 4193–4204.

Gurau G., Rodriguez H., Kelley S. P., Janiczek P., Kalb R. S., and Rogers R. D., *Angew. Chem. Int. Ed.*, **2011**, 50, 12024 –12026.

Handford B. M. E., Abanades J. C., Anthony E. J., Blunt M. J., Brandani S., Dowell N. M., Fern´andez J. R., Ferrari M. C., Gross R., Hallett J. P., Haszeldine R. S., Heptonstall P., Lyngfelt A., Makuch Z., Mangano E., Porter R. T. J., Pourkashanian M., Rochelle G. T., Shah N., Yao J. G. and Fennell P. S., *Energy Environ. Sci.*, **2014**, 7, 130–189.

Hao L., Li P., Yang T., Chung T. S., *J. Membr. Sci.,* **2013**,436, 221–231.

Haszeldine R. S., *Science*, **2009**, 325, 1647-1652.

Hellums M. W., Koros W. J., Husk G. R., Paul D. R., *J. Membr. Sci.*, **1989**, 46, 93–112.

Hibbs M. R., Fujimoto C. H. and Cornelius C. J., *Macromolecules*, **2009**, 42, 8316–8321.

Hirao M., Akita K. I. and Ohno H., *Polym. Adv. Technol.,* **2000**, 11, 534±538.

Hoogers, G.; Fuel Cell Technology Handbook; CRC Press: Boca Raton, FL, **2003**.

Hu X., Tang J., Blasig A., Shen Y., Radosz M., *J. Membr. Sci.,* **2006***,* 281, 130–138.

Hu Y. F., Liu Z. C., Xu C. M. and Zhang X. M., *Chem. Soc. Rev.*, **2011**, 40, 3802–3823.

Hudiono Y. C., Carlisle T. K., Bara J. E., Zhang Y., Gin D.L., Noble R. D., *J. Membr. Sci.,* **2010**, 350, 117–123.

Hudiono Y. C., Carlisle T. K., LaFrate A. L., Gin D. L., Noble R. D., *J. Membr. Sci.,* **2011***,* 370, 141–148.

Hunley M. T., England J. P. and Long T. E., *Macromolecules,* **2010**, 43, 9998–10005.

Iojoiu C., Chabert F., Mar´echal M., Kissi N. El., Guindet J., Sanchez J.-Y., *J. Power Sources*, **2006**, 153, 198–209.

Ito K., Nishina N. and H. Ohno, *Electrochim. Acta*, **2000**, 45, 1295–1298.

Jacobson M. Z., *Energy Environ. Sci.*, **2009**, 2, 148–173.

Javaid A., *Chem. Eng. J.*, **2005**, 112, 219–226.

Jeffery G. H., Bassett J., Mendham J., Denney R. C., Vogel's Textbook of Quantitative Chemical Analysis, *British Library Cataloguing in Publication Data*, 5th edn, **1989**.

Jheng L., Hsu S. L., Lin B., Hsu Y., *J. Membr. Sci.*, **2014**, 460, 160-170.

Jindaratsamee P., Ito A., Komuro S., Shimoyama Y., *J. Membr. Sci.,* **2012***,* 423–424, 27-32.

Jung M. J., Arges C. G. and Ramani V., *J. Mater. Chem.*, **2011**, 21, 6158.

Kammakakam I., Kim H. W., Nam S. Y., Par H. B., Kim T. H., *Polymer,* **2013**, 54, 3534-3541.

Kanehashi S., Nagai K., *J. Membr. Sci.,* **2005**, 253, 117–138.

Kapantaidakis G. C., Koops G. H., Wessling M., Kaldis S. P. and Sakellaropoulos G. P., *AIChE J*, **2003**, 49, 1702-1711.

Karadkar P. B., Kharul U. K., Bhole Y. S., Badhe Y. P., Tambe S. S., Kulkarni B. D., *J. Membr. Sci.*, **2007**, 303, 244–251.

Karas F., Hnat J., Paidar M., Schauer J., Bouzek K., *Int. J. Hydrogen Energy*, **2014**, 39, 5054-5062.

Kenarsari S. D., Yang D., Jiang G., Zhang S., Wang J., Russell A. G., Weif Q. and Fan M., *RSC*

Adv., **2013**, 3, 22739-22773.

Kesting R. E., Fritzsche A. K., *Polymeric gas separation membranes*, Wiley, New York **1993**.

Kim S. Y., Kim S. and Park M. J., *Nat. Commun.,* **2016**, DOI: 10.1038/ncomms1086.

Koch V. R., Nanjundiah C., Carlin R. T., Nashua N. H., US Patent 5827602; **1997**.

Kohno Y. and Ohno H., *Phys. Chem. Chem. Phys.*, **2012**, 14, 5063–5070.

Koros W. J. and Fleming G. K., *J. Membr. Sci.*, **1993**, 83, l-80.

Koros W. J., Chan A. H. and Paul D. R., *J. Membr. Sci.*, **1977**, 2, 165-190.

Koros W. J., Mahajan R., *J. Membr. Sci.,* **2000**, 175, 181–196.

Koros W. J., Paul D. R., *J. Polym. Sci. Polym. Phys.*, **1976,** 14, 1903–1907.

Kreuer K. D., *Chem. Mater.* **1996,** *8,* 610-641.

Kreuer K. D., Paddison S. J., Spohr E. and Schuster M., *Chem. Rev.*, **2004,** 104, 4637-4678.

Kumbharkar S. C., Bhavsar R. S. and Kharul U. K., *RSC Adv.*, **2014**, 4, 4500–4503.

Kumbharkar S. C., Karadkar P. B., Kharul U. K., *J. Membr. Sci.*, **2006**, 286, 161–169.

Kumbharkar S. C., Kharul U. K., *Eur. Polym. J.*, **2009**, 45, 3363–3371.

Kumbharkar S. C., Kharul U. K., *J. Membr. Sci.*, **2010**, 357, 134–142.

Laskoski H. L. R. and Snow A. W., *J. Am. Chem. Soc.*, **2006**, 128, 12402–12403.

Lee S. Y., Ogawa A., Kanno M., Nakamoto H., Yasuda T. and Watanabe M., J. Am. Chem. Soc.
  2010b, 132, 9764–9773.

Lee S. Y., Yasuda T., Watanabe M., *J. Power. Sources,* **2010a**, 195, 5909–5914.

Lee S., *Chem. Commun.*, **2006**, 1049–1063.

Li J. L. and Chen B. H., *Sep. Purif. Technol.,* **2005**, 41, 109–122.

Li P., Paul D. R. and Chung T. S., *Green Chem.*, **2012**, 14, 1052-1063.

Li P., Zhao Q., Anderson J. L., Varanasi S., Coleman M. R., *J. Polym. Sci. Part A: Polym. Chem.*, **2010**, 48, 4036–4046.

Li Q., He R., Jensen J. O. and Bjerrum N. J., *Chem. Mater,* **2003,** 15, 4896-4915.

Li Q., Jensen J. O., Savinell R. F., Bjerrum N. J., *Prog. Polym. Sci.*, **2009**, 34, 449–477.

Lin B., Cheng S., Qiu L., Yan F., Shang S. and Lu J., *Chem. Mater.,* **2010a**, 22, 1807–1813.

Lin B., Chu F., Ren Y., Jia B., Yuan N., Shang H., Feng T., Zhu Y., Ding J., *J. Power Sources,* **2014**, 266, 186-192.

Lin B., Qiu L., Lu J. and Yan F., *Chem. Mater.,* **2010b**, 22, 6718–6725.

Liu Y., Wang Z. U. and Zhou H. C., *Greenhouse Gas Sci Technol.,* **2012***,* 2, 239–259.

Mader J., Xiao L., Schmidt T. J. and Benicewicz B. C., *Adv. Polym. Sci.*, **2008**, 216, 63–124.

Makhija S., Pearce E. M., Kwei T. K. and Liu F., *Polym. Eng. Sci.*, **1990**, 30, 798-801.

Mamlouk M., Ocon P. and Scott K., *J. Power Sources,* **2014**, 245, 915-926.

Marcilla R., Blazquez J. A., Fernandez R., Grande H., Pomposo J. A., Mecerreyes D., *Macromol. Chem. Phys*., **2005**, 206, 299–304.

McHattie J. S., Koros W. J., Paul D. R., Polymer, **1992**, 33, 1701–1711.

Mecerreyes D., Applications of Ionic Liquids in Polymer Science and Technology2015, *Springer Heidelberg New York Dordrecht London,* **2015**.

Mecerreyes D., *Prog. Polym. Sci.,* **2011**, 36, 1629–1648.

Mehnert C. P., *Chem. Eur. J.*, **2005**, 11, 50 – 56.

Merle G., Wessling M. and Nijmeijer K., *J. Membr. Sci.*, **2011**, 377, 1– 35.

Michaels A. S. and Bixler H. J., *J. Poly Sci.*, **1961**, L, 393-412.

Miquel M. G., Bedia J., Abrusci C., Palomar J. and Rodriguez F., *J. Phys. Chem. B,* **2013**, 117, 3398−3406.

Mishra A. K., Kim N. H. and Lee J. H., *J. Membr. Sci.*, **2014**, 449, 136-145.

Mishra A. K., Kuila T., Kim D., Kim N. H. and Lee J. H., *J. Mater. Chem.*, **2012**, 22, 24366-24372.

Mondal M. K., Balsora H. K., Varshney P., *Energy*, **2012**, 46, 431-441.

Morgan D., Ferguson L. and Scovazzo P., *Ind. Eng. Chem. Res.,* **2005,** *44,* 4815-4823.

Mulder M., *Basic principles of membrane technology*, Kluwer Academic Publisher, Dordrecht, **1996.**

Muldoon M. J., Aki S. N. V. K., Anderson J. L., Dixon J. K. and Brennecke J. F., *J. Phys. Chem. B,* **2007**, 111*,* 9001-9009.

Musto P., Karaszt F. E., MacKnight W. J., *Polymer*, **1993**, 34, 2934–2946.

Neves L. A., Crespo J. G. and Coelhoso I. M., *J. Membr. Sci.*, **2010***,* 357, 160–170.

Neves L. A., Nemestothy N., Alves V. D., Cserjesi P., Belafi-Bako K., Coelhoso I. M., *Desalination*, **2009**, 240, 311-315.

Nguyen P. T., Wiesenauer E. F., Gin D. L. and Noble R. D., *J. Membr. Sci.,* **2013**, 430, 312–320.

Nobel R. D., *J. Membr. Sci.,* **2011***,* 378, 393– 397.

Noonan K. J. T., Hugar K. M., Kostalik IV H. A., Lobkovsky E. B., Abruna H. D. and Coates G. W., *J. Am. Chem. Soc*., **2012**, 134, 18161−18164.

Ogihara W., Washiro S., Nakajima H., Ohno H., *Electrochim. Acta*, **2006**, 51, 2614–2619.

Ohno H., Yoshizawa M. and Ogihara W., *Electrochim. Acta*, **2004**, 50, 255–261.

Olajire A. A., *Energy*, **2010**, 35, 2610-2628.

Oliveira F. S., Pereiro A. B., Arau´jo J. M. M., Bernardes C. E. S., Lopes J. N. C., Todorovic S., Feio G., Almeida P. L., Rebelo L. P. N. and Marrucho I. M., *Phys.Chem. Chem. Phys.,* **2013**, 15, 18138.

Paddison S. J. and Paul R., *Phys. Chem. Chem. Phys*., **2002**, 4, 1158–1163.

Pan J., Chen C., Li Y., Wang L., Tan L., Li G., Tang X., Xiao L., Lu J. and Zhuang L., *Energy Environ. Sci.*, **2014**, 7, 354–360.

Pan X., Xiao S., Wang C., Cai P., Lu X., Lu Q., *Opt. Commun,* **2009**, 282, 763–768.

Park J. Y. and Paul D. R., *J. Membr. Sci.*, **1997**,125, 23–39.

Peckham T. J. and Holdcroft S., *Adv. Mater.,* **2010**, *22*, 4667–4690.

Pennarun P. Y., Jannasch P., *Solid State Ion.*, **2005**, 176, 1849–1859.

Plasynski S. I. and Chen Z. Y., Review of CO_2 capture technologies and some important opportunities, US DOE National Energy Technology Laboratory, **2000**.

Plechkova N. V. and Seddon K. R., *Chem. Soc. Rev.*, **2008**, 37, 123–150.

Powell C. E., Qiao G. G., *J. Membr. Sci.,* **2006**, 279, 1–49.

Price S. C., Ren X., Jackson A. C., Ye Y., Elabd Y. A. and Beyer F. L., *Macromolecules,* **2013**, 46, 7332−7340.

Privalova E. I., Arvela P. M., Murzin D. Y., Mikkola J. P., *Russ. Chem. Rev.*, **2012**, 81,435-457.

Pu H., *Polym. Int.*, **2003**, 52, 1540-1545.

Qiu B., Lin B., Si Z., Qiu L., Chu F., Zhao J., Yan F., *J. Power Sources*, **2012**, 217, 329-335.

Ramani V., The Electrochemical Society Interface*, Spring,* **2006**.

Ran J., Wu L., Varcoe J. R., Ong A. L., Poynton S. D., Xu T., *J. Membr. Sci.*, **2012**, 415–416, 242–249.

Renard I., Li H., Marsan B., *Electrochim. Acta*, **2003**, 48, 831-844.

Rewar A. S., Bhavsar R. S., Sreekumar K., Kharul U. K., *J. Membr. Sci.*, **2015**, 481, 19–27.

Robeson L.M., *J. Membr. Sci.*, **2008**, 320, 390–400.

Sadrabadi M. M. H., Dashtimoghadam E., Majedi F. S., Kabiri K., Hashjin M. S., Moaddel H., *J. Membr. Sci.*, **2010**, 365, 286–293.

Salerno H. L. S., Beyer F. L., Elabd Y. A., *J. Polym. Sci., Part B: Polym. Phys.*, **2012**, 50, 552–562.

Salleh W. N. W., Ismail A. F., Matsuura T. and Abdullah M. S., *Sep. Purif. Rev.*, **2011**, 40, 261–311.

Sanders D. F., Smith Z. P., Guo R., Robeson L. M., McGrath J. E., Paul D. R., Freeman B. D., *Polymer*, **2013**, 54, 4729-4761.

Sannigrahi A., Ghosh S., Maity S. and Jana T., *Polymer*, **2011**, 52, 4319-4330.

Scott K. and Shukla A. K., *Rev Environ Sci Biotechnol,* **2004***,* 3, 273–280.

Scovazzo P., Havard D., McShea M., Mixon S., Morgan D., *J. Membr. Sci.*, **2009**, 327, 41–48.

Scovazzo P., Kieft J., Finan D. A., Koval C., DuBois D., Noble R., *J. Membr. Sci.,* **2004**, 238, 57–63.

Sekhon S. S., Park J. S., Cho E. K., Yoon Y. G., Kim C. S. and Lee W. Y., *Macromolecules,* **2009**, *42*, 2054-2062.

Shaligram S. V., Wadgaonkar P. P., Kharul U. K., *J. Membr. Sci.*, **2015**, 493, 403–413.

Shannon M. S. and Bara J. E., *Sep. Sci. Technol.*, **2012**, 47, 178–188.

Shao L., Low B. T., Chung T. S., Greenberg A. R., *J. Membr. Sci.*, **2009**, 327, 18–31.

Shaplov A. S., Lozinskaya E. I., Vygodskii Y.S., Electrochemical Properties and Applications of Ionic Liquids, **2010,** 203-298.

Sharkh A. B. F., Yahaya G. O., Ali S. A., Hamad E. Z., Abu-Reesh I. M., *J. Appl. Polym. Sci.*, **2003**, 89, 2290–2300.

Shekhawat D., Luebke D. R. and Pennline H. W., A Review of Carbon Dioxide Selective Membranes**,** DOE/NETL-**2003**/1200.

Shen C. H., Hsu S. L., Bulycheva E. and Belomoina N., *J. Membr. Sci.,* **2012**, 11, 399–400.

Shimekit B. and Mukhtar H., Natural Gas Purification Technologies – Major Advances for CO_2 Separation and Future Directions, *Advances in Natural Gas Technology*, 235-271, **2012**, ISBN 978-953-51-0507-7.

Silva R. F., Francesco M. D. and Pozio A., *J. Power Sources*, **2004**, 134, 18-26.

Sistla Y. S., Jain L and Khanna A., *Sep. Puri. Technol.*, **2012**, 97, 51-64.

Sistla Y. S., Jain L. and Khanna A., *Sep. Purif. Technol.*, **2012**, 97, 51-64.

Sistla Y. S., Khanna A., *Chem. Eng. J.,* **2015***,* 273, 268–276.

Smiglak M., Reichert W. M., Holbrey J. D., Wilkes J. S., Sun L., Thrasher J. S., Kirichenko K., Singh S., Katritzky A. R. and Rogers R. D., *Chem. Commun.*, **2006**, 2554–2556.

Smith G. D., Borodin O., Li L., Kim H., Liu Q., Bara J. E., Gin D. L. and Nobel R., *Phys. Chem. Chem. Phys*., **2008**, 10, 6301–6312.

Soo K. J. W. Y., An investigation into polybenzimidazoles as anion exchange membranes, M.Sc. dessertation, **2009**, Simon Fraser University, Canada.

Soria V., Gomez C. M., Rodriguez P., Parets M. J. and Campos A., *Colloid Polym. Sci*., **1994**, 272, 497-503.

Sprague I. B., Byun D. and Dutta P., *Electrochim. Acta*, **2010**, 55, 8579-8589.

Sridhar S., Bee S. and Bhargava S. K., Membrane-based Gas Separation: Principle, Applications and Future Potential, **2014**.

Stern S. A. and Saxena, *J. Membr. Sci.*, **1980**, 7, 47-59.

Stern S. A., Gareis P. J., Sinclair T. F., and Mohr P. H., *J. Appl. Polym. Sci.*, **1963**, 7, 2035-2051.

Stern S. A., *J. Membr. Sci.*, **1994**, 94, l-65.

Suarez P. A. Z., Dullius J. E. L., Einloft S., DeSouza R. F., Dupont J., Polyhedron, **1996**, 15, 1217–1219.

Tang J., Shen Y., Radosz M. and Sun W., *Ind. Eng. Chem. Res.,* **2009,** *48,* 9113–9118.

Tang J., Tang H., Sun W., Plancher H., Radosz M. and Shen Y., *Chem. Commun.*, **2005a**, 3325–3327.

Tang J., Tang H., Sun W., Radosz M., Shen Y., *J. Polym. Sci., Part A: Polym. Chem.*, **2005b**, 43, 5477–5489.

Tang J., Tang H., Sun W., Radosz M., Shen Y., *Polymer*, **2005c**, 46, 12460–12467.

Tay S. W., Zhang X., Liu Z., Hong L. and Chan S. H., *J. Membr. Sci.,* **2008**, 321, 139-145.

Thomas O. D., Soo K. J. W. Y., Peckham T. J., Kulkarni M. P. and Holdcroft S., *Polym. Chem.*, **2011**, 2, 1641–1643.

Thomas O. D., Soo K. J. W. Y., Peckham T. J., Kulkarni M. P. and Holdcroft S., *J. Am. Chem. Soc.*, **2012**, 134, 10753−10756.

Tin P. S., Chung T. S., Liu Y., Wang R., Liu S. L., Pramod K. P., *J. Membr. Sci.*, **2003**, 225, 77–90.

Tome L. C., Aboudzadeh M. A., Rebelo L. P. N., Freire C. S. R., Mecerreyes D. and Marrucho I. M., *J. Mater. Chem. A*, **2013**, 1, 10403–10411.

Tome L. C., Development of new membranes based on ionic liquid materials for gas separation, *PhD dessertation*, **2014**a, Instituto de Tecnologia Química e Biológica António Xavier, Universidade Nova de Lisboa, Portugal.

Tome L. C., Patinha D. J. S., Ferreira R., Garcia H., Pereira C. S., Freire C. S. R., Rebelo L. P. N. and Marrucho I. M., *Chem Sus Chem,* **2014b**, 7, 110 – 113.

Tominaga Y. and Ohno H., *Chem. Lett.*, **1998**, 955-956.

Tsujita Y., *Prog. Polym. Sci.*, **2003**, 28, 1377–1401.

Varcoe J. R., Slade C. T., *Fuel cell*, **2005**, 5, 187-200.

Ven E. V. D., Chairuna A., Merle G., Benito S. P., Borneman Z., Nijmeijer K., *J. Power Sources,* **2013**, 222, 202-209.

Vieth W. R., Howell J. M., Hsieh J. H., *J. Membr. Sci.*, **1976**, 1, 177–220.

Vygodskii Y. S., Melnik O. A., Shaplov A. S., Lozinskaya E. I., Malyshkina I. A. and Gavrilova N. D., *Polymer Science, Ser. A*, **2007**, 49, 256–261.

Walden P., *Bull. Russian Acad. Sci.*, **1914**, 405–422.

Wang C., Guo Y., Zhu X., Cui G., Li H. and Dai S., *Chem. Commun.*, **2012**, 48, 6526–6528.

Wang C., Luo X., Luo H., Jiang D., Li H., and Dai S., *Angew. Chem. Int. Ed.*, **2011**, 50, 4918 – 4922.

Wang G., Hou W., Xiao F., Geng J., Wu Y. and Zhang Z., *J. Chem. Eng. Data*, **2011**, 56, 1125–1133.

Wang J. S., Naito Y. and Kamiya Y., *J. Polym. Sci.: Part B: Polym. Phy.*, **1996**, 34, 2027-2033.

Wang J. T. and Hsu S. L., *Electrochim. Acta*, **2011**, 56, 2842-2846.

Wang J., Li S. and Zhang S., Macromolecules, **2010**, 43, 3890–3896.

Weber A. Z. and Newman J., *AIChE J.,* **2004b**, 50, 3215-3226.

Weber A. Z. and Newman J., *Chem. Rev.*, **2004a,** 104, 4679-4726.

Wilke A., Yuan J., Antonietti M. and Weber J., *ACS Macro Lett.*, **2012**, 1, 1028−1031.

Winter M. and Brodd R. J., *Chem. Rev.,* **2004,** 104, 4245-4269.

Wu C., Senftleb T. P. and Schneider W. F., *Phys. Chem. Chem. Phys.*, **2012**, 14, 13163–13170.

Xiao Y., Dai Y., Chung T. S., Guiver M. D., *Macromolecules*, **2005**, 38, 10042–10049.

Xiong Y. B., Wang H., Wang Y. J. and Wang R. M., *Polym. Adv. Technol.*, **2012**, 23 835–840.

Xu C., Cao Y., Kumar R., Wu X., Wang X. and Scott K., *J. Mater. Chem.*, **2011**, 21, 11359.

Xu C., Du H., Li B., Kang F., and Zeng Y., *J. Electrochem. Soc.*, **2009**, 156**,** A435-A441 2009.

Yang Z. Z., Zhao Y. N. and He L. N., *RSC Adv.*, **2011**, 1, 545–567.

Ye H., Huang J., Xu J. J., Kodiweera N. K. A. C., Jayakody J. R. P. and Greenbaum S. G., *J. Power Sources*, **2008**, 178, 651-660.

Ye Y. and Elabd Y. A., *Macromolecules*, **2011**, 44, 8494–8503.

Yu C. H., Huang C. H., Tan C. S., *Aerosol Air Qual. Res.*, **2012**, 12, 745–769.

Yu H., Wu Y. T., Jiang Y. Y., Zhou Z. and Zhang Z. B., *New J. Chem.*, **2009**, 33, 2385–2390.

Yuan J. and Antonietti M., *Polymer*, **2011**, 52, 1469-1482.

Yuan J., Mecerreyes D., Antonietti   M., *Prog. Poly. Sci.*, **2013**, 38, 1009– 1036.

Zhang F., Zhang H. and Qu C., *J. Mater. Chem. A*, **2011**, 21, 12744-12752.

Zhang Q., Li S. and Zhang S., *Chem. Commun.,* **2010**, 46, 7495–7497.

Zhang X., Zhang X., Dong H., Zhao Z., Zhang S. and Huang Y., *Energy Environ. Sci.*, **2012**, 5, 6668–6681.

Zhao T.S., Li Y.S. and Shen S.Y., *Energy Power Eng. China*, **2010**, 4, 443–458.

Zhao W., He G., Zhang L., Ju J., Dou H., Nie F., Li C., Liu H., *J. Membr. Sci.*, **2010**, 350, 279– 285.

Zhijun Z., Haifeng D. and Xiangping Z., *Chin. J. Chem. Eng.*, **2012**, 20, 120-129.

Zhou Y., Yang J., Su H., Zeng J., Jiang S. P. and Goddard W. A., *J. Am. Chem. Soc.,* **2014**, 136, 4954−4964.

Zuo Z., Fu Y. and Manthiram A., *Polymer*, **2012**, 4, 1627-1644.

	Synopsis of the Thesis to be submitted to the Academy of Scientific and Innovative Research for Award of the Degree of Doctor of Philosophy in Chemistry
Name of the Candidate	Ms. Anita S. Rewar
Degree Enrolment No. & Date	Ph. D in Chemical Sciences (10CC11J26069); January 2011
Title of the Thesis	Investigations towards applicability of polybenzimidazole (PBI) based polymeric ionic liquids (PILs) for gas permeation and fuel cells
Research Supervisor	Dr. Ulhas K. Kharul (AcSIR, CSIR-NCL, Pune)

Introduction

Climate changes related to global warming caused by increased CO_2 concentration in the atmosphere is a major challenges. The burning of the fossil fuel results into increase of CO_2 concentration in the atmosphere. To overcome this issue, there can be two solutions (1) development of the methods which would effectively reduce the CO_2 concentration in the atmosphere and (2) development of new renewable energy sources that can replace use of fossil fuel. Membrane based CO_2 separation have benefits over the other process [1] and could be a possible solution to mitigate CO_2 concentration in the atmosphere. On the other hand, proton exchange membrane based fuel cell (PEMFC) and anion exchange membrane based fuel cell (AEMFC) are emerging as an alternate energy generating system. Polymeric ionic liquid (PIL) are emerging as a new generation membrane materials for CO_2 separation due for to their specific properties [2,3,4]. Room temperature ionic liquid (RTIL) based blend membranes are being investigated due to their improved ion-transport properties [5,6].

Statement of Problem, Aims and Objectives

Applicability of ionic liquids in CO_2 separation and in PEMFC/AEMFC although is well demonstrated, it has drawbacks associated with their liquid phase. Polymeric ionic liquids (PILs) are projected as emerging CO_2 separation membrane materials. Reported PILs are brittle in nature and cannot be used for practical applicability involving high pressures. In view of potentials of PILs (limitless anion and cation combination, high CO_2 sorption, etc.), there is a need for developing mechanically stable PILs membranes for CO_2 separation. As RTILs are demonstrated to elevate performance in PEMFC, it would be worth to evaluate PILs as membrane materials in PEMFC/AEMFC, which became the aim of present work.

Following are objectives of the this work that would enhance an understanding towards applicability of PILs for CO_2 separation and as PEMFC/AEFC materials.

1) To investigate effects of partial ionic character in regulating gas sorption and diffusion (especially for CO_2) in rigid rod, film forming PBI based PILs.

2) To investigate effects of amino acids as an anion in PBI-based PILs for gas sorption.

2) To evaluate applicability of PILs as a membrane material for PEMFC and AEMFC.

Methodology used

1. With chosen polybenzimidazole backbone and a bulky *4-tert*-butylbenzyl group as a substituent (to ease the gas diffusion) for partial *N*-quaternization of PBI-BuI, develop a family of PILs possessing partial ionic character and investigate their gas sorption, diffusion and transport properties. Elucidation of physical properties of this new family of polymers would help in understanding their permeation properties.

2. Synthesis and characterization of PILs with amino acid as an anion for investigating CO_2 sorption characteristics of PILs. The selection of amino acid was based on variation in chain length, number and type of 'N' functionality.

3. Perform incremental incorporation of PIL in PBI and evaluate proton transport of resulting blend membranes in PEMFC. The partial *N*-quaternization of PBI-I by using allyl groups would generate PILs character as well as crosslinking ability. Choose *N*-substituents with specific aims to enhance stability of PIL in alkaline condition, induce ionic character and crosslinking ability in PILs.

Key Findings

Scheme 1. *Polymeric ionic liquids (PILs) possessing partial ionic liquid character: Gas permeation studies*

A structural balance between *N*-substitution and *N*-quaternization was performed by the controlled *N*-quaternization of PBI-BuI by a bulky group, *4-tert*-butylbenzyl. Homogeneous blend based on a PIL (fully *N*-quaternized PBI-BuI) and *N*-substituted PBI-BuI were obtained. Both these methodologies of incorporating partial ionic character in the membrane conveyed that at a low ionic character incorporation of ~ 10-13 %, a balance of ionic character and bulky *N*-substituent led to highest gas permeability. At higher ionic character, increased chain interaction predominates and as a result, permeability decreased.

Scheme 2. *PILs possessing partial ionic liquid character: Effects of anion exchange on their physical and gas permeation properties*

Two PILs ([TBzPBI-BuI][Br]$_{10}$ and [TBzPBI-BuI][Br]$_{18}$) from above study were chosen for anion exchange with three chosen anions, Tf_2N^-, BF_4^- and Ac^- based on their CO_2 specific nature. Among formed PILs, the one with BF_4^- anion showed higher CO_2 permeability as well as selectivity. This study concludes that combination of partial ionic character and anions is crucial in elevating CO_2 permeation properties.

Scheme 3. *Effect of amino acid as an anion on physical and gas sorption properties of PBI based polymeric ionic liquids*

A series of PILs containing amino acid as an anion was synthesized. The AAPIL with L-Arginine as anion showed higher CO_2 sorption as well as CO_2 based sorption selectivity than that of other anions. This was attributed to the presence effective *N*-sites for CO_2 sorption.

Scheme 4. *PIL-PBI blend membranes: Physical and electrochemical evaluations towards their applicability as membranes for PEMFC and AEMFC*

Blending of polymeric ionic liquids (PILs) with PBI for applicability was performed and resultant membranes were analyzed for high temperature proton exchange membrane fuel cell (HT-PEMFC) as well as anion exchange membrane fuel cell (AEMFC). The PBI-PIL blend membranes shown a significant improvement in the proton conductivity (almost double the performance as that of PBI membranes) as well as hydroxide ion conductivity.

Scheme 5. *Novel elegant stable polymeric ionic liquid (PIL) membrane materials for fuel cell (PEMFC and AEMFC)*

The new family of PILs with crosslinking ability was synthesized based on allyl substituent. These PILs could be crosslinked without use of any external crosslinkers or catalysts and showed good proton conductivity of 0.0013-0.016 S.cm^{-1}. Alkali stable PIL membranes were prepared based on bulky *N*-substituent. A high hydroxide ion conductivity (0.03-0.07 S.cm^{-1}) and stability evaluation for few months indicated the significance of this strategy of obtaining new generation OH$^-$ transporting membranes.

References

[1] D. F. Sanders, *et al*., *Polymer* **54** (2013) 4729–4761.

[2] D. Mecerreyes, *Progr. Polym. Sci.* **36** (2011) 1629-1648.

[3] J. Yuan, *et al*., *Progr. Polym. Sci.* **38** (2013) 1009-1036.

[4] S. Zulfiqar, *et al*., *Polym. Chem.* **6** (2015) 6435-6451.

[5] J. T. Wang, *et al*., *Electrochim. Acta.* **56** (2011) 2842-2847.

[6] C. H. Shen, *et al*., *J. Membr. Sci.* **399-400** (2012) 11-15.

Signature of the	Signature of the	Signature of the
Candidate	Ph.D. co- supervisor	Ph.D. supervisor
(Ms. Anita S. Rewar)	(Dr. K. Sreekumar)	(Dr. Ulhas. K. Kharul)

List of publications

1) **S. Rewar**, S. V. Shaligram, U. K. Kharul, Polybenzimidazole based polymeric ionic liquids possessing partial ionic character: Effects of anion exchange on their gas permeation properties, J. Membr. Sci. 497 (2015) 2828-288.

2) **S. Rewar**, R. S. Bhavsar, K. Sreekumar, U. K. Kharul, Polybenzimidazole based polymeric ionic liquids (PILs): Effects of controlled degree of *N*-quaternization on physical and gas permeation properties, J. Membr. Sci. 481 (2015)19–27.

3) **S. Rewar**, H. D. Chaudhari, R. Illathvalappil, K. Sreekumar and U. K. Kharul, New approach of blending polymeric ionic liquid with polybenzimidazole (PBI) for enhancing physical and electrochemical properties, J. Mater. Chem. A, 2 (2014) 14449- 14458.

4) R. S. Bhavsar, S. C. Kumbharkar, **A. S. Rewar**, U. K. Kharul, Polybenzimidazole based film forming polymeric ionic liquids: Synthesis and effects of cation-anion variation on their physical properties, Polym. Chem. 5 (2014) 4083-4096.

5) S. V. Shaligram, **A. S. Rewar**, P. P. Wadgoankar, U. K. Kharul, Incorporation of rigid polyaromatic groups in polybenzimidazole-based polymeric ionic liquids: Assertive effects on gas permeation properties submitted to RSC Advance.

6) **A. S. Rewar** and U. K. Kharul, Effect of amino acid as an anion on physical and gas sorption properties of PBI based polymeric ionic liquids, to be communicated.

7) **A. S. Rewar,** K. Sreekumar and U. K. Kharul, PIL-PBI blend membranes: Physical and electrochemical evaluations towards their applicability as membranes for PEMFC and AEMFC, under preparation.

Patent:

- U. K. Kharul**,** K. Sreekumar, **A. S. Rewar**, H. D. Chaudhari, Blend membranes based on polybenzimidazole (PBI) and polymeric ionic liquids (PILs) and process for the preparation thereof, US/2015/132797 A1.

Oral Presentation:

- ❖ **Anita S. Rewar** and Ulhas K.Kharul, "Polymeric ionic liquids based on polybenzimidazoles: Effects of variation in anion on physical and gas sorption properties" presented at '3rd International Conference on Membrane (ICM-2015), held at Kochi, India; 21 – 24 August

2015.

- **Anita S. Rewar**, K. Sreekumar and Ulhas K. Kharul, "Blend membranes based on polyionic liquid and polybenzimidazole: physical and electrochemical properties"; presented at '2nd International Conference on Membrane (ICM-2013), held at M. G. University, Kottayam, India; 3 – 6 October 2013.

Poster presentations:

- **Anita S. Rewar**, K. Sreekumar and Ulhas K. Kharul, "Polybenzimidazole- Polymeric Ionic Liquid blend membranes for Alkaline Membrane Fuel Cell", presented at International Conference on Membrane based Separations (MEMSEP 2015) held at M. S. University, Vadodara, India; 21-23 March 2015.

- **Anita S. Rewar**, K. Sreekumar and Ulhas K. Kharul, "New approach of blending polymeric ionic liquid with polybenzimidazole (PBI) for enhancing physical and electrochemical properties", presented at International Symposium on polymer science and technology, *MACRO 2015*, held at IACS, Kolkata, India; 23 – 26 January 2015.

- **Anita S. Rewar**, K. Sreekumar and Ulhas. K. Kharul "Polymeric Ionic Liquids Possessing Partial Ionic Character: Synthesis and Gas Permeation Studies"; presented at '3rd International Symposium, *FAPS* Polymer Congress and *MACRO 2013* on Frontiers in Polymer Science, held at IISc, Bangalore, India; 15 – 18 May 2013.

- **Anita S. Rewar**, K. Sreekumar and Ulhas. K. Kharul "Polymeric Ionic Liquids Possessing Partial Ionic Character: Synthesis and Gas Permeation Studies" during National Science Day 2013, National Chemical Laboratory, Pune, India.

- **Anita S. Rewar**, K. Sreekumar and Ulhas. K. Kharul "New Blend Membranes Based on Polyionic Liquid and Polybenzimidazole: Physical and Electrochemical properties" during National Science Day 2012, National Chemical Laboratory, Pune, India.